

ATP-sensitive Potassium Channels and Cardiac Arrhythmia

Mark James Specterman

MBBS BSc MRCP

Submitted in partial fulfilment of the requirements of
the Degree of Doctor of Philosophy

Queen Mary, University of London

2019

Declaration

I, Mark James Specterman, confirm that the research included within this thesis is my own work or that where it has been carried out in collaboration with, or supported by others, that this is duly acknowledged below and my contribution indicated. Previously published material is also acknowledged below.

I attest that I have exercised reasonable care to ensure that the work is original, and does not to the best of my knowledge break any UK law, infringe any third party's copyright or other Intellectual Property Right, or contain any confidential material.

I accept that the College has the right to use plagiarism detection software to check the electronic version of the thesis.

I confirm that this thesis has not been previously submitted for the award of a degree by this or any other university.

The copyright of this thesis rests with the author and no quotation from it or information derived from it may be published without the prior written consent of the author.

Signature:

Date:

Abstract

ATP-sensitive potassium channels (K_{ATP}) open in response to metabolic challenge. They form of pore subunits (Kir6.1 or Kir6.2) and modulatory subunits (SUR1, SUR2A or SUR2B) and are ubiquitously expressed. Differential subunit composition between cardiac chambers was investigated, as were atrial anti-arrhythmic effects of K_{ATP} modulation.

Selective pharmacology of K_{ATP} openers and inhibitors was confirmed in a heterologous expression system through whole-cell patch clamp. Isolated HL-1 cells (a murine atrial cardiomyocyte model) and murine atrial cardiomyocytes showed identical K_{ATP} pharmacological responses representing Kir6.2/SUR1 channels. Relative quantification of murine whole atrial RNA concurred, and was distinct from the ventricles (Kir6.2/SUR2). Human whole heart RNA from normal hearts exhibited a different pattern with no obvious chamber specificity.

Kir6.1^{-/-} and Kir6.2^{-/-} mice demonstrated that both pore types contribute to electrophysiological parameters in isolated atrial cardiomyocytes, but Kir6.2 appears more important. In atrial tissue (Langendorff hearts), Kir6.2^{-/-} more than Kir6.1^{-/-} mice demonstrated increased effective refractory periods and reduced conduction velocity at baseline, and during hypoxia, compared to wildtype. A trend to reduced arrhythmogenicity was observed during programmed electrical stimulation in the Kir6.2^{-/-} mouse.

In syncytia of spontaneously beating HL-1 cells, K_{ATP} activation with diazoxide was met with rotational to uniform wavefront organisation and silencing of electrical activity in a dose-dependent manner, reversed with channel blockade. In Langendorff mouse hearts K_{ATP} inhibition reversed hypoxia induced slowing of spontaneous sinus node activation, but pharmacological activation alone did not, suggesting different mechanisms with hypoxic channel activation.

Thus, both pore subunits contribute to the cardiac electrophysiology of murine atria, but Kir6.2 appears more important. HL-1 cells exhibit identical K_{ATP} pharmacology to murine atrial myocytes, which have a differential subunit composition compared to the ventricle. Any human cardiac K_{ATP} differential

subunit expression needs further exploration. K_{ATP} activation and inhibition have anti-arrhythmic effects and this might be explored further clinically.

Acknowledgements

My principle academic thanks for the completion of this project go to my primary supervisor Professor Andrew Tinker. He has always been available for advice and direction with a style that never overbears, and has inspired my passion for cardiac cellular electrophysiology continuously since we first discussed pursuit of this project.

Thanks to my secondary supervisors Professor Richard Schilling and Professor Pier Lambiase, both who are clinical and scientific inspirations. They have helped me maintain a translational approach to my work. I thank Dr Malcolm Finlay in providing support in many aspects including his Matlab scripts, his experience with the Langendorff preparation and his expertise with optics and calcium imaging.

Thanks to the members (present and former) of Professor Tinker's lab: Dr Qadeer Aziz, Dr Muriel Nobles, Dr Alison Thomas, Dr Stephen Harmer, Dr Keat-Eng Ng, Dr Sonia Sebastian, Ms Naomi Anderson, Dr Yiwen Li, Ms Leona Ojake, Dr James Cartwright, Ms Grace Salisbury, Dr Elena Tsisanova and Dr Mustafa Hassan, thanks for tirelessly putting up with my incessant questions.

A specific debt of gratitude goes to Dr Qadeer Aziz for tutoring me. Thanks to him I can actually patch clamp. He also performed the whole-cell action potential recordings and their analysis for this study. Thanks to Dr Muriel Nobles for the culture of the HL-1 cells, Dr Aziz and Dr Thomas for previously deriving the SUR2B-containing, Kir6.2/SUR1 and Kir6.2/SUR2A stable cell lines, Ms Leona Ojake for performing relative RNA quantification on the Kir6.2 global knockout mouse line, Dr Thomas for performing relative RNA quantification for the human tissue samples collected through The Barts Cardiovascular Registry (BCVR), and I must acknowledge The BCVR for providing access to these samples. The HL-1 cells were a kind gift from Professor Claycomb's lab.

A humongous thanks to my wife Haley for almost single-handedly bringing up the kids for the last 2 years! She has been incredibly supportive despite the fact I'm sure she thought it would never end. Thanks to my parents, who first ever put me in a position to achieve this and to my brother Robert for his constant positivity. Thanks to our daughters Elsie and Ivy, you don't know it yet, but this is, and I hope much more is, for you.

This work was supported by The Medical Research Council MR/L016230/1.

Table of Contents

Declaration	2
Abstract	3
Acknowledgements	5
Table of Contents	6
List of Figures	11
List of Tables	15
Abbreviations	16
Presentations, Publications, Awards	23
Section 1: Introduction	24
1.1 The Human Cardiac Action Potential and Excitation-Contraction Coupling	25
1.1.1 The Action Potential	25
1.1.2 Depolarisation Propagation and Gap Junctions	35
1.1.3 Ion Channel / Connexin Expression and Regional Specialisation	38
1.1.4 Autonomic and G-protein Linked Regulation	44
1.2 Atrial Fibrillation	48
1.2.1 Definition and Proposed Mechanisms.....	48
1.2.2 Management and Therapies	54
1.2.3 Drug Development for AF	59
1.3 ATP-sensitive Potassium Channels	62
1.3.1 ATP-sensitive Potassium Channel Structure, Function and Modulation.....	62
1.3.2 ATP-sensitive Potassium Channel Pharmacology.....	69
1.3.3 Cardiac ATP-sensitive Potassium Channels.....	73
1.3.4 ATP-sensitive Potassium Channels and Cardiac Chamber Subunit Specificity	78
1.4 The Mouse Heart as a Model for Investigating Arrhythmia Mechanisms and Therapies	85
1.5 Hypotheses	88

1.6 Aims	89
Section 2: Methods.....	90
2.1 Molecular Biology and Cell Culture.....	91
2.1.1 HEK293 stable cell lines expressing K _{ATP} subunits.....	91
2.1.1.1 Materials.....	91
2.1.1.2 Derivation and culture of HEK293 cell line stably overexpressing Kir6.1/SUR1 K _{ATP} Channels.....	92
2.1.1.3 Derivation and culture of HEK293 cell line stably overexpressing Kir6.1/SUR2A K _{ATP} Channels	94
2.1.1.4 Revival and culture of HEK293 cell lines stably overexpressing Kir6.1/SUR2B, Kir6.2/SUR2B, Kir6.2/SUR1 and Kir6.2/SUR2A K _{ATP} Channels.....	95
2.1.1.5 Transforming bacteria to amplify plasmids and cDNA	95
2.1.1.6 Isolation and Purification of Plasmid DNA.....	96
2.1.2 HL-1 Cells	97
2.1.2.1 Materials.....	99
2.1.2.2 Culturing HL-1 Cells	100
2.1.2.3 Passaging HL-1 Cells.....	101
2.1.2.4 Freezing and Reviving Cells	102
2.2 Generation of Knockout Mice	104
2.2.1 <i>Kcnj8</i>	104
2.2.2 <i>Kcnj11</i>	106
2.3 Animal Husbandry	108
2.4 Genotyping	109
2.4.1 <i>Kcnj8</i> Global Knockout.....	109
2.4.2 <i>Kcnj8</i> Cardiac Conditional Knockout.....	111
2.5 mRNA Quantification	113
2.5.1 Murine RNA.....	113
2.5.2 Human RNA	114
2.5.3 Quantitative real-time reverse transcriptase polymerase chain reaction (qRT-PCR).....	115
2.6 Isolation of Murine Atrial Myocytes.....	121
2.7 Patch Clamp Recordings from Isolated Cells	123
2.7.1 The Patch Clamp Technique.....	123

2.7.1.1 The Equilibrium Potential	123
2.7.1.2 Patch Clamp Equipment set-up	125
2.7.1.3 Single-Channel Recording	126
2.7.1.4 Whole-Cell Recording	130
2.7.1.5 Pipette and Cell Capacitance, and Series Resistance	131
2.7.1.6 Pros and Cons of the different configurations	136
2.7.1.7 Perforated-Patch Whole-Cell Recording	137
2.7.2 Experimental Conditions	138
2.8 Electrophysiology from Cardiac Tissue	142
2.8.1 Signal analysis via the surface electrogram	142
2.8.2 Langendorff Heart Preparations	146
2.8.3 FlexMEA Signal Analysis	149
2.9 Calcium Transient Measurement from HL-1 Syncytia	156
2.10 Statistical Analyses	158
Section 3: Results.....	159
3.1 Confirmation of Selective Pharmacology of K_{ATP} Openers and Inhibitors using HEK293 Stable Cell Lines	160
3.1.1 SURx subunit pharmacology	160
3.1.2 Kir6x subunit pharmacology	164
3.1.3 Representative recordings	165
3.1.4 Untransfected HEK293 cells	168
3.1.5 Summary	170
3.2 Generation of knockout mice.....	171
3.2.1 Attempt to generate a cardiomyocyte conditional <i>Kcnj8</i> knockout mouse.....	171
3.2.2 <i>Kcnj8</i> global knockout	175
3.2.3 <i>Kcnj11</i> global knockout	178
3.2.4 Summary	180
3.3 Isolated murine atrial cardiomyocytes demonstrate a functional expression and predominance for sarcolemmal K_{ATP} channels comprising Kir6.2/SUR1 subunits	181
3.3.1 Differential cardiac K_{ATP} subunit mRNA expression	181
3.3.2 Kir6.2 deletion, but not Kir6.1 deletion, abolishes the K_{ATP} current in isolated murine atrial cardiomyocytes	182

3.3.3 Kir6.2 but not Kir6.1 contributes to the resting membrane potential in isolated murine atrial cardiomyocytes	187
3.3.4 Knockout of either K_{ATP} pore-forming subunit does not lead to hypertrophy in isolated atrial cardiomyocytes	190
3.3.5 Kir6.2 contributes to the resting membrane potential in isolated atrial cardiomyocytes - reproducible with whole-cell action potential analysis.....	190
3.3.6 Kir6.2 deletion leads to a failure of action potential shortening on K_{ATP} activation	194
3.3.7 Summary	197
3.4 K_{ATP} activation slows automaticity in a murine atrial tissue model utilising HL-1 cells	199
3.4.1 HL-1 cells exhibit a K_{ATP} current and the functional expression is one of Kir6.2/SUR1 subunit composition.....	199
3.4.2 HL-1 cell syncytia exhibit spontaneous rotational activity that can be abolished by application of the K_{ATP} opener diazoxide	202
3.4.3 Summary	206
3.5 K_{ATP} activation during hypoxia contributes to sinus node depression, but pharmacological activation alone does not.....	207
3.5.1 Pharmacological K_{ATP} activation does not slow sinus node rate in a whole heart model	207
3.5.2 Inhibition of K_{ATP} during hypoxia prevents sinus node rate slowing .	208
3.5.3 Summary	210
3.6 Both K_{ATP} pore-forming subunits contribute to tissue-level electrophysiology of the atria in murine whole heart.....	211
3.6.1 Both K_{ATP} pore-forming subunits affect the atrial effective refractory period, and Kir6.2 is crucial to preventing its prolongation during hypoxia	211
3.6.2 Both K_{ATP} pore-forming subunits affect the atrial conduction velocity	215
3.6.3 Kir6.2 deletion, and pharmacological K_{ATP} inhibition, cause prolongation of atrial minimum wavefront path length during hypoxia	218
3.6.4 Kir6.2 deleted mice display reduced arrhythmia inducibility to programmed electrical stimulation during hypoxia / reperfusion	221

3.6.5 Summary	223
3.7 Whole heart RNA quantification suggests the presence of all	
K_{ATP} subunits except SUR1 in the human heart.....	225
3.7.1 Commercially available human whole heart RNA.....	225
3.7.2 Human whole heart RNA from The Barts Cardiovascular Registry .	227
3.7.3 Summary	228
Section 4: Discussion	229
4.1 Unique findings and addressment of the hypotheses and aims	230
4.2 K_{ATP} subunit pharmacology	232
4.3 Kir6.2 is the predominant pore-forming subunit, but is there a	
role for Kir6.1 in murine atrial cardiomyocytes?	234
4.4 K_{ATP} channel activation organises rotational wavefronts to	
straight uniform wavefronts, and slows automaticity	241
4.5 Pharmacological K_{ATP} activation does not impact on sinus node	
automaticity	244
4.6 Human cardiac K_{ATP}	245
4.7 Clinical implications and translational aspects	246
4.8 Limitations	249
4.9 Future directions	251
Section 5: References	252

List of Figures

Figure 1.1	The human cardiac action potential.....	26
Figure 1.2	Excitation-contraction coupling.....	31
Figure 1.3	Connexon channel structure.....	36
Figure 1.4	Autonomic inputs to the heart.....	44
Figure 1.5	Autonomic regulation of cardiomyocytes.....	45
Figure 1.6	Mechanisms of arrhythmia.....	49
Figure 1.7	Proposed AF mechanisms.....	50
Figure 1.8	Schematic of functional re-entry.....	50
Figure 1.9	Spiral waves.....	54
Figure 1.10	K _{ATP} structure.....	63
Figure 1.11	Cryo-EM structure of a Kir6.2/SUR1 channel.....	67
Figure 1.12	Pharmaco-topology of K _{ATP} openers and inhibitors.....	72
Figure 1.13	Comparison of human and mouse action potentials.....	85
Figure 2.1	Schematic of constructs for the <i>Kcnjx</i> knockout allele.....	105
Figure 2.2	Schematic for Cre recombinase mediated knockout of the floxed allele.....	106
Figure 2.3	Simplified map of <i>Kcnj8</i> and primer binding sites for genotyping.....	110
Figure 2.4	Reverse Transcription step for qRT-PCR.....	116
Figure 2.5	Quantitative Real-Time PCR.....	117
Figure 2.6	Demonstration of Equilibrium Potential.....	124
Figure 2.7	Cell-attached patch clamp configuration.....	126
Figure 2.8	Inside-out patch clamp configuration.....	129
Figure 2.9	Whole-cell patch clamp configuration.....	131
Figure 2.10	Electronic equivalent circuits demonstrating cell-attached and whole-cell patch clamp configurations.....	133
Figure 2.11	Perforated patch clamp configuration.....	137
Figure 2.12	Action potential measurements.....	139
Figure 2.13	Generation of unipolar and bipolar electrograms.....	143
Figure 2.14	The FlexMEA.....	147
Figure 2.15	Langendorff set up.....	148
Figure 2.16	The <i>EcgSplitter</i> GUI.....	150

Figure 2.17	The <i>EcgSplitter</i> manual window selection tool.....	152
Figure 2.18	Calculation of conduction velocity from a regression surface.....	154
Figure 3.1	Selective pharmacology for the SUR subunit.....	161
Figure 3.2	Effects of HMR1098 and Tolbutamide.....	163
Figure 3.3	PNU37883A K_{ATP} pore selectivity.....	165
Figure 3.4	Representative recordings for SUR1 containing channels.....	166
Figure 3.5	Representative recordings for SUR2A containing channels.....	167
Figure 3.6	Representative recordings for SUR2B containing channels.....	168
Figure 3.7	Effects of K_{ATP} openers and inhibitors in untransfected HEK293 cells.....	169
Figure 3.8	Genomic DNA PCR for the cardiomyocyte conditional Kir6.1 knockout mice.....	172
Figure 3.9	Tissue specific ΔC_t values for Kir6.1-cKO mice "non-knockout" genotypes.....	173
Figure 3.10	Relative expression as compared to WT of Kir6.1 between tissue types in Kir6.1-cKO mice.....	174
Figure 3.11	Genomic DNA PCR for the Kir6.1 global knockout mouse.....	176
Figure 3.12	Relative expression as compared to WT of Kir6.1 between tissue types in Kir6.1-gKO mice.....	177
Figure 3.13	Relative expression compared to WT of K_{ATP} subunits in the Kir6.1-gKO heart.....	178
Figure 3.14	Relative expression compared to WT of Kir6.2 between tissue types in Kir6.2-gKO mice.....	179
Figure 3.15	Relative expression compared to WT of K_{ATP} subunits in the Kir6.2-gKO heart.....	180
Figure 3.16	Relative expression of mRNA encoding for the various K_{ATP} subunits in wild-type murine whole heart.....	182
Figure 3.17	Demonstration of a K_{ATP} current in wild-type murine atrial cardiomyocytes with the pharmacological signature of Kir6.2/SUR1 subunits.....	184

Figure 3.18	Kir6.1 deletion does not reduce K_{ATP} current activation in isolated murine atrial cardiomyocytes.....	185
Figure 3.19	Kir6.2 deletion leads to an absence of activated K_{ATP} current in isolated murine atrial cardiomyocytes.....	186
Figure 3.20	Kir6.2 deletion abolishes, but Kir6.1 deletion increases, the tolbutamide-sensitive diazoxide-activated current in isolated murine atrial cardiomyocytes.....	187
Figure 3.21	Kir6.2 deletion but not Kir6.1 deletion leads to a more depolarised resting membrane potential in isolated murine atrial cardiomyocytes.....	189
Figure 3.22	K_{ATP} pore deletion does not affect the size of isolated atrial cardiomyocytes.....	190
Figure 3.23	Representative action potentials from isolated atrial cardiomyocytes.....	192
Figure 3.24	Kir6.2 deletion leads to changes in the parameters of the action potential in isolated atrial cardiomyocytes.....	193
Figure 3.25	Kir6.2 deletion does not alter the APD of isolated atrial cardiomyocytes at baseline but does lead to failure to shorten the APD on K_{ATP} activation.....	195
Figure 3.26	Kir6.2 deletion leads to altered action potential morphology in isolated atrial cardiomyocytes and differential momentary membrane potential.....	196
Figure 3.27	HL-1 cells exhibit a K_{ATP} current activated by diazoxide but not pinacidil.....	200
Figure 3.28	The K_{ATP} current in HL-1 cells is inhibited by tolbutamide but not PNU37883A.....	201
Figure 3.29	Diazoxide but not pinacidil hyperpolarises the resting membrane potential of HL-1 cells.....	202
Figure 3.30	Example HL-1 syncytia demonstrating rotational wavefront propagation.....	203
Figure 3.31	HL-1 syncytia - diazoxide slows the frequency of spontaneous rotational / automatic activity.....	205
Figure 3.32	HL-1 syncytia - diazoxide can re-organise activation wavefronts from rotational to straight and uniform.....	206

Figure 3.33	Pharmacological K_{ATP} activation does not slow spontaneous sinus node rate in the whole heart.....	208
Figure 3.34	Inhibition of K_{ATP} during hypoxia prevents sinus node rate slowing.....	209
Figure 3.35	Baseline heart rate was unaffected by either K_{ATP} pore knockout.....	212
Figure 3.36	Atrial ERP is prolonged in both K_{ATP} pore knockout mice and Kir6.2 is crucial to maintain it during hypoxia.....	214
Figure 3.37	Atrial CV is lower in both K_{ATP} pore knockout mice.....	216
Figure 3.38	Example isochronal activation maps from Langendorff hearts.....	217
Figure 3.39	Atrial steady state CV falls through hypoxia at the same rate in both K_{ATP} pore knockout mice as WT.....	218
Figure 3.40	Kir6.2 deletion, and pharmacological K_{ATP} inhibition, cause prolongation of atrial minimum wavefront path length during hypoxia.....	220
Figure 3.41	Kir6.2 deleted mice display reduced arrhythmia inducibility to programmed electrical stimulation during hypoxia / reperfusion.....	222
Figure 3.42	Example trace of arrhythmia induced by programmed electrical stimulation.....	223
Figure 3.43	Relative quantification of K_{ATP} subunit transcripts in human whole "normal heart" RNA.....	226
Figure 3.44	Relative quantification of K_{ATP} subunit mRNA transcripts from human atrial samples through The Barts Cardiovascular Registry.....	227

List of Tables

Table 1	Summary of human diseases or traits in which mutations or genomic variants in K_{ATP} occur.....	82
Table 2	Summary of the investigated effects of K_{ATP} openers and inhibitors.....	170

Abbreviations

[x]_i	Intracellular concentration of species x
[x]_o	Extracellular concentration of species x
ABCC8	Gene encoding adenosine triphosphate sensitive potassium channel sulphonylurea receptor subunit 1
ABCC9	Gene encoding adenosine triphosphate sensitive potassium channel sulphonylurea receptor subunit splice variants 2A and 2B
ACEi	Angiotensin converting enzyme inhibitor
ADP	Adenosine diphosphate
AF	Atrial fibrillation
APD	Action potential duration
APD₉₀	Action potential duration at 90% repolarisation of its absolute amplitude
ARB	Angiotensin II receptor blocker
ARI	Activation-recovery interval
AT-1	Angiotensin II receptor
ATP	Adenosine triphosphate
AVN	Atrioventricular node
BEGM	Bipolar electrogram
Ca²⁺	Calcium ion
CACNA1C	Gene encoding long-acting L-type calcium current pore-forming subunit
CACNA1G	Gene encoding transient-acting T-type calcium current pore-forming subunit Cav3.1
CACNA1H	Gene encoding transient-acting T-type calcium current pore-forming subunit Cav3.2
CACNA2D1	Gene encoding long-acting L-type calcium current auxiliary subunit Cava α 2 δ
CACNB2	Gene encoding long-acting L-type calcium current auxiliary subunit Cav β 2
cAF	Chronic or persistent atrial fibrillation
cAMP	Cyclic adenosine monophosphate

Cav1.2	Long-acting L-type calcium current pore forming subunit
Cav3.1	Transient-acting T-type calcium current pore-forming subunit
Cav3.2	Transient-acting T-type calcium current pore-forming subunit
Cavα2δ	Long-acting L-type calcium current auxiliary subunit
Cavβ2	Long-acting L-type calcium current auxiliary subunit
CICR	Calcium induced calcium release
CL	Cycle length
CT	Computed Tomography
CV	Conduction velocity
Cx40	Connexin 40
Cx43	Connexin 43
Cx45	Connexin 45
DAD	Delayed after-depolarisation
DAG	Diacylglycerol
DZX	Diazoxide
EAD	Early after-depolarisation
E_i	Equilibrium potential of ion i
emf	Electromotive force
ERP	Effective refractory period
ET_A	Endothelin-1 receptor
FBS	Foetal bovine serum
FlexMEA	Flexible microelectrode array
Fluo-4,AM	Fluo-4 acetoxymethyl ester
GDP	Guanosine diphosphate
G_i	G-inhibitory protein
GIRK	G-Protein linked inwardly-rectifying potassium channel
GLIB	Glibenclamide
G_q	G _q protein
G_s	G-stimulatory protein
GTP	Guanosine triphosphate
g_x	Conductance of species x
G_{ai}	G-inhibitory protein alpha subunit
G_{aq}	G _q protein alpha subunit
G_{βγ}	G-inhibitory protein beta subunit

HCN	Hyperpolarisation-activated cyclic nucleotide-gated cation channel (funny current) pore forming subunit
HCN4	Gene encoding hyperpolarisation-activated cyclic nucleotide-gated cation channel (funny current) pore-forming subunit
hERG1	Rapid delayed rectifier potassium current pore-forming subunit
His	His bundle
HMR	HMR1098
I_{CaL}	Long-acting L-type calcium current
I_{CaT}	Transient-acting T-type calcium current
ICD	Implantable cardioverter defibrillator
I_f	Funny current
I_{K1}	Strongly inwardly-rectifying potassium current
$I_{KACh,Ado}$	Acetylcholine / Adenosine activated potassium current
I_{KATP}	Adenosine triphosphate sensitive potassium current
I_{Kr}	Rapid delayed rectifier potassium current
I_{Ks}	Slow delayed rectifier potassium current
I_{Kslow1}	Murine delayed rectifier potassium current 1
I_{Kslow2}	Murine delayed rectifier potassium current 2
I_{Kur}	Ultra-rapid delayed rectifier potassium current
I_{Na}	Sodium current
$I_{Na/Ca}$	Sodium-calcium exchange current
$I_{Na/K}$	Sodium-potassium ATPase pump
I_{NaL}	Late persistent sodium current
I_{NaPeak}	Peak inward sodium current
I_p	Sodium-potassium ATPase pump current
IP₃	Inositol-1,4,5-triphosphate
$I_{to,f}$	Transient outward potassium current with fast recovery
$I_{to,s}$	Transient outward potassium current with slow recovery
K⁺	Potassium ion
K_{ATP}	Adenosine triphosphate sensitive potassium channel
KChIP2	Transient outward potassium current with fast recovery auxiliary subunit
KCNA4	Gene encoding transient outward potassium current with slow recovery pore-forming subunit

KCNA5	Gene encoding the ultra-rapid delayed rectifier potassium current pore-forming subunit
KCNAB1	Gene encoding the ultra-rapid delayed rectifier potassium current auxiliary subunits Kv β 1.2 and Kv β 1.3
KCNAB2	Gene encoding the ultra-rapid delayed rectifier potassium current auxiliary subunit Kv β 2.1
KCND3	Gene encoding transient outward potassium current with fast recovery pore-forming subunit
KCNE1	Gene encoding slow delayed rectifier potassium current auxiliary subunit
KCNE1	Suggested slow delayed rectifier potassium current auxiliary subunit
KCNE2	Gene encoding rapid delayed rectifier potassium current auxiliary subunit
KCNE2	Suggested rapid delayed rectifier potassium current auxiliary subunit
KCNH2	Gene encoding rapid delayed rectifier potassium current pore-forming subunit
KCNIP2	Gene encoding transient outward potassium current with fast recovery auxiliary subunit
KCNJ11	Gene encoding adenosine triphosphate sensitive potassium channel pore-forming subunit Kir6.2
KCNJ2	Gene encoding strongly inwardly-rectifying potassium current I _{K1} current pore-forming subunit
KCNJ3	Gene encoding G-protein linked inwardly rectifying potassium channel pore-forming subunit Kir3.1
KCNJ5	Gene encoding G-protein linked inwardly rectifying potassium channel pore-forming subunit Kir3.4
KCNJ8	Gene encoding adenosine triphosphate sensitive potassium channel pore-forming subunit Kir6.1
KCNK3	Gene encoding suggested inward leak potassium channel
KCNQ1	Gene encoding slow delayed rectifier potassium current pore-forming subunit
KCO	Potassium channel (K _{ATP}) opener

Kir2.1	Strongly inwardly-rectifying potassium I_{K1} current pore-forming subunit
Kir3.1	G-protein linked inwardly-rectifying potassium channel pore-forming subunit
Kir3.4	G-protein linked inwardly-rectifying potassium channel pore-forming subunit
Kir6.1	Adenosine triphosphate-sensitive potassium channel pore-forming subunit
Kir6.1-cKO	Kir6.1 cardiomyocyte conditional knockout mouse
Kir6.1-gKO	Kir6.1 global knockout mouse
Kir6.2	Adenosine triphosphate-sensitive potassium channel pore-forming subunit
Kv1.4	Transient outward potassium current with slow recovery pore-forming subunit
Kv1.5	Ultra-rapid delayed rectifier potassium current pore-forming subunit
Kv4.3	Transient outward potassium current with fast recovery pore-forming subunit
Kv7.1	Slow delayed rectifier potassium current pore-forming subunit
Kvβ1.2	Ultra-rapid delayed rectifier potassium current auxiliary subunit
Kvβ1.3	Ultra-rapid delayed rectifier potassium current auxiliary subunit
Kvβ2.1	Ultra-rapid delayed rectifier potassium current auxiliary subunit
LA	Left Atrium
LAA	Left atrial appendage
LQT1	Long-QT Syndrome 1
LQT2	Long-QT Syndrome 2
LQT3	Long-QT Syndrome 3
LV	Left ventricle
MAP	Monophasic action potential
MAP₉₀	Monophasic action potential duration at 90% repolarisation of its absolute amplitude
MDP	Maximum diastolic potential
MEA	Microelectrode array
Mg²⁺	Magnesium ion

mitoK_{ATP}	Mitochondrial ATP-sensitive potassium channel
MRI	Magnetic Resonance Imaging
Na⁺	Sodium ion
Nav1.5	Sodium channel pore-forming subunit
Navβ1	Sodium channel auxiliary subunit β1
Navβ2	Sodium channel auxiliary subunit β2
Navβ3	Sodium channel auxiliary subunit β3
NBF	Nucleotide binding fold
pAF	Paroxysmal atrial fibrillation
PBS	Phosphate buffered saline
PCR	Polymerase chain reaction
PIN	Pinacidil
PIP₂	Phosphatidylinositol-4,5-bisphosphate
PKA	Protein Kinase A
PKC	Protein Kinase C
PNU	PNU37883A
PP-1	Protein-phosphatase 1
PV	Pulmonary vein
PVI	Pulmonary vein isolation
qRT-PCR	Quantitative real-time reverse transcriptase polymerase chain reaction
RA	Right atrium
RV	Right ventricle
RyR	Ryanodine receptor
SAN	Sino-atrial node
SCN1B	Gene encoding the sodium channel auxiliary subunit β1
SCN2B	Gene encoding the sodium channel auxiliary subunit β2
SCN3B	Gene encoding the sodium channel auxiliary subunit β3
SCN5A	Gene encoding the sodium channel pore-forming subunit Nav1.5
SERCA	Sarcoplasmic reticulum calcium transport ATPase
SR	Sarcoplasmic reticulum
SUR1	Adenosine triphosphate-sensitive potassium channel sulphonylurea receptor subunit 1

SUR2A	Adenosine triphosphate-sensitive potassium channel sulphonylurea receptor subunit 2 splice variant 2A
SUR2B	Adenosine triphosphate-sensitive potassium channel sulphonylurea receptor subunit 2 splice variant 2B
$t_{1/2}$	Time to half maximum activation
TASK-1	Suggested inward leak potassium channel
TdP	Torsades de Pointes
TMD	Transmembrane domain
TOLB	Tolbutamide
UEGM	Unipolar electrogram
$V_{1/2}$	Potential at which activation reaches half-maximum
VF	Ventricular fibrillation
$V_{h0.5}$	Membrane potential at which 50% of channels are inactivated
$V_{j1/2}$	Transjunctional voltage gradient of half maximal activation/inactivation
V_m	Membrane potential
V_{max}	Action potential phase 0 maximum upstroke velocity
V_T	Threshold voltage for activation
WFPL	Minimum wavefront path length
WT	Wild-type mouse
$\alpha 1$	Alpha adrenergic receptor 1
$\beta 1$	Beta adrenergic receptor 1
τ_a	Exponential time constant of activation
τ_d	Exponential time constant of deactivation
τ_i	Exponential time constant of inactivation
τ_{rec}	Exponential time constant of recovery from inactivation

Presentations, Publications, Awards

Meeting Abstract and Presentation

Specterman M, Aziz Q, Finlay M, Nobles M, Anderson N, Ng K-E, Schilling R, Tinker A (2016). K_{ATP} channels as a drugable target for inappropriate sinus and ectopic atrial tachycardia. *J Interv Card Electrophysiol* **45(3)**, 278 (European Cardiac Arrhythmia Society 2016 Annual Congress special issue).

Meeting Presentation and Award

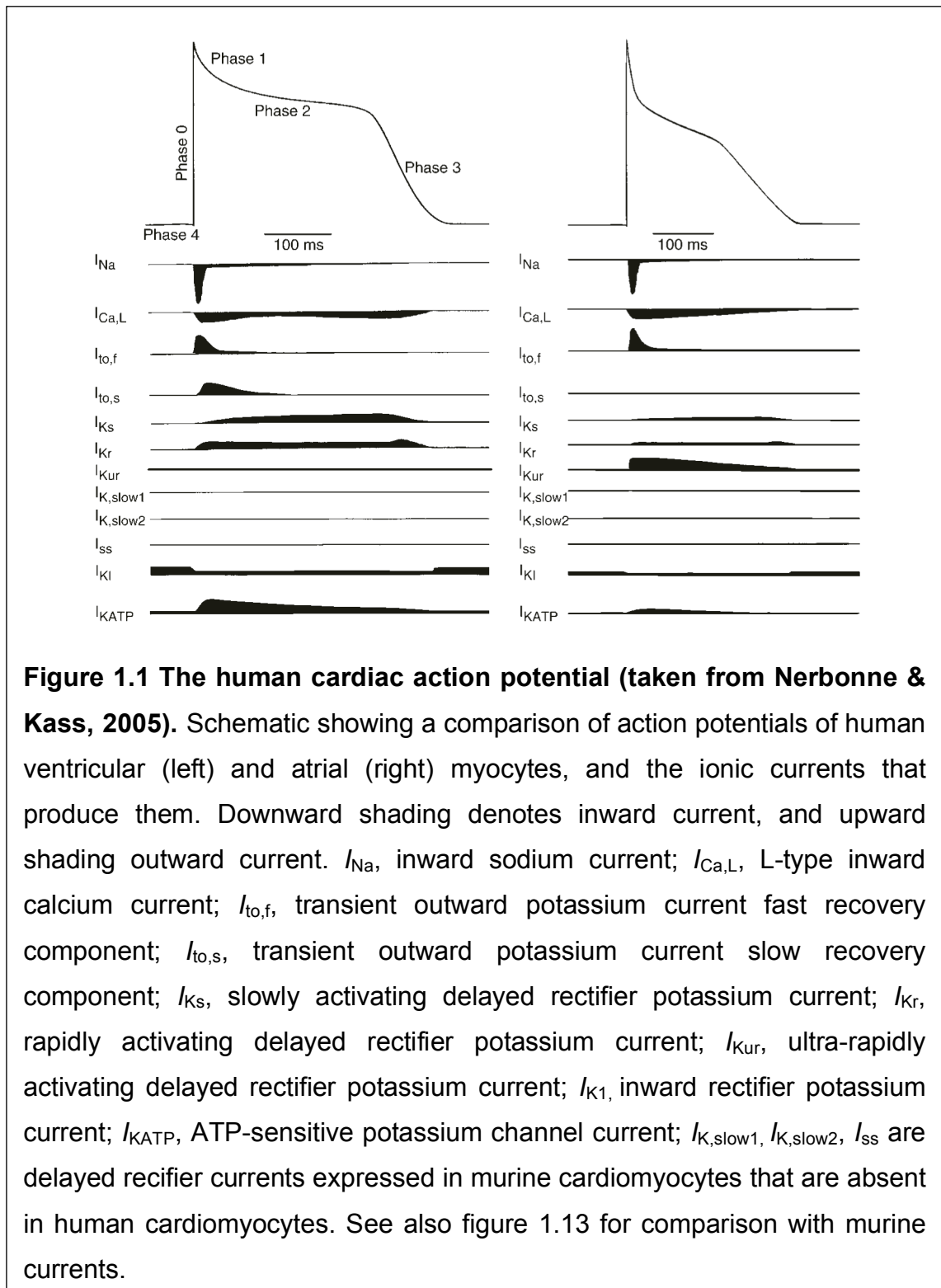
Young Investigator of the Year Award 2016, Heart Rhythm Congress, Birmingham, UK - The K_{ATP} channel opener diazoxide reduces automaticity in an in vitro atrial cell model - potential for K_{ATP} channels as a drug target for atrial arrhythmias.

Section 1: Introduction

1.1 The Human Cardiac Action Potential and Excitation-Contraction Coupling

1.1.1 The Action Potential

Contraction of the myocardium and the action of the heart as a pump requires the flow of various ionic currents in and out of cardiomyocytes. The rhythmic beating of the heart requires the propagation of these currents from groups of cells in one region, conducted to groups of cells in neighbouring and distant regions. The currents are carried by sodium (Na^+), calcium (Ca^{2+}) and potassium (K^+) ions through pores called ion channels in the membranes of cardiomyocytes. Ionic flow is dependent on an electrochemical gradient defined by their concentrations on either side of the cell membrane (diffusion) and the potential difference across the membrane at any particular moment, exerting an electromotive force on the ion. The equilibrium potential (or reversal potential) for an ion (E_i), is the potential difference across the membrane, that results in no flow of that particular ion given the concentrations of it either side of the membrane (discussed in more detail in section 2.7.1 on patch clamp electrophysiology). If the membrane potential of the cell (V_m) is more positive to E_i for a given cation, then that cation will carry outward current (assuming a permeable ion channel is open) and the opposite is true if the membrane potential of the cell is more negative to E_i . Ultimately, it is the depolarisation of a cardiomyocyte where the cytoplasmic face of the cell membrane is transformed at rest from a negative potential difference relative to the extracellular face, to that of a positive one by inward Na^+ and Ca^{2+} ions, and the binding of Ca^{2+} to intracellular myofilaments, that cause the cell to contract. The cell must then be able to relax again and repolarise ready for the next beat and this requires the extrusion of Na^+ and Ca^{2+} ions, the re-sequestration of Ca^{2+} ions back into the sarcoplasmic reticulum (SR), and the outward flow of potassium ions. This process is what constitutes the action potential and excitation-contraction coupling. The classic cardiac action potential in large mammals consists of 4 phases (see Figure 1.1).



Action Potential Phase 0

The upstroke of the action potential is produced by the inward sodium current (I_{Na}). Cardiac sodium channels are voltage-gated and composed of an α pore-forming subunit and either 1 or 2 β (regulatory) subunits (Nerbonne & Kass,

2005). The α subunit consists of four domains each with six transmembrane-spanning regions and the predominant cardiac α subunit across species is Nav1.5 encoded by the *SCN5A* gene (Fozzard, 2002; Nerbonne & Kass, 2005). Three β subunits Nav β 1, Nav β 2 and Nav β 3 encoded by *SCN1B*, *SCN2B* and *SCN3B* respectively contribute to the expression and trafficking of the channel to the sarcolemma and its voltage-gating (Nerbonne & Kass, 2005). Based on Hodgkin and Huxley's original model of ion channel gating it can be said that sodium channels have both activation and inactivation gates (Hodgkin & Huxley, 1952). Nav1.5 containing channels have very fast activation kinetics with a time to half maximal activation at 20°C ($t_{1/2}$) of \sim 0.8ms, a threshold voltage for activation (V_T) of \sim -55mV and a voltage producing half maximal conductance ($V_{1/2}$) of \sim -50mV (Ulbricht, 2005). This is followed by fast voltage-dependent inactivation with an exponential time constant (τ_i) of the rapid component of inactivation at $V_m=+20$ mV of \sim 0.4ms, before fast recovery from this inactivation with a time constant (τ_{rec}) at $V_m=-100$ mV of \sim 40ms and deactivation at $V_m=-60$ mV back to the resting state of both gates during repolarisation (Nerbonne & Kass, 2005; Ulbricht, 2005; Armstrong, 2006; Mangold *et al.*, 2017). Estimates suggest that at membrane potentials corresponding to the plateau phase \sim +10mV (phase 2) of the action potential in ventricular myocytes, \sim 99% of the sodium channels are inactivated (Nerbonne & Kass, 2005). Recovery from inactivation requires that the membrane potential becomes repolarised and the probability of recovery from inactivation increases as the membrane potential drops from the plateau potential (Ulbricht, 2005). Loss of function mutations in the Nav1.5 channel are thought to underpin, in part, the mechanisms behind the Brugada syndrome (Wilde *et al.*, 2010; Kusano, 2013). Changes in ventricular depolarisation (slower phase 0, reduced peak amplitude in phase 0) and repolarisation and subsequent accentuated heterogeneous dispersion of action potential duration (APD) predisposes to triggered and re-entrant arrhythmia leading to polymorphic VT/VF and sudden death (Wilde *et al.*, 2010; Kusano, 2013).

Action Potential Phase 1

The transient outward potassium currents (I_{to}) produce the “notch” and the early initial repolarisation of the action potential (Liu *et al.*, 1993; Wettwer *et al.*,

1994). These currents are part of a family of voltage-gated potassium channels activated by the depolarisation of the cell. Voltage-gated potassium channels in general, consist of a pore-forming α subunit composed of tetramers of six transmembrane domain proteins and associate with β subunits which contribute to the expression and trafficking of the channel to the sarcolemma and its voltage-gating (Nerbonne & Kass, 2005). Voltage-gated potassium channels are outwardly rectifying whereby pore opening on depolarisation of the cardiomyocyte leads to outward potassium current. The transient outward potassium current activates and inactivates quickly at membrane potentials positive to $\sim -30\text{mV}$ (Wettwer *et al.*, 1994; Nerbonne & Kass, 2005). Two types of transient outward potassium current exist namely $I_{to,f}$ (fast activation with time to peak activation $\sim 10\text{ms}$, fast inactivation $\tau_i \sim 60\text{ms}$ at $V_m = +60\text{mV}$, fast recovery kinetics $\tau_{rec} \sim 25\text{ms}$ at $V_m = -100\text{mV}$) and $I_{to,s}$ (fast activation and moderately fast inactivation with similar time constants to $I_{to,f}$, but slower recovery kinetics $\tau_{rec} \sim 340\text{ms}$) (Liu *et al.*, 1993; Wettwer *et al.*, 1994; Nerbonne & Kass, 2005). I_{to} has a narrow window current with a steady-state voltage dependence of inactivation such that the potential at which 50% of channels are inactivated ($V_{h0.5}$) is of the order of $\sim -30\text{mV}$. $I_{to,f}$ appears to consist of Kv4.3 α subunits encoded by *KCND3* and KChIP2 β subunits encoded by *KCNIP2* probably in a 4:4 stoichiometry (Nerbonne & Kass, 2005). The α subunit of $I_{to,s}$ is Kv1.4 encoded by *KCNA4* but the β subunit is not well defined (Nerbonne & Kass, 2005).

The voltage-gated I_{Kur} (ultra-rapid) current also contributes to phase 1 repolarisation with very fast activation at $V_T \sim -30\text{mV}$ and a time constant of activation (τ_a) of $\sim 2\text{ms}$ at $V_m = +50\text{mV}$, but very slow inactivation kinetics and, essentially, does not functionally inactivate. For example current is reduced by only $\sim 16\%$ moving from $V_m = -80\text{mV}$ to $+40\text{mV}$ via a 1000ms pre-pulse to -20mV (Wang *et al.*, 1993; Ravens & Wettwer, 2011). It consists of Kv1.5 α subunits encoded by *KCNA5* and associates with Kv β 1.2 and Kv β 1.3 β subunits encoded by splice variants of *KCNAB1*, and Kv β 2.1 subunits encoded by *KCNAB2* (Nerbonne & Kass, 2005; Ravens & Wettwer, 2011). I_{Kur} appears to be expressed specifically in the atria (Ravens & Wettwer, 2011).

The sodium/potassium-ATPase pump ($I_{Na/K}$) extrudes Na^+ and imports K^+ with a stoichiometry of three Na^+ ions to two K^+ ions (Glitsch, 2001). It is activated by a high intracellular sodium concentration ($[Na^+]_i$) and/or a high extracellular potassium concentration ($[K^+]_o$) and given the stoichiometry of flux, produces an outward pump current of positive ions (I_p) (Glitsch, 2001). It contributes to repolarisation, the maintenance of a negative resting membrane potential and the maintenance of intra- and extracellular ion concentrations necessary for normal cellular function. It is constitutively active throughout the action potential.

Action Potential Phase 2

A balance of inward calcium and sodium currents, and outward potassium currents, produces the plateau phase. The depolarisation caused by I_{Na} activates voltage-gated calcium channels. Calcium channels, like sodium channels, are formed from an α subunit comprising 4 domains each with six transmembrane-spanning regions. Long-acting (L-type) calcium channels (I_{CaL}) are high-voltage activating (HVA) opening rapidly ($\tau_a \sim 2.3ms$) at $V_T \sim -20mV$ and are long-acting owing to a slow time-course of inactivation ($\tau_i \sim 1s$). They recover from inactivation over $\sim 400ms$ at $V_m = -80mV$. They are the predominant current contributing to the classic atrial and ventricular myocyte action potential (Bean, 1985; Hirano *et al.*, 1989; Koschak *et al.*, 2001; Nerbonne & Kass, 2005; Catterall, 2011). In the atria and ventricle they are formed of a Cav1.2 α subunit encoded by *CACNA1C* and the predominant cardiac accessory subunits Cav β 2, encoded by *CACNB2*, and Cav α 2 δ , encoded by *CACNA2D1* which both contribute to the expression and trafficking of the channel to the sarcolemma and its voltage-gating (Nerbonne & Kass, 2005). I_{CaL} in the sinus node is produced predominantly by channels with Cav1.3 subunits encoded by *CACNA1D* (Mangoni *et al.*, 2003). They activate at more negative membrane potentials ($V_T \sim -45mV$), more rapidly ($\tau_a \sim 0.8ms$), and inactivate more slowly ($\tau_i \sim 1.7s$) than Cav1.2 channels (Koschak *et al.*, 2001). Cav1.3 channels also undergo the phenomenon of voltage dependent facilitation during recovery from inactivation at hyperpolarised potentials, post a depolarising pulse (Christel *et al.*, 2012). These properties owing to Cav1.3 channels serve function to a pacemaking role in the sinus node as is discussed below. L-type calcium channels also undergo calcium-dependent-inactivation whereby their opening

and subsequent influx of calcium also promotes their inactivation (Bers, 2002; Catterall, 2011).

Transient-acting (T-type) calcium channels (I_{CaT}) are low-voltage activating (LVA) and open rapidly at $V_T \sim -50\text{mV}$. They are more densely expressed in the atria and pacemaker/nodal tissues contributing to automaticity, particularly in nodal tissues, and inactivate more rapidly than L-type channels with $\tau_i \sim 20\text{ms}$ at $V_m = +10\text{mV}$ (Bean, 1985; Perez-Reyes, 2003; Nerbonne & Kass, 2005; Catterall, 2011). They recover from inactivation more slowly than L-type calcium channels $\sim 800\text{ms}$ at $V_m = -80\text{mV}$ (Hirano *et al.*, 1989). They are formed of Cav3.1 and Cav3.2 α subunits encoded by *CACNA1G* and *CACNA1H* respectively and it appears that they are expressed at the sarcolemma in the absence of a β subunit (Perez-Reyes, 2003; Nerbonne & Kass, 2005).

A small population of Nav1.5 sodium channels is slow to inactivate during phase 1 and phase 2 and this contributes a persistent late sodium current (I_{NaL}) to the plateau phase (Liu *et al.*, 1993; Sakmann *et al.*, 2000; Nerbonne & Kass, 2005). The kinetics and voltage-dependency of inactivation and the degree of I_{NaL} are governed in part by the associated Nav β -subunit (Nerbonne & Kass, 2005; Ulbricht, 2005). Mutations in Nav1.5 channels leading to increased I_{NaL} underpin heterogeneous action potential duration (APD) prolongation in Long-QT syndrome 3 (LQT3) leading to triggered polymorphic VT/VF and sudden death (Schwartz *et al.*, 2012).

The sodium/calcium (Na/Ca) exchanger is constitutively active and is reversible with a stoichiometry of moving three Na^+ ions to one Ca^{2+} ion (Blaustein & Lederer, 1999; Bers, 2002; Eisner & Sipido, 2004). As such when calcium is extruded from the cell there is a net inward positive current ($I_{Na/Ca}$), and the opposite is true when calcium enters the cell when $I_{Na/Ca}$ is outward (reverse mode). The equilibrium potential of the Na/Ca exchanger is given by $E_{Na/Ca} = 3E_{Na} - 2E_{Ca}$. During the early part of phase 2 the concentration of intracellular Na^+ ($[\text{Na}^+]_i$) is high and the membrane potential is more positive to $E_{Na/Ca}$ and so $I_{Na/Ca}$ is outward and calcium enters the cell in reverse mode (Bers, 2002). During the end of phase 2 the membrane potential drops below $E_{Na/Ca}$ and

intracellular Ca^{2+} ($[\text{Ca}^{2+}]_i$) is high and so $I_{\text{Na/Ca}}$ is inward and calcium is extruded (Bers, 2002). This is forward mode.

Intracellular Ca^{2+} activates the ryanodine receptor (RyR) located in the sarcoplasmic reticulum (SR) membrane. In turn Ca^{2+} is released from the SR through the RyR in a process called calcium-induced-calcium-release (CICR) (Bers, 2002). Thus, whilst the Na/Ca exchanger may be in reverse mode with outward $I_{\text{Na/Ca}}$, the inward flow of Ca^{2+} through the exchanger can prolong the plateau phase through CICR at the SR (Bers, 2002).

It is during phase 2 that there is high $[\text{Ca}^{2+}]_i$ and Ca^{2+} binding to Troponin C causing the tropomyosin complex to move off the actin active site and allow the myosin head to bind actin. With ATP hydrolysis the myosin head then pulls the actin filament closer in towards the sarcomere for contraction (Bers, 2002; de Tombe, 2003; Gordan *et al.*, 2015) (see Figure 1.2).

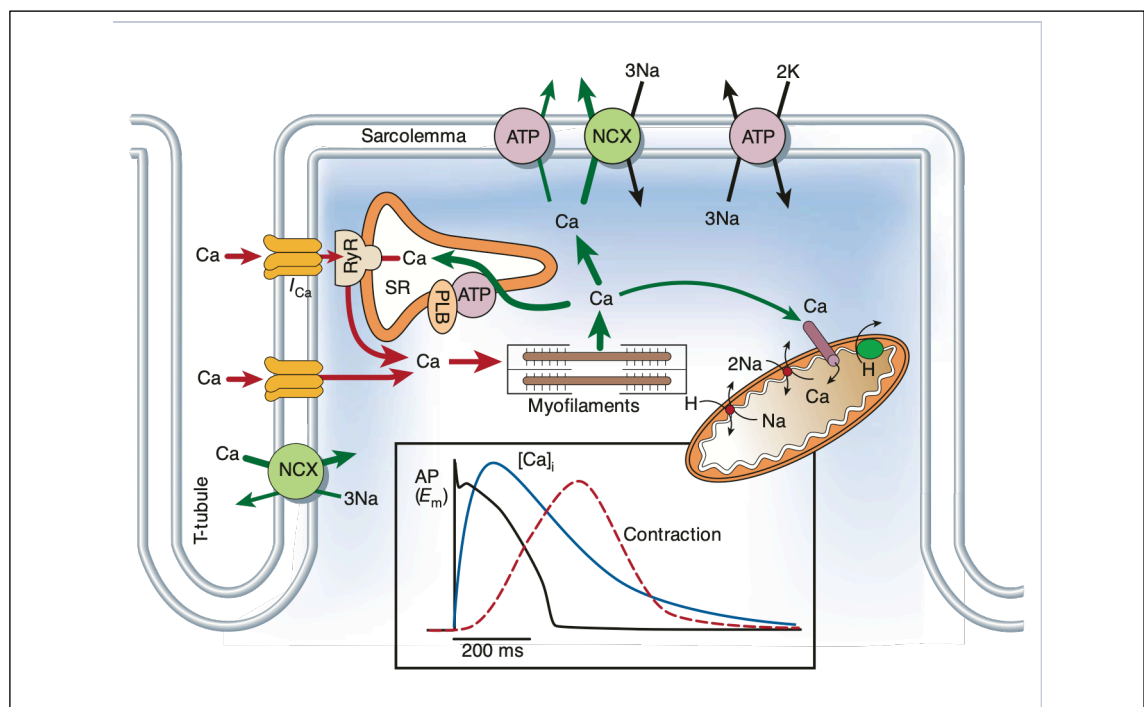


Figure 1.2. Excitation-contraction coupling (taken from Bers, 2002).

Schematic demonstrating the processes of excitation-contraction coupling and Ca^{2+} extrusion from the cytosol. The inset shows the time course of an action potential, Ca^{2+} transient and contraction measured, in this case, from a rabbit ventricular myocyte at 37°C. NCX, sodium-calcium exchanger; ATP, ATPase pump; PLB, phospholamban; SR, sarcoplasmic reticulum.

Outward potassium currents have been described for phase 1 namely the transient outward currents and I_{Kur} . Late in phase 2 activation of the rapid delayed rectifier potassium current I_{Kr} contributes to repolarisation. This current is produced by an outwardly rectifying voltage-gated potassium channel made up of hERG1 α subunits encoded by *KCNH2* and, most likely, a MiRP1 β subunit encoded by *KCNE2* (Nerbonne & Guo, 2002; Schram *et al.*, 2002; Nerbonne & Kass, 2005). It activates moderately fast with a $\tau_a \sim 127$ ms whilst also inactivating and recovering from inactivation with fast kinetics ($\tau_i \sim 4$ ms at $V_m = 0$ mV ; $\tau_{rec} \sim 8$ ms at $V_m = -80$ mV) (Nerbonne & Kass, 2005; Vandenberg *et al.*, 2012). It deactivates very slowly with a time constant of deactivation (τ_d) of ~ 300 ms at $V_m = -70$ mV (Vandenberg *et al.*, 2012). Loss of function mutations in hERG underpin heterogeneous action potential duration (APD) prolongation in Long QT syndrome 2 (LQT2) leading to triggered polymorphic ventricular tachycardia (VT) / ventricular fibrillation (VF) and sudden death (Schwartz *et al.*, 2012).

Action Potential Phase 3

Repolarisation occurs when outward potassium currents predominate after inactivation of voltage-gated inward cation currents. In addition to I_{Kur} and I_{Kr} the slow delayed rectifier potassium current I_{Ks} contributes. This current is produced by an outwardly rectifying voltage-gated potassium channel made up of Kv7.1 α subunits encoded by *KCNQ1* and a β subunit encoded by *KCNE1* (Nerbonne & Kass, 2005; Tinker & Harmer, 2010). It activates very slowly over the order of seconds at positive membrane potentials ($\tau_a \sim 800$ ms) with no inactivation and deactivates slowly $\tau_d \sim 150$ ms (Gintant, 1995; Nerbonne & Kass, 2005; Tinker & Harmer, 2010). In the absence of *KCNE1*, activation is not attenuated and is fast (Nerbonne & Kass, 2005; Tinker & Harmer, 2010). Owing to slow activation kinetics and a lack of inactivation, I_{Ks} accumulates at higher heart rates and contributes to action potential shortening at short diastolic intervals (Volders *et al.*, 2003). Loss of function mutations in *KCNQ1* underpin heterogeneous action potential duration (APD) prolongation in Long-QT syndrome 1 (LQT1) leading to triggered polymorphic VT/VF and sudden death (Schwartz *et al.*, 2012).

During phase 3 the Na/Ca exchanger is in its calcium extrusion mode owing to high $[Ca^+]_i$. The inward $I_{Na/Ca}$ is unable to overcome the large repolarising potassium currents and the cell repolarises. Ca^{2+} dissociates from myofilaments and undergoes uptake back into the SR via the sarcoendoplasmic reticulum calcium transport ATPase (SERCA), an ATPase pump associated with the SR membrane protein phospholamban (Bers, 2002; de Tombe, 2003; Gordan *et al.*, 2015). Ca^{2+} is also extruded via a Ca^{2+} -ATPase pump at the sarcolemma and via uptake into mitochondria via the mitochondrial Ca^{2+} uniport (Bers, 2002). In doing so the myofilaments relax back to their original Ca^{2+} unbound state.

An inward rectifier potassium channel (see below 'Other Potassium Currents' for description) formed by a tetramer of Kir2.1 pore subunits encoded by *KCNJ2* produces the I_{K1} current (Nerbonne & Kass, 2005). It is constitutively active and non-voltage-gated as per the inward rectifier family (Hibino *et al.*, 2010). It undergoes strong inward rectification (see below 'Other potassium currents') and contributes only a small outward potassium current between membrane potentials of $\sim -70mV$ and $-30mV$, and a larger inward potassium current at membrane potentials more negative to the equilibrium potential of potassium (E_K) $\sim -80mV$ (Nerbonne & Kass, 2005; Hibino *et al.*, 2010). It thus contributes to the end of repolarisation in phase 3 and helps set the resting membrane potential.

Action Potential Phase 4

Inward leak K^+ currents which might represent TASK-1 channels encoded by *KCNK3* cause very slow depolarisation of membrane potential in phase 4 of atrial and ventricular myocytes (Nerbonne & Kass, 2005; Tinker & Harmer, 2010). Otherwise phase 4 is largely quiescent in these cells and the overall permeability to K^+ ions, driven in large part by I_{K1} , sets the resting membrane potential, and where the Na^+/K^+ -ATPase pump ensures a chemical gradient for K^+ ions. The hyperpolarisation-activated cyclic nucleotide-gated cation channel (HCN), encoded by *HCN4*, is expressed at high levels in sinoatrial nodal (SAN) and atrioventricular nodal (AVN) cells, and to a lesser degree in Purkinje fibre cells (Schram *et al.*, 2002; Nerbonne & Kass, 2005; DiFrancesco, 2010). It is a

non-specific cation channel permeable to both sodium and potassium ions and activates at membrane potentials below $\sim -40\text{mV}$ (DiFrancesco, 2010). Owing to its permeability to sodium and potassium its reversal potential is $\sim -10\text{mV}$ and therefore carries inward current I_f where "f" denotes the "funny" current. It is named so given its activation at hyperpolarised membrane potentials, which was in stark difference to other ion channels known at the time of discovery in the late 1970s (DiFrancesco, 2010). The "funny" current is physiologically highest in density in SAN cells and therefore the rate of rise of the depolarisation slope is largest in SAN cells making them the predominant pacemaking cells in the heart (Schram *et al.*, 2002; Lakatta & DiFrancesco, 2009; DiFrancesco, 2010; Park & Fishman, 2011).

Other Potassium Currents

Two other members of the inward rectifier potassium channel family (along with Kir2.1, I_{K1}) contribute to the cardiac action potential, namely the G-protein linked acetylcholine/adenosine activated potassium channel (GIRK), and ATP-sensitive potassium channels (K_{ATP}). Inward rectifier potassium channels are characterised by a tetramer of pore-forming subunit proteins each with two transmembrane-spanning regions and a connecting H5 region homologous to that of the voltage-gated potassium channels that provides the K^+ -selectivity filter (see schematic for K_{ATP} channel Figure 1.10) (Hibino *et al.*, 2010). Inward rectification is provided by a degree of block from the intracellular side of the pore by magnesium ions (Mg^{2+}) and polyamines at membrane potentials more positive to their respective reversal potentials (Hibino *et al.*, 2010). This serves to produce an overall greater inward channel conductance. However, given the channel selectivity for potassium, and that the membrane potential does not deviate grossly negative to E_K , functionally these channels contribute more to repolarisation and membrane hyperpolarisation (Nerbonne & Kass, 2005; Hibino *et al.*, 2010; Tinker & Harmer, 2010). GIRK and Kir2.1 channels show strong inward rectification and K_{ATP} channels weak inward rectification (Hibino *et al.*, 2010). K_{ATP} channels therefore will produce relatively larger outward currents at more positive membrane potentials. Inward rectifier channels are not voltage-gated and are either constitutively open as in Kir2.1 channels, or open

in response to receptor-linked activation (GIRK) or changes in the metabolic environment (K_{ATP}) (Hibino *et al.*, 2010).

GIRK channels in the heart are formed by a tetramer of two Kir3.1 subunits, encoded by *KCNJ3*, and two Kir3.4 subunits, encoded by *KCNJ5*, and are expressed largely in the atria and sinus node (Nerbonne & Kass, 2005; Hibino *et al.*, 2010; Tinker & Harmer, 2010). They are linked to G-inhibitory proteins (G_i) that are activated by M2 muscarinic receptors in the heart in response to the binding of acetylcholine, and A1 adenosine receptors activated by adenosine (Lerman & Belardinelli, 1991; Hibino *et al.*, 2010). When activated, guanosine diphosphate (GDP) bound by the G_i -protein Coupled Receptor α subunit ($G_{\alpha i}$) is released owing to conformational change, and guanosine triphosphate (GTP), present in high concentration binds instead. This causes separation and activation of the two subunits $G_{\alpha i}$ and $G_{\beta\gamma}$ of the G-inhibitory protein (Hibino *et al.*, 2010). The $G_{\beta\gamma}$ subunit then activates a linked potassium channel increasing its open probability (Hibino *et al.*, 2010). Inactivation of G_i is through GTP hydrolysis to GDP. Owing to activation by acetylcholine and adenosine the current has been denoted $I_{KCh,Ado}$.

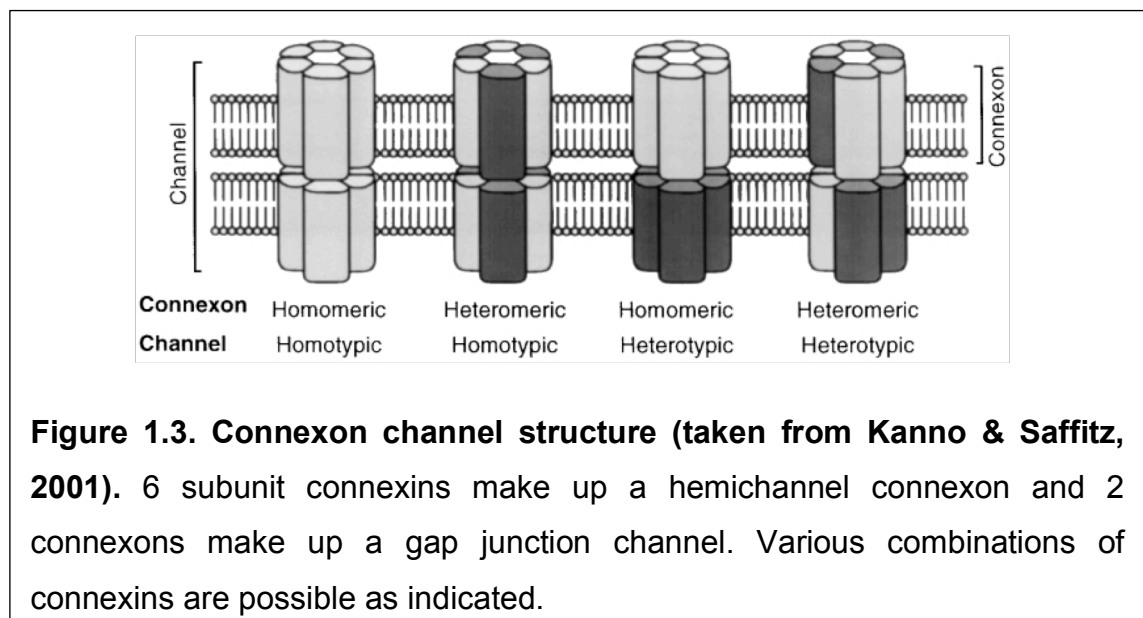
Kir2.1 channels (I_{K1}) have been discussed previously and K_{ATP} channels will be discussed in greater detail in later sections.

1.1.2 Depolarisation Propagation and Gap Junctions

In a normal heart beat the rhythm is initiated in the sinus node located in the roof of the right atrium (RA) between the vena cavae. The depolarisation wave exits into the RA and propagates first through the RA. Propagation then moves to the left atrium (LA) and occurs directly via a collection of parallel fibres known as Bachmann's bundle which traverses from the RA superiorly and posteriorly across the interatrial roof and groove over to the LA and inserts into the lateral wall between the left atrial appendage (LAA) and the orifice of the left upper pulmonary vein (LUPV) (Ariyarajah & Spodick, 2006; van Campenhout *et al.*, 2013). The LAA is the last area of the atria to activate (Durrer *et al.*, 1970; Ramanathan *et al.*, 2006). The depolarisation wave then reaches the AV node that exerts a delay in conduction down through the His-Purkinje system that in

turn depolarises the ventricles. In this manner blood is first pumped from the atria into the ventricles during ventricular diastole and then from ventricles into the arterial circulation during ventricular systole.

For heart rhythm and synchronisation to be under the control of pacemaker tissue, cardiomyocytes need to be coupled to allow propagation of waves of depolarisation through the heart. As cells in one region depolarise, this needs to initiate activation of the next group of cells. Cardiomyocytes are coupled at the intercalated disc by gap junctions that allow the flow of ions from one cell directly to another. This speeds up the propagation of the wave of depolarisation from one cell to another, and from one region to another. Evidence exists that gap junctions co-localise with Nav1.5 channels at the intercalated disc. This facilitates conduction as Na⁺ entry in one cell can then diffuse down its electrochemical gradient into a neighbouring cell thereby activating it (Rohr, 2004). Each cell contributes hemichannels or connexons to the junction and connexons are made up of 6 subunit connexins (Grant, 2009) (see Figure 1.3).



Connexins have 4 transmembrane-spanning regions, cytosolic N- and C-termini and 2 extracellular loops making up the pore (Kanno & Saffitz, 2001).

There are three major types connexin 40 (Cx40), connexin 43 (Cx43) and connexin 45 (Cx45) (Kanno & Saffitz, 2001). They each have different gating mechanisms being sensitive to changes in pH, voltage and Ca^{2+} and each have different unitary conductance (Ahir & Pratten, 2014). Cx43 is the most widely expressed in the heart and is relatively voltage insensitive with a transjunctional voltage gradient of half maximal activation/inactivation ($V_{j1/2}$) of $\sim\pm 60\text{mV}$ and single channel conductance of $\sim 50\text{pS}$ (Kanno & Saffitz, 2001; van Veen *et al.*, 2001). Cx40 is more voltage-sensitive, $V_{j1/2} \sim\pm 50\text{mV}$, and has a larger unitary conductance $\sim 100\text{pS}$ (van Veen *et al.*, 2001; Ahir & Pratten, 2014). Cx45 has a lower unitary conductance $\sim 30\text{pS}$ and is steeply voltage sensitive $V_{j1/2} \sim\pm 20\text{mV}$ (van Veen *et al.*, 2001; Ahir & Pratten, 2014). Connexins contribute to anisotropy whereby conduction is favoured in a certain direction. This can be in part because of preferential voltage-sensitive gating. For example, connexins can form heterotypic channels at cell junctions (eg. a connexon made up of Cx40 followed in series by a connexon made up of Cx43 both embedded either side in the sarcolemma of separate cells). In such heterotypic channels it has been shown that Cx40 gates preferentially with positive polarity and Cx43 with negative polarity (Valiunas *et al.*, 2000; Kanno & Saffitz, 2001). Conduction is facilitated when the Cx40 cell is depolarised and the Cx43 cell not (Valiunas *et al.*, 2000; Kanno & Saffitz, 2001). Physiologically this can facilitate anterograde conduction from Purkinje fibres, with a predominant expression of Cx40, to ventricular myocytes with predominant expression of Cx43, and inhibiting retrograde conduction (Valiunas *et al.*, 2000). Anisotropy also develops in the context of source-sink mismatch. If a smaller mass of excited tissue connects with a larger mass, and connexin expression is high between all the cells in that 3D structure, then crudely, the current load from each tissue mass is distributed evenly to the other. If a depolarisation wave is travelling from smaller to larger tissue mass, the probability that there will be enough current to bring all the cells of the larger tissue mass to threshold will be low and there is likely to be conduction block which would constitute a low safety factor (Rohr, 2004). This is not true for the opposite direction (larger tissue mass to smaller tissue mass). However, if connexin expression in the larger tissue mass is low, then the current load from the smaller tissue mass might be preferentially distributed only to cells in the larger tissue mass coupled by connexins, and there will effectively be more current load per cell. The probability of threshold being reached is

much higher and conduction is more likely to ensue (high safety factor), albeit that conduction velocity might be slow (Rohr, 2004).

1.1.3 Ion Channel / Connexin Expression and Regional Specialisation

Ion channels are differentially expressed throughout heart regions providing different action potential morphologies that serve the function of that particular region. K_{ATP} channels are ubiquitously expressed throughout the body and this goes too for the different regions of the heart. It is suggested though that K_{ATP} subunit expression could itself have cardiac chamber specificity. This will be discussed in greater depth in later sections and K_{ATP} is not included in the following overview.

Sinoatrial Node

The SA node consists of a central chief pacemaking region and towards the periphery a transitional zone where ionic properties gradually become more "atrial-like". The central pacemaking cells have a high density of HCN channels and I_f is large and contributes to the prominent phase 4 depolarisation in these cells. Phase 0 upstroke is relatively slow owing to a lack of fast activating sodium current. There is a high density of Cav3.1, Cav3.2, Cav1.2 and Cav1.3 containing channels reflecting important contributions of the I_{CaT} and I_{CaL} currents respectively to the upstroke of the action potential (Boyett *et al.*, 2000; Mangoni *et al.*, 2003; Park & Fishman, 2011). The delayed rectifier K_V currents are both expressed in the central node but there is a smaller I_{Kr} current relative to the periphery and atria. I_{Ks} is also present (Schram *et al.*, 2002). There is also a small I_{to} current but a lack of I_{K1} . This all translates into a more prolonged action potential duration (APD) in the central node with a more positive maximum diastolic potential (MDP) ~ -50 mV. Kir3.1/3.4 containing channels are also expressed providing modulation by the parasympathetic nervous system (Park & Fishman, 2011). Controversy exists as to the driving mechanisms behind pacemaker activity (Lakatta & DiFrancesco, 2009). Some are proponents that I_f drives diastolic depolarisation in phase 4, and others that there is rhythmic release of Ca^{2+} from RyRs at the SR that causes inward $I_{Na/Ca}$ and depolarisation, a phenomenon known as the "calcium clock" (Park &

Fishman, 2011). The "calcium clock" has been reported to be more important in smaller mammals (Bogdanov *et al.*, 2001; Lakatta & DiFrancesco, 2009). Cav1.3 channels are reported to be the predominant carrier of I_{CaL} in the sinus node and their activation at more negative membrane potentials with faster activation and slower inactivation than Cav1.2 channels supports automaticity (Mangoni *et al.*, 2003; Christel *et al.*, 2012). Cav1.3 channels have also been shown to localise with ryanodine receptors in sarcomeric structures and produce a greater frequency of spontaneous local calcium induced calcium release events from RyRs that increase the frequency of automaticity (Torrente *et al.*, 2016). This frequency is also sensitive to the direct effects of β -adrenergic stimulation on Cav1.3 channels (Torrente *et al.*, 2016). Loss of function mutations affecting Cav1.3 strongly impact on pacemaking function both in the sinus node and the AV node (Mesirca *et al.*, 2015). The I_f current may be more sensitive to parasympathetic inhibition and slowing of heart rate and the "calcium clock" more sensitive to β -adrenergic stimulation and increases in heart rate (DiFrancesco, 2010). In order to maintain a more positive MDP the central node needs to be insulated from the periphery and atria but such that depolarisation can still propagate to the atria. This is served by SAN anatomy and connexin expression. The central node has a low expression of small conductance Cx45 containing connexons and a lack of Cx40/Cx43. At the periphery the expression of Cx45 increases along with Cx40 and Cx43 and atrial fibres extend into the node with finger-like projections minimising connecting surface area (Coppen *et al.*, 1999; Verheijck *et al.*, 2001). In this manner source-sink mismatch is reduced and the smaller tissue mass of the sinus node is able to conduct and propagate into a smaller proximal mass of atrial fibres. As connexin expression then increases the increasing activated atrial mass is able to depolarise with high conduction velocity. Similarly, due to low conductance, the more central regions are shielded from the hyperpolarising effects of the atria (Joyner & van Capelle, 1986; Coppen *et al.*, 1999; Verheijck *et al.*, 2001). There is a significant degree of connective tissue between the central node and crista terminalis which also minimises the surface area of SAN in contact with the atria (Coppen *et al.*, 1999). Heterotypic connexons containing Cx43/Cx45 might exist at the periphery connecting nodal and atrial cells and such connexons could have rectifying properties (White *et al.*, 1994). If inserted into the membrane in the correct orientation they would

facilitate current to flow from SAN to atria and not in a retrograde fashion that also helps to insulate the SAN from the hyperpolarising effects of the atria (Verheijck *et al.*, 2001). Expression of Nav1.5 channels increases towards the SAN periphery, which also aids to overcome source-sink mismatch with the larger mass of the atria (Unudurthi *et al.*, 2014).

Atria

Atrial cells show much lower expression of I_f current and have little or no phase 4 depolarisation (Porciatti *et al.*, 1997; Schram *et al.*, 2002). They exhibit a large I_{Na} current and have a fast upstroke translating to rapid tissue conduction (Sakakibara *et al.*, 1992). T-type calcium current is present to a higher degree in atria than ventricle and Cav1.2 channels are also abundant (Schram *et al.*, 2002). The I_{K1} current is smaller in the atria than ventricle leading to a more positive MDP ~ -70 mV than ventricle (Li *et al.*, 2001). The I_{Kr} current is larger in LA than RA leading to shorter APD and shorter effective refractory period (ERP) in the LA (Li *et al.*, 2001). The I_{Kur} current appears to be atrial specific (Ravens & Wettwer, 2011). There is a much larger inducible $I_{KACh,Ado}$ current in the atria than the ventricle (Schram *et al.*, 2002; Tinker & Harmer, 2010). An $I_{to,f}$ current exists likely of the Kv4.3 molecular correlate (Wang *et al.*, 1999). There appear to be no differences between RA and LA for the I_{Kur} , I_{to} or I_{K1} densities (Schram *et al.*, 2002). Evidence exists suggesting that I_{KACh} density is greater in the LA compared to the RA (Sarmast *et al.*, 2003). Cx43 is the major atrial connexin though close to the SAN there is co-expression with Cx40 (Vozzi *et al.*, 1999; Schram *et al.*, 2002).

Atrioventricular Node

The AVN, like the SAN, has distinct regions of cellular function. Rod-shaped cells predominate at the junction of the atria and node that have ionic mechanisms more akin to atrial cells. Ovoid-shaped cells are present towards the compact central AVN and towards the His bundle (Munk *et al.*, 1996; Schram *et al.*, 2002). Ovoid cells express a significant I_f current providing their automatic pacemaker capability but no I_{Na} and the action potential upstroke is provided by I_{CaT} and I_{CaL} though I_{CaL} predominates (Hancox & Mitcheson, 1997).

Similar to SAN cells there is a small I_{to} current, however, repolarisation is reliant on I_{Kr} with little or no I_{Ks} and thus APD is longer than in the SAN (Schram *et al.*, 2002). AVN cells exhibit post-repolarisation refractoriness (Munk *et al.*, 1996) most likely secondary to reliance on I_{CaL} for the upstroke with its slower activation, longer recovery time and more positive activation voltage to that of I_{Na} . The MDP is also more positive than the atria and ventricle ~ -60 mV, owing to a lack of I_{K1} (Hancox & Mitcheson, 1997). I_{KACh} is present and enables modulation by the parasympathetic nervous system (Harvey & Belevych, 2003). Like the SAN the predominant gap junction protein is Cx45 and conduction is slow in the AVN compared to non-nodal tissues (Schram *et al.*, 2002).

His-Purkinje System

These cells exhibit a fast upstroke owing to Nav1.5, Cav3.1 and Cav3.2 channel expression (Schram *et al.*, 2002; Nerbonne & Kass, 2005). The plateau phase is less depolarised than in ventricular cells owing to less I_{CaL} current (Tseng & Boyden, 1989; Schram *et al.*, 2002). The action potential is longer than in ventricular muscle that might be explained by reduced expression of delayed rectifier potassium channel mRNA, though I_{Kr} and I_{Ks} are detectable (Schram *et al.*, 2002). APD might also be prolonged due to a smaller $I_{to,f}$ current and a larger I_{NaL} than in ventricular myocytes but the presence of I_{to} still gives rise to a "spike and dome" morphology of the action potential (Carmeliet, 1987; Schram *et al.*, 2002; Niwa & Nerbonne, 2010). I_{K1} is present and governs a negative MDP of ~ -80 mV akin to ventricular myocytes but there is also a low expression of HCN4 and I_f current that enables phase 4 diastolic depolarisation and automaticity (Kus & Sasyniuk, 1975; Schram *et al.*, 2002; Nerbonne & Kass, 2005). I_{KACh} is also expressed albeit to a much lesser degree than the nodal and atrial tissues (Nerbonne & Kass, 2005). The His-Purkinje system appears to contain abundant amounts of all three connexins and this contributes to the rapid conduction of these tissues (Davis *et al.*, 1995).

Ventricle

Ventricular cardiomyocytes have little or no phase 4 depolarisation owing to very low expression of an I_f current (Hoppe *et al.*, 1998; DiFrancesco, 2010).

The MDP is ~ -85 to -90 mV secondary to a large I_{K1} current and this also renders any residual I_f expression defunct (Davis & Temte, 1969; Wettwer *et al.*, 1994; Konarzewska *et al.*, 1995; DiFrancesco, 2010). The upstroke is fast secondary to a large I_{Na} (Fozzard, 2002; Nerbonne & Kass, 2005; Rook *et al.*, 2012). The plateau phase is driven largely by L-type calcium current and late persistent sodium current I_{NaL} as previously described for the typical phase 2 of the action potential. Repolarisation is governed by I_{to} and I_{K1} , and to a lesser extent by I_{Kr} and I_{Ks} (Wettwer *et al.*, 1994; Konarzewska *et al.*, 1995; Nerbonne & Guo, 2002). As will be described in later sections I_{KATP} also contributes significantly to repolarisation during ischaemia. The predominant connexon in the ventricle is Cx43 (Vozzi *et al.*, 1999; Schram *et al.*, 2002).

In the ventricle, transmural and regional heterogeneity in expression and function of these currents determines variations in action potential duration and repolarisation times and it is heterogeneity of repolarisation that is mechanistically important in arrhythmogenesis. Increased heterogeneity of repolarisation makes re-entry and/or fibrillatory conduction more likely. A large body of evidence from canine wedge preparations suggests the presence of 3 layers of cell types endocardial, midmyocardial (M-cell) and epicardial (Antzelevitch *et al.*, 1991). M-cells appear to have longer action potentials than endocardial myocytes, which in turn have longer action potentials than epicardial myocytes. This is thought to arise due to a lower expression of I_{Ks} , a larger I_{NaL} and larger $I_{Na/Ca}$ current in M-cells as compared to epicardial or endocardial myocytes (Viswanathan *et al.*, 1999; Zygmunt *et al.*, 2001; Nerbonne & Guo, 2002). Epicardial myocytes and M-cells have a larger I_{to} current than endocardial myocytes with a particularly large $I_{to,f}$ in epicardial cells contributing to a shorter action potential than M-cells and endocardial myocytes (Antzelevitch *et al.*, 1991). Expression of I_{to} is contingent on expression of both the pore-forming subunit and the β -subunit KChIP2 and evidence suggests it is varied transmural expression of KChIP2 that governs differences in transmural current density of I_{to} (Nerbonne & Guo, 2002). Given the kinetics of recovery from inactivation are faster for $I_{to,f}$ and M-cells appear to have a greater $I_{to,s}$ density, M-cells have a steep slope of restitution of action potential duration, epicardial myocytes less steep and endocardial myocytes a lesser rate-dependence of action potential duration still. With longer diastolic intervals there

is greater I_{to} recovery between beats. This may then seem paradoxical but the existing theory is that as less I_{Ks} is recruited at slower rates, the greater degree of notch produced in phase 1 actually slows the activation of I_{Kr} and I_{CaL} which in turn prolongs the action potential phases 2 and 3. At shorter diastolic intervals I_{Ks} is recruited and less I_{to} recovers between beats, especially $I_{to,s}$, leading to restitution and shortening of action potential duration (Antzelevitch *et al.*, 1991; Viswanathan *et al.*, 1999). On top of transmural heterogeneity in action potential duration (APD), evidence across species suggests that in general, APD is shorter in the right ventricle (RV) than the left ventricle (LV) largely owing to greater expression of I_{to} and I_{Ks} (Molina *et al.*, 2016). In canine hearts evidence suggests greater expression of these two currents at the apex compared to the base in both current measured from isolated cells and protein quantification via western blot (Szentadrassy *et al.*, 2005). Results of protein study for human heart were similar (Szentadrassy *et al.*, 2005). This would suggest shorter APD at the apex compared to the base. In the dog this then follows that the sequence of repolarisation crudely follows that of activation (ie. anterior septum through apex and free wall and up to base) and would explain discordant T wave polarity to that of the QRS complex on the surface ECG. In human, however, there is concordance between T wave polarity and that of the QRS. Given local repolarisation time is contingent on the activation time together with the action potential duration, evidence exists that T wave/QRS concordance exists in humans due to an inverse relationship between activation time and repolarisation time and that repolarisation proceeds from base to apex (Opthof *et al.*, 2009; Janse *et al.*, 2012). *In silico* modelling suggests that all three of transmural, apico-basal and interventricular gradients of repolarisation are involved in the inscription of the T wave on the ECG (Zheng *et al.*, 2016). Above all these gradients of repolarisation and the heterogeneity of action potential duration are critical in arrhythmogenesis and increased heterogeneity in disease states makes tissue more arrhythmogenic. Mapping and targeting of susceptible areas of tissue is important for therapeutic aim both by surgical/catheter-based and pharmacological means, and further delineation of species specific gradients of ion channel expression in health and disease will aid the search for new therapeutic approaches.

1.1.4 Autonomic and G-protein Linked Regulation

Fine-tuning of the underlying properties of action potential generation, propagation and excitation-contraction coupling are afforded by a balance of the effects of the sympathetic and parasympathetic nervous systems. Both circulating adrenaline and noradrenaline released from penetrating post-ganglionic sympathetic nerve fibres, are responsible for activating β -adrenergic G_s -protein coupled receptors (stimulatory G-proteins) throughout the myocardium and conduction system (Salazar *et al.*, 2007; Gordan *et al.*, 2015) (see Figure 1.4).

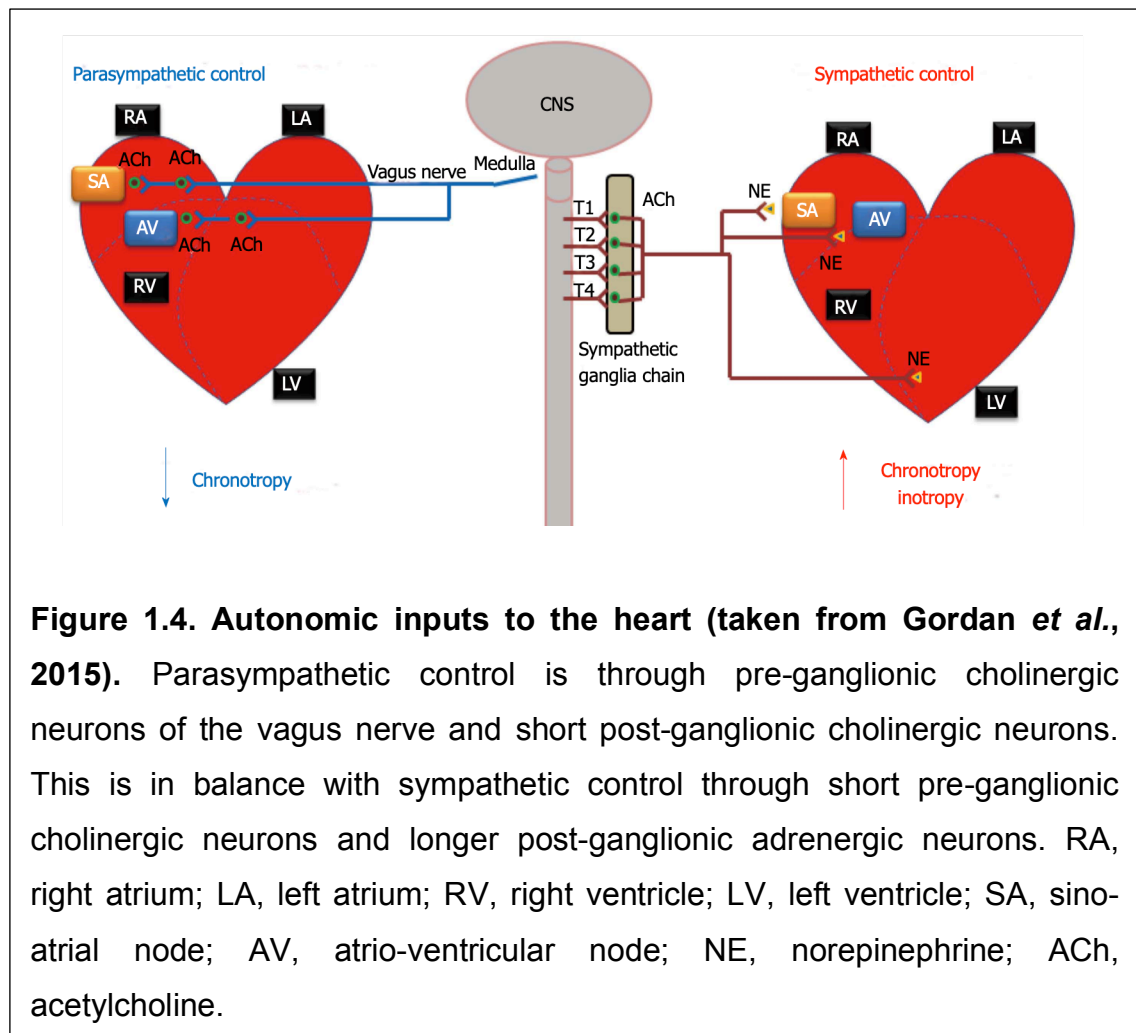


Figure 1.4. Autonomic inputs to the heart (taken from Gordan *et al.*, 2015). Parasympathetic control is through pre-ganglionic cholinergic neurons of the vagus nerve and short post-ganglionic cholinergic neurons. This is in balance with sympathetic control through short pre-ganglionic cholinergic neurons and longer post-ganglionic adrenergic neurons. RA, right atrium; LA, left atrium; RV, right ventricle; LV, left ventricle; SA, sinoatrial node; AV, atrio-ventricular node; NE, norepinephrine; ACh, acetylcholine.

On activation by receptor-ligand binding, the heterotrimeric G-protein complex separates through exchange of GDP to GTP releasing the $G_{\alpha s}$ subunit (Lymeropoulos *et al.*, 2013) (see Figure 1.5).

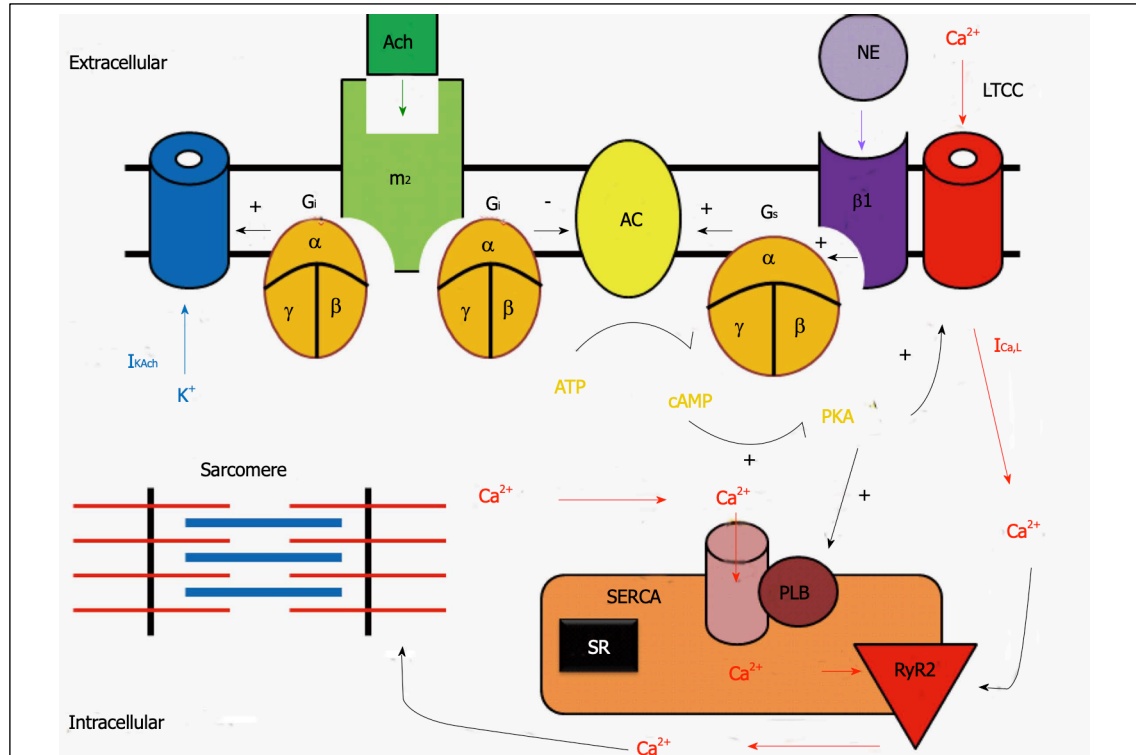


Figure 1.5. Autonomic regulation of cardiomyocytes (taken from Gordan *et al.*, 2015). Acetylcholine from parasympathetic post-ganglionic neurons activates at muscarinic M2 receptors through inhibitory G-protein leading to reduced cAMP production and an increase in outward potassium currents linked to these G-proteins. Noradrenaline from sympathetic post-ganglionic neurons has the opposite effect through activation of β_1 receptors and stimulatory G-protein leading to increased cAMP production. cAMP leads to protein kinase A activation and phosphorylation of various downstream targets including the inward calcium current and phospholamban leading to increased sarcoplasmic calcium uptake and release. NE, norepinephrine; β_1 , beta1-adrenergic receptor; G_s , stimulatory G-protein; Ach, acetylcholine; M2, muscarinic receptor type 2; G_i , inhibitory G-protein; AC, adenylate cyclase; PKA, protein kinase A; $I_{Ca,L}$, L-type calcium channel; RyR2, ryanodine receptor 2; SERCA, sarcoplasmic reticulum Ca^{2+} -ATPase2a; PLB, phospholamban.

This activates adenylate cyclase converting ATP to cyclic AMP (cAMP), which in turn activates Protein Kinase A (PKA) (Lympelopoulou *et al.*, 2013). Through phosphorylation by PKA of T-type and L-type calcium channels there is increased inward calcium that leads to a positive inotropic effect. In SAN tissue this leads to increased calcium uptake into the SR that in turn leads to an increased likelihood, and therefore rate of, calcium release and forward mode $I_{Na/Ca}$ current leading to increased automaticity (Lakatta & DiFrancesco, 2009). PKA signalling also positively modulates ryanodine receptor (RyR) calcium release increasing automaticity (Vinogradova *et al.*, 2002). This is coupled to a direct positive effect of cAMP on the I_f current shifting the open state to more depolarised potentials and thus shortening the cycle length of automaticity in the SAN (DiFrancesco & Tortora, 1991). PKA phosphorylation of phospholamban and Troponin I induces a positive lusitropic effect by way of enhanced release of calcium from myofilaments and increased re-uptake into the SR through release of phospholamban-inhibition of SERCA (Bers, 2002). This in turn enhances SR calcium content leading to a positive inotropic effect. PKA phosphorylation increases I_{Ks} current leading to accelerated repolarisation to counter the action potential prolonging effects of an increased inward calcium current and allow for higher heart rates (Volders *et al.*, 2003). There is also a positive dromotropic effect that may be due to an increased gap junction conductance particularly with respect to Cx40 and Cx45 in nodal tissue, and also an increased I_{Na} expression and conductance (Abriel, 2007; Salameh & Dhein, 2011; Rook *et al.*, 2012). β -adrenergic modulation occurs throughout the myocardium and conduction system.

Acetylcholine release at post-ganglionic parasympathetic nerve fibres and the effects of adenosine lead to opening of inhibitory G-protein (G_i) linked potassium channels (GIRK) and an increased outward potassium current as previously described (see also Figure 1.5). $I_{K_{ACh,Ado}}$ is a hyperpolarising current opposing the effects of I_f and slowing automaticity in nodal tissue, and also reduces calcium load and automaticity through the "calcium clock" (Brodde & Michel, 1999). The G_{oi} subunit released on activation also reduces adenylate cyclase activity having an inhibitory effect on PKA activation. GIRK channels and parasympathetic innervation is abundant in sinoatrial tissue but not so in the ventricle (Brodde & Michel, 1999).

The endothelin-1 receptor ET_A, angiotensin II receptor AT-1, adrenergic α₁ receptor and muscarinic acetylcholine receptor M3 are all coupled to G_q-proteins. Activation leads to heterotrimeric separation of the G_{αq} subunit via exchange of GDP for GTP, which in turn activates phospholipase C leading to generation of diacylglycerol (DAG) and inositol-1,4,5-triphosphate (IP₃) from phosphatidylinositol-4,5-bisphosphate (PIP₂) (Tinker *et al.*, 2016). IP₃ release leads to sustained calcium release from the SR. Whilst this calcium release might initially be positively inotropic, it also enables calcium-dependent DAG activation of protein kinase C (PKC) groups through which phosphorylation pathways mediate myocardial apoptosis, necrosis and hypertrophy pathways (Salazar *et al.*, 2007). PKC signalling pathways also activate protein phosphatase-1 (PP-1), which dephosphorylates phospholamban causing inhibition of SERCA, reduced SR calcium uptake and an ensuing negative inotropic effect (Braz *et al.*, 2004). IP₃ itself also has a nuclear envelope receptor, which is involved with nuclear calcium signalling and coupled gene expression through a calcineurin pathway leading to hypertrophy (Salazar *et al.*, 2007; Nakayama *et al.*, 2010). As such the neurohumoral stress agonists mentioned above, through the IP₃ / DAG pathway linked to G_q-protein-coupled receptors, play an important role in the pathophysiology and tissue remodelling in heart failure.

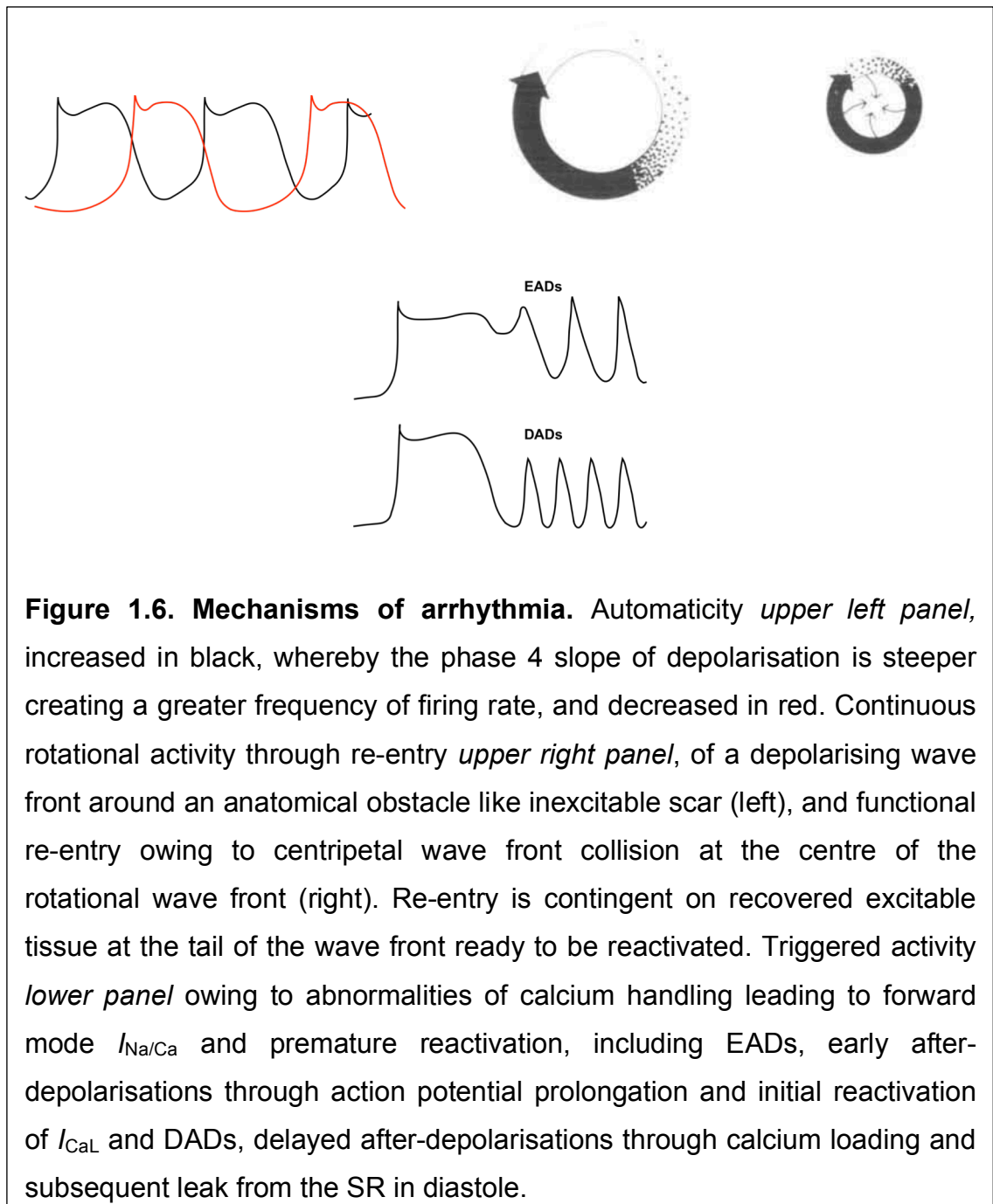
1.2 Atrial Fibrillation

1.2.1 Definition and Proposed Mechanisms

Atrial Fibrillation (AF) is the most common sustained arrhythmia (Lip & Tse, 2007). It has an estimated prevalence in the developed world of 1.5-2% of the general population, and is associated with a five-fold risk of stroke and a three-fold incidence of congestive heart failure, and higher mortality (Camm *et al.*, 2012). The current European Society of Cardiology (ESC) guidelines for the management of AF, declare that "...this arrhythmia remains one of the major causes of stroke, heart failure, sudden death, and cardiovascular morbidity in the world. Furthermore, the number of patients with AF is predicted to rise steeply in the coming years" (Kirchhof *et al.*, 2016).

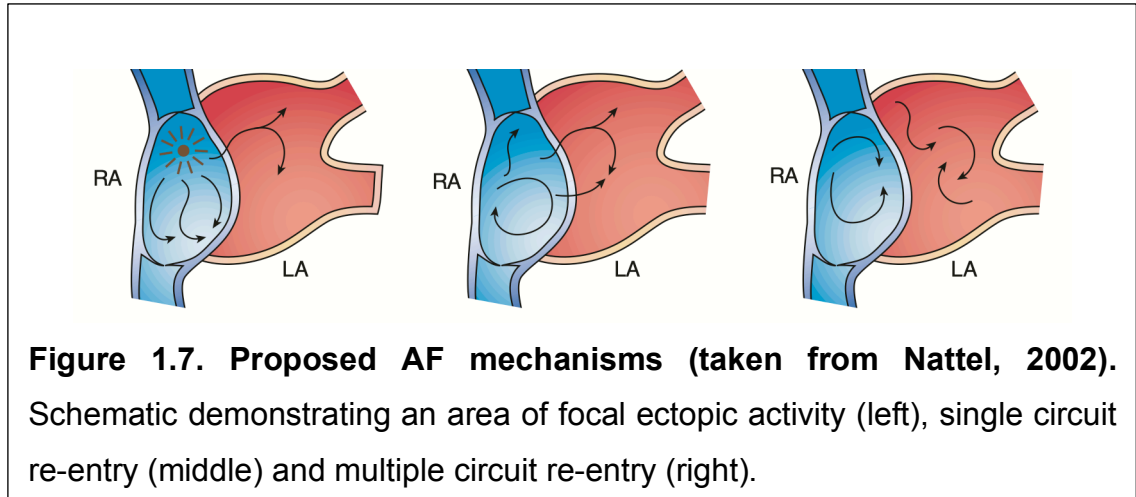
Fibrillation is defined by rapid, disorganised and chaotic activation of excitable tissue. The random chaotic impulses propagating through the atria activate the AV node in a random pattern thus causing a completely irregularly irregular depolarisation of the ventricles. Where the AV node functions well it can conduct these random impulses at high rates and thus the ventricular rate can be very rapid causing symptoms of palpitations, light-headedness and breathlessness. Atrial systole is effectively lost and the absence of active atrial transport of blood to the ventricles during ventricular diastole can worsen heart function, contributing to symptoms, and can cause heart failure. The increased residual volume in the atria leads to volume overload and increased atrial pressure, which in turn can promote the pathophysiological changes that cause perpetuation of the arrhythmia. A prothrombotic state is produced by an inflammatory response to the increased atrial stretch and fibrosis caused by volume overload, and by the stasis of blood that ensues in the atria whilst they are fibrillating (Kirchhof *et al.*, 2016). This is particularly apparent in the left atrial appendage where the velocity of blood can be very low. Clot can then embolise causing various sequelae including devastating stroke, ischaemic gut and limbs. As such the arrhythmia can cause a large degree of morbidity and associated mortality.

All arrhythmogenic mechanisms of automaticity, triggered and re-entry (see Figure 1.6) have been implicated in AF whether with regards the initiation or perseveration of the arrhythmia. Atrial ionic remodelling appears to ensue whereby prolonged bouts serve to further potentiate the arrhythmia (Hobbs *et al.*, 1999; Nattel, 2002).



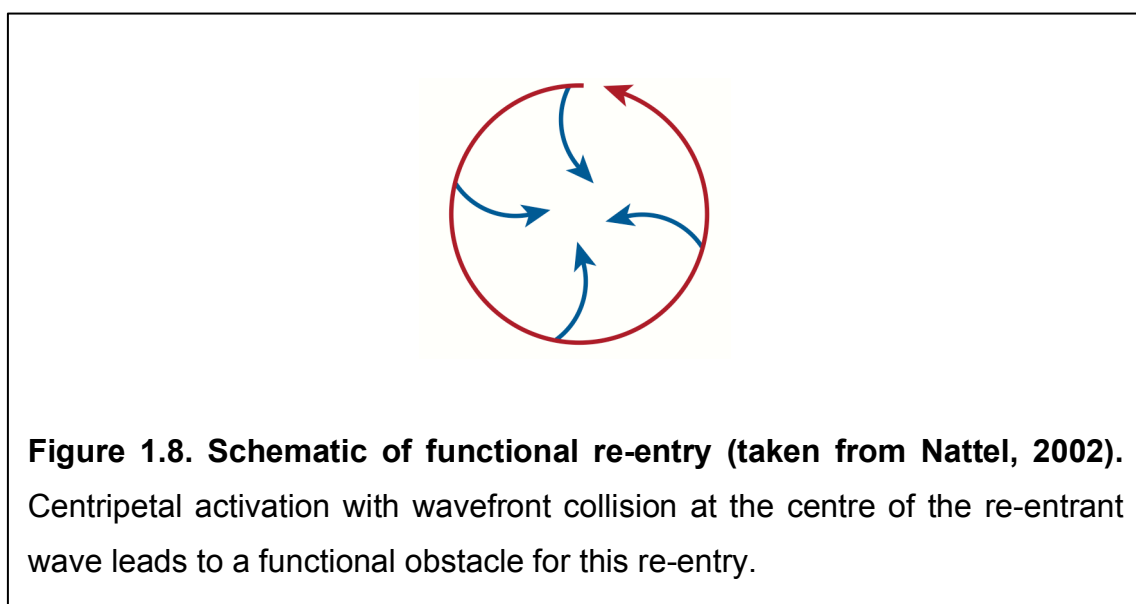
Classical postulated mechanisms of AF involve rapidly firing ectopic foci (particularly in the pulmonary veins, superior vena cava and ligament of marshall), single circuit re-entry and multiple circuit re-entry (Moe *et al.*, 1964;

Allessie *et al.*, 1977; 1985; Haïssaguerre *et al.*, 1998; Doshi *et al.*, 1999; Tsai *et al.*, 2000) (see Figure 1.7). It remains to be confirmed whether AF drivers are due in part to automatic, triggered or re-entrant foci and all mechanisms may be in play (Schotten *et al.*, 2011).



Classical Re-entry

The work of Allessie and colleagues promoted the concept of the leading circle theory, re-entry around a functional rather than anatomical obstacle, and that of the minimum wavefront path length (WFPL) to sustain a re-entrant arrhythmia as a product of the effective refractory period (ERP) and the conduction velocity (CV) in the tissue (see Figure 1.8).



The shorter this path length, the more likely a re-entrant wave to set up in a tissue of given mass, and the more likely for multiple re-entrant circuits. This idea underpins one proposed mechanism of anti-arrhythmic drug action. That their effects on ERP and CV combine to a product of a longer minimum WFPL, that reduces the likelihood of single or multiple re-entrant waves (Wang *et al.*, 1990; 1994; 1995).

Atrial electrophysiology remodels as a consequence of chronic AF with changes in ion channel expression and/or regulation and gating. The inward calcium current I_{Ca} is reduced in density (Workman *et al.*, 2008; Heijman *et al.*, 2014) and this corresponds with a shorter action potential duration and loss of rate adaptation of APD (Van Wagoner *et al.*, 1999). Potassium channel functional remodelling also occurs. For example, Kir2.1 expression, basal I_{K1} density and open probability is higher in right atrial appendage myocytes from patients with chronic AF compared to those in sinus rhythm (Dobrev *et al.*, 2005). I_{KACH} appears to be constitutively active when investigated in the same myocytes in an agonist-independent manner with a greater open probability and this is thought to be driven by abnormalities in protein kinase C (PKC) channel phosphorylation (Dobrev *et al.*, 2005). On the other hand transient outward and ultra-rapid delayed-rectifier potassium current densities appear to be reduced (Workman *et al.*, 2008; Heijman *et al.*, 2014). Cholinergic activation of I_{KACH} at times of high vagal tone, and reductions in APD particularly in the left atrium, has been implicated as a mechanistic step to the initiation of AF by ectopic foci (Wakimoto *et al.*, 2001; Kneller *et al.*, 2002; Sarmast *et al.*, 2003). The proposed overall effect is a reduction in APD that translates to a shorter effective refractory period that contributes to perseveration and increased burden of arrhythmia.

Gap junction expression and distribution is also affected by chronic AF with an enhanced Cx40 expression and a shift of distribution to the lateral membrane from the polar membrane of both Cx43 and Cx40 in atrial cardiomyocytes (Polontchouk *et al.*, 2001). This is associated with a functional reduction in the physiological anisotropy of the atrial tissue promoting conduction perpendicular to the fibre axis as well as in parallel (Polontchouk *et al.*, 2001). This reduction in anisotropy promotes re-entry due to multiple directions of impulse

propagation and for the fact that there is an increase in source-sink mismatch for depolarising current being distributed to a greater number of adjacent cells. This reduces conduction velocity and shortens the minimum wavefront path length.

The myocardial sleeve extensions into the pulmonary veins from the left atrium show histological features of fibrosis, akin to that produced by ischaemia, and slow conduction would lend itself as a fertile substrate for re-entry (Saito *et al.*, 2000; Ho *et al.*, 2001). Stable micro-reentry has been shown within the pulmonary veins particularly under the influence of acetylcholine (Po *et al.*, 2005).

Automaticity and Triggered Activity

Ectopy arising from areas such as the pulmonary veins, superior vena cava and ligament of Marshall, can initiate the arrhythmia and there is a body of evidence to suggest that automaticity, triggered activity and micro-reentrant circuits could all be responsible for ectopy arising from these sites (Schotten *et al.*, 2011). Pulmonary vein myocytes at the LA-PV junction have been seen to have a morphology akin to nodal cells, exhibit a current resembling I_f , and in patients with AF, gene expression at the LA-PV junction favours a nodal phenotype that would lend itself to automatic activity (Schotten *et al.*, 2011; Yeh *et al.*, 2013).

Delayed after-depolarisations (DADs) are caused by leak of calcium either from an overloaded SR or leaky RyRs. The calcium sparks cause forward mode $I_{Na/Ca}$ current leading to depolarisations that, if propagate to surrounding tissue, can initiate ectopic activity. In atrial cardiomyocytes from both patients with paroxysmal and chronic AF there appears to be a greater diastolic calcium leak and incidence of triggered activity via DADs because of increased SERCA uptake in the former, and increased RyR and $I_{Na/Ca}$ activity in the latter (Voigt *et al.*, 2012; 2014).

Early after-depolarisations (EADs) occur classically with action potential prolongation whereby a prolonged phase 2 leads to activation of an inward calcium window current and subsequent forward mode $I_{Na/Ca}$ leading to a new

upstroke and action potential in phase 2 (Antzelevitch & Burashnikov, 2011). Late phase 3 EADs occur when there is a combined sympathovagal tone causing both calcium loading and action potential shortening respectively. This leads to strong calcium release from the SR that persists long into phase 3 of the action potential by which time the membrane potential is repolarised enough beyond the equilibrium potential of $I_{Na/Ca}$ to allow forward mode current and lead to a new action potential (Burashnikov & Antzelevitch, 2006). Late phase 3 EADs are suggested to play a role in immediate recurrences of AF (Burashnikov & Antzelevitch, 2003).

Whilst vagotonically induced AF is commonly explained by APD shortening due to increased $I_{K_{ACh}}$, acetylcholine also activates muscarinic M3 receptors and the G_q linked IP_3 / DAG pathway as previously discussed and IP_3 release causes sustained SR calcium release that could induce after-depolarisations and triggered activity (Tinker *et al.*, 2016).

Spiral Wave Theory

A developing hypothesis for rotational wavefront generation are spiral waves or rotors with a constantly excitable core, termed a phase singularity owing to this core displaying no definable cyclical presence of activity and where all other markers of the spatiotemporal phase of the rotor converge (Beaumont *et al.*, 1998; Pandit & Jalife, 2013). Aspects of spiral wave theory lend themselves to explaining why anti-arrhythmic drugs that block sodium (Na^+) channels, reducing excitability and slowing conduction, but not necessarily increasing minimum wavefront path length, can terminate AF (Wijffels *et al.*, 2000; Kawase *et al.*, 2003). Evidence has shown reducing excitability through Na^+ channel blockade, can enlarge the excitable core of rotors through "source-sink" mismatch and increase the radius of rotation (Wijffels *et al.*, 2000; Cosío & Delpón, 2002; Kawase *et al.*, 2003). Enlarging the excitable gap at the centre of these rotors increases the chance of fusion of wavefronts and extinguishing the rotor (Wijffels *et al.*, 2000; Nattel, 2002; Cosío & Delpón, 2002; Kawase *et al.*, 2003) (see Figure 1.9).

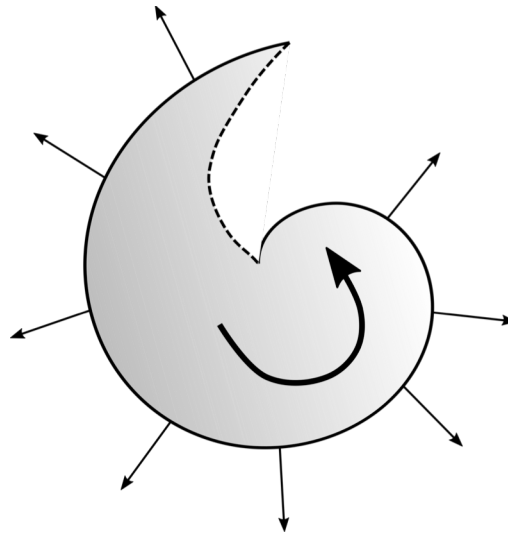


Figure 1.9. Spiral waves. Schematic demonstrating propagation outwards from a spiral wave. Where tissue has low excitability, the central core will be enlarged and the radius of arc of activation larger.

1.2.2 Management and Therapies

Reducing the risk of stroke in the context of AF is enabled by the use of anti-coagulation strategies using drugs such as warfarin or the novel oral anticoagulants. At present, reducing the morbidity associated with the arrhythmia is mainly via the use of anti-arrhythmic drugs and/or catheter ablation.

Anti-arrhythmic drugs

The classical mechanism of action of anti-arrhythmic drugs is via prolongation of the action potential duration and effective refractory period to reduce the likelihood of sustained re-entry by prolonging the wavefront path length. Potassium channel blockade prolongs phase 3 of the action potential.

Class Ia and Ic sodium channel blockers reduce the maximum upstroke velocity of phase 0 of the action potential (V_{max}) due to slow offset kinetics. This in turn slows conduction velocity and excitability of the tissue (Osadchii, 2017). This might be seen as paradoxical as the WFPL would be shortened and might

promote re-entrant arrhythmias and indeed in some instances, particularly ischaemic hearts and those with high scar burden from previous infarct, this is the case as was demonstrated in the CAST study (Echt *et al.*, 1991). However, most are not pure sodium channel blockers and have some potassium channel blocking effects on I_{to} and hERG also prolonging phase 3 and APD (Wang *et al.*, 1990; 1995; Melgari *et al.*, 2015). Sodium channel blockers also cause post-repolarisation refractoriness due to delaying recovery from inactivation of the sodium channel and this in turn prolongs the ERP (Coronel *et al.*, 2012; Osadchii, 2017). Sodium channel blockade causing reduction of tissue excitability and AF termination is in support of spiral waves as a mechanism of AF given the angle of curvature at the centre of a spiral wave is contingent on tissue excitability. With reduced excitability the angle of curvature that can be maintained is less acute. The more acute the angle of curvature of the rotor, the greater the volume of tissue directly in front of the curving wavefront, and the greater the sink of tissue that must be activated by the rotor wavefront. It follows that greater tissue excitability is required for greater curvature (Pandit & Jalife, 2013). Sodium channel blockade, thus, reduces the acuteness of the angle of curvature of the rotor and in turn increases the rotor wavefront path length, and also increases the excitable gap at the centre of the rotor. All this makes wavefront collision and rotor extinction more likely.

Beta-blockers serve to block sympathetically driven recruitment of potassium currents such as I_{Ks} thus prolonging APD and also reduce inward calcium reducing the SR calcium load and probability of triggered and automatic activity (Chen *et al.*, 1999; Kühlkamp *et al.*, 2000).

In a meta-analysis of randomised controlled trials comparing anti-arrhythmics vs. placebo or no treatment after cardioversion, sodium channel blockers (disopyramide, quinidine, flecainide and propafenone), pure potassium channel blockade (dofetilide), potassium channel blockade plus beta-blockade class 3 (sotalol), or mixed ion channel blockade plus anti-sympathetic effects class 3 (amiodarone, dronedarone) significantly reduced the recurrence rate of AF at 1 year (OR 0.19 to 0.7) (Lafuente-Lafuente *et al.*, 2015). However, given the recurrence rate in the control arms was as high as 84% at 1 year, most would agree this is only a modest practical reduction, and side effects were frequent in

all groups. This is also in the context that all but amiodarone and propafenone were associated with pro-arrhythmia. Amiodarone and standard beta-blockers (eg. bisoprolol, metoprolol succinate) are the only anti-arrhythmics with an adequate safety profile to use in those with depressed LV function, though success rates at rhythm control with standard beta-blockers are limited (OR 0.62), and amiodarone in particular is associated with side effects, most notably abnormal liver and thyroid function, pulmonary fibrosis and corneal deposits (Camm *et al.*, 2010; Lafuente-Lafuente *et al.*, 2015). All Class I and III anti-arrhythmics are prone to prolonging the QT interval and predisposing to Torsades de Points (TdP) (Camm *et al.*, 2010). Thus, there is a desire to develop new anti-arrhythmics with higher specificity for the atria compared to the ventricle, or those that have desirable effects in the atria with the same or neutral effects in the ventricle.

Catheter ablation

Catheter ablation for AF has developed significantly as a treatment strategy over the past 15 years. The empirical strategy is to produce lines of block around the pulmonary vein (PV) ostia (pulmonary vein isolation; PVI) to prevent ectopic firing from the PVs into the left atrium (Haïssaguerre *et al.*, 1998). The PVs appear to have a tissue architecture distinct from the LA with myocardial sleeve projections from the LA inter-digitating with fibrotic areas with slow conduction providing a substrate for re-entry (Nattel, 2003; Chard & Tabrizchi, 2009). This is coupled with the fact that PV myocytes have been shown to have a shorter APD than the LA owing to a smaller I_{Ca} and larger delayed rectifier potassium currents (Nattel, 2003). PV myocytes also appear to have a phenotype displaying automatic behaviour and a propensity to triggered activity through differences in calcium handling where SR loading capability is less and open to leak (Chard & Tabrizchi, 2009). Postganglionic autonomic nerve fibres, particularly cholinergic, also richly innervate the PVs that might cause autonomically driven pro-arrhythmic effects as previously described in section 1.1.4 (Chard & Tabrizchi, 2009).

Success rates from PVI for an AF-free 1 year period can be as high as ~90% in skilled hands and taking into account the need for multiple procedures (Jaïs *et*

al., 2008). It appears to be a successful treatment modality in most patients with paroxysmal AF. One recent large randomised controlled trial has now also demonstrated a survival/hospitalisation benefit at 1.5 years in patients with persistent or paroxysmal AF. This was in the context of severely impaired LV systolic dysfunction with an implantable cardioverter defibrillator (ICD), who were largely intolerant of anti-arrhythmic drugs, undergoing pulmonary vein isolation as compared to medical therapy (ventricular rate control or pursued attempts at chemical rhythm control) (Marrouche *et al.*, 2018). The primary outcome measure correlated with better maintenance of sinus rhythm.

Nevertheless catheter ablation is not without risk of major complication. In one survey reporting the outcome of more than 1000 AF ablation procedures, acute severe complication rates were 0.6% for stroke, 1.3% for tamponade, 1.3% for peripheral vascular complications and 2% for pericarditis (Arbelo *et al.*, 2012; Camm *et al.*, 2012). These data were from high volume centres with experienced operators and thus rates are likely to be higher globally.

Most studies thus far have been in those with no or minimal structural heart disease and success rates are not as high in those with persistent AF where episodes last greater than 7 days. Where persistent AF has developed, this may derive from a completely different mechanism to the paroxysmal form, or this mechanism may even be a progression based on remodelling of the atria to frequent paroxysms (Hobbs *et al.*, 1999; Camm *et al.*, 2010). Current proposed mechanistic approaches suggest areas of slow conduction in the LA body due to fibrosis that promote re-entry, but attempts to improve outcomes beyond those with PVI alone, by targeting complex fractionated electrograms thought to be emanating from areas of scar in persistent AF have been met with mixed results (Verma *et al.*, 2010; 2015).

Similarly attempts to use software capable of defining rotor activity through mapping phase singularities at the rotor core, and ablating areas with rotors of dominant frequency, has also been met with mixed results (Narayan *et al.*, 2012; 2014; Buch *et al.*, 2016; Steinberg *et al.*, 2017).

Whilst it appears PVI with catheter ablation is superior to medical therapy alone in the heart failure population with severely impaired LV systolic dysfunction, certainly men aged below 70 years of age where the LV ejection fraction was still over 25%, this is the cohort that had the largest benefit and no obvious harm in the aforementioned study (Marrouche *et al.*, 2018), results of an even larger randomised controlled trial comparing catheter ablation to PVI in all-comers with all types of AF, appears to demonstrate no clear hard outcome primary endpoint benefit in an intention-to-treat analysis. The results of the CABANA trial have been presented through a conference, but the study data are yet to be formally published. The authors have stipulated a large crossover from the medical to the ablation arm and that in an on-treatment analysis a benefit of ablation can be seen, but there was inadequate powering of the trial for such an analysis and it is open to confounding. Thus far it can only be seen as hypothesis generating. Another qualm with all trials comparing ablation and medical therapy to date is that the control medical arm contains no "sham" methodology. A placebo effect of ablation cannot be discounted.

A large growing body of evidence has shown that obesity is an independent risk factor for incidence and increasing burden of AF (Lavie *et al.*, 2017). Apart from links with atherosclerosis and hypertension that are themselves associated with an increased burden of AF, haemodynamic effects of obesity are such that circulating blood volume increases as does a demand for greater cardiac output. This leads to left ventricular hypertrophy and at least diastolic if not systolic LV dysfunction and subsequent atrial stretch and fibrosis (Lavie *et al.*, 2017). Obesity is also associated with a greater volume of epicardial and pericardial fat, particularly around the posterior left atrium and pulmonary veins. Fat here is secretory of various pro-inflammatory cytokines (eg. IL-6) and growth factors (eg. TGF- β 1) amongst other metabolic, angiogenic and neurohumoural factors. This all serves to increase fibrotic changes around the pulmonary vein ostia and left atrium which in turn has detrimental effects on calcium handling and reduces conduction velocity promoting the substrate for re-entry and AF triggers (Wong *et al.*, 2017). Epicardial adipose tissue (EAT) itself also interdigitates the atrial myocardium adding to conduction slowing (Lavie *et al.*, 2017).

Direct correlation has been shown between volume or thickness of epicardial fat and AF burden via Computed Tomography (CT) / Magnetic Resonance Imaging (MRI) studies (Gaeta *et al.*, 2017). However, a large heterogeneity exists with regards the absolute volumes reported in the separate studies suggesting it is hard to label any cut-off value to risk. Structured cardiovascular risk factor and weight loss management programmes have been shown in both randomised controlled trials and observational studies to reduce the burden of AF and improve outcomes following catheter ablation (Abed *et al.*, 2013; Pathak *et al.*, 2014; 2015).

1.2.3 Drug Development for AF

The search continues for an effective atrial specific drug that does not produce pro-arrhythmia in the ventricle.

Blocking potassium channels has the effect of prolonging the APD and ERP and blocking sodium channels reduces excitability and also prolongs the ERP. As previously explained this in turn increases the minimum wavefront path length for re-entry and reduces the likelihood of fibrillatory conduction. A corollary to this is that without atrial specificity of these drugs, they also increase APD and ERP in a very heterogeneous manner in the ventricle. Sotalol, for example, is highly specific for I_{Kr} block and preferentially prolongs APD in the mid-myocardial layer of the ventricle (Nerbonne & Guo, 2002). This in turn increases the likelihood of early after-depolarisations (EADs), spontaneous depolarisations occurring prior to full repolarisation because of excess intracellular calcium during a prolonged phase 3 of the action potential, that in turn cause forward mode of the $I_{Na/Ca}$ exchanger with net inward current (Priori & Corr, 1990). If EADs propagate to tissue no longer refractory, this can set up re-entry and/or fibrillatory conduction and constitutes a risk of sudden death of malignant ventricular arrhythmias.

Work has been performed to test the efficacy of blockers of I_{Kur} (such as vernakalant) and I_{KACh} given the suggested atrial specificity of these currents. Vernakalant has been shown to terminate AF when given intravenously but this is probably due to its Na^+ blocking effect for it is not a specific blocker of I_{Kur}

(Ravens & Wettwer, 2011). Pure I_{Kur} block has not yet been demonstrated to suppress AF, its block actually shortens APD in atrial cardiomyocytes in sinus rhythm and I_{Kur} is downregulated in chronic AF all questioning how useful a drug target it will be (Ravens & Odening, 2016). Despite promising results of I_{KACH} blockers in dogs, a recent clinical trial of the agent BMS 914392 failed to show a reduction in AF burden in patients with paroxysmal AF (Podd *et al.*, 2016).

Another atrial specific target has been the late persistent sodium current I_{NaL} . The inactivation curve of the atrial Nav1.5 channel appears to be left shifted towards more negative potentials and given the resting membrane potential of atrial cardiomyocytes is more positive than ventricular cardiomyocytes, for any particular resting state there is a greater population of Nav1.5 channels in an inactivated state in the atria compared to the ventricle (Maier & Sossalla, 2013). Ranolazine is a drug licensed for use as an anti-anginal whereby its mechanism of action is suggested to inhibit the late sodium current thereby reducing $[Na]_i$ and consequently reducing reverse mode of the $I_{Na/Ca}$ exchange current and reducing calcium load on the cell. This in turn reduces energy requirements and improves LV diastolic function reducing supply/demand mismatches during ischaemia. It exhibits use-dependent block with a selectivity for Nav1.5 channels but can also block in a pre-open state when only a limited number of activation gates are open at less positive membrane potentials (Zygmunt *et al.*, 2011). It has fast release from block but only when the channel has recovered from inactivation and as such at short diastolic intervals, such as during an atrial arrhythmia, there will ensue a high degree of block in the atria given the differences in the inactivation curves of the sodium channel between the atria and ventricle. Thus, its effect on the peak sodium current, I_{NaPeak} , is more pronounced in the atria and presumably reduces excitability either causing a source-sink mismatch at the centre of rotors, or prolonging post-repolarisation refractoriness (Zygmunt *et al.*, 2011; Vizzardi *et al.*, 2012). Its anti-arrhythmic properties are accentuated by its, albeit weaker, I_{Kr} blocking effect and the favourable metabolic sequelae from inhibiting I_{NaL} (Vizzardi *et al.*, 2012). The MERLIN-TIMI 36 trial randomised 6500 acute coronary syndrome patients to ranolazine in addition to standard therapy or standard therapy alone (Scirica *et al.*, 2007). Although no difference in the combined primary outcome of cardiovascular death, myocardial infarction or recurrent ischaemia, further

analysis did show a trend towards a reduced AF and supraventricular tachycardia burden. A more recent trial looked at use of ranolazine alone and in combination with dronedarone in patients with pAF, found no benefit with either drug alone, but significantly reduced AF burden compared to placebo when the drugs were used in combination (Reiffel *et al.*, 2015). No safety concerns were raised from the trial but we know that dronedarone has a significant negatively inotropic effect and is contraindicated in patients with structural heart disease thus putting up a barrier to the widespread use of this drug combination.

Other avenues explored include upstream therapies. Angiotensin converting enzyme inhibitors (ACEi) and angiotensin II receptor blockers (ARB) have shown mixed results. A randomised controlled trial examining the effect of olmesartan in patients with lone paroxysmal AF (no AF risk factors) demonstrated no benefit on AF burden (Goette *et al.*, 2012) whilst a retrospective matched case-control study in hypertensive patients with no other AF risk factors demonstrated a benefit for reduced AF burden amongst patients on an ACEi or ARB as compared with β -blockers or diuretics, but not calcium channel antagonists (Marott *et al.*, 2014). The suggestion is such therapy is useful in conjunction with reducing other AF risk factors, and in line with general cardiovascular disease prevention reducing AF burden rather than being an independent modifier of AF risk. This too can be said for statin therapy whereby any signal for their effect on AF burden reduction is most likely due to reduced burden of vascular disease as an associated AF risk factor (Fang *et al.*, 2012; Alves-Cabratosa *et al.*, 2017).

1.3 ATP-sensitive Potassium Channels

1.3.1 ATP-sensitive Potassium Channel Structure, Function and Modulation

ATP-sensitive potassium channels (K_{ATP}) are weak inwardly-rectifying potassium (K^+) channels displaying no voltage-dependent gating and instead link cellular excitability to the cell's metabolic state. Inward rectification is produced by block of the cytosolic side of the pore by magnesium and polyamines but this block is weak affording still a strong outward current when the membrane potential is more positive to E_K . Their structure consists of a hetero-octamer of subunits. The pore forming subunits are designated Kir6.1 and Kir6.2, and regulatory sulphonylurea receptor (SUR) subunits SUR1, SUR2A and SUR2B (Inagaki *et al.*, 1996). Four of each make up the channel (Clement *et al.*, 1997; Inagaki *et al.*, 1997; Shyng & Nichols, 1997) (see Figure 1.10).

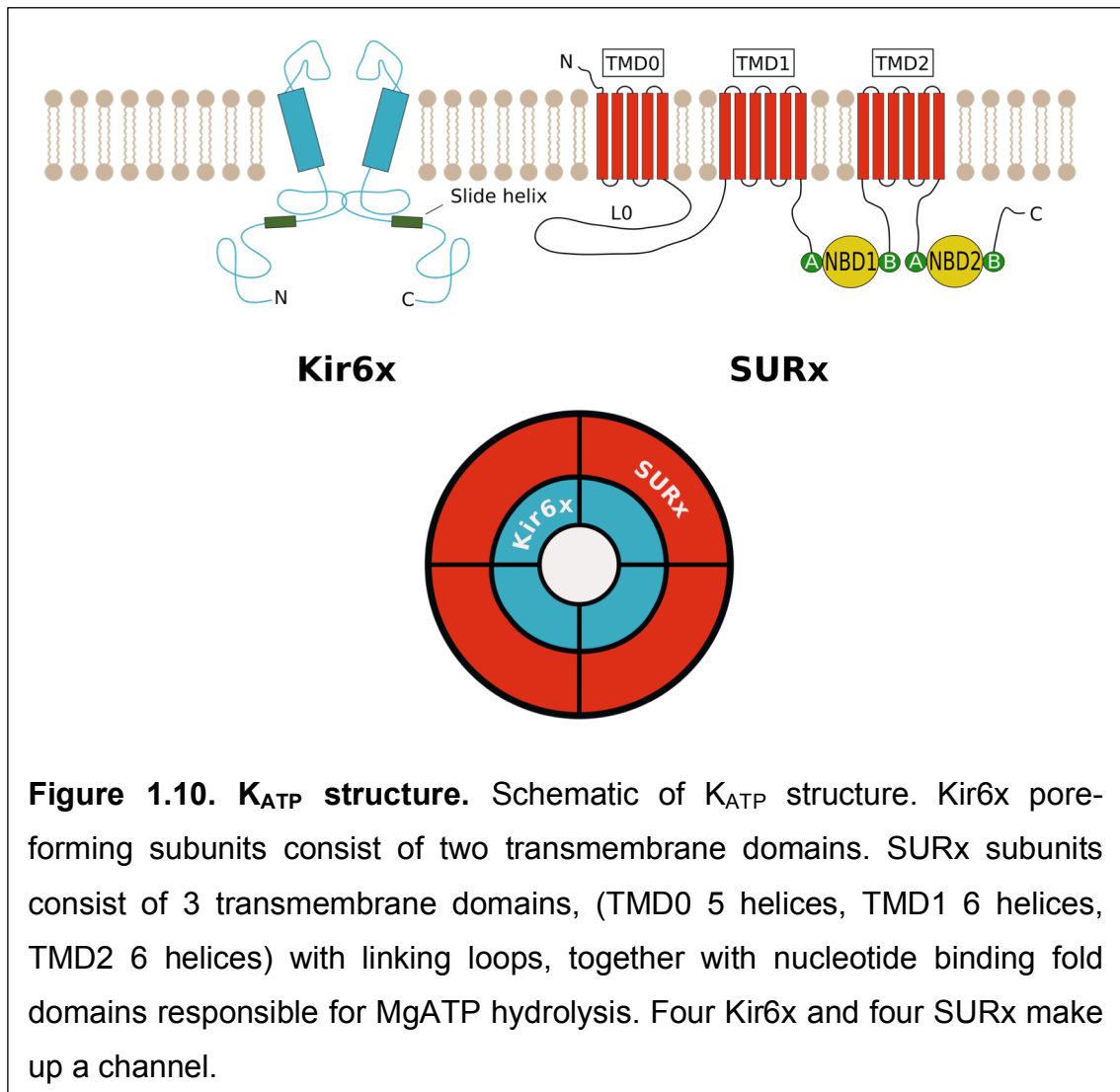


Figure 1.10. K_{ATP} structure. Schematic of K_{ATP} structure. Kir6x pore-forming subunits consist of two transmembrane domains. SURx subunits consist of 3 transmembrane domains, (TMD0 5 helices, TMD1 6 helices, TMD2 6 helices) with linking loops, together with nucleotide binding fold domains responsible for MgATP hydrolysis. Four Kir6x and four SURx make up a channel.

In native cells, transport of the Kir subunit to the sarcolemma is contingent on co-expression with SUR, which covers up an ER-retention motif (Neagoe & Schwappach, 2005). The genes *KCNJ8* and *KCNJ11* encode the two isoforms of the pore forming subunit Kir6.1 and Kir6.2 respectively (Inagaki *et al.*, 1995b; 1995a). SUR1 is encoded by *ABCC8* and SUR2 encoded by *ABCC9*, with two RNA splice variants of SUR2 namely SUR2A and SUR2B (Inagaki *et al.*, 1995a; Chutkow *et al.*, 1996). *KCNJ8* and *ABCC9* are adjacent to each other on chromosome 12p12.1 and *KCNJ11* and *ABCC8* likewise on chromosome 11p15.1 (Inagaki *et al.*, 1995a; Chutkow *et al.*, 1996).

The Kir subunits have two trans-membrane domains (TMDs) with cytosolic N and C termini and an H5 segment with homology of the voltage gated K⁺ channels and which is responsible for the channel's K⁺ selectivity (Flagg *et al.*, 2010). In addition, running parallel to the cytoplasmic surface of the cell

membrane, there is an amphipathic "interfacial" or "slide" helix thought to provide part of the physical link with adenosine triphosphate (ATP) gating (Ribalet *et al.*, 2006; Enkvetchakul *et al.*, 2007; Flagg *et al.*, 2010). Conductances between the two isoforms differs, Kir6.2 ~80pS and Kir6.1 ~35pS (Inagaki *et al.*, 1995a; 1996; Yamada *et al.*, 1997; Kondo *et al.*, 1998). There is direct magnesium (Mg^{2+}) independent nucleotide tri-phosphate, and to a lesser extent nucleotide di-phosphate inhibition at the Kir subunits (Tucker *et al.*, 1998; Babenko & Bryan, 2001).

The SUR subunits consist of 3 TMDs (17 helices) and nucleotide binding folds (NBFs) associated with TMD2 that have Walker A and B motifs responsible for Mg^{2+} dependent binding of nucleotide di- and tri-phosphates on the cytoplasmic side of the membrane (Gribble *et al.*, 1997a; Shyng *et al.*, 1997; Flagg *et al.*, 2010). Such Mg^{2+} dependent binding allosterically regulates activity of the Kir subunit via interaction with cytoplasmic TMD0 and linker (or lasso) L0 regions (Lederer & Nichols, 1989; Smith *et al.*, 2002; Babenko & Bryan, 2003). Mg^{2+} -dependent hydrolysis of ATP to adenosine diphosphate (ADP), or a lowering of the intracellular $MgATP/MgADP$ ratio, leads to NBF dimerisation and confers an increase in Kir opening by allosterically releasing the Kir subunit from nucleotide di- or tri-phosphate inhibition (Hopkins *et al.*, 1992; Ueda *et al.*, 1999; Matsuo *et al.*, 2000).

When expressed in the absence of SUR by deletion of the ER-retention motif, the pore-forming subunits display differing effects to the influence of adenine nucleotides. Kir6.2 is directly inhibited (IC_{50} ~100 μ mol/L) whereas Kir6.1 not (Tucker *et al.*, 1997; Farzaneh & Tinker, 2008). When either Kir6x are expressed along with SUR both have been shown to display adenine nucleotide inhibition even in Mg^{2+} -free solution and the presence of SUR1 with Kir6.2, for example, decreases the IC_{50} to ~10 μ mol/L (Babenko & Bryan, 2001). R50, K185, I182, F333, G334, Y330, L205 are key residues implicated in ATP binding and gating of Kir6.2 (Tucker *et al.*, 1998; Drain *et al.*, 1998; Li *et al.*, 2000a; Ribalet *et al.*, 2003; John *et al.*, 2003; Antcliff *et al.*, 2005; Tammaro *et al.*, 2006). They have been delineated to a pocket associated with the "interfacial" helix and region of interaction of the L0 linker region to the pore in the area parallel to the submembrane space in a recently described cryo-EM

crystal structure of the Kir6.2/SUR1 channel (Martin *et al.*, 2017). Most if not all residues have demonstrated importance of ATP binding via mutant studies owing to charged side chains important in phosphate species binding of ATP (Tucker *et al.*, 1998; Drain *et al.*, 1998; Li *et al.*, 2000a; Ribalet *et al.*, 2003; Antcliff *et al.*, 2005). Kir6.1 does not share all of these residues. However, it may be that co-expression with SUR produces subsequent subtle folding of the pore that enables binding of ATP that can reconcile the findings that a truncated Kir6.1 expressed in the absence of SUR displays no direct ATP inhibition, but that expressed with SUR, does display ATP inhibition despite the absence of magnesium (Babenko & Bryan, 2001; Farzaneh & Tinker, 2008). Another specific feature of Kir6.1-containing species is their dependence on ADP for activation (Beech *et al.*, 1993; Yamada *et al.*, 1997; Satoh *et al.*, 1998).

Activation and inhibition is in fine balance. With co-expression of SUR the pore-forming subunits appear sensitised to Mg^{2+} -free adenine nucleotide inhibition but also the SUR subunit confers the ability to allosterically free the Kir subunit from this inhibition on Mg^{2+} -dependent hydrolysis of ATP to ADP at the NBFs that lead to their dimerisation (Babenko & Bryan, 2001; Flagg *et al.*, 2010). In the physiological setting cytosolic concentrations of ATP nearly always saturate inhibition at either pore type. In turn the activation/inhibition balance is largely driven by the MgATP/MgADP ratio at the SUR subunit (Babenko & Bryan, 2001). Sensitising effects of co-expressed SUR on either pore type appear to be in a hierarchy with SUR1 ~ SUR2B > SUR2A and Kir6.1 appears more sensitive to the effects of co-expressed SUR (Isomoto *et al.*, 1996; Babenko *et al.*, 1998; 1999). Kir6.1 species, thus, tend to display an intrinsically greater open probability.

Phosphatidylinositol 4,5-bisphosphate (PIP_2) interaction at the membrane is crucial to maintain channel activation and with its depletion there is channel inhibition (Tinker *et al.*, 2014). PIP_2 binding directly competes or at least inhibits ATP binding at the pore. In the recently described cryo-EM structures of the Kir6.2/SUR1 channel, the PIP_2 binding site is delineated and in one case PIP_2 appears to be seen bound to the pore at the cytosolic domain close to the "interfacial" helix and in very close proximity to the ATP binding site just below (Li *et al.*, 2017; Martin *et al.*, 2017). All of these structures surround the area of

the inner helix gate on the pore and it is easy to reconcile that allosteric pressure from these species can alter the aperture of this gate. The structures are in keeping with previous homology modelling of the channel that has described the association and stoichiometry of Kir6x and SURx subunits (see Figure 1.10) (Clement *et al.*, 1997; Antcliff *et al.*, 2005). The structures have given further insight into the molecular mechanics governing channel gating. Rotation of TMDs 1 and 2 during NBF dimerisation from a "propeller" shape to a "quatrefoil" shape appears to release pressure from the TMD0, and crucially, the lasso L0 structure on the region of ATP binding preventing buttressing of the ATP molecule and promoting its release, thus causing increased aperture of the inner helix gate and opening of the pore (Lee *et al.*, 2017). Figure 1.11 demonstrates 2D class averages, EM density maps and ribbon representations depicted from the recent publications of the cryo-EM structure of Kir6.2/SUR1 channels.

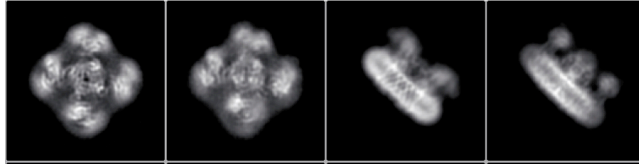
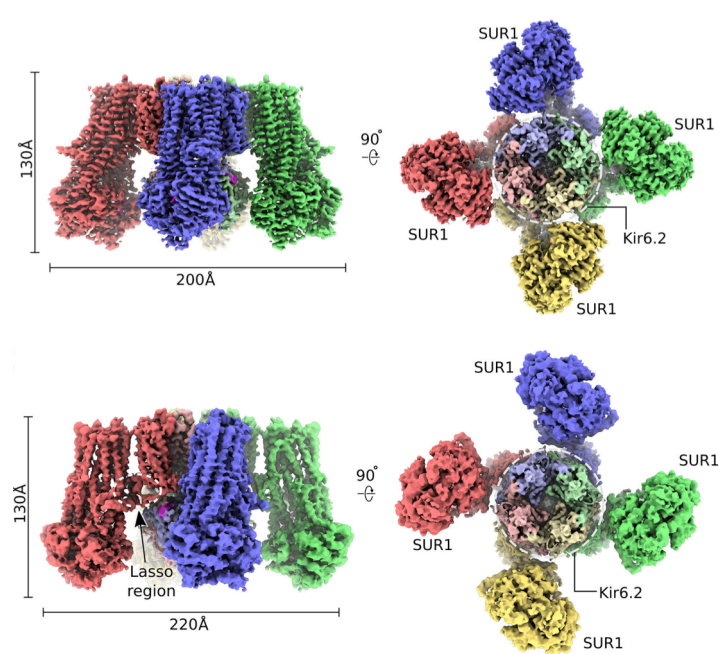
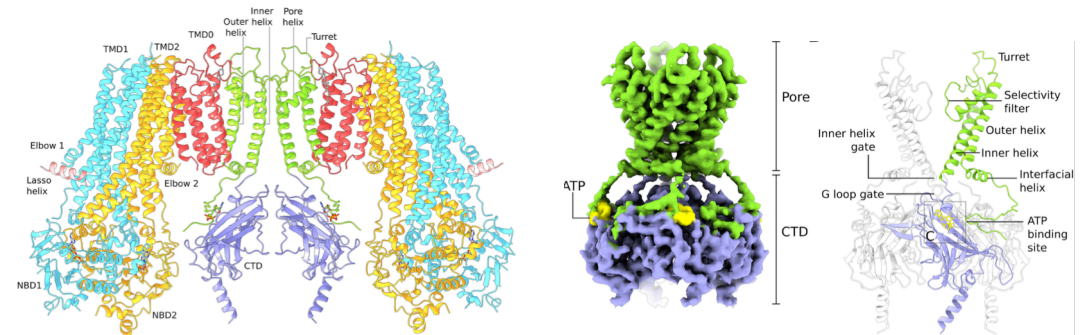
A**B****C**

Figure 1.11. Cryo-EM structure of a Kir6.2/SUR1 channel. A. 2D class averages of channels in top view and side view from a cryo-EM micrograph (taken from Martin *et al.*, 2017). B. Side view and view from below of (top) quatrefoil and (bottom) propeller forms of the channel showing the Lasso abutting the inner helix gate in the propeller form (taken from Lee *et al.*, 2017). C. (Left) Ribbons representation of two Kir6.2/SUR1 fusion protomers in the quatrefoil form, (Right) EM density and ribbons representations of the Kir6.2 tetramer with EM density of the bound ATP molecule in yellow (taken from Lee *et al.*, 2017).

Changes in the ATP/ADP ratio at different compartments in the subcellular space are transmitted via diffusion through the 2 phosphotransfer pathways controlled by creatine kinase (CK) and adenylate kinase (AK) (Carrasco *et al.*, 2001; Crawford *et al.*, 2002; Selivanov *et al.*, 2004; Flagg *et al.*, 2010). The CK pathway is able to amplify subtle changes in ATP concentration from one compartment to another such that small reductions in the bulk cellular concentration of ATP are amplified at the submembrane space and can be sensed by K_{ATP} (Selivanov *et al.*, 2004). This occurs as the stoichiometry of flux of submembrane creatine phosphate (CrP) required to correct for reductions in bulk ATP concentration is much larger than that required for the reverse process (Selivanov *et al.*, 2004). The AK pathway is able to fine-tune this to avoid large oscillations in ATP and ADP at the submembrane (Selivanov *et al.*, 2004).

There is also modulation by downstream effects of G-protein linked protein kinase A (PKA) phosphorylation with subsequent phosphorylation of both the Kir and SUR subunits. In vascular smooth muscle (VSM) for example this activates the channel (Tinker *et al.*, 2014). In cardiac myocyte channels this is less well examined but also appears to have the same effect (Zingman *et al.*, 2002; Flagg *et al.*, 2010; Kim *et al.*, 2012). Apart from β -adrenergic activation via PKA, adenosine also activates the channel via this pathway in the vasculature through stimulatory G protein coupled adenosine A_2 receptors (Kleppisch & Nelson, 1995).

The modulation by phosphorylation of protein kinase C (PKC) also has heterogeneous effects dependent on the specific subunit composition, activating K_{ATP} at the cardiomyocyte sarcolemma and inhibiting at the VSM cell membrane (Flagg *et al.*, 2010; Tinker *et al.*, 2014).

Thus, in a metabolically challenging environment with a low intracellular ATP/ADP ratio and thus high MgADP/MgATP ratio, there is a tendency to accelerate repolarisation or hyperpolarise the membrane. In cardiac myocytes there is acceleration of phase 3 of the action potential through increased channel activity and thus action potential duration (APD) shortening (Lederer *et al.*, 1989; Venkatesh *et al.*, 1991; Kubota *et al.*, 1993; Tinker *et al.*, 2014).

The channel expressed in pancreatic β cells links cellular metabolism to insulin secretion. Active glucose uptake after a meal when circulating glucose levels are high, leads to a higher ATP/ADP ratio conferring closure of the channel, with reduced K^+ efflux leading to depolarisation of the cell membrane and opening of voltage-gated calcium channels. The inward flow of calcium leads to exocytosis of insulin (Ashcroft, 1988; Aguilar-Bryan *et al.*, 1995; Inagaki *et al.*, 1996).

It is also expressed in the brain, skeletal muscle and vascular smooth muscle (VSM) (Flagg *et al.*, 2010). Ablation of K_{ATP} currents in VSM cells produces hypertensive animals and coronary artery spasm through prolonged smooth muscle depolarisation and contraction (Miki *et al.*, 2002; Chutkow *et al.*, 2002). Its expression and function in the heart will be discussed further in later sections.

1.3.2 ATP-sensitive Potassium Channel Pharmacology

K_{ATP} channels involve a rich pharmacology. This has been exploited through the use of sulphonylureas in the treatment of diabetes. Drugs such as tolbutamide and glibenclamide inhibit K_{ATP} . Binding and allosteric modulation at the SUR subunit causes closed state stability and increased interburst closed times. This prolongs depolarisation of the cell (in this case the pancreatic β -cell), with inward Ca^{2+} current triggering exocytosis and increased release of insulin (Aguilar-Bryan *et al.*, 1995; Sola *et al.*, 2015). There are also a variety of K_{ATP} channel openers (KCOs) including diazoxide, pinacidil, nicorandil and cromakalim with effects mediated via Mg^{2+} -dependent hydrolysis of ATP to ADP at the SUR subunit (Schwanstecher *et al.*, 1998; Babenko *et al.*, 2000; Bienengraeber *et al.*, 2000).

Inhibitors

These drugs have specificity for particular SUR subunits. Tolbutamide is more specific to SUR1 than SUR2A with TMD2 helices 12-16 being implicated for high affinity binding and inhibition (Ashfield *et al.*, 1999; Babenko *et al.*, 1999). An interaction with tolbutamide and the N-terminus of the pore-forming subunit

also appears to be crucial to its effect whilst inhibition is also augmented by its interference with the action of MgADP at the NBFs promoting unbalanced Mg²⁺-independent inhibition at the pore (Gribble *et al.*, 1997b; Reimann *et al.*, 1999; Babenko *et al.*, 1999). SUR1 containing protein complexes can be inhibited by micromolar concentrations of tolbutamide while glibenclamide is less specific between SUR1 and SUR2A where its binding site in biochemical studies using truncated protein implicates the L0 cytosolic loop, TM helices 15/16 and the cytosolic loop 8 between them (Gribble *et al.*, 1998; Ashfield *et al.*, 1999; Babenko *et al.*, 1999; Mikhailov *et al.*, 2001). In one of the recently defined crystal structures it is implied that a density befitting of glibenclamide can be seen associated with a region involving both the above cytosolic loops that would support the previous putative binding site data (Lee *et al.*, 2017). It is also suggested that this position would serve to keep the NBFs forced apart preventing dimerisation and thus maintaining the buttressing effect of the L0 loop on the inner helix gate providing a mechanistic explanation to the inhibitory effect of glibenclamide on channel opening (Lee *et al.*, 2017). However, the authors stipulate that further studies with greater resolution of structures will be needed to confirm this.

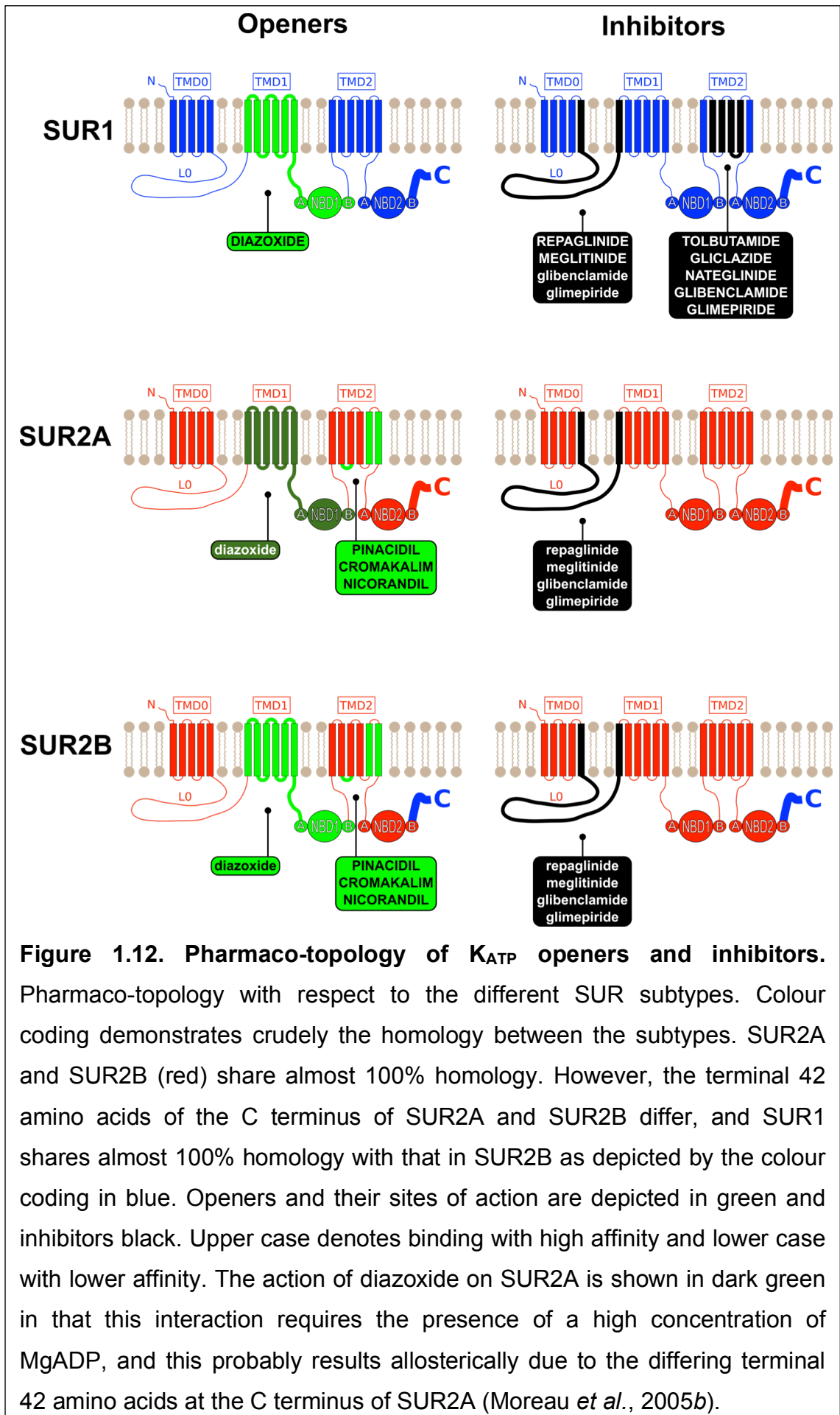
HMR1883 and its sodium salt HMR1098 are sulphonylurea derivatives thought to have a selective inhibition of SUR2A containing channel complexes over SUR1 though this has also been challenged recently (Gögelein *et al.*, 1998; Russ *et al.*, 2001; Manning Fox *et al.*, 2002; Zhang *et al.*, 2011). PNU37883A is unique in that it is thought to be a direct pore blocker of the Kir subunit and it has been suggested exhibits selectivity for Kir6.1 containing channel complexes over Kir6.2 but again this is also a matter of contention (Cui *et al.*, 2003; Kovalev *et al.*, 2004). It is also implicated in blocking other ion channels with K⁺ and Ca²⁺ conductance (Teramoto, 2006a).

Openers

Diazoxide is relatively SUR1-specific at micromolar concentrations owing to residues at TMD1 helices 6-11 and NBF1 and pinacidil SUR2 specific at similar concentrations owing to residues at TMD2 helices 12-17 (Babenko *et al.*, 2000; Dabrowski *et al.*, 2002; Hambrock *et al.*, 2004). Similar findings to pinacidil

relate to cromakalim and its analogues (Uhde *et al.*, 1999; Babenko *et al.*, 2000; Moreau *et al.*, 2000; 2005b). Indeed transfer of residues at TM17 in SUR2A to SUR1 confers the SUR2A KCO sensitivity patterns in SUR1 (Moreau *et al.*, 2000; Hambrook *et al.*, 2004). Pinacidil, cromakalim and to a lesser extent, diazoxide, all have opener activity on SUR2B-containing channels (Schwanstecher *et al.*, 1998; Uhde *et al.*, 1999; Matsuoka *et al.*, 2000; Moreau *et al.*, 2005b). Whilst diazoxide is thought not to activate SUR2A-containing channels with great efficacy, reports have shown a binding affinity and ability to activate dependent on the presence of MgADP (Schwanstecher *et al.*, 1998; D'hahan *et al.*, 1999; Matsuoka *et al.*, 2000).

The pharmaco-topology of drug-SUR selective binding as determined by the site directed mutagenesis and chimaeric studies described above, is summarised in Figure 1.12.



1.3.3 Cardiac ATP-sensitive Potassium Channels

Cardiac protection

K_{ATP} channels are expressed throughout the heart in the atria, ventricles and the cardiac conduction system. They appear to be closed under normal metabolic conditions (Noma, 1983; Zünkler *et al.*, 1997; Babenko *et al.*, 1998; Pelzmann *et al.*, 2001). Shortening of phase 3 of the action potential, through K_{ATP} opening in response to metabolic stress (a reduction of intracellular ATP concentration $[ATP]_i$ and an increase in intracellular ADP concentration $[ADP]_i$ in the presence of Mg^{2+}), is thought to provide a protective mechanism during these periods. In one study looking at guinea pig ventricular myocytes, action potential duration (APD) was reduced by as much as 50% when as little as 0.7% of the maximum K_{ATP} conductance was active (Nichols *et al.*, 1991). Excessive calcium (Ca^{2+}) loading confers cellular toxicity (Bers, 2008). Shortening of APD allows for reduced calcium (Ca^{2+}) loading together with conservation of cellular ATP, and this has been shown to be executed by K_{ATP} opening in response to ischaemia (McPherson *et al.*, 1993; Jovanović *et al.*, 1998; 1999; Suzuki *et al.*, 2002; Baumann *et al.*, 2002). This effect can also be diminished with ablation of K_{ATP} current and in animal models K_{ATP} inhibition, both through knockout and pharmacological modulation, has been shown to increase infarct size after ischaemic insults (Gross & Auchampach, 1992; Jovanović *et al.*, 1998; Suzuki *et al.*, 2002; 2003; Aziz *et al.*, 2017).

There is also evidence that shortening of APD via K_{ATP} opening is important for exertional capacity at higher heart rates during β -adrenergically driven stress and the “fight/flight” response (Zingman *et al.*, 2002).

K_{ATP} channel activation appears fundamental to the process of ischaemic preconditioning in cardiac and skeletal muscle, where short bursts of ischaemia lead to conditioning of tissue and reduced injury to future, more prolonged bouts of ischaemia (Murry *et al.*, 1986; Gross & Auchampach, 1992). Whether this is due solely to activation of sarcolemmal currents still remains to be seen and there is a vast amount of work, reviewed extensively by Yellon and Downey, supporting the theory that a mitochondrial K_{ATP} current (mito K_{ATP}) is responsible

(Yellon & Downey, 2003). Opening of the mitochondrial channel and influx of K^+ into mitochondria is thought to cause osmotic swelling altering the ability to phosphorylate ADP. ADP cannot enter the intermembrane space due to swelling. Instead creatine is phosphorylated and this is a more efficient means of transmitting energy to the cytoplasm (Yellon & Downey, 2003). An influx of K^+ through mito K_{ATP} opening also reduces toxic Ca^{2+} entry and prevents the opening of the mitochondrial transition pore through which other toxic substrates can enter during prolonged bouts of ischaemia (Yellon & Downey, 2003).

With increases of afterload, Ca^{2+} overload can lead to cardiac hypertrophy through activation of the calcineurin-NFAT signal transduction cascade that drives the expression of hypertrophy genes (Wilkins & Molkenin, 2004). Ablation of K_{ATP} currents in knockout animals has been shown to correlate with cardiac hypertrophy and heart failure phenotypes and that this is likely to be directly related to APD prolongation and Ca^{2+} overload (Kane *et al.*, 2006; Yamada *et al.*, 2006). Consistent with a role of K_{ATP} in heart failure phenotypes, there is convincing human evidence that a frame-shift mutation in the region encoding the NBF of SUR2A, which causes defective catalysis of ATP hydrolysis and reduced channel function, is associated with an otherwise, idiopathic, dilated cardiomyopathy (Bienengraeber *et al.*, 2004). Reduced K_{ATP} activity is also implicated in the reduced downstream activity of peroxisome proliferator-activated receptor γ coactivator (PGC)-1 α and a group of energy metabolism related genes at both protein and mRNA levels that leads to a heart failure phenotype (Hu *et al.*, 2008; Zlatkovic *et al.*, 2009).

Arrhythmia

As explained in section 1.2.1 arrhythmia mechanisms described include re-entry (anatomical, functional and spiral wave), abnormal automaticity and triggered events (EADs and DADs) (Tse, 2016). In guinea pig ventricular myocytes action potential duration (APD) was reduced by as much as 50% when as little as 0.7% of the maximum K_{ATP} conductance was active (Nichols *et al.*, 1991) and the opening of K_{ATP} channels leads to faster repolarisation and a shorter QT interval on the surface ECG, a marker of the activation-recovery

interval (Kubota *et al.*, 1993; Lu *et al.*, 2008). In turn this gives a reduced effective refractory period, which in principle can predispose to re-entrant circuits and a pro-fibrillatory state. Pro-fibrillatory effects of K_{ATP} openers have been shown in numerous animal models and a major factor in this is likely to involve heterogeneous dispersion of APD effects both in an interventricular, and intraventricular manner between layers of the myocardium (Wolleben *et al.*, 1989; Chi *et al.*, 1990; Furukawa *et al.*, 1991; Di Diego & Antzelevitch, 1993; Wolk *et al.*, 1999; Uchida *et al.*, 1999). In a Kir6.2 knockout (KO) mouse model surface ECG recordings showed absence of ST elevation in response to ischaemia in the knockouts that was present in the wild-type (WT) mice (Li *et al.*, 2000*b*). In epicardially mapped dogs regional ST elevation was seen in response to regionally induced ischaemia by coronary ligation of the left anterior descending artery (LAD) that was very similar to regional injection of the KCO pinacidil in the same artery, and in both, ST elevation was reversed with the K_{ATP} inhibitor glibenclamide (Kubota *et al.*, 1993). Similar glibenclamide reversal of ischaemia-induced T wave changes was seen in another canine study (Kondo *et al.*, 1996). The component of ST deviation seen in response to ischaemia that can be attributed to K_{ATP} opening, is explained by a heterogeneous dispersion of transmural expression such that there is higher expression in the epicardium relative to the endocardium (Furukawa *et al.*, 1991). Increased outward K^+ current in response to ischaemia in the epicardium thus provides a transmural voltage gradient seen on the surface ECG.

The corollary is that blocking K_{ATP} would be anti-arrhythmic. Studies in rat and canine models have looked at ventricular fibrillatory potential in the context of ischaemia and shown that this is reduced in the presence of K_{ATP} blocking drugs (Wolleben *et al.*, 1989; Kantor *et al.*, 1990; Billman *et al.*, 1998). This has been replicated in a Langendorff-perfused explanted cardiomyopathic human heart model (Farid *et al.*, 2011).

Studies have also investigated arrhythmia inducibility in atrial preparations. In a rat model isoproterenol-induced metabolic stress led to a reduced intracellular ATP concentration and an increased atrial tachyarrhythmia inducible state that was reversed with the K_{ATP} inhibitor glibenclamide (Kim *et al.*, 2012). In a murine model with salt-induced hypertension, atrial K_{ATP} upregulation was seen

coinciding with shortened APD and ERP and increased atrial arrhythmia inducibility (Lader *et al.*, 2011). In human hearts obtained at transplantation, KCOs were seen to increase atrial arrhythmia inducibility that was then terminated with a K_{ATP} inhibitor (Fedorov *et al.*, 2011). Pro-fibrillatory effects of K_{ATP} openers have also been shown in rat, canine, rabbit and feline models (Wolleben *et al.*, 1989; Chi *et al.*, 1990; Furukawa *et al.*, 1991; Di Diego & Antzelevitch, 1993; Wolk *et al.*, 1999; Uchida *et al.*, 1999).

Perhaps paradoxically, however, in clinical trials in patients with cardiac ischaemia, patients using the K_{ATP} opener and nitric oxide donor nicorandil had improved outcomes and no increased arrhythmic risk (IONA Study Group, 2002; Simpson & Wellington, 2004). In fact the drug was even found to reduce arrhythmic risk in one study (Ueda *et al.*, 2004). This is despite its ability to activate both the proposed smooth muscle and classic cardiac sarcolemmal channel (Reimann *et al.*, 2001). Indeed, whilst K_{ATP} opening during ischaemia may well be pro-fibrillatory, its pharmacological blockade during ischaemic insults leads to increased infarct size in animal models (Gross & Auchampach, 1992; Suzuki *et al.*, 2002; 2003). Thus, from a translational perspective, particularly with regards the ventricle, pursuit of an anti-arrhythmic mechanism from channel blockade in this setting may well be counter-productive.

Atrial electrophysiology remodels as a consequence of changes in ion channel expression and/or regulation and gating with AF (Dobrev *et al.*, 2005; Workman *et al.*, 2008; Heijman *et al.*, 2014). Conflicting evidence exists for remodelling of K_{ATP} current in human chronic AF. Two studies have looked at differences in K_{ATP} current density in isolated right atrial appendage myocytes between sinus rhythm and chronic AF patients and showed opposing results (Balana *et al.*, 2003; Wu *et al.*, 2005). Another report looking at mRNA expression of a variety of potassium channel genes in AF patients demonstrated a reduced expression of *KNCJ11* (Brundel *et al.*, 2001). It is unclear how these findings might relate to the maintenance of the arrhythmia though a reduction in current might serve to promote re-entry through conduction slowing if diastolic membrane potential is more depolarised. A reduction in repolarising current might also promote triggered activity.

The early repolarisation pattern (“J wave”) on the ECG is commonly seen in healthy individuals. Though in documented kindreds it can represent something more malignant and the early repolarisation pattern (“J wave syndromes”) may predispose individuals to ventricular fibrillation and sudden death (Antzelevitch, 2012). A rare variant in KCNJ8 (S422L) has been associated with early repolarisation and ventricular fibrillation (Haïssaguerre *et al.*, 2009). Other groups have also described similar findings with the same mutation (Medeiros-Domingo *et al.*, 2010; Barajas-Martínez *et al.*, 2012). This mutant Kir6.1 subunit, co-expressed with SUR in mammalian cells, leads to an increase in current density compared to wild-type, owing to a decrease in sensitivity and inhibition by ATP (Haïssaguerre *et al.*, 2009; Medeiros-Domingo *et al.*, 2010; Barajas-Martínez *et al.*, 2012). The mutation has also been associated with lone atrial fibrillation in conjunction with early repolarisation in another case study (Delaney *et al.*, 2012).

Whilst channel opening might open up tissue to the increased likelihood of re-entry, in the case of abnormal automaticity or triggered activity, it is also possible that hyperpolarisation of the membrane will lead to the arrhythmia being extinguished. Effects of K_{ATP} modulation on automaticity have largely been investigated in isolated nodal cell or Purkinje fibre preparations and confirm that an increased outward potassium flux and membrane hyperpolarisation on channel opening slows spontaneous firing rate and suppresses automaticity (Yanagisawa & Taira, 1981; Satoh & Hashimoto, 1984; Imanishi *et al.*, 1984; Lathrop *et al.*, 1990). Hypoxia-induced spontaneous cycle length prolongation was blunted in Kir6.2 deleted Langendorff hearts suggesting a prominent role for K_{ATP} in sinus node automaticity (Fukuzaki *et al.*, 2008). Pinacidil has been shown to abolish EADs produced after drug-induced APD prolongation and DADs produced after ouabain induced calcium overload in canine ventricular myocytes (Spinelli *et al.*, 1991). Similar effects have been shown using nicorandil (Lathrop *et al.*, 1990). Indeed, nicorandil can abolish transmural dispersion of repolarisation and triggered activity in canine long QT models (Shimizu & Antzelevitch, 2000; Chinushi *et al.*, 2002), and when given intravenously, has been shown to abolish EADs and ventricular fibrillation in a patient with long QT syndrome (Sato *et al.*, 1995) and abolish Torsades de Pointes in a patient with atrio-ventricular block and bradycardia induced QTc

prolongation (Watanabe *et al.*, 1999). Loss of K_{ATP} function has also been shown to promote triggered activity. For example, Kir6.2 deletion was met with defective action potential shortening and EADs in isoproterenol challenged Langendorff mouse hearts (Liu *et al.*, 2004). A similar mechanism was proposed in a patient with lone Atrial Fibrillation (AF) emanating from the Vein of Marshall who was found to have a missense mutation Thr1547Ile in the ABCC9 gene encoding the SUR2A subunit (Olson *et al.*, 2007). Thus, the exact role of K_{ATP} in arrhythmia is complex and substrate dependent.

1.3.4 ATP-sensitive Potassium Channels and Cardiac Chamber Subunit Specificity

With the notion that manipulation of K_{ATP} current might influence arrhythmia inducibility in the clinical setting, an attractive aspect for K_{ATP} as a potential pharmacological target is its subunit composition and that there might be differences in expression between atria and ventricle. This might lead to the development of novel drugs that target the atria, circumventing the problems discussed above of unwanted effects on the ventricle of many pre-existing drugs used in clinical practice today.

A general picture has emerged with regards subunit expression and composition. The classic cardiac ventricular K_{ATP} channel comprises Kir6.2 and SUR2A. For example, the K_{ATP} properties of ventricular myocytes, including human, have been recapitulated in heterologous expression systems with this combination of subunits (Inagaki *et al.*, 1996; Babenko *et al.*, 1998). Ventricular myocytes of Kir6.2^{-/-} or SUR2^{-/-} mice lack K_{ATP} currents (Suzuki *et al.*, 2001; Chutkow *et al.*, 2001) and are unaffected in SUR1^{-/-} mice (Elrod *et al.*, 2008). The opposite is true of SUR1^{-/-} murine atrial myocytes and in this case K_{ATP} currents are absent (Flagg *et al.*, 2008). This finding was reproduced in experiments with SUR1^{-/-} murine atrial and ventricular myocytes with a variety of SUR isotype specific KCOs and inhibitors showing ablation of atrial but not ventricular currents (Glukhov *et al.*, 2010). Ablation of both atrial and ventricular currents in Kir6.2^{-/-} mice has also been demonstrated (Glukhov *et al.*, 2010). The importance of Kir6.2 in the mouse atria has also been established in another set of experiments with a mouse with global deletion (Saegusa *et al.*,

2005). In a murine model, the atrial channel appears to be represented at least in part by Kir6.2/SUR1.

In the sino-atrial node (SAN) cells of the rabbit it was shown that SUR2 specific openers caused hyperpolarisation of the maximum diastolic potential (MDP) and reduced automaticity but the single channel K_{ATP} conductance was an intermediate 52 ± 8 pS suggesting both pore-forming subunits could be present (Han *et al.*, 1996). K_{ATP} currents present in SAN cells of WT mice have, however, been ablated in Kir6.2 KO mice suggesting the importance of this pore-forming subunit in this model (Fukuzaki *et al.*, 2008). Recently our lab has demonstrated direct electrophysiological effects on SAN cells of conduction system-specific knockout of Kir6.1 in the mouse heart and in the majority of cells K_{ATP} current was activated by diazoxide and sensitive to tolbutamide (Aziz *et al.*, 2018). An ATP-sensitive K^+ current that increases with metabolic inhibition has also been demonstrated in the atrio-ventricular nodal (AVN) cells of the rabbit (Kakei & Noma, 1984). The single channel conductance was in keeping with that of Kir6.1 as forming the pore but there has been little other work that demonstrates this.

The presence of K_{ATP} has also been demonstrated in the Purkinje system of the mouse heart whereby the current was more sensitive to activation by MgADP when compared to ventricular myocytes, and where Kir6.1 mRNA expression was higher than Kir6.2 in the Purkinje system compared to the ventricle (Bao *et al.*, 2011). In this study currents in the Purkinje system were responsive to diazoxide and levcromakalim, and only levcromakalim in the ventricle. SUR2B mRNA expression was higher than SUR2A in the Purkinje system compared to the ventricle. There were similar findings both pharmacologically and with slope conductance in another study all suggesting a predominance of a Kir6.1/SUR2B composition (Light *et al.*, 1999).

Whilst the classic cardiac sarcolemmal channel has been described as Kir6.2/SUR2A and in the rodent atria Kir6.2/SUR1, mRNA encoding Kir6.1 is consistently detected at high levels in human heart (Erginel-Unaltuna *et al.*, 1998; Gaborit *et al.*, 2007; Fedorov *et al.*, 2011). There appears to be some association between gain-of-function *KCNJ8* mutations and ECG

findings/arrhythmia (Haïssaguerre *et al.*, 2009; Medeiros-Domingo *et al.*, 2010; Delaney *et al.*, 2012; Barajas-Martínez *et al.*, 2013). Various studies have recognised the capability for heteromultimerisation of the pore-forming subunits that would explain intermediate single channel conductances (Baron *et al.*, 1999; Cui *et al.*, 2001; Pountney *et al.*, 2001). Expression of pore mutations in Kir6.1 and Kir6.2 have both caused reductions in K_{ATP} current in rat cardiomyocytes (van Bever *et al.*, 2004). Heteromultimers of the SUR subunit have also been demonstrated (Cheng *et al.*, 2008; Wheeler *et al.*, 2008), though the likelihood of this, particularly in native cells, has been questioned (Giblin *et al.*, 2002; Tricarico *et al.*, 2006).

Changes in expression patterns have also been demonstrated in response to hypoxia and ischaemic insults. SUR1 expression has been seen to increase post-infarct in the infarct border zone in the ventricles of rat hearts (Isidoro Tavares *et al.*, 2007), whereas SUR2A expression was seen to increase in rat embryonic heart cells in response to hypoxia (Crawford *et al.*, 2003). In another study in rat embryonic heart cells, hypoxia appeared to up-regulate Kir6.1 expression and down-regulate Kir6.2 expression (Melamed-Frank *et al.*, 2001). This may be co-ordinated by a Forkhead transcription factor signalling pathway (Philip-Couderc *et al.*, 2008; Raeis *et al.*, 2010). A study on human hearts obtained at transplantation found SUR2A to be present in both atria and ventricle of non-failing hearts but a signal for SUR1 only in the ventricle. Both SURs appeared to be present in atria and ventricles of failing hearts suggesting an up-regulation of SUR1 in this setting (Fedorov *et al.*, 2011).

Conflicting reports are available with regards the subunit expression in vascular smooth muscle though the general picture appears to be that of Kir6.1/SUR2B or Kir6.2/SUR2B (Flagg *et al.*, 2010; Tinker *et al.*, 2014). In skeletal muscle reports suggest Kir6.2 is expressed with either SUR1 or SUR2A depending on fibre type (Tricarico *et al.*, 2006; Flagg *et al.*, 2010). In the pancreas a more cemented opinion has been formed that the composition is that of Kir6.2/SUR1 (Yokoshiki *et al.*, 1998).

One approach to defining the importance of K_{ATP} subunit expression in different tissues is to see the effect of mutations leading to pathology and disease traits. A summary of this is provided in Table 1.

CLINICAL CONDITIONS	GENE	MECHANISMS AND OBSERVATIONS	REFERENCES
CARDIAC			
Brugada syndrome, Early repolarisation ("J wave") syndrome, atrial and ventricular fibrillation	<i>KCNJ8</i>	S422L GOF has been associated with these conditions	(Haïssaguerre <i>et al.</i> , 2009; Medeiros-Domingo <i>et al.</i> , 2010; Barajas-Martínez <i>et al.</i> , 2012; Delaney <i>et al.</i> , 2012)
	<i>ABCC9</i>	V734I and S1402C GOF mutations implicated	(Hu <i>et al.</i> , 2014)
Atrial Fibrillation	<i>ABCC9</i>	Missense mutation T1547I leading to loss of function and implicated in AF initiating from the Vein of Marshall	(Olson <i>et al.</i> , 2007)
Sudden Infant Death Syndrome	<i>KCNJ8</i>	In frame deletion E332del and missense mutation V346I each cause loss of function and have been associated with this condition	(Tester <i>et al.</i> , 2011)
Increased LV size and Heart Failure	<i>KCNJ11</i>	E23K mutant appears over-represented in heart failure patients	(Reyes <i>et al.</i> , 2008; 2009)
	<i>ABCC9</i>	Missense mutation A1513T or frameshift mutation and stop codon introduction at L1524 - both impair nucleotide hydrolysis at NBF2 causing reduced function and associated with DCM patients	(Bienengraeber <i>et al.</i> , 2004)
Coronary spasm and Myocardial Infarction	<i>ABCC9</i>	Association with V734I mutation which causes both reduced ATP inhibition and reduced MgNDP activation when mutant co-expressed with SUR2B	(Smith <i>et al.</i> , 2013)

Table 1. Summary of human diseases or traits in which mutations or genomic variants in K_{ATP} occur.

INSULIN SECRETION			
Congenital Hyperinsulinism	<i>KCNJ11</i>	Recessive mutations leading to loss of K _{ATP} channels at the membrane and ER retention eg. H259R	(Marthinet <i>et al.</i> , 2005)
	<i>KCNJ11</i>	Recessive mutations producing non-functional protein eg. Y12X, L147P	(Thomas <i>et al.</i> , 1996; Nestorowicz <i>et al.</i> , 1997)
	<i>KCNJ11</i>	Dominant mutation causing impaired pore-opening eg. in-frame deletion I284del	(Kapoor <i>et al.</i> , 2011)
	<i>ABCC8</i>	Recessive mutations leading to loss of K _{ATP} channels at the membrane and ER retention eg. F1388del	(Sharma <i>et al.</i> , 1999; Cartier <i>et al.</i> , 2001; Yan <i>et al.</i> , 2007; Taneja <i>et al.</i> , 2009)
	<i>ABCC8</i>	Recessive mutations causing loss of MgADP and drug sensitivity despite membrane resident channels eg. T1139M, R1215Q	(Shyng <i>et al.</i> , 1998)
	<i>ABCC8</i>	Dominant mutations causing reduced sensitivity to metabolic inhibition and drug activation eg. V187D, E1506K	(Otonkoski <i>et al.</i> , 1999; Huopio <i>et al.</i> , 2000; Kapoor <i>et al.</i> , 2011)
Neonatal Diabetes	<i>KCNJ11</i>	Missense mutations causing ATP insensitivity and GOF eg. E227K, E229K	(Gloyn <i>et al.</i> , 2004; Girard <i>et al.</i> , 2006; Vedovato <i>et al.</i> , 2016)
	<i>KCNJ11</i>	In-frame deletion Kir6.2-28Δ32 causing ATP insensitivity and GOF	(Craig <i>et al.</i> , 2009)
	<i>ABCC8</i>	Missense mutations causing ATP insensitivity and GOF eg. L213R, I1424V	(Babenko <i>et al.</i> , 2006)

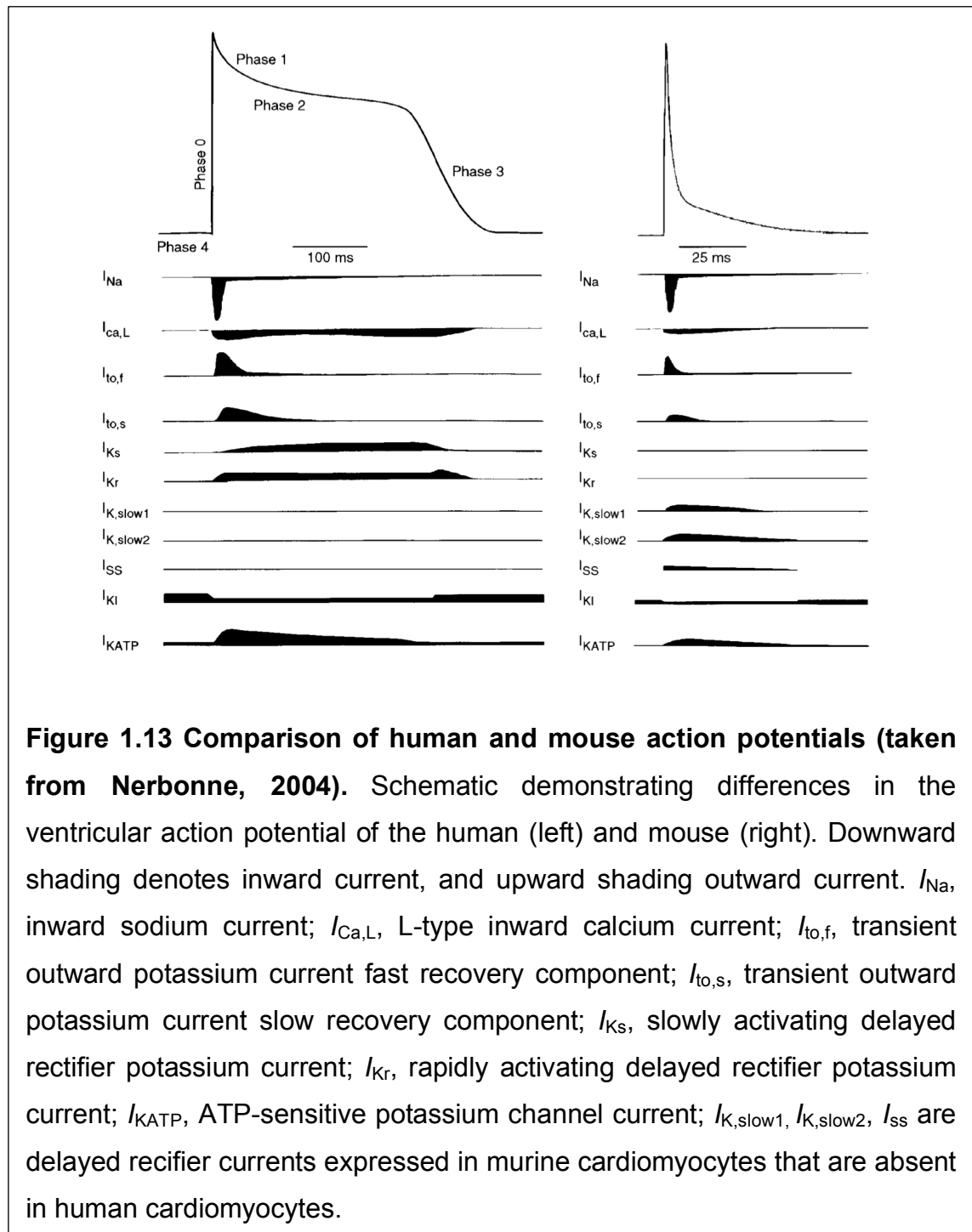
(Table 1 Continued)

Type 2 Diabetes	<i>KCNJ11</i>	E23K mutant causing modest ATP insensitivity and GOF	(Gloyn <i>et al.</i> , 2003)
	<i>ABCC8</i>	S1369A variant when co-expressed with <i>KCNJ11</i> E23K variant causes ATP insensitivity and GOF	(Hamming <i>et al.</i> , 2009)
<i>CANTÚ SYNDROME</i>			
Hypertrichosis, Osteochondrodysplasia, Cardiomegaly and concentric hypertrophy	<i>KCNJ8</i>	Missense non-synonymous variant V65M, functional characteristics not confirmed	(Brownstein <i>et al.</i> , 2013)
	<i>ABCC9</i>	Missense mutations leading to reduced ATP sensitivity or increased MgADP activation and GOF eg. P432L, A478V, C1043Y	(Harakalova <i>et al.</i> , 2012; van Bon <i>et al.</i> , 2012; Cooper <i>et al.</i> , 2015)

(Table 1 Continued)

1.4 The Mouse Heart as a Model for Investigating Arrhythmia Mechanisms and Therapies

The stark differences in body surface area to volume ratio of the mouse compared to larger mammals are exhibited again by differences in cardiac electrophysiological properties. The murine heart rate ranges from 500-700 beats per minute (bpm) as compared to the normal human range ~40-180bpm



and the murine action potential is markedly shorter (~50-80ms) than the human (~250-300ms) (Kaese & Verheule, 2012) (see Figure 1.13).

Where similar ion channel expression occurs between mice and human so too largely does the molecular composition (Nerbonne & Kass, 2005). The only exception is with regards the fast recovering transient outward current, $I_{to,f}$ where the pore-forming subunit in the mouse is made up of a heteromultimer of Kv4.2 and Kv4.3 subunits as opposed to a homomultimer of Kv4.3 subunits in human (Nerbonne, 2004). Murine nodal cells share similar ion channel and gap junction protein expression, together with nodal structure, to that of human but $I_{to,s}$ is the major repolarising current (Nerbonne & Kass, 2005; Kaese & Verheule, 2012). In the atria and ventricles the fast depolarising phase 0 upstroke is supplied, as in human, by the Nav1.5 sodium channel (Nerbonne, 2004). There is, however, a much lower contribution of inward calcium current and late persistent sodium current in the mouse and as such there is merely a gradual repolarisation and no spike and notch of phase 1 and a loss of dome in phase 2 (Nerbonne, 2004; Kaese & Verheule, 2012). This is also compounded by ~90% of calcium extrusion being through SERCA at the SR and only a small contribution by forward mode $I_{Na/Ca}$ current. In the human this is more like 70:30 in favour of SERCA under steady state conditions (Bers, 2002). Calcium handling, is therefore, different in the mouse and this will have implications on arrhythmia mechanisms. The major repolarising currents in mouse atria and ventricle are I_{Kslow1} (Kv1.5, the molecular correlate of which in the human produces the atrial specific I_{Kur} current) and I_{Kslow2} (Kv2.1), along with I_{to} (Nerbonne, 2004). There is negligible expression of I_{Kr} and I_{Ks} . KChIP2 also provides the auxiliary subunit for I_{to} as it does in human, except regional and transmural expression is dependent on pore expression rather than KChIP2 expression, as in the human ventricular wall (Nerbonne, 2004). Mice share molecular correlates for I_{KATP} , I_{K1} and $I_{KACH,Ado}$ (Nerbonne & Kass, 2005). Connexon expression largely mirrors that of humans (Kaese & Verheule, 2012). Conduction velocity in the mouse is not too dissimilar to larger mammals (~50-60cm/s) and thus surface ECG parameters and timings are much shorter given the shorter distances impulses must travel in the murine heart (Kaese & Verheule, 2012). Owing to the murine myocardial wall being much thinner than the human, and due to much more subtle dispersion in repolarisation times, the

surface T wave of the mouse is a much more subtle feature. Despite the above, incidence of arrhythmias still appears higher when there is increased dispersion of repolarisation (Nerbonne, 2004). Despite the small area and volume of murine atria and ventricles, and the small wavefront path length that would be required for re-entry, re-entrant arrhythmias have been demonstrated in murine hearts and cholinergic atrial fibrillation with shortening ERP has also been demonstrated (Wakimoto *et al.*, 2001; Opel *et al.*, 2015). Induced fibrosis has also contributed to arrhythmogenicity as we see in human (Choi *et al.*, 2012; Kaese & Verheule, 2012). Spiral waves too have been observed as have triggered induced mechanisms for both ventricular and atrial arrhythmia (Comtois *et al.*, 2005; Kaese & Verheule, 2012). Transgenic mice with knockdown of I_{to} and I_{Kslow} have shown QT prolongation and a higher incidence of ventricular arrhythmias (Nerbonne, 2004).

Transgenic models might alter gene expression in different ways in the mouse compared to the human, the species' do not share identical ion channel expression patterns and of course the mouse heart size introduces technical issues. However, all proposed human arrhythmia substrates are demonstrable in the mouse and with similar mechanisms. This together with the relative ease of housing smaller animals and breeding transgenic models means costs are also lower and logistics favourable. The mouse is still a reasonable model for studying cardiac arrhythmia.

Other possible models with similar logistical ease might be the zebrafish, though it does not share the same structural cardiac similarities to human that the mouse affords and, thus, as a whole heart model is not as favourable (Verkerk & Remme, 2012). Inducible pluripotent stem cells re-programmed from, for example, skin cells received from patients, are an exciting area of development but experience from our own lab shows how early we are with this model. Cells are immature and do not exhibit the full array of currents and another disadvantage is the lack of a whole heart model, though strides are being made to overcome this (Tiscornia *et al.*, 2011; Jackman *et al.*, 2015; Tzatzalos *et al.*, 2016; Lemoine *et al.*, 2018).

1.5 Hypotheses

A

1. Kir6.1, in addition to Kir6.2, is an important pore-forming subunit in atrial cardiomyocytes.
2. There is a differential K_{ATP} subunit expression between cardiac chambers that would make it plausible to pharmacologically manipulate K_{ATP} channels in the atria selectively as a drug target for atrial arrhythmias.

B

Manipulation of K_{ATP} channels in cardiac muscle can be anti-arrhythmic:

1. Channel opening will hyperpolarise cardiomyocytes tending to reduce automaticity and/or triggered activity.
2. Channel inhibition will prolong ERP theoretically attenuating the inducibility of re-entrant arrhythmias.

1.6 Aims

1. To define the K_{ATP} subunit expression and current characteristics in the atria and ventricles of mouse heart and to compare this with human atria.
2. To examine the role of K_{ATP} channels in the genesis of abnormal atrial rhythm using pharmacological approaches in a murine model with global deletion of either Kir6.1 or Kir6.2, and utilising HL-1 cells.

Section 2: Methods

2.1 Molecular Biology and Cell Culture

2.1.1 HEK293 stable cell lines expressing K_{ATP} subunits

My first task was to develop a system by which I could use subunit-specificity of K_{ATP} openers and inhibitors to delineate the K_{ATP} subunit composition of a population of K_{ATP} channels in a cell.

K_{ATP} channels composed of all combinations of a homomultimer of pore-forming subunits with a homomultimer of sulphonylurea receptor subunits were stably overexpressed in HEK293 cells, originally acquired by the laboratory as a gift from Professor L. Y. Jan (University of California, San Francisco, USA).

Whole-cell patch clamp would be performed on these cells in the presence of K_{ATP} openers and inhibitors.

2.1.1.1 Materials

cDNAs encoding the Kir6x pore-forming subunits were propagated in the pcDNA3.1/Zeo(+) mammalian expression vector (Life Technologies Ltd Invitrogen Division, Paisley, UK) and had been previously obtained by the laboratory as a gift from Professor S. Seino (Chiba University School of Medicine, Chiba, Japan). cDNAs encoding the SURx subunits were propagated in the pcDNA3 mammalian expression vector (Life Technologies Ltd Invitrogen Division, Paisley, UK). SUR1 cDNA had been previously obtained as a gift from Professor J. Bryan (Baylor College of Medicine, Houston, USA). SUR2A and SUR2B cDNAs had been previously obtained as a gift from Professor Y. Kurachi (Osaka University, Osaka, Japan). Sanger sequencing performed at the William Harvey Research Institute Genome Centre, confirmed the identity and species of the cDNAs: Kir6.1 cDNA belonged to rat; Kir6.2 cDNA belonged to mouse; SUR1 cDNA belonged to hamster; SUR2A and SUR2B cDNAs belonged to mouse (Inagaki *et al.*, 1995a; Hambrock *et al.*, 1999). The Qiagen[®] Plasmid Midi Kit (Qiagen, Manchester, UK) was used when required for plasmid amplification, G-418 disulphate from Melford Laboratories Ltd (Ipswich, UK) and

Zeocin from Life Technologies Ltd Invitrogen Division (Paisley, UK). Cell culture medium was Gibco™ MEM (+Earle's salts; +L-Glutamine) Ref 31095-029.

2.1.1.2 Derivation and culture of HEK293 cell line stably overexpressing Kir6.1/SUR1 K_{ATP} Channels

Owing to failure to derive a stable line using circular plasmids, the plasmids containing cDNA for Kir6.1 and SUR1 were first linearised. Restriction enzymes were chosen from a selection advised in the manufacturer's guidelines to cut at one site on the plasmid. The chosen restriction enzymes were then checked against the New England Biolabs database NEBcutter V2.0 (www.nc2.neb.com) so as to ensure they would not cut in the sequence of the gene of interest. The restriction enzyme MfeI (with Cutsmart Buffer) was used to linearise Kir6.1 and PvuI (with Buffer 3.1) to linearise SUR1. Enzymes and buffers were obtained from New England Biolabs (Hitchin, UK). Buffers were chosen as per the manufacturer's guidelines. A reaction mixture consisted of 5µg of plasmid cDNA, 10U of restriction enzyme, 2µl of 1X buffer and all made up to 20µl with double-distilled water. All reagents were kept on ice until the start of the reaction, which took place incubated at 37°C for 2 hours as per the manufacturer's guidelines. The reaction products were then purified using the Qiagen QIAquick PCR Purification Kit from Qiagen (Manchester, UK) as per the manufacturer's instructions. The concentration of DNA was analysed using a NanoDrop® 1000 spectrophotometer.

The purified cDNA was transfected into HEK293 cells using Lipofectamine® 2000 transfection reagent (Life Technologies Ltd Invitrogen Division, Paisley, UK) as per the manufacturer's guidelines. Briefly, 5µl Lipofectamine® 2000 was added to 195µl Opti-MEM® I (Life Technologies Ltd Invitrogen Division, Paisley, UK). Separately, 250ng of Kir6.1 cDNA and 1000ng SUR1 cDNA were made up to 200µl with Opti-MEM® I. The Lipofectamine® 2000/Opti-MEM® I mixture was then mixed gently with the Opti-MEM® I/cDNA mixture and left for 20 minutes at room temperature.

Wild-type HEK293 cells had been cultured in 6-well (9.62cm² per well) plates to ~70% confluence in each well with ~3mls of standard media (Gibco™ MEM

containing 10% foetal bovine serum + 1% penicillin/streptomycin). The media were removed and the cells washed in 1ml of Opti-MEM® I before incubating the cells in 1ml of Opti-MEM® I. The Lipofectamine® 2000/Opti-MEM® I/cDNA mixture from above was then added drop by drop to the cells and the cell/reagent mixture incubated at 37°C/5% CO₂ for 4 hours. The Lipofectamine® 2000/Opti-MEM® I/cDNA mixture was then removed from the cells and they were washed in pre-warmed (37°C) phosphate buffered saline (PBS). The cells were trypsinised with 400µl of trypsin and seeded at 1:100, 1:1000 and 1:10000 dilutions in 100mm dishes and in 10mls antibiotic-free media (Gibco™ MEM + 10% foetal bovine serum) and incubated for 24 hours at 37°C and 5% CO₂. When cells were deemed to have seeded adequately the media were switched to the selection media (Gibco™ MEM containing 10% foetal bovine serum + 1mM G418 disulphate + 350µM Zeocin). The media were then changed every 3 to 4 days. Cell death would occur but individual "islands" of cells representing clones of individual transfection events conferring resistance to the antibiotics in the media would develop and be spatially separated. After ~3 weeks of continued selection, large and distinct colonies were "picked off" the bottom of the dishes using sterilised cotton buds, and reseeded into separate 9.62cm² wells of a 6-well plate with 3mls of selection media. Media were changed twice a week. When ~70% confluent, media were removed and cells from each well washed in warmed PBS, trypsinised with 400µl trypsin and reseeded in separate 25cm² flasks with 5mls of selection media. Selection media were then changed twice a week. When ~70% confluent media were removed, the cells washed in warmed PBS and trypsinised with 1.5mls of trypsin. Trypsin was deactivated by making up to 5mls with selection media. A proportion of cells were reseeded onto 10mm coverslips in a 6-well plate at 10-15% confluence and incubated in 3mls selection media. The rest of the cells were reseeded into a 75cm² flask made up to 10mls selection media. Media were always changed twice a week. Forty-eight hours later, cells seeded onto coverslips were suitable for electrophysiology experiments (30-40% confluent). Cells in 75cm² flasks were passaged into new 75cm² flasks at 70% confluence by removing media, washing with warmed PBS and trypsinising with 3mls trypsin. Trypsin was deactivated by the addition of selection media (up to 10mls) and a proportion, usually a 1:20 dilution, was transferred to a new 75cm² flask and made up to 10mls with selection media.

Alternatively trypsinised cells made up to 10mls with standard media could be frozen for future use by spinning at 800rpm for 3 minutes, discarding supernatant, and the pellet resuspended in 5mls of 90% foetal bovine serum/10% DMSO. 1ml aliquots of this were then placed in cryovials and frozen slowly ($\sim -1^{\circ}\text{C}/\text{min}$) in a freezing jar submerged in isopropanol in a -80°C freezer and stored thereafter at -80°C . When needed, aliquots were revived by fast thawing at 37°C in a water bath, spun at 800rpm for 3 minutes, FBS + 10% DMSO removed and the pellet resuspended in standard media and seeded into a 25cm^2 flask. 24 hours later when adequately stuck down the media were changed to selection media and passaging could continue usually with all cells being first reseeded into a 75cm^2 flask as previously described. When required, a proportion of trypsinised cells from the 75cm^2 flask could always be seeded onto 10mm coverslips in a 9.62cm^2 well at 10-15% so that in 48 hours the cells would be at 30-40% ready for patch clamp experiments (see section 2.7).

2.1.1.3 Derivation and culture of HEK293 cell line stably overexpressing Kir6.1/SUR2A K_{ATP} Channels

In this instance plasmid cDNAs for Kir6.1 and SUR2A (as described above) were used. For transfection FuGENE® HD transfection reagent (Promega Ltd, Southampton, UK) was used as per the manufacturer's guidelines. Briefly, $7\mu\text{l}$ FuGENE® HD, 500ng Kir6.1 cDNA and 2000ng SUR2A cDNA were made up to $100\mu\text{l}$ with Opti-MEM® I, mixed gently and left for 15 minutes at room temperature. Wild-type HEK293 cells had been cultured on 6-well (9.62cm^2 per well) plates at $\sim 70\%$ confluence in each well with $\sim 3\text{mls}$ of Gibco™ MEM (containing 10% foetal bovine serum + 1% penicillin/streptomycin). The FuGENE® HD/Opti-MEM® I/cDNA mixture was then added directly to the media in the 9.62cm^2 well and incubated at $37^{\circ}\text{C}/5\% \text{CO}_2$ for 4 hours. The mixture was then removed from the cells; they were washed with warmed PBS and trypsinised with $400\mu\text{l}$ of trypsin. All the trypsinised cells were then transferred to 10mls of standard media in a 100mm dish. After 24 hours when adequately stuck down the media were changed to selection media and this changed every 3 to 4 days. Cell death would occur but individual "islands" of cells representing clones of individual transfection events conferring resistance to the antibiotics in the media would develop and be spatially separated. After

~3 weeks of continued selection, large and distinct colonies were "picked off" the bottom of the dishes using sterilised cotton buds, and reseeded into separate 9.62cm² wells of a 6-well plate with 3mls of selection media. The process thereafter as per the derivation of the Kir6.1/SUR1 stable line would then be repeated.

2.1.1.4 Revival and culture of HEK293 cell lines stably overexpressing Kir6.1/SUR2B, Kir6.2/SUR2B, Kir6.2/SUR1 and Kir6.2/SUR2A K_{ATP} Channels

These cell lines had been derived previously by the laboratory using the FuGENE® HD method as described in section 2.1.1.3. 1ml aliquots stored at -80°C in FBS + 10% DMSO could be fast thawed at 37°C and revived by the process described above for the Kir6.1/SUR1 stable line.

2.1.1.5 Transforming bacteria to amplify plasmids and cDNA

When required more cDNA for the K_{ATP} subunits could be produced as follows. Lysogeny broth (LB) is a nutritionally rich medium created by Giuseppe Bertani used in promoting the growth of bacteria. The pcDNA3 and pcDNA3.1/Zeo(+) vectors confer a resistance to various antibiotics including carbenicillin. LB-Agar-carbenicillin plates were made from an autoclaved solution of two LB tablets (Sigma Aldrich Co Ltd) and 1.5g Agar (Sigma Aldrich Co Ltd) in 100ml double distilled water. Carbenicillin (Thermofisher Scientific) was made as a 100mg/ml stock and 100µL added to the 100ml LB-Agar solution making 100µg/ml solution. Plain LB was made from an autoclaved solution of two LB tablets in 100ml double distilled water for later use. Per transformation, 50µL of competent *Escherichia Coli* cells were thawed on ice to which 50-100ng (1µL of a 1:10 dilution) of cDNA-containing plasmid was added. The cell-DNA mix was further incubated on ice for 30 minutes. As a control 1µL of culture grade water (Sigma Aldrich Co Ltd) was added to a separate sample of 50µL competent cells and incubated on ice for 30 minutes. The cells were heat-shocked at 42°C for 90 seconds in a heat block to promote uptake of the exogenous plasmid and then placed on ice for a further 2 minutes. 800µL of pre-warmed (37°C) LB was then added to the cDNA-cell or H₂O-cell mixture. This mixture was then incubated at 37°C for 1 hour in a water bath. Thereafter, 100µL of the LB-

cDNA-cell or LB-H₂O-cell mixture was plated on a LB-Agar-carbenicillin plate using a spreader until all had appeared to be absorbed into the plate. The plate was incubated at 37°C overnight in an oven to promote growth.

The following morning, colonies were counted and starter cultures were initiated in LB containing carbenicillin (100µg/ml final concentration). Sterile pipette tips were used to pick off individual colonies of interest, and placed in separate falcon tubes containing 10ml of LB-carbenicillin (100µg/ml) mixture. The tubes were then placed in a shaking incubator at 37°C and at 210rpm for 5 hours to promote growth.

In the meantime, an autoclaved conical flask containing 50ml LB-carbenicillin was prepared. After 5 hours the most turbid of the starter cultures was poured into the conical flask, the top covered with foil and incubated overnight with shaking (210rpm) at 37°C.

The next morning the contents of the flask were emptied into a tube suitable for centrifugation and spun at 4000rpm at 4°C for 30 minutes and the supernatant removed leaving the bacterial pellet.

2.1.1.6 Isolation and Purification of Plasmid DNA

Plasmid DNA was isolated and purified using the Qiagen[®] Plasmid Midi Kit following the manufacturer's instructions (Qiagen, 2012). Briefly, this involves first resuspension of the bacterial pellet in Qiagen[®] resuspension buffer (containing 50mM Tris-Cl, pH 8.0; 10mM EDTA and 100µg/ml RNase A). Then lysis of the bacteria is performed using Qiagen[®] lysis buffer (200mM NaOH, 1% SDS (w/v)). Neutralisation of the lysis mixture is then achieved with Qiagen[®] neutralisation buffer (3M potassium acetate, pH 5.5). This produces a precipitate containing genomic DNA, proteins, cell debris, and potassium dodecyl sulfate. This mixture is passed through filter paper to remove the precipitated debris. QIAGEN-tips are a column allowing gravity flow of solution through a resin that binds plasmid DNA. The filtered solution is passed through a column where the resin has been equilibrated with Qiagen[®] equilibration buffer (750mM NaCl, 50mM MOPS, pH 7.0; 15% isopropanol (v/v); 0.15%

Triton[®] X-100 (v/v)). The plasmid DNA collected in the resin is then washed using Qiagen[®] wash buffer (1.0M NaCl, 50mM MOPS, pH 7.0; 15% isopropanol (v/v)) to remove contaminants including large amounts of carbohydrates. The plasmid DNA is then eluted from the resin using Qiagen[®] elution buffer (1.25M NaCl; 50mM Tris-Cl, pH 8.5; 15% isopropanol (v/v)) before being precipitated with isopropanol. The precipitated plasmid DNA is collected as a pellet via centrifugation and washed with 70% ethanol to remove precipitated salt. The 70% ethanol is also more volatile than isopropanol and in replacing it, makes the DNA easier to redissolve. After air-drying the pellet of the 70% ethanol it can be re-dissolved in RNase/DNase-free water. The concentration of DNA was checked for purity with spectrophotometry (NanoDrop[®] 1000) to ensure a 260/280 absorbance ratio of 1.8 or above.

2.1.2 HL-1 Cells

HL-1 cells are the first cell line established that can maintain the differentiated cardiomyocyte phenotype and contractile activity *in vitro* (Claycomb *et al.*, 1998). They were established by Professor William Claycomb's group (New Orleans, USA) by culturing AT-1 cells under specific conditions. AT-1 cells are murine atrial cardiomyocyte tumour cells that have been grown in a transgenic mouse in which expression of the simian virus 40 (SV40) large T antigen was targeted for expression in atrial cardiomyocytes via the atrial natriuretic factor (ANF) promoter (Field, 1988; Claycomb *et al.*, 1998). These tumour cells could be harvested and transplanted subcutaneously as ectopic grafts in other syngeneic hosts such that they would propagate as new subcutaneous tumours (Steinhelper *et al.*, 1990). On harvesting tumour cells after each transplantation, AT-1 cells would retain their cardiomyocyte phenotype in culture (Lanson *et al.*, 1992; Borisov & Claycomb, 1995). This included functional, biochemical and ultrastructural features characteristic of adult atrial myocytes. However, the phenotype was not sustainable during passage and thus it was necessary to use them as primary cells (Claycomb *et al.*, 1998).

Further investigation led to the discovery that under certain conditions, when AT-1 cells were cultured and passaged in specific media termed "Claycomb Medium" supplemented with 100µM norepinephrine, 10% FBS of a specific

batch, and 2mM L-glutamine, this would maintain the cell line and the mature cardiomyocyte phenotype even during multiple passages (Claycomb *et al.*, 1998). This cell line has been termed the HL-1 cell line. The Claycomb Medium formula remains proprietary to Sigma-Aldrich Co Ltd.

HL-1 cells have been shown to harbour an array of cardiac myocyte currents (I_f , I_{Na} , I_{CaL} , $I_{Na/Ca}$, I_K , I_{KATP}), gap junctions (Cx40, Cx43, Cx45), sarcomeric proteins (Alpha-myosin heavy chain (α MHC), Troponin, Titin, α -actin) and sarcoplasmic reticulum proteins (Ryanodine receptor (RyR2), FK506-binding protein (FKBP)) (White *et al.*, 2004; Fox *et al.*, 2005). Together with their ultrastructural features characteristic of atrial myocytes and their ability to beat both in isolation and in clusters setting up activating wavefronts, they represent a promising tool and model for cardiac myocyte electrophysiological study and investigation of arrhythmia mechanisms.

Limitations of their use include cellular heterogeneity that has been demonstrated by differences in calcium current density, connexin expression and conduction velocity between selectively cultured clones, such that there is a non-uniformity in the above parameters in non-clone-selective syncytia (Dias *et al.*, 2014). Conduction velocity across HL-1 syncytia has also been shown to be significantly slower than in mouse atrial myocytes (Dias *et al.*, 2014). An alternative argument is that heterogeneities in properties such as conduction velocity and action potential duration, together with slow conduction, appear crucial for arrhythmogenesis, and so this as a starting point in experimental cultures could also be seen as an advantage.

I wanted to first characterise, using whole-cell patch clamp, the K_{ATP} current in isolated HL-1 cells. I would then utilise the ability of clusters of HL-1 cells to beat spontaneously, to test the effects of K_{ATP} activation and inhibition on this spontaneous beating. For this I would use calcium fluorescence imaging of HL-1 syncytia.

The lab follows the instructions set out by Sigma Aldrich Co Ltd and Professor Claycomb's lab.

2.1.2.1 Materials

All materials were obtained from Sigma Aldrich Co Ltd except the HL-1 cells, which were a kind gift from Professor Claycomb. The FBS was pre-ordered to obtain a batch that had been pretested by the Claycomb lab for use with HL-1 cells to ensure a beating phenotype.

100ml of supplemented Claycomb Medium consists of: Claycomb Medium 87ml, FBS 10ml (10%), Penicillin/Streptomycin 1ml (100U/ml; 100µg/ml), Norepinephrine 1ml (from a 10mM stock; 0.1mM), L-Glutamine 1ml (from a 200mM stock; 2mM). The Claycomb Medium bottle was wrapped in aluminium foil as it is light sensitive. After two weeks the L-Glutamine was replenished.

Norepinephrine[(±)-arterenol] was first prepared by making ascorbic acid 30mM stock by adding 0.59g of ascorbic acid to 100ml of cell culture grade distilled water. 80mg of norepinephrine was then added to 25ml of the 30mM ascorbic acid. This was then filter-sterilised using a 0.2µM syringe-driven filter. 1ml volumes were aliquoted into sterile microtubes and stored at -20°C. 1ml of this 10mM stock was then used per 100ml of medium for a 0.1mM final concentration. Norepinephrine was made up fresh monthly.

L-Glutamine came as a 100X solution and was aliquoted into working volumes before addition to the medium. Otherwise it was frozen at -20°C ready for future use.

Soybean Trypsin Inhibitor was prepared by dissolving 25mg of dessicate soybean trypsin inhibitor in 100ml of Dulbecco's phosphate buffered saline (PBS; Ca²⁺-free and Mg²⁺-free). This was then filter-sterilised using a 0.2µM syringe-driven filter and stored at 4°C.

Gelatin/Fibronectin was prepared by adding 0.1g gelatin to 500ml of distilled water and autoclaved. The final concentration of dissolved gelatin was 0.02%. The fibronectin was received in a tube in liquid form at 1mg/ml and 1ml of this was added to 199ml of the 0.02% gelatin and mixed gently. Aliquots of 6ml

were then placed immediately into 15ml sterile plastic tubes and frozen to -20°C ready for future use.

2.1.2.2 Culturing HL-1 Cells

Cultures were fed 5ml for a T25 flask or 10ml for a T75 flask with supplemented Claycomb Medium every weekday. If necessary, 20ml of supplemented Claycomb Medium was added to each T75 flask on Friday afternoons and this medium was then changed again the following Monday morning.

2.1.2.3 Passaging HL-1 Cells

T75 flasks were prepared by coating the base with 3ml of gelatin/fibronectin and incubating at 37°C for 1 hour. The T75 flask of confluent HL-1 cells to be passaged had its medium removed and the cells washed with 6ml of warmed PBS. 3ml of 0.05% trypsin/EDTA was then added and the flask incubated at 37°C for 1 minute. The 0.05% trypsin/EDTA was removed and a fresh 3ml was added before further incubation at 37°C for 2 minutes. When cells had become non-adherent 3ml of wash medium (containing only Claycomb Medium + 5% FBS + Penicillin/Streptomycin 100µg/ml) was added directly to cells to inactivate the trypsin. The cells in this 6ml mixture were then transferred into a 15ml tube for centrifugation along with an extra 8ml wash medium used to rinse the flask to obtain the last remaining cells, making a total of 14ml in the 15ml tube. This was then centrifuged at 500xg for 5 minutes. Meanwhile, the gelatin/fibronectin used to coat the new T75 flasks was removed from the flasks and 9ml supplemented Claycomb Medium was added and the flask set-aside at 37°C. After centrifugation the supernatant was removed from the 15ml tube and the pellet of HL-1 cells was gently resuspended in 3ml of supplemented Claycomb Medium. 1ml of the cell suspension was then added to the 9ml of supplemented Claycomb Medium in the T75 flask for a 1:3 split.

If cells were to be used for patch clamp experiments (see also section 2.7) 10mm glass coverslips were pre-coated with 1µl gelatin/fibronectin in a 6 well plate and allowed to air dry in the culture hood for at least 1 hour. 3ml supplemented Claycomb Medium was used per well. Assuming the cells at the time of passage were ~80% confluent in a T75, and knowing that the area of each well of a 6-well plate is of the order of 9.62cm², ~80µl of resuspended cells (post centrifugation) was added to each well of medium/coverslips in the 6-well plate and gentle swirling applied to spread the cells evenly in the medium. This volume of suspension would mean cells settled in the well at ~15% confluence. Patch clamp experiments were performed ~48 hours later when the cells were ~40% confluent. The supplemented Claycomb Medium in the 9.62cm² wells was changed every day.

If cells were to be used for fluorescence microscopy experiments (see also section 2.9) they were seeded into a perfusion chamber of a multielectrode array (MEA) (Multichannel Systems, Germany). The MEA was chosen as it could be used with a compatible temperature controller (TC02, Multichannel Systems, Germany), and potentially adapted for simultaneous electrogram and fluorescence measurement though this was not implemented in my work. MEAs were pre-coated with 300 μ l gelatin/fibronectin and incubated at 37°C for 1 hour. The excess gelatin/fibronectin was then removed and the perfusion chamber washed twice with 1ml PBS. 1ml supplemented Claycomb Medium was then added per perfusion chamber. Assuming the cells at the time of passage were ~80% confluent in a T75, and knowing that the area of each perfusion chamber is of the order of 5.5cm², then ~220 μ L of resuspended cells (post centrifugation) was added to each MEA perfusion chamber and gentle swirling applied to spread the cells evenly in the medium. This volume of suspension would mean cells settled in the perfusion chamber at ~80% confluence. The medium would be changed every day. Experiments would take place 48 hours after the cells were seeded.

2.1.2.4 Freezing and Reviving Cells

The contents of one confluent T75 flask were frozen down per cryovial. The T75 flask of confluent HL-1 cells was briefly rinsed with 5ml of PBS warmed to 37°C and then removed by aspiration. 3ml 0.05% trypsin/EDTA was added to the flask, which was then incubated at 37°C for 2 minutes. After checking under microscopy that cells had become non-adherent, 3ml of soybean trypsin inhibitor was added to the flask and this 6ml mixture was then transferred to a 15ml tube for centrifugation. The flask was also rinsed with 8ml of wash medium and this 8ml added to the 15ml tube making a total volume of 14ml in the 15ml tube. The tube was centrifuged for 5 minutes at 500xg. Thereafter the supernatant was aspirated and the pellet of HL-1 cells gently resuspended in 1.5ml of freezing medium (95% FBS / 5% DMSO). The resuspended cells were then pipetted into a cryovial and this placed into a freezing jar containing room temperature isopropanol. This was then placed into a freezer at -80°C allowing the cells to freeze slowly at a rate of -1°C/minute. Cells would thereafter be stored at -80°C.

To revive cells, a T75 flask was first coated with gelatin/fibronectin for at least an hour at 37°C as previously described. The gelatin/fibronectin was removed and replaced with 10ml of supplemented Claycomb medium and the flask placed back into the incubator at 37°C to be used later. Then 10ml of wash medium was added into an empty 15ml tube and this incubated in a water bath at 37°C. A cryovial of frozen cells was fast thawed at 37°C in a water bath and transferred into the 15ml tube containing wash medium at 37°C. This was then centrifuged at 500xg for 5 minutes, the supernatant removed by aspiration and the pellet of cells gently resuspended in 5ml of supplemented Claycomb medium. This was then added to the 10ml of Medium at 37°C already in the T75 flask. When the cells had become adherent (after ~4 hours), the medium was replaced with 15ml of fresh supplemented Claycomb medium.

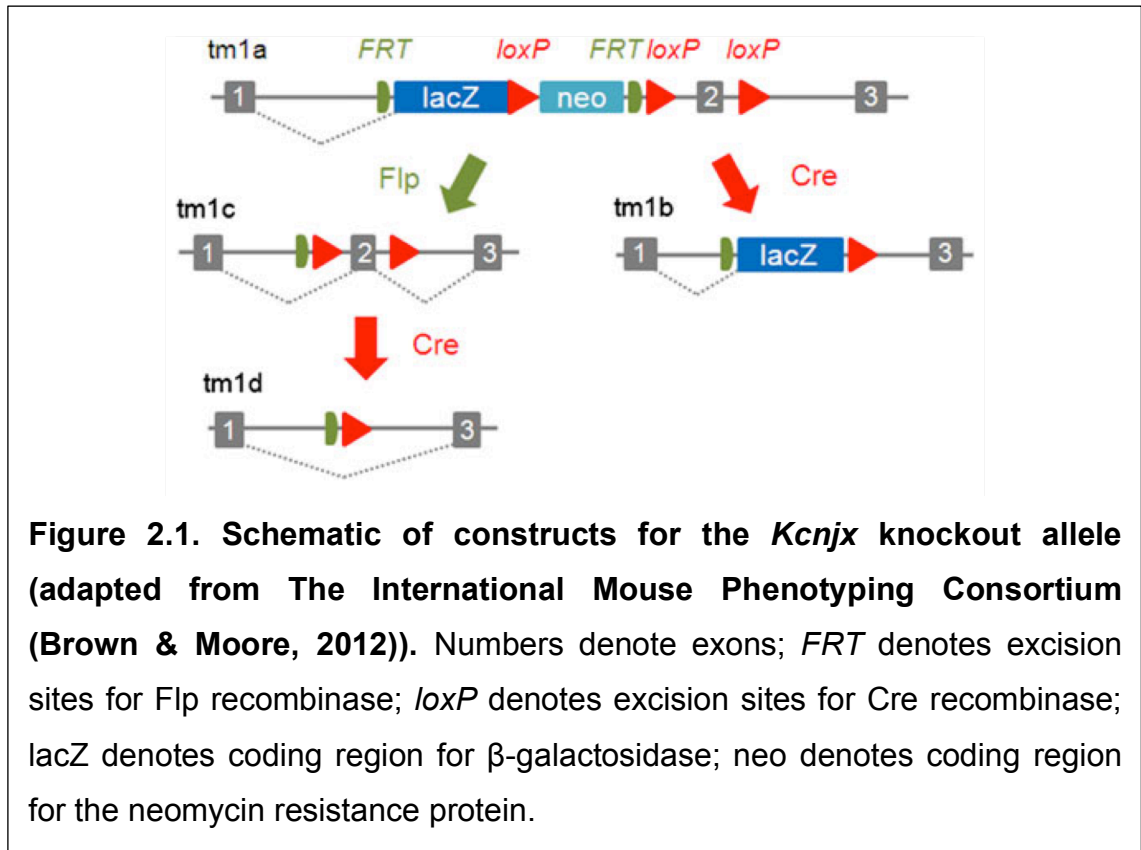
2.2 Generation of Knockout Mice

2.2.1 *Kcnj8*

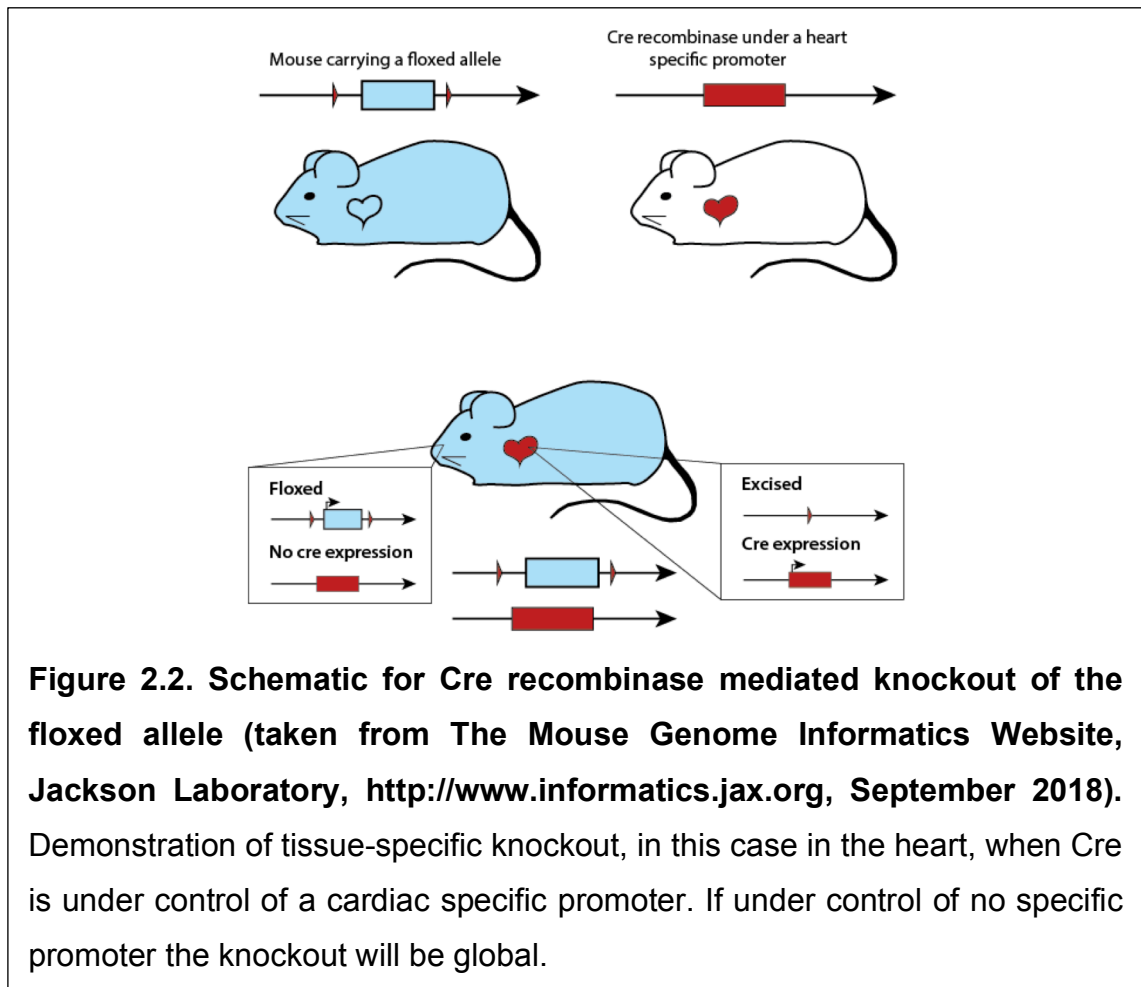
The initial aim was to produce a mouse with cardiomyocyte conditional knockout of Kir6.1 (Kir6.1-cKO) to investigate the importance of this pore-forming subunit with respect to heart muscle electrophysiology and arrhythmia. A conditional knockout would potentially circumvent concerns that the hypertensive phenotype of a global knockout (see section 1.3.1) might lead to electrophysiological changes indirectly, through an increased afterload-induced tissue substrate of both fibrosis, and stretch-induced K_{ATP} opening, or from ischaemia (Miki *et al.*, 2002; Chutkow *et al.*, 2002; Lader *et al.*, 2011).

Mice with suggested cardiomyocyte conditional, and later another line with global deletion, of exon 2 of the *Kcnj8* gene encoding the Kir6.1 subunit (rendering deletion of the ATG translation initiation codon) were produced with the help of genOway[®] (Lyon, France; project number genOway/EV/TIN1- *Kcnj8* 070206) using Cre-lox, and Flp-recombinase technology. Briefly, Flp and Cre are recombinases that will excise DNA flanked by regions known as FRT or loxP sites respectively. Homologous recombination through homology arms either side of a construct containing exon 2 of the *Kcnj8* gene and a neomycin resistance cassette, all flanked by loxP sites, enable its introduction into the specific site in the genome. FRT sites also flank the neomycin resistance cassette itself. Such a vector can be transfected into embryonic stem cells (ESCs) harvested from a developing blastocyst. ESCs exhibiting the transfected loxP flanking sequence can be selectively cultured in antibiotic-containing media since the neomycin resistance gene is expressed. The cultured ESCs are then injected back into a blastocyst before re-implantation into a pseudopregnant female (Bouabe & Okkenhaug, 2013). Chimeric pups are born and genetically modified ESCs can contribute to germ-cell formation. Flp and Cre are introduced into the genome by additive transgenesis. In additive transgenesis, the Flp or Cre carrying vector is injected directly into the pronucleus of the developing embryo and the sequence will find its way to a random site in the genome. If chimeric pups are crossed with mice expressing Flp-recombinase, pups are born where the neomycin resistance cassette is

excised. An example of one such possible group of constructs is shown in figure 2.1. Crossing animals harbouring Cre with animals harbouring the floxed allele will produce pups heterozygous for the knockout allele. Further crossing of these animals will produce pups homozygous for the knockout allele.



If Cre expression is under the control of a tissue specific promoter ablation should occur solely in that tissue (see Figure 2.2).



2.2.2 *Kcnj11*

I sought to compare, through identical experiments, the importance of each of the K_{ATP} pore-forming subunits in the murine atria. As such a mouse with global deletion of the *Kcnj11* gene encoding the Kir6.2 subunit was produced with the help of The Medical Research Council Centre for Mouse Genetics, Harwell Campus, Oxfordshire, UK (MRC Harwell) in collaboration with the International Mouse Phenotyping Consortium (Brown & Moore, 2012). Gene trapping was performed using a construct containing a *lacZ* sequence followed by a neomycin-resistance cassette (for antibiotic selective culture) followed by the exon of *Kcnj11*. The *lacZ* sequence and neomycin-resistance cassette are flanked by FRT sites and the neomycin-resistance cassette and *Kcnj11* exon are flanked by loxP sites. This construct is termed tm1a (see Figure 2.1). Homologous recombination through homology arms either side of the construct enable its integration into the specific site in the genome. A vector containing

the construct was transfected into embryonic stem cells (ESCs) harvested from a developing blastocyst. ESCs exhibiting the transfected sequence were selectively cultured in antibiotic containing media. The cultured ESCs were then injected back into a blastocyst and implanted into a pseudo-pregnant female. Chimeric pups are born and crossed with wild-type mice to enable germ line transmission. Thereafter tm1a sperm can be isolated and in-vitro fertilisation (IVF) performed in the presence of soluble Cre thus mediating excision of the loxP flanked neomycin-resistance cassette and *Kcnj11* exon, and generating pups heterozygous for the knockout tm1b allele (see Figure 2.1). When crossed these mice will give rise to litters containing pups homozygous for the knockout tm1b allele. The presence of the *lacZ* sequence under the control of the endogenous promoter means the allele can, if required, be used as a reporter for spatial *Kcnj11* gene expression as the encoded enzyme β -galactosidase forms a blue precipitate in the presence of 5-bromo-4-chloro-3-indolyl- β -D-galactopyranoside (X-gal).

All mice were of a C57BL/6N background strain.

2.3 Animal Husbandry

Animals and their offspring were maintained at Queen Mary University of London (QMUL) animal core facilities under UK Home Office guidelines relating to animal welfare. All mice were kept in a pathogen-free temperature controlled environment (21-23°C) with 12hr day/12hr night light cycles. Animals were allowed access to standard rodent chow and water. Mice were studied between 12-24 weeks of age under standardised conditions. Use of animals in all the studies was in accordance with the United Kingdom Animal (Scientific Procedure) Act of 1986. Mice showing signs of poor health and barbarisation were excluded from use. Purely owing for the need to conserve housing space, the *Kcnj11* knockout colony was bred and genotyped offsite at MRC Harwell. Experimental homozygous knockout animals and the wild-type littermate controls were transported over to QMUL animal core facilities at 6-8 weeks of age, and were acclimatised until experimental age of 12-24 weeks.

All experiments were conducted in accordance with the Guide for the Care and Use of Laboratory Animals published by the British Home Office and the US National Institutes of Health (NIH Publication No. 85-23, revised 1996). The animal work was approved by the QMUL Animal Welfare and Ethical Review Body and covered by UK Home Office project licence PPL/7665.

2.4 Genotyping

Mice were ear marked at 3-4 weeks of age for identification purposes and genomic DNA was isolated from the ear clips using 125µL of lysis buffer 402-E (proprietary of Viagen Biotech, Inc., Los Angeles, USA) containing 0.4mg/ml proteinase K (Sigma Aldrich Co Ltd). As per the manufacturer's instructions ear clips were incubated at 55°C for at least 3 hours and the proteinase K was deactivated by incubating at 85°C for 45 minutes before being cooled at room temperature for 10 minutes. The tubes were then placed in a centrifuge at 14,000rpm for a minute to pellet any undigested material such as hair. The samples were then stored at -20°C or used immediately for polymerase chain reaction (PCR).

PCR was performed using BioMix™ Red (Bioline Reagents Ltd, UK) the contents of which are proprietary but it is a ready-to-use 2x reaction mix containing a stable *Taq* DNA polymerase and an inert red dye that permits easy visualisation and direct loading onto a gel. Volumes were used as per the manufacturer's instructions:

Genomic DNA PCR mix	
BioMix™ Red	12.5µL
DNase/RNase-free Water	6.5µL
Forward Primer	2µL
Reverse Primer	2µL
DNA	2µL

2.4.1 *Kcnj8* Global Knockout

The following primers were used:

For the wild type allele -

Forward primer 21841flp-TIN1 5' ACTAGCACCTCTATCCCCAGCTCCTACC 3'

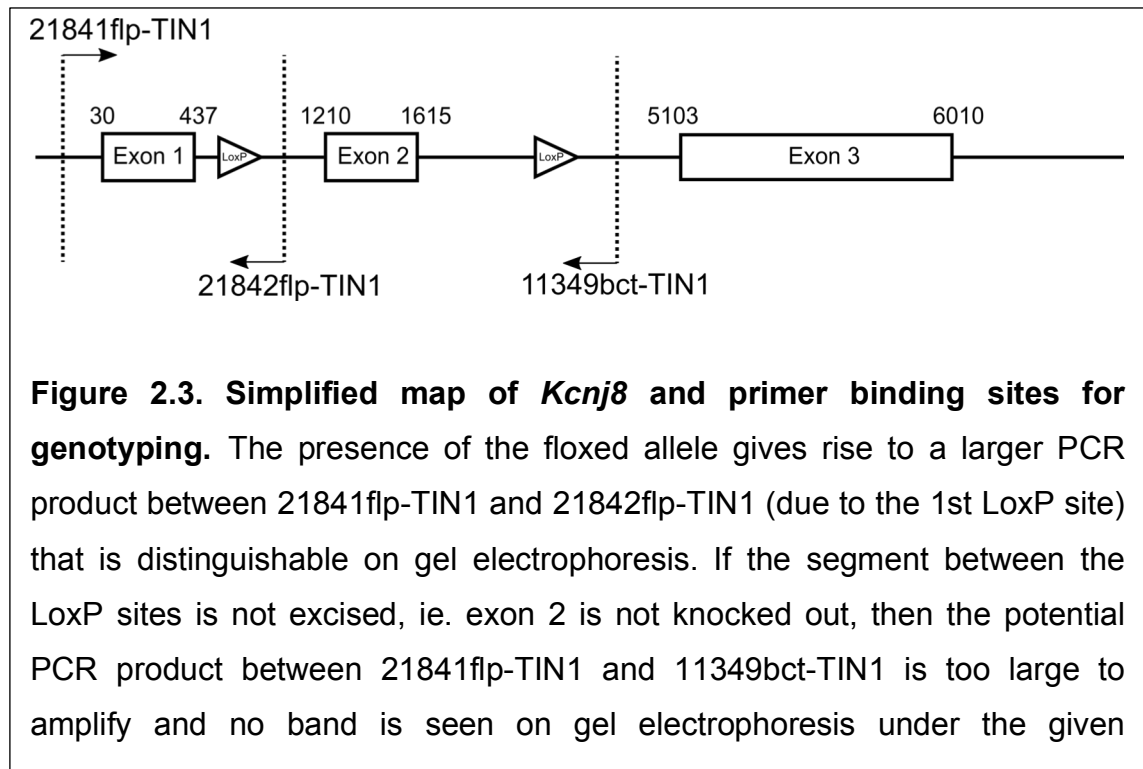
Reverse primer 21842flp-TIN1 5' CCGCCCCTCCCTCTGAACCTATATC 3'.

For the knock out allele -

Forward primer 21841flp-TIN1 5' ACTAGCACCTCTATCCCCAGCTCCTACC 3'

Reverse primer 11349bct-TIN1 5' CTGACACCAAAGCTGCCTGACAACA 3'.

Figure 2.3 demonstrates a simplified map of the *Kcnj8* gene and where the primers bind.



The following reaction conditions were followed:

Genomic DNA PCR programme <i>Kcnj8</i> Global KO	
94°C for 2 minutes	} for 35 cycles
94°C for 30 seconds	
65°C for 30 seconds	
68°C for 40 seconds	
68°C for 8 minutes	
8°C for ∞	

2.4.2 *Kcnj8* Cardiac Conditional Knockout

The following primers were used:

To determine the presence of the floxed allele -

Forward primer 21841flp-TIN1 5' ACTAGCACCTCTATCCCCAGCTCCTACC 3'

Reverse primer 21842flp-TIN1 5' CCGCCCCTCCCTCTGAACCTATATC 3'.

(See Figure 2.3).

To determine the presence of alphaMHCCre -

Forward primer CRE-ORF F [TM1408] 5' ATCCGAAAAGAAAACGTTGA 3'

Reverse primer CRE-ORF R [TM1409] 5' ATCCAGGTTACGGATATAGT 3'

The following reaction conditions were used:

Genomic DNA PCR programme alphaMHCCre	
94°C for 2 minutes	} for 34 cycles
94°C for 30 seconds	
60°C for 30 seconds	
72°C for 60 seconds	
72°C for 8 minutes	
8°C for ∞	

Genomic DNA PCR programme floxed allele	
94°C for 2 minutes	} for 35 cycles
94°C for 30 seconds	
63°C for 30 seconds	
68°C for 60 seconds	
68°C for 8 minutes	
8°C for ∞	

Products were then run on a 1% agarose gel with 5µL of Midori Green stain (Nippon Genetics Europe, Germany) per 100ml of gel.

In the case of the *Kcnj11* global knockout mice genotyping had kindly been performed at The Medical Research Council Centre for Mouse Genetics,

Harwell Campus, Oxfordshire, UK (MRC Harwell). Further characterisation of the mice was carried out using a quantitative real-time reverse transcriptase polymerase chain reaction (qRT-PCR described below).

2.5 mRNA Quantification

I sought to determine any differential expression of K_{ATP} subunits across the heart, and any differences between mouse and human using qRT-PCR.

2.5.1 Murine RNA

After undergoing schedule 1 cull via cervical dislocation, animals were harvested for cardiac atria and ventricles, the aorta and liver. Hearts were immersed in and flushed with PBS before the atrial appendages were removed and the ventricles from mid portion to apex. The aorta was also immersed in PBS and stripped and removed of para-aortic fat. Atrial appendages for each animal were combined together for RNA extraction, as were the ventricles. Not more than 30mg of each tissue type was collected. Tissue was placed in 1.5ml RNase-free tubes and placed in *RNAlater*[®] (Sigma Aldrich Co Ltd) to reduce RNA degradation.

A pestle and mortar were treated with *RNaseZap*[™] (Sigma Aldrich Co Ltd) to remove RNase and reduce RNA degradation. Tissue was then transferred to the mortar and flash frozen in liquid nitrogen before being crushed with a pestle. The crushed tissue was then transferred to a 2ml RNase-free tube.

Thereafter, RNA was extracted using the *Qiagen*[®] *RNeasy*[®] Fibrous Tissue Mini Kit as per the manufacturer's instructions (Qiagen, 2010). Briefly, this involves first disrupting and homogenising the tissue in a lysis buffer (*Qiagen*[®] RLT buffer). The composition of this remains proprietary but it contains guanidine isothiocyanate that supports the binding of RNA to the silica membrane in the RNA collection columns. Before use 10 μ L of β -mercaptoethanol (Sigma Aldrich Co Ltd) is added per 1ml of RLT buffer, which helps to inactivate RNase. Tissue disruption and homogenisation was performed with a 21-gauge needle on the end of a 1ml sterile syringe with repeated aspiration and expelling of fluid and crushed tissue until a homogenous solution had developed. After dilution with RNase-free water, 10 μ L proteinase K is added, the solution mixed and then incubated at 55°C in a heat block for 10 minutes. The addition of proteinase K helps to digest contractile proteins, connective tissue, and collagen. These

digested elements are then removed with centrifugation and the supernatant kept and mixed with an aliquot of 70% ethanol. It was then transferred to an "RNeasy column" which is a collecting column allowing flow of solution through a silica membrane under centrifugation. The silica membrane binds RNA of size > 200 nucleotides, thus allowing ribosomal and transfer RNA to pass through the membrane, and saving mRNA in the membrane. It also allows the passage of genomic DNA. A wash buffer (Qiagen[®] RW1 buffer) is then passed through the membrane under centrifugation. The composition of this remains proprietary but it too contains guanidine isothiocyanate, which supports the binding of RNA to the silica membrane. It also contains ethanol, and the buffer is said to remove biomolecules such as carbohydrates, proteins and fatty acids, that are non-specifically bound to the silica membrane. At the same time, RNA molecules larger than 200 bases remain bound to the membrane. Another milder wash buffer (Qiagen[®] RPE buffer) is then passed through the membrane under centrifugation. The composition of this remains proprietary but it contains ethanol and its main function is to remove traces of salts, which are still left on the membrane due to buffers used earlier in the protocol. Prolonged centrifugation helps to dry the membrane of residual RPE buffer or ethanol before mRNA bound to the membrane is eluted under centrifugation using RNase-free water. The concentration and purity was then checked with the use of spectrophotometry (NanoDrop[®] 1000) to ensure a 260/280 absorbance ratio of the order of 2 or above.

2.5.2 Human RNA

Isolated human total RNA from all four heart chambers (right atrium, left atrium, right ventricle and left ventricle) from three separate donors said to be "normal" with regards to no past medical history and normal cardiac structure and function, was purchased from AMS Biotechnology (Europe) Limited. Donors consisted of a 49 year old male, 69 year old male and 65 year old male.

Fifty micrograms of RNA was available for each donor-chamber sample, all with RIN of 5 or above. All the samples were diluted to 100ng/μL and separated into 10μL aliquots to be stored at -80°C before reverse transcriptase polymerase chain reaction to convert each 10μL aliquot to complementary DNA (cDNA).

Access was also obtained to fresh human atrial appendage tissue obtained from patients undergoing cardiac bypass. This was under the auspices of The Barts Cardiovascular Registry (BCVR). The BCVR is an umbrella project to collect and store biological samples and data from a multitude of patients at The Barts Heart Centre creating a bio-bank resource. The BCVR has ethical approval for a number of biosample collection processes with patients giving informed consent. Any investigator can apply to the BCVR to access these biosamples or data. I attended the operating theatre to receive fresh atrial appendage tissue from the cardiothoracic surgeon and flash freeze in *RNAlater*[®] (Sigma Aldrich Co Ltd). RNA was extracted on tissue thawed on ice using the same method as per the murine tissue (see above Qiagen[®] RNeasy[®] Fibrous Tissue Mini Kit) barring one difference. For human tissue an added optional DNase step was performed as per the manufacturer's instructions after the RW1 buffer wash step. A DNase stock is mixed with a buffer (Qiagen[®] RDD buffer). The composition of this remains proprietary but it is said to provide efficient on-column digestion of DNA and also ensures that the RNA remains bound to the column. After this DNase step there was a further RW1 buffer wash before proceeding with the same protocol as per murine tissue (see section 2.5.1).

2.5.3 Quantitative real-time reverse transcriptase polymerase chain reaction (qRT-PCR)

A two-step protocol was used to quantify the relative mRNA expression for the genes encoding the K_{ATP} subunits.

Reverse transcription (see Figure 2.4) was first performed using the High Capacity cDNA Reverse Transcription Kit (Applied Biosystems[™]).

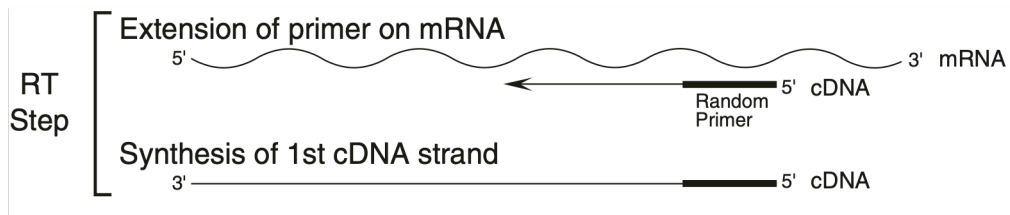


Figure 2.4. Reverse Transcription step for qRT-PCR (taken from TaqMan® Gene Expression Mastermix Protocol, Applied Biosystems™, 2010). In the first step mRNA strands are reverse transcribed to single cDNA strands. Such is the efficiency and capacity of the reaction mixture, assuming not more than 2µg of mRNA go in to the reaction mix, all mRNA is reverse transcribed.

Briefly, this involves making a reaction mix on ice and then processing in a thermal cycler as per the manufacturer's instructions:

Reverse transcription reaction mix	
10X Reverse Transcription buffer	2µL
Deoxynucleotide triphosphate mix	0.8µL
Random primers	2µL
Reverse Transcriptase	1µL
RNase Inhibitor	1µL
DNase/RNase-free Water	3.2µL
RNA (2-200ng/µL)	10µL

Reverse transcription programme
25°C for 10 minutes
37°C for 120 minutes
85°C for 5 minutes
4°C for ∞

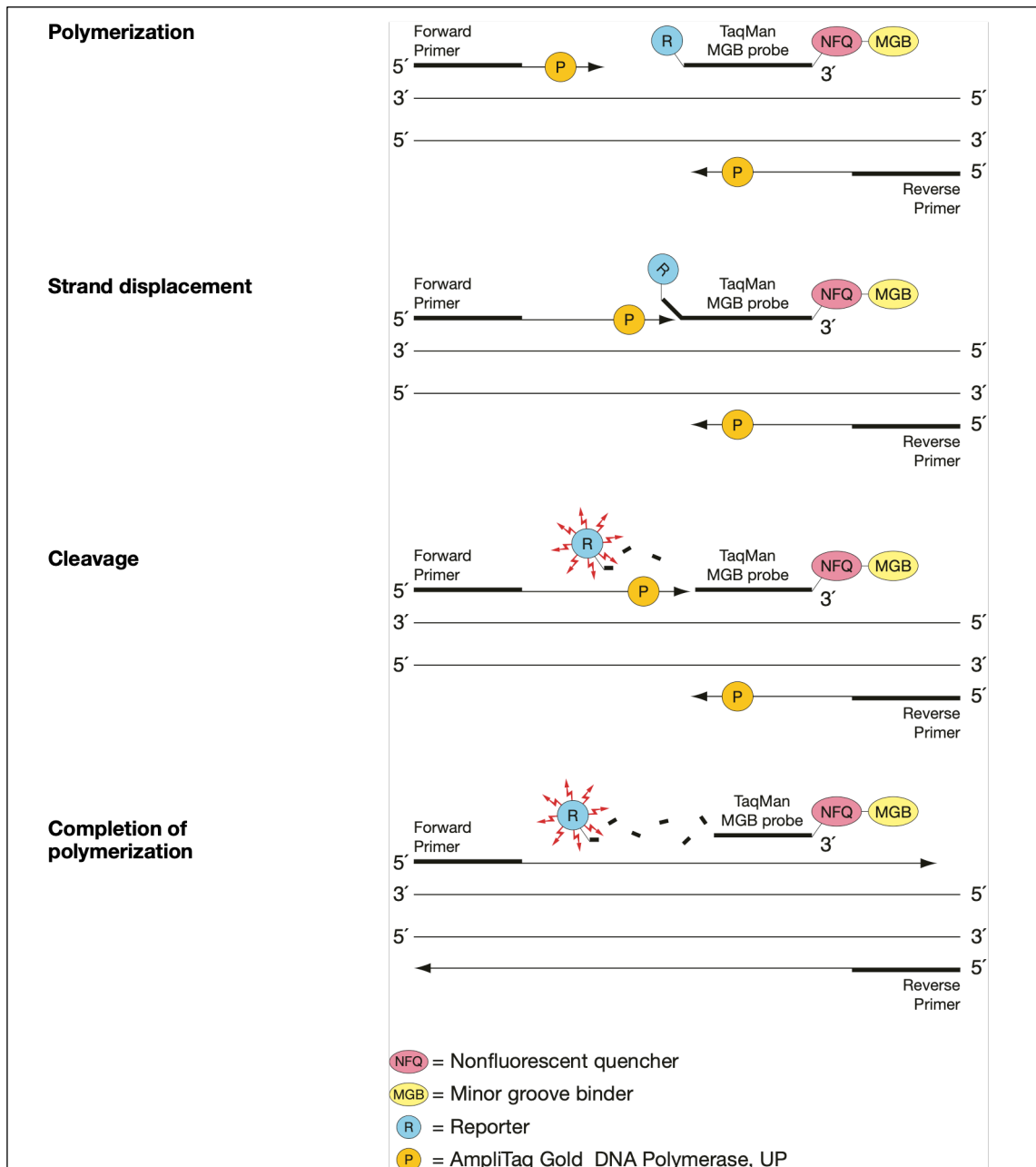


Figure 2.5. Quantitative Real-Time PCR (taken from TaqMan® Gene Expression Mastermix Protocol, Applied Biosystems™, 2010). In the second step of qRT-PCR TaqMan® probes bind specifically to sequences on the target of interest. Reporter dye is initially quenched due to Förster Resonance Energy Transfer (FRET) by the quencher end of the probe but during PCR the reporter is cleaved off allowing for fluorescence emission. This repeats itself during the PCR owing to the large amount of reaction mix available. The number of cycles required to reach a threshold fluorescence is recorded. The greater the amount of target, the lower the cycle number required to reach threshold. Fluorescence builds in an exponential fashion.

The concentration and purity of the single-stranded cDNA synthesised by this step was then quantified with spectrophotometry (NanoDrop[®] 1000) to ensure a 260/280 absorbance ratio of 1.8 or above.

Subsequently, quantitative real-time PCR was performed using inventoried TaqMan[®] gene expression assays (Applied Biosystems[™]) with FAM as the reporter dye and GAPDH as the housekeeping gene (see Figure 2.5). For each reaction cDNA was diluted in RNase-free water such that 90ng of murine cDNA and 50ng of human cDNA were used per 20 μ L reaction mix.

In the case of murine cDNA, *Kcnj8* was quantified using Assay ID: Mm00434620_m1 whose probe spans exon junction 2-3; *Kcnj11* was quantified using Assay ID: Mm00440050_s1 whose probe was designed within the exon of the gene; *Abcc8* was quantified using Assay ID: Mm00803450_m1 whose probe spans exon junction 28-29 and *Abcc9* was quantified using Assay ID: Mm00441638_m1 whose probe spans exon junction 30-31.

In the case of human cDNA, *KCNJ8* was quantified using Assay ID: Hs00958961_m1 whose probe spans exon junction 2-3; *KCNJ11* was quantified using Assay ID: Hs00265026_s1 whose probe was designed within the exon of the gene; *ABCC8* was quantified using Assay ID: Hs01093770_m1 whose probe spans exon junction 3-4; *ABCC9* transcript variant SUR2A was quantified using Assay ID: Hs02514422_s1 whose probe was designed within exon 38A and *ABCC9* transcript variant SUR2B was quantified using Assay ID: Hs02515384_s1 whose probe was designed within exon 38B. It should be noted that exon 38 at the 3' end of *ABCC9* defines the two splice variants. Variant SUR2A is encoded with exon 38A and SUR2B encoded with exon 38B.

The following mixture and PCR programme were used as per the manufacturer's instructions:

Quantitative Real-Time PCR reaction mix

TaqMan Gene Expression Master Mix (2X)	10µL
TaqMan Gene Expression Assay (20X)	1µL
cDNA Template + H ₂ O	9µL

Quantitative Real-Time PCR programme

95°C for 10 minutes
95°C for 15 seconds x 40 cycles
60°C for 1 minutes x 40 cycles

All genes were assayed in triplicate for all tissues and relative gene expression was then quantified using the $2^{-\Delta\Delta Ct}$ method (Livak & Schmittgen, 2001). Using this method, the exact copy number of target molecules is not required to measure the relative quantification between two different sets of target. Instead the number of cycles of real-time PCR reaction required of a target to reach threshold fluorescence can be used. If X_T is the number of target molecules when threshold fluorescence has been reached, then

$$X_T = X_0 \cdot (1 + E_x)^{Ct,x} = K_x \quad [1]$$

where X_0 is the initial number of target molecules, E_x is the efficiency of target amplification, Ct,x is the threshold cycle number for target amplification and K_x is a constant. Avoiding the use of absolute copy number requires normalising to an internal control reference gene that will have stability in expression through a range of experimental conditions. Standard housekeeping genes, such as GAPDH, make for good reference genes and GAPDH was chosen for this study based on its attributes in this context (Livak & Schmittgen, 2001; Vandesompele *et al.*, 2002). Equation 1 can then be applied to the reference

$$R_T = R_0 \cdot (1 + E_R)^{Ct,R} = K_R \quad [2]$$

where R_T is the number of reference molecules when threshold fluorescence has been reached, R_0 is the initial number of reference molecules (which should

be stable between preparations and only depend on the quality of the preparation affecting both reference and target), E_R is the efficiency of reference amplification, $Ct_{,R}$ is the threshold cycle number for reference amplification and K_R is a constant. Therefore, if

$$X_N = X_0/R_0 = \text{amount of target } X \text{ normalised to reference } R \text{ [3]}$$

and,

$$X_T/R_T = K \text{ (a constant) [4]}$$

and assuming the efficiencies of the target and reference are the same, then dividing equation 1 by equation 2 and rearranging gives,

$$X_N = K.(1 + E)^{-\Delta Ct} \text{ [5]}$$

where ΔCt is the difference in threshold cycles for target and reference ($Ct_{,X} - Ct_{,R}$). If the same process is performed for a separate experimental condition or different gene target, in order to make a relative comparison, then the amount of target 1 q normalised to a reference (in this case GAPDH) and relative to a calibrator target 2 cb is given by,

$$X_{N,q} / X_{N,cb} = K.(1 + E)^{-\Delta Ct,q} / K.(1 + E)^{-\Delta Ct,cb} = (1 + E)^{-\Delta\Delta Ct} \text{ [6]}$$

where $-\Delta\Delta Ct = -(\Delta Ct,q - \Delta Ct,cb)$. In this study utilising the commercially available probes and reaction mixtures, the efficiency is close to 1 and thus equation 6 can be re-written

$$\text{amount of target relative to calibrator} = 2^{-\Delta\Delta Ct} \text{ [7]}$$

2.6 Isolation of Murine Atrial Myocytes

Apart from relative expression using qRT-PCR, I wanted to perform whole-cell patch clamp on isolated murine atrial myocytes. I would utilise the pharmacological tools developed using the HEK293 stable lines to delineate the K_{ATP} subunit composition in the murine atrial myocytes. I would also detect any changes in current in the knockout mice.

Animals underwent schedule one killing via cervical dislocation. Hearts were then rapidly excised and placed in a warm Tyrode's solution at 37°C consisting of (in mM); NaCl 140, KCl 5.4, KH_2PO_4 1.2, $CaCl_2$ 1.8, $MgCl_2$ 1, HEPES-NaOH 5, D-Glucose 5.5 (adjusted to pH 7.4 with NaOH). Using a small incision, the ventricles were flushed with Tyrode's to remove blood and then the left and right atrial appendages were removed and each cut into 4 pieces. Piece-meal atria were then placed in a low Mg^{2+}/Ca^{2+} solution for 6 minutes at 37°C containing (in mM); NaCl 140, KCl 5.4, KH_2PO_4 1.2, $CaCl_2$ 0.2, $MgCl_2$ 0.5, HEPES-NaOH 5, D-Glucose 5.5, Bovine serum albumin (BSA) 1mg/ml, Taurine 50 (adjusted to pH 6.9 with NaOH). This solution helps to disrupt intercellular connections at the intercalated discs. The tissue was then digested for 20 minutes in low Mg^{2+}/Ca^{2+} solution at 37°C also containing 1mg/ml Collagenase Type 2 (Worthington Biochemical Corporation), 1mg/ml Bacterial Protease Type 14 (Sigma Aldrich Co Ltd) and $CaCl_2$ 400µM. Gentle agitation with a fire-polished Pasteur pipette was applied every 5 minutes. The tissue was then washed 4 times (total of 12 minutes) in modified Kraft-Brühe solution (KB) at 37°C containing (in mM); KCl 20, KH_2PO_4 10, BSA 1mg/ml, Taurine 10, L-Glutamic acid 70, KOH 80, HEPES-KOH 10 (adjusted to pH 7.4 with KOH). The KB solution stops enzymatic dissociation. Atrial cells were further dissociated manually in the KB solution using a fire-polished Pasteur pipette and allowed to rest for 5 minutes prior to re-adaptation. Cells were allowed to re-adapt to physiological levels of Na^+ and Ca^{2+} by incremental addition of a solution containing 10mM NaCl and 1.8mM $CaCl_2$ and finally Tyrode's solution with 1mg/ml BSA.

Cells were centrifuged at 700rpm for 7 minutes after which some of the supernatant was removed before gentle resuspension to make a more

concentrated mixture of cells. Cells were then plated on laminin-coated 10mm coverslips and left for 30 minutes at 37°C before being bathed in Tyrode's solution with 1mg/ml BSA at 37°C for a further 30 minutes prior to patch clamp recordings.

2.7 Patch Clamp Recordings from Isolated Cells

2.7.1 The Patch Clamp Technique

2.7.1.1 The Equilibrium Potential

If a selectively permeable membrane separates two ionic solutions of differing ionic concentrations, selective ions will tend to flow from one side of the membrane to the other from the side of highest concentration to that of the lower concentration, i.e. down the concentration gradient, until the potential difference set up by the net flow of charge opposes the concentration gradient. This potential difference is said to be the “Equilibrium Potential” and is dependent on the different concentrations of the selectively permeable ions on either side of the membrane (Molleman, 2003). In a simple example of two solutions, one containing sodium chloride (NaCl) and the other potassium chloride (KCl) each of the same concentration, and separated by a potassium (K^+) selective permeable membrane, potassium ions will flow down their concentration gradient from the KCl solution to the NaCl solution (see Figure 2.6). Initially the net charge on either side of the membrane is equal, but as now only K^+ ions are flowing a net negative charge develops on the original KCl side of the membrane and a net positive charge on the original NaCl side of the membrane. As more K^+ ions flow the potential difference across the membrane builds until the electrochemical gradient is neutral for K^+ . That is the concentration gradient is balanced by the electrical gradient driving K^+ back across the membrane.

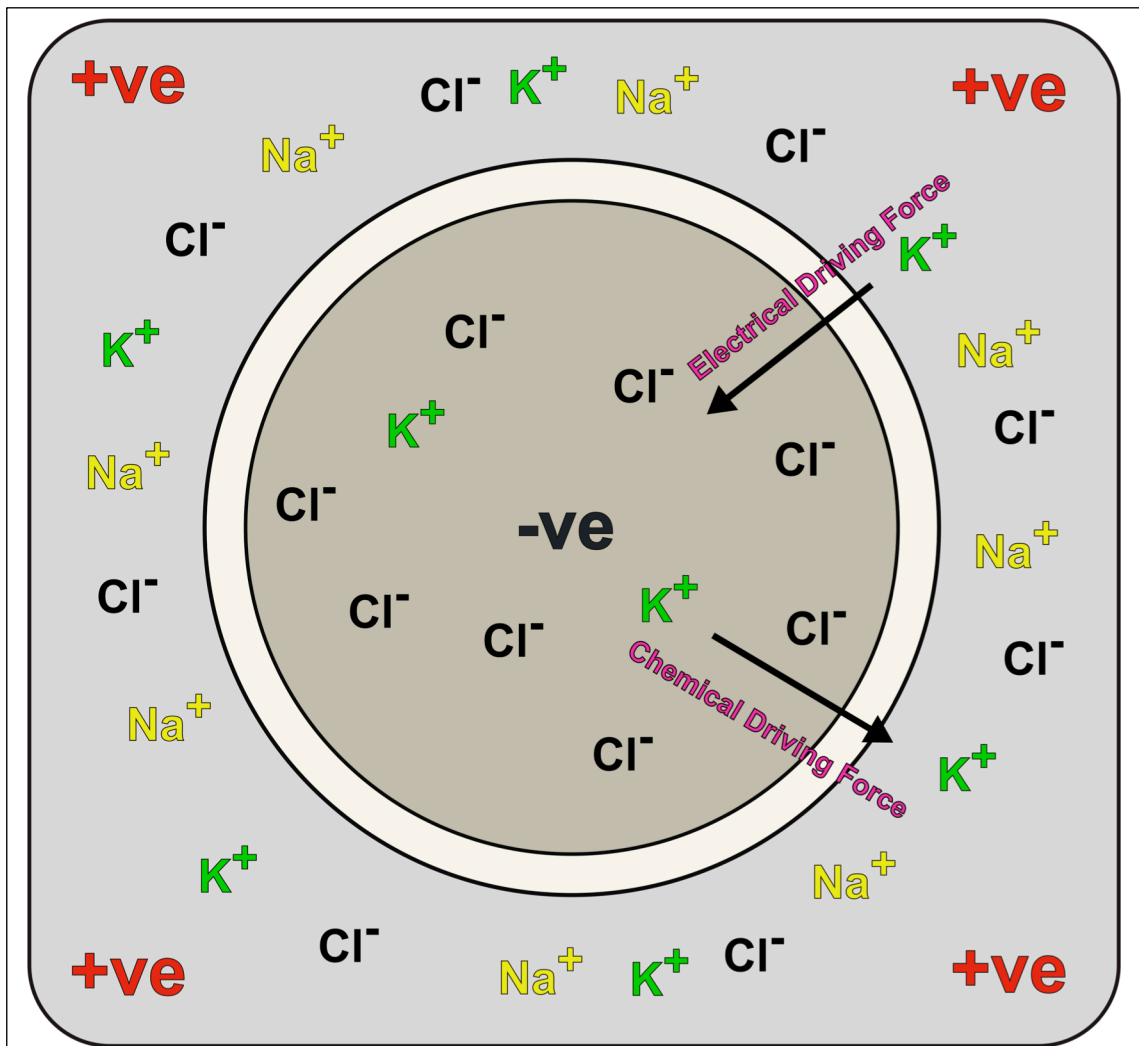


Figure 2.6. Demonstration of Equilibrium Potential. If equal concentrations of NaCl and KCl solutions exist either side of a potassium selective permeable membrane, potassium ions flow down their chemical gradient until the chemical driving force is equal to the electrical driving force created by the ensuing electrical gradient. At this point no further potassium ion flow ensues and the current will be zero. The potential difference across the membrane at this point is equal to the equilibrium potential for potassium for this set of circumstances.

If the compartments either side of the membrane are thought of as the cytosolic and extracellular sides of a cell separated by the cell membrane, then at this point of equilibrium, depending on the concentrations of an ion on either side of the membrane, the Equilibrium Potential for the ion (E), is given by the equation founded by Walter Hermann Nernst (1864-1941) known as the *Nernst Equation*:

$$E = \frac{RT}{zF} \ln \frac{[ion]_o}{[ion]_i}$$

where R is the universal gas constant (8.31 J mol⁻¹ K⁻¹), T is the temperature in Kelvin, z is the oxidation state (charge) of the ion under consideration, F is the Faraday constant (9.65 x 10⁴ C mol⁻¹), [ion]_o is the concentration of the ion under consideration on the extracellular side and [ion]_i is that on the intracellular side (Molleman, 2003).

At rest in a standard physiological extracellular solution, the mammalian cell membrane is predominantly permeable to K⁺. The intracellular concentration of K⁺ tends to be of the order of 140mM and the extracellular concentration of the order of 5mM. These concentrations are maintained largely by the Na⁺/K⁺ ATPase pump transporting Na⁺ out of the cell and K⁺ inwardly. Thus the Na⁺ concentration is higher on the extracellular side. The equilibrium potential of K⁺ at these concentrations is of the order of -80mV. However, there is still some permeability to other ions and the net resting membrane potential, after contribution of all equilibrium potentials, is usually somewhere between -50mV to -90mV. In ventricular cardiac myocytes it is more of the order of -90mV (Nerbonne & Kass, 2005). The negative sign denotes that the intracellular side is of a more negative potential with respect to the extracellular side of the cell by the magnitude indicated.

2.7.1.2 Patch Clamp Equipment set-up

Glass microelectrode capillaries can be pulled in two stages using a vertical microelectrode puller (Narishige, Japan) to create micropipettes. The capillary glass is melted via a heating coil through which the capillary is placed and centred. Pulling occurs via gravity at two temperatures resulting in separation of

the capillary and two tapered pipettes each open at the tapered end through a very small aperture of the order of 0.5-1 μ m (Hamill *et al.*, 1981). The pipettes can be backfilled with solution of desired ionic composition and then placed onto a chlorided silver wire that makes contact with a gold pin at the back of a commercially available pipette holder (Axon Instruments Inc., USA). This gold pin is then incorporated into circuitry incorporating a headstage (CV-203 BU, Axon Instruments Inc., USA), which then connects to an amplifier (Axopatch 200B, Axon Instruments Inc., USA) that controls inputs and outputs out of a command module. Analog signals are then digitised through a low-noise data acquisition system (Digidata 1440A, Axon Instruments Inc., USA) and a computer with the relevant software (pClamp 10, Axon Instruments Inc., USA) enables the user to visualise and manipulate the data in real-time. As such voltage and current commands can be sent to the probe and transmitted through the electrode in the pipette solution. The circuitry is completed via another earth electrode that sits in the “bath” solution that incubates the experimental isolated cells (see Figure 2.10). If the pipette is merely dipped into the bath, a potential difference between the pipette electrode and bath electrode is set up and a current, carried by the ions in the bath and pipette solutions thus ensues.

2.7.1.3 Single-Channel Recording

1). Cell-attached (See Figure 2.7)

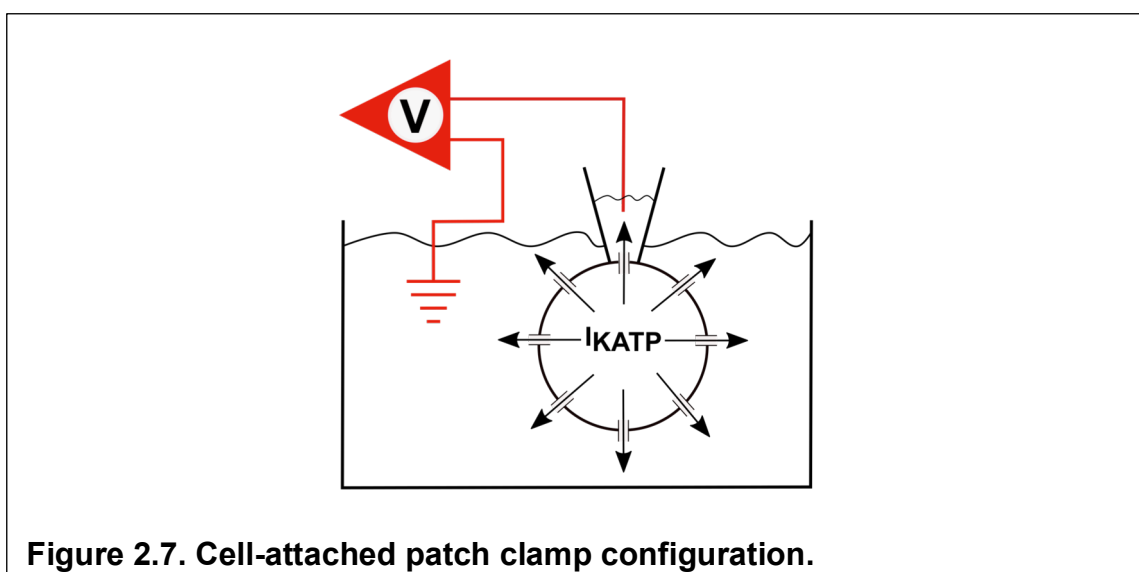


Figure 2.7. Cell-attached patch clamp configuration.

If the tip of a pipette is lowered under microscopy very lightly onto the cell surface, a seal with the cell membrane can be formed via light suction (negative pressure) through tubing connected to a side-port of the pipette holder. This seal can have a high resistance $>1\text{G}\Omega$ (known as a Giga-seal) and thus electrically isolates the patch of membrane directly subtended by the pipette tip in a configuration known as “cell-attached” (Hamill *et al.*, 1981). The resting membrane potential of the cell may not be known exactly, but it can be estimated as close to the equilibrium potential for K^+ ions (E_k). If the bath is a physiological extracellular solution with $[\text{K}^+] \sim 5\text{mM}$, E_k would be of the order of -80mV (Molleman, 2003). Given the patch of membrane subtended by the pipette tip is small relative to the surface area of the rest of the cell membrane, its resistance is very much higher than the rest of the cell membrane. Any command potential difference set up between the pipette electrode and the bath earth electrode will be dropped across the test patch of membrane due to the laws governing resistors in series (DeFelice, 1997). This added command voltage does not in essence affect the resting membrane potential of the cell as a whole, just the voltage clamped across the patch (discussed further below in section 2.7.1.5). The voltage clamped across the patch E_{patch} is then calculated as the difference between the resting membrane potential of the cell E_m (relative to the bath electrode) calculated by the Nernst equation, and the potential of the pipette electrode E_p (relative to the bath electrode):

$$E_{\text{patch}} = E_m - E_p$$

Dependent on the ion channel composition of the cell membrane and the voltage clamped across the patch or the presence of activating or inhibiting molecules, certain ion channels may or may not be contributing to the membrane permeability at that voltage clamp. If they are open and the voltage clamp is either side of the equilibrium potential of the respective ions at the concentrations governed by the cytosolic solution and pipette solution, there will be an electromotive driving force (emf) on the ions, they will move through the respective open ion channels, and current will flow. In voltage clamp, the computer and software measure this current by injecting through the amplifiers the exact opposite current needed to maintain the voltage clamp across the patch. If the opposite current was not injected, the voltage across the patch

would change until the new overall equilibrium potential, dependent on the ionic permeability of the membrane and ionic concentrations either side of the membrane with respect to this permeability was reached.

In membrane attached patch configurations such as cell-attached patch, the current through the number of ion channels in the patch subtended by the pipette tip is measured. This is a very small number compared to the total number of ion channels in the cell membrane as a whole and with pipette tips of resistance towards 5MΩ and above, conferring a pipette tip diameter of ~0.5μM or less, this can be limited in some cases to as little as 10 or fewer ion channels in the patch (Hamill *et al.*, 1981; Molleman, 2003). Openings of channels can be seen as deflections from the baseline current. The baseline current is due merely to leak current through the membrane. Single channel currents can be delineated as the smallest current deflection or smallest “level” of deflection from this baseline. Larger current deflections can be produced by a multiple number of channels open at that moment and will thus be multiples of the single channel deflection. In the case of only one type of channel in the patch, designating baseline as a level itself then there will be n+1 current levels that can be seen where n is the number of channels in the patch. It is possible to measure a single ion channel current (I) for a particular driving force (emf, electromotive force supplied by the voltage clamp of the amplifier) and then the single channel unitary conductance (g) via the equation:

$$g = emf \cdot I$$

Similarly single channel current-voltage (I-V) relationship plots can also be produced.

It is also possible to measure the open probability of the channel under the experimental conditions (driving force, ionic concentrations, and presence of opening or blocking molecules). The time that is spent at each current level can be plotted in a histogram. Due to thermal noise the current trace tends to “quiver” at each current level. The distribution of the current trace around the level due to this noise is Gaussian and this is represented in the current level amplitude histogram (Molleman, 2003). The peak of the Gaussian distribution

will represent the actual value of the current level and events due to noise lie around this mean. Using automated software packages it is possible to manually set thresholds for each current level that take into account the distribution of events around the level due to noise. This then creates an idealised trace of the dwell time at each current level and can cut down dramatically the amount of data to be stored and analysed compared with looking at the pure amplitude histogram. Open probability $P(o)$ is then the open dwell time as a proportion of the total dwell time of the recording:

$$P(o) = \frac{\sum t \text{ open}}{\sum t \text{ open} + \sum t \text{ closed}}$$

The dwell times take into account the number of channels involved in the open or closed time. i.e. time spent at a current level of 3 involves 3 channels open and a multiplication factor of 3 will be applied to the open dwell time apportioned to this level. If the total number of channels in the patch is 4, then 1 channel must be closed at a current level of 3, and therefore this contributes to the closed dwell time of the recording with a multiplication factor of 1.

2). *Inside-Out Patch (See Figure 2.8)*

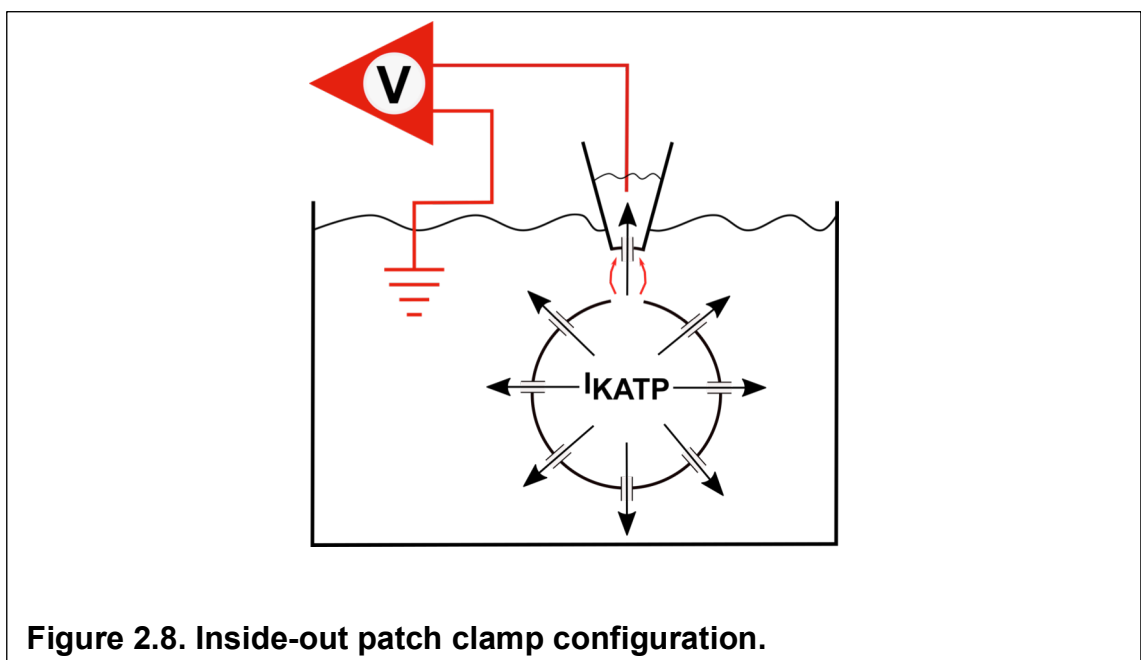


Figure 2.8. Inside-out patch clamp configuration.

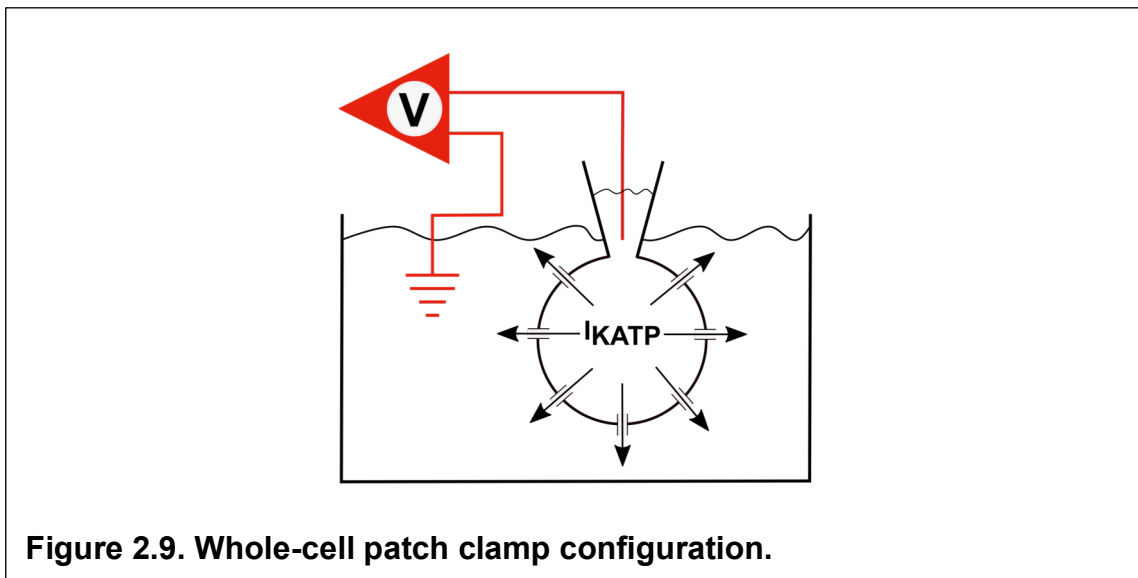
The main disadvantage of the cell-attached configuration is the requirement to estimate the resting membrane potential of the cell and thus not knowing exactly the voltage clamp and driving force across the patch subtended by the pipette tip (Molleman, 2003). Given that the seal generated between the pipette and the cell membrane can be very tight, it is possible to lift the pipette off the cell pulling with it the piece of membrane subtended by the pipette tip together with excess membrane that then forms a vesicle at the tip of the pipette. If the pipette is then lifted momentarily out of the bath the vesicle disperses leaving just the piece of membrane subtended by the pipette. This piece of membrane is such that if the pipette is lowered back into the bath, what was the intracellular side of the membrane is facing outwards and is in contact with the bath solution ("inside-out"), and what was the extracellular side of the membrane subtended by the pipette tip and in contact with the pipette solution remains so. As such, any voltage clamp command between the pipette electrode and the bath electrode is directly dropped across the patch (E_{patch}) without the need to factor in the resting membrane potential of the cell (Molleman, 2003). An added advantage of this configuration is that with superfusion systems connected to the bath supply, dynamic changes to the virtual "intracellular" environment can be maintained and thus experimented with.

3. Outside-Out Patch

This as it suggests is similar to Inside-Out Patch but for the fact that what was the extracellular side of the membrane is now facing outwards and is in contact with the bath solution and what was the intracellular side of the membrane now becomes subtended by the pipette tip and in contact with the pipette solution. This configuration is achieved by lifting the pipette off the cell whilst in the whole-cell configuration which will be discussed below.

2.7.1.4 Whole-Cell Recording (See Figure 2.9)

After formation of a giga-seal, it is possible to rupture the patch of membrane subtended by the pipette tip by applying further negative pressure through the tubing connected to the side port of the pipette holder.



After rupture, the cell membrane still creates a seal on either side of the pipette tip, but the pipette solution is now in direct contact with the intracellular compartment through the opening of the pipette. This allows control of the voltage and current clamp of the whole of the cell membrane, hence, the name “whole-cell” recording. A process of dialysis also occurs where the pipette solution will mix through diffusion with the intracellular fluid of the cell. Given the amount of solution in the pipette is vastly greater than that of the intracellular fluid, the pipette solution will, after a period of 3-5 minutes, effectively engulf and become the intracellular fluid composition (Molleman, 2003).

2.7.1.5 Pipette and Cell Capacitance, and Series Resistance

Figure 2.10 demonstrates measuring equipment (a) and equivalent electronic schematic (b) diagrams of RC circuits moving from placing a pipette in the bath solution to getting a giga-seal in cell-attached patch and going to the whole-cell configuration. E_{pc} , R_{pc} and C_{pc} represent the driving force of the patch clamp amplifier, the resistance in the patch clamp amplifier and any stray capacitance in the amplifier circuit when the pipette is in the air. The switch S_{cpip}/S_{rpip} is a double switch that closes on entering the pipette into the bath thus exposing the amplifier to the pipette capacitance C_{pip} and pipette resistance R_{pip} . The switch S_{seal} is closed short-circuiting away from the circuit that will be provided by the cell that is not yet present. When a seal is made with the cell, S_{seal} opens exposing this circuit provided by the cell (DeFelice, 1997). R_{cap} is the resistance afforded by the cell-attached patch of membrane subtended by the

pipette tip and R_{seal} the resistance afforded by the sides of the seal itself that may have a tiny degree of leak. The hope is R_{seal} will be very large signifying a tight and not leaky seal. In cell-attached configuration it can be noted that the driving force of the amplifier is now exposed to the effects of the driving force of the membrane potential of the cell E_m , the membrane resistance of the cell R_m and the capacitance effect of the cell membrane C_m . However, what with R_{cap} being relatively large, the voltage applied by the amplifier is dropped over the patch of membrane subtended by the pipette and does little to influence the membrane potential of the cell as a whole (DeFelice, 1997). In fact therefore, the membrane potential of the cell contributes to that across the pipette-subtended patch as previously explained in the section on cell-attached patch (2.7.1.3). When the patch is ruptured going to whole-cell configuration, and simulated by closing of switch S_{acc} , this short circuits R_{cap} given the access resistance R_{acc} is much lower than R_{cap} . R_{acc} is ideally very low such that the capacitance of the membrane can be charged easily and quickly by the controlling voltage of the amplifier as a large current then flows across the pipette tip to affect the cell membrane (DeFelice, 1997). Thus the membrane potential E_m is itself then controlled by that of the amplifier by charging the membrane.

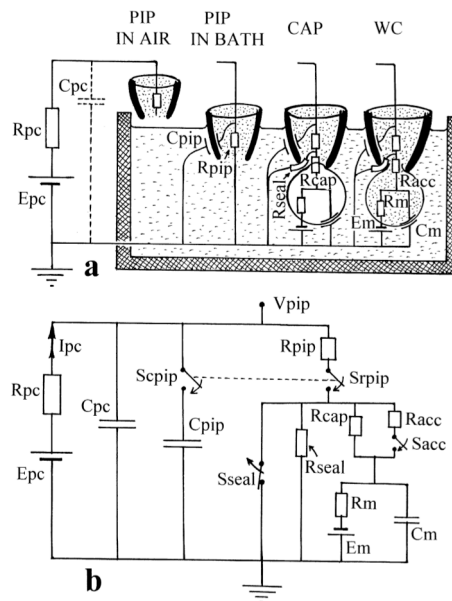


Figure 2.10. Electronic equivalent circuits demonstrating cell-attached and whole-cell patch clamp configurations (taken from DeFelice, 1997).

E_{pc} , R_{pc} and C_{pc} represent the driving force of the patch clamp amplifier, the resistance in the patch clamp amplifier and any stray capacitance in the amplifier circuit when the pipette is in the air. The switch S_{cpip}/S_{rpip} is a double switch that closes on entering the pipette into the bath thus exposing the amplifier to the pipette capacitance C_{pip} and pipette resistance R_{pip} . S_{seal} is a switch that when opens on contact with the cell exposing to the cell circuit. R_{cap} is the resistance afforded by the cell-attached patch of membrane subtended by the pipette tip and R_{seal} the resistance afforded by the sides of the seal itself that may have a tiny degree of leak. In cell-attached configuration (CAP) E_{pc} is now exposed to the effects of the driving force of the membrane potential of the cell E_m , the membrane resistance of the cell R_m and the capacitance effect of the cell membrane C_m . R_{cap} is relatively large and E_{pc} is dropped near solely over the patch of membrane subtended by the pipette. When the patch is ruptured going to whole-cell configuration, and simulated by closing of switch S_{acc} , this short circuits R_{cap} given the access resistance R_{acc} is much lower than R_{cap} . When R_{acc} is low, the capacitance of the membrane can be charged easily and quickly by E_{pc} as a large current then flows across the pipette tip to affect the cell membrane. The membrane potential E_m is itself then controlled by that of the amplifier by charging the membrane.

The pipette glass and, after membrane rupture in the whole-cell configuration, the cell membrane, both have a capacitance to store charge. As such in applying a potential difference through the circuitry there is a delay in the attainment of that potential difference across the cell membrane and as such a delay in the attainment of the driving force. The glass of the pipette and the cell membrane have capacitance (C) governed by the equation:

$$C = \frac{\epsilon \epsilon_0 A}{d}$$

where ϵ_0 is the polarisability of free space ($8.85 \times 10^{-12} \text{ CV}^{-1}\text{m}^{-1}$), ϵ is the dielectric constant of the insulator between two plates of a capacitor each of area A and separated by distance d (Axon Instruments Inc, 1993). In this case the plates are the two sides of the glass pipette or the individual layers of the lipid bilayer of the cell membrane and the insulators are the material between these layers. Ions in solution move towards the two sides of the pipette glass and cell membrane until the charge stored provides an equal and opposite potential difference across the capacitor that opposes the driving voltage of the amplifier (DeFelice, 1997). Only then is this intended voltage applied across the cell membrane.

The amount of charge Q moving towards the plates of a capacitor is related to the driving voltage E and capacitance C by the equation:

$$C = \frac{Q}{E}$$

As the charge moves it carries a current that is manifest in the recording as an excess current peak or transient that decays as the potential difference across the capacitor rises towards the driving voltage. This decay of current transient I and rise of potential difference E are described by the exponential functions:

$$I = I_0 e^{-\frac{t}{RC}}$$

$$E = E_0(1 - e^{-\frac{t}{RC}})$$

where I_0 and E_0 are the starting current and final potential difference respectively, t is the time since the driving voltage was applied by the amplifier, R is the total resistance in series of the circuit and C is the capacitance. These relationships constitute the principles governing capacitors and resistors in series known as RC circuits (DeFelice, 1997).

These capacitance current transients are not current carried across the cell membrane but will be represented in the recording unless they are accounted for. A parallel circuit that contains a variable RC circuit enables this cancellation. The parallel capacitor and resistor can be adjusted such that they provide an equal and opposite capacitance to the cell and pipette thus effectively cancelling them (Axon Instruments Inc, 1993).

The aim of voltage clamp experiments is to measure the current across the cell membrane being clamped at the driving voltage. Unfortunately, the resistances of the pipette and pipette electrode reduce the voltage that is finally dropped over the membrane, and thus the current measured, because they are in series with it and are known as the “series resistance” (Molleman, 2003). The series resistance can be estimated in the capacitance transient cancellation process because it contributes to the RC circuit as a whole. A compensatory mechanism can then be enforced where the amplifier is instructed to inject slightly more current than would be necessary to clamp at a particular voltage to compensate for the proportion of the voltage that will be dropped across the series resistance. For most cells, the amount of compensation that can be practically enforced is about 70%, with any more than this usually being detrimental to the cell because of current oscillations set up in the RC circuit (Axon Instruments Inc, 1993).

With voltage clamp the cell membrane is clamped at the controlling voltage. In order for this the resistance in the amplifier/pipette aspect of the circuit needs to be significantly lower than that of the membrane to allow fast charging (via a large current) of the pipette capacitance. This in turn enables a large potential difference to be dropped across the membrane fully charging its capacitance (DeFelice, 1997). If the resistance of the amplifier is significantly large, the various capacitances of the circuit never become fully charged as the current

passing is too small and this too includes that of the cell membrane. Whilst then the voltage of the membrane cannot be clamped this albeit small current passing through can, and if there are any endogenous variations in the membrane potential affecting this current, they can be calculated and represented by the software. This then is current clamp. If a cell activates and produces an action potential, the voltage waveform can be produced on screen by the software.

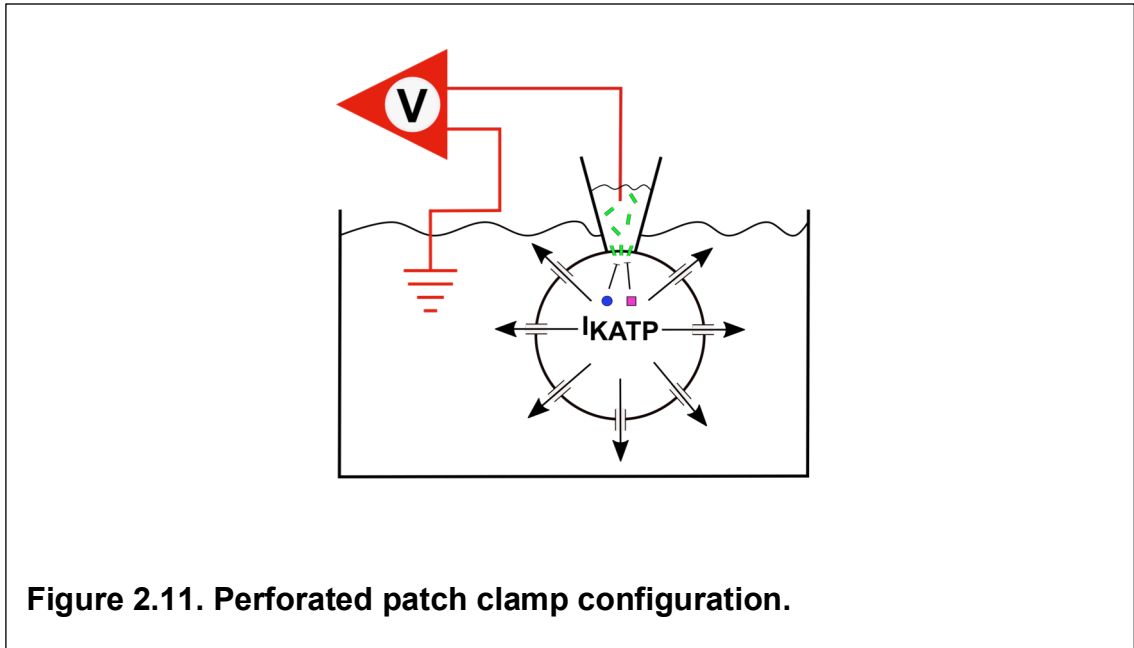
2.7.1.6 Pros and Cons of the different configurations

Whole-cell recording allows for experimenting with different environments on the intracellular side of the cell membrane as well as the extracellular environment without the added technical difficulty of achieving inside-out or outside-out patch. That said, for obtaining dose-response relationships for changes in environment on the intracellular side of the membrane, inside-out patch is superior given the ability to superfuse the bath solution with the required concentrations of investigatory ligand and gain data for these different concentrations from the same cell.

Whilst cell-attached patch would appear the most direct configuration, tight seals reaching at least $5\text{G}\Omega$ are required to limit noise on the baseline of the recording, a factor very important to delineate single channel openings (Hamill *et al.*, 1981). However, whole-cell recordings also give a whole-cell current, and thus, real-time assessment of current responses to drugs, for example, can be easier in the whole-cell configuration (Molleman, 2003). Whole-cell conductance can also be measured and whilst it is not known exactly how many ion channels exist in the whole of the cell membrane, the whole-cell current can be normalised to the cell capacitance estimated during the capacitance transient cancellation process explained above. Cell capacitance is a surrogate for the area of the cell membrane, and whilst assumptions are made that the membrane ion channel density between cells is similar, nonetheless the capacitance thus provides an estimate of the number of ion channels in the cell (Molleman, 2003). Whole-cell current can then be normalised to the cell capacitance and expressed as the current density.

A possible problem with whole-cell recording, particularly during long recording experiments, is that dialysis of the cell contents is met by the loss of molecules potentially critical to ion channel function and thus the phenomenon of “run-down” of current can ensue. The phenomenon can be overcome by Perforated Patch Whole-Cell recording.

2.7.1.7 Perforated-Patch Whole-Cell Recording (See Figure 2.11)



This involves adding an antibiotic such as amphotericin to the pipette solution. Before back filling the pipette with this antibiotic-containing solution, the pipette tip is dipped in standard pipette solution without antibiotic in order to draw up a very small amount into the pipette tip by capillary action. Thus the antibiotic containing solution will rest on top of the standard solution in the pipette and the antibiotic will slowly diffuse towards the pipette tip down its concentration gradient (Molleman, 2003). This gives just enough time to achieve a tight seal onto a cell before the antibiotic starts to make contact with the cell membrane. Antibiotics such as amphotericin, then act by slowly forming pores in the cell membrane that happen to be permeable to ions, but impermeable to the majority of intracellular and membrane bound protein species such that they are maintained in the intracellular environment. In due course, there are enough pores in the membrane to simulate a ruptured membrane in whole-cell configuration and whole-cell current can be measured by clamping voltage

across the whole-cell membrane by the access to the cell conferred by the antibiotic pores. The problem of “run-down” is also largely eliminated. The downside to perforated-patch whole-cell recording is the length of time it can take to achieve a perforated patch and the yield of good quality perforated patches achieved. Indeed it can take up to 45 minutes to achieve a cell ready for recording. In that time the cell’s health in general may have deteriorated (Molleman, 2003).

2.7.2 Experimental Conditions

Whole-cell patch clamp recordings were performed. Capacitance transients and series resistance were compensated electronically by using amplifier circuitry (Axopatch 200B). Data were filtered at 2kHz (four-pole Bessel) and sampled at 10kHz using a Digidata 1550 (Axon Instruments). Currents were acquired and analysed using pClamp10 (Axon Instruments). Whole-cell currents were recorded using a voltage-ramp protocol (-150 to +50mV over 1s at 0.1Hz). Baseline current density was taken after 3 minutes of dialysis if there was no change in current from developing the whole-cell configuration, or at plateau of current if there was any change in current after developing the whole-cell configuration. Similarly, maximum drug action was measured at plateau of any change in current. Mean current-density values at +40mV were taken from the 5 sweeps of the voltage ramp protocol after plateau was reached.

Whole-cell action potentials were recorded using the current-clamp configuration. Action potentials were triggered by 600pA/5ms square pulses at 1Hz. Data were analysed using pClamp10 (Axon Instruments) and Clampfit10 (Axon Instruments). After 3 minutes dialysis action potentials were recorded for 2 minutes with each drug condition. The last 10 action potentials of each recording period were averaged. Measurements were taken as per the schematic example in figure 2.12. V_{max} (dV/dt) was taken as the mean gradient of the upstroke of the action potential given by the change from resting to peak membrane potential (Δ) over the time for this change.

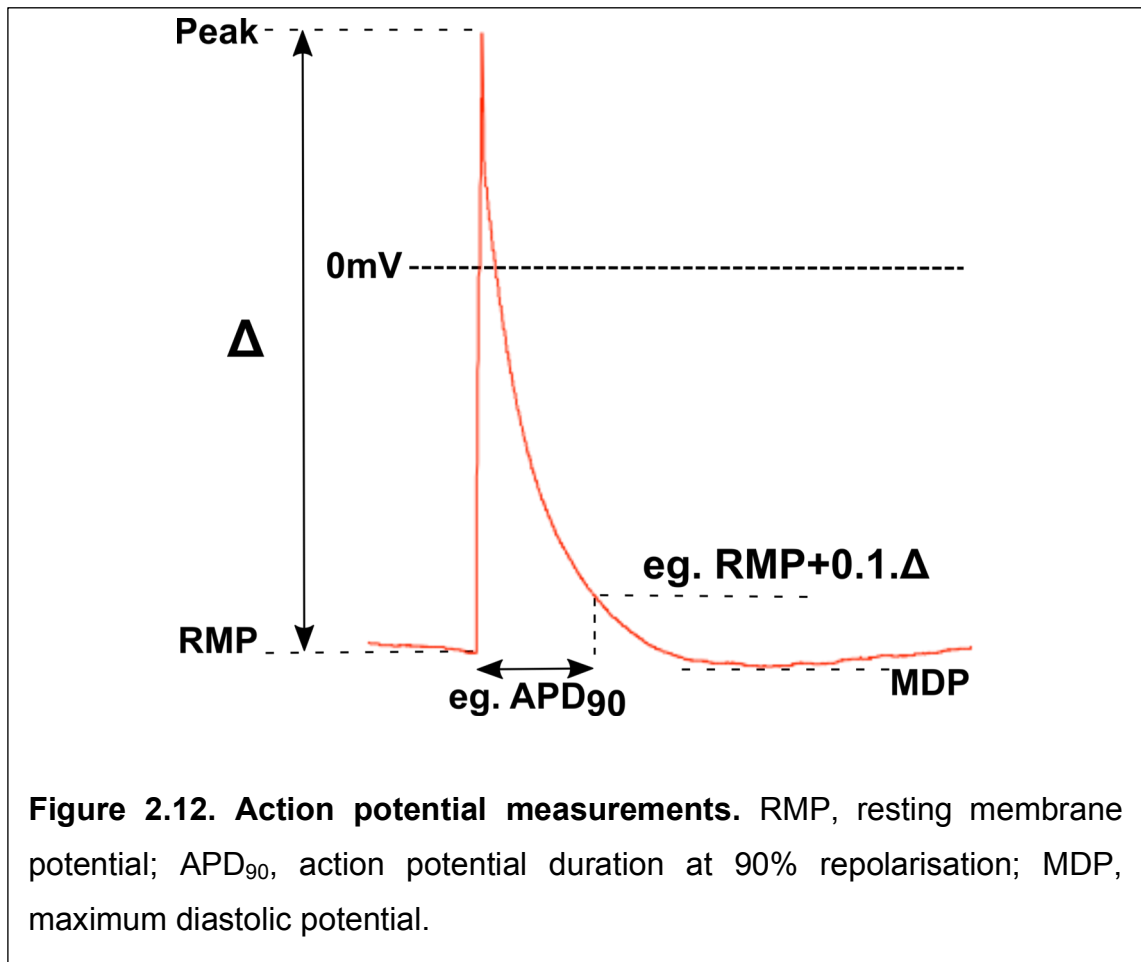


Figure 2.12. Action potential measurements. RMP, resting membrane potential; APD₉₀, action potential duration at 90% repolarisation; MDP, maximum diastolic potential.

Glass micropipettes were pulled from capillary tubes made of borosilicate with filament, 1.5mm outer diameter, 1.17mm inner diameter, 100mm length (Harvard Apparatus, USA). Pipette resistance varied between 2-3M Ω .

The pipette solution for voltage-clamp contained (mM): KCl 110, MgCl₂ 1, HEPES 10, EGTA 10, MgATP 3, Na₂ADP 1, pH 7.2 with KOH and final [K⁺] ~ 150. The bath solution contained (mM): NaCl 130, KCl 4, CaCl₂ 1.8, MgCl₂ 1, HEPES 10, D-Glucose 10, pH 7.35 with NaOH and final [Na⁺] ~ 135.

The pipette solution for current-clamp recordings contained (mM); K-Gluconate 110, KCl 20, HEPES 10, EGTA 0.05, MgCl₂ 0.5, MgATP 5, Na₂-GTP 0.3, Na₂-phosphocreatine 5, pH 7.4 using KOH.

Pipettes were backfilled with intracellular solution and the pipette tip then dipped in Sigmacote® (Sigma Aldrich Co Ltd) which is a liquid siliconising reagent that will coat glass and render it electrically inert. It is hydrophobic and thus will not coat the aperture of the pipette that is filled with pipette solution. The Sigmacote® thus helps to reduce the pipette capacitance by shielding from the bath solution when immersed.

K_{ATP} channel opening drugs diazoxide (DZX) and pinacidil (PIN) (Sigma Aldrich Co Ltd) and inhibitors glibenclamide (GLIB) and tolbutamide (TOLB) (Sigma Aldrich Co Ltd), and the inhibitor HMR1098 (HMR) (Axon Medchem BV, Netherlands), were dissolved in \geq 99.5% dimethylsulfoxide (DMSO, Sigma Aldrich Co Ltd) to make stock solutions. Stock was further diluted in extracellular solution for use in experiments. Stock solutions of diazoxide and tolbutamide were made to 100mM and those of pinacidil, glibenclamide and HMR1098 to 10mM. The suggested pore blocker PNU37883A (PNU) (Axon Medchem BV, Netherlands) was dissolved in double distilled water to make a stock solution at 10mM before further dilution in extracellular solution for use in experiments. Final concentrations for experiments were chosen based on selectivity for subunits defined by the literature (see section 1.3.2) and were as follows: diazoxide and tolbutamide 100 μ M; pinacidil, glibenclamide and HMR1098 10 μ M and PNU37883A 50 μ M. A maximum of DMSO 0.2% was used in drug-containing extracellular solutions and an extracellular solution

containing the addition of DMSO 0.2% alone was prepared as a control. Extracellular perfusate was then introduced to the bath via a gravity driven superfusion system running at ~1.5ml/minute. All experiments were conducted at room temperature.

2.8 Electrophysiology from Cardiac Tissue

Apart from looking for any significance of K_{ATP} current modulation in isolated atrial myocytes, I wanted to look for any further differences at the tissue level. Specifically, I wanted to test for differences in ERP and CV, electrophysiological parameters that contribute to arrhythmogenicity.

2.8.1 Signal analysis via the surface electrogram

When measuring electrical activity by means of electrodes placed on the surface of tissue, it is the charge build-up in the extracellular space directly beneath the electrode that leads to the potential difference measured via the electrode. Two configurations may be utilised as described below and depicted in Figure 2.13.

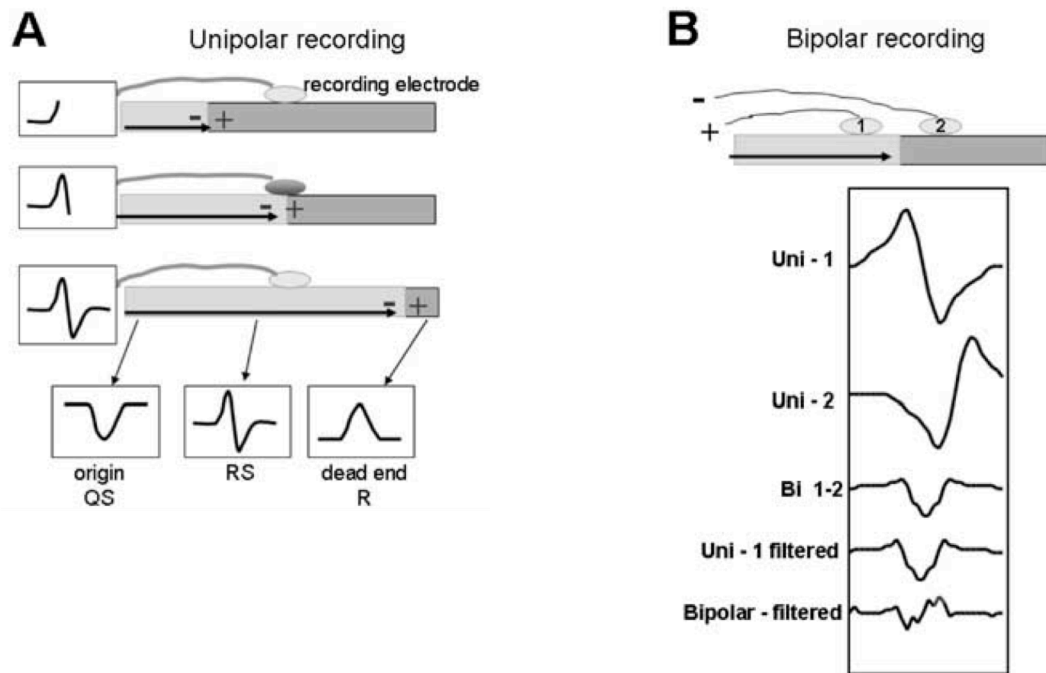


Figure 2.13. Generation of unipolar and bipolar electrograms (taken from Stevenson & Soejima, 2005). In the case of unipolar electrograms (A), the developing wavefront of activation passes underneath the exploring electrode and the potential difference in the extracellular space is measured with respect to a remote indifferent electrode (not shown). As the wavefront moves towards and then passes the exploring electrode the extracellular space develops a more negative potential difference with respect to the indifferent electrode giving different morphologies of electrogram as shown dependent on the position of the exploring electrode. In the case of bipolar electrograms (B), the instantaneous sum of the potential differences in the extracellular space between two local unipolar electrodes is measured. One unipolar signal is inverted given it is attached to the negative input of the amplifier.

1). Unipolar electrograms (UEGM)

In panel A of Figure 2.13 an exploring electrode resting on the surface of, for example, cardiac tissue, would be connected to the positive terminal of a recording amplifier and a second electrode, referred to as the indifferent electrode, would be placed at a distance, ideally infinite, away from the tissue and connected to the negative terminal. As a depolarisation wave spreads across the tissue towards the exploring electrode, the extracellular space surrounding depolarised cells becomes negatively charged and the exploring electrode transiently sits above extracellular space that is relatively more positively charged. A current thus flows across the extracellular space down the voltage gradient. The amplifier detects the potential that is set up. It becomes gradually more positive as the wave of depolarisation approaches the exploring electrode. At the point of depolarisation, or activation, of the tissue directly beneath the exploring electrode, the extracellular space directly beneath the electrode rapidly becomes negatively charged and this is reflected in the voltage waveform which develops a sharp transition and downward deflection to negative values before resetting to zero as the wave of depolarisation passes. The bottom 3 inset waveforms show how recording at either extreme end of the wavefront demonstrates directionality. If the wavefront moves completely away from an electrode the UEGM is solely negative, and it is solely positive if the wavefront moves only towards an electrode. It has been shown that at the point where the first derivative (dV/dt) of the unipolar electrogram is most negative, corresponds to the activation time of the tissue directly beneath the exploring electrode, as given by the point where the first derivative of a simultaneous monophasic action potential (MAP) is at its most positive (during the upstroke) (Wyatt *et al.*, 1981; Millar *et al.*, 1985; Coronel *et al.*, 2006). This also corresponds well with the greatest flux of sodium during the upstroke.

A wave of repolarisation then follows and also produces gradients of charge and, therefore, voltage, in the extracellular space. In a unipolar electrogram the T wave inscribes this gradient of repolarisation. In human, the T wave is distinct and can usually be clearly demarcated. It either has positive or negative polarity. Some groups argue that the point of the greatest modular value of the first derivative of the second limb of a T wave, descending for a positive T wave

and ascending for a negative T wave, marks the moment of local repolarisation, and that this correlates with the MAP_{90} , the point at which the MAP is repolarised by 90% of its absolute amplitude (Yue *et al.*, 2004; Yue, 2007). However, this notion does not fit with the first principles that govern the mechanics for the morphology of the unipolar electrogram for activation as described above. More in keeping with these first principles is the finding that the point where the first derivative of the T wave is most positive, on the ascending limb of either a positive or negative T wave, correlates with local repolarisation (Coronel *et al.*, 2006; Potse *et al.*, 2007; 2009).

It is attractive to measure the activation-recovery interval (ARI), as there is good correlation with the duration of the MAP and therefore the APD. However, whilst visualisation and assessment of the UEGM activation waveform in murine cardiac tissue can be performed with relative ease, it is notoriously difficult to discern and assess the T wave. What's more, controversies exist as to exactly where local repolarisation time is inscribed on the murine UEGM (Knollmann *et al.*, 2001; Boukens *et al.*, 2014). This makes it difficult to measure an ARI in the mouse as a surrogate for APD. One might make an attempt to measure a MAP and whilst this is possible, it too is technically challenging given the size and friability of the mouse heart and tissue. Changes in ERP correlate well with changes in APD, and under albeit normal conditions, ERP has been shown to be on average 85% of APD_{90} (Knollmann *et al.*, 2001). Thus, it is reasonable to monitor changes in ERP as a surrogate for APD and ERP itself has important implications for arrhythmogenicity, certainly with regards re-entrant mechanisms.

Whilst the UEGM can demonstrate directionality of a wavefront and has properties that allow for measurement of activation time and in some cases repolarisation time, it is open to far-field contamination from surrounding areas not local to the area directly beneath the electrode and also to noise.

2). Bipolar electrograms (BEGM)

In panel B of Figure 2.13 the sum of the potential differences at any moment between two closely spaced unipolar electrodes records the BEGM. Since

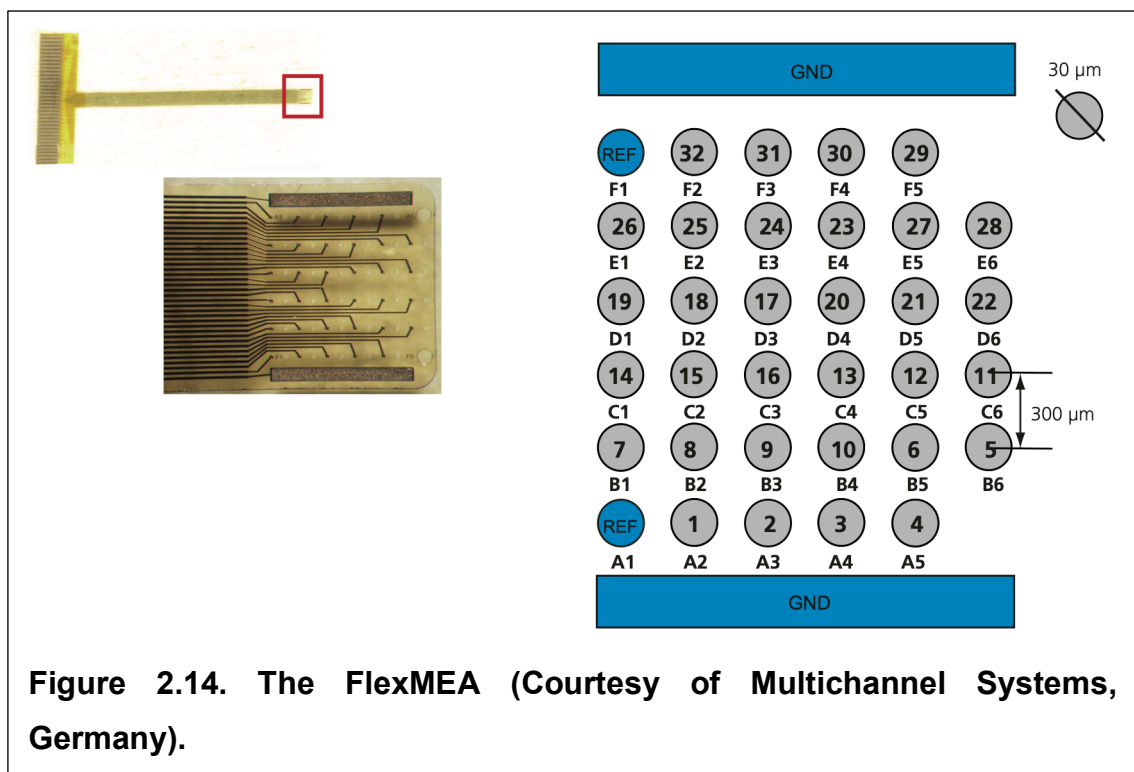
electrode 2 is connected to the negative terminal of the amplifier, its output is also inverted. Noise and far-field contamination are, thus, subtracted from the signal.

Whilst the BEGM is useful to help eliminate noise and far-field contamination, it is virtually impossible to delineate exactly where between the electrodes the local activation of the tissue occurs and controversies exist as to whether to take the onset of the BEGM or the peak of the BEGM as the activation time. It is also virtually impossible to assess the directionality of a wavefront and if the wavefront moves near perpendicular to the axis of the electrodes, a very low amplitude signal will be seen as there will be near no potential difference between the electrodes (Cantwell *et al.*, 2015).

2.8.2 Langendorff Heart Preparations

After schedule one killing via cervical dislocation, hearts were excised following thoracotomy and placed briefly in ice-cold oxygenated (95% O₂/5% CO₂) Krebs solution containing (mM) NaCl 118, KCl 4.75, MgSO₄·7H₂O 1.19, NaHCO₃ 25, KH₂PO₄ 1.19, D-glucose 5, CaCl₂ 1.4 and C₃H₃NaO₃ 2. Hearts were then quickly cannulated on ice via the aorta with a 14G aortic cannula (ADInstruments, Oxford), held in place with a clip, and mounted onto a modified Langendorff setup. Hearts were retrogradely perfused via the ascending aorta with warmed Krebs solution (contents as above) at constant flow of 2 ml min⁻¹ via a peristaltic pump. The temperature of the perfusate was maintained at 37.0±0.5 °C using an automated temperature controller and heatable perfusion cannula with temperature sensor (TC02, Multichannel Systems, Germany). Hypoxic conditions were produced by pre-bubbling Krebs with 95% N₂/5% CO₂. Drug containing Krebs solutions were made in the same manner and to the same concentrations as described in section 2.7.2. Solutions could be switched seamlessly using a custom-made manifold perfusion system. Experimental protocols were commenced after a 10 minute stabilisation period. A custom-made plastic cup was pressed lightly against the anterior surface of the heart and helped support and stabilise it during beating.

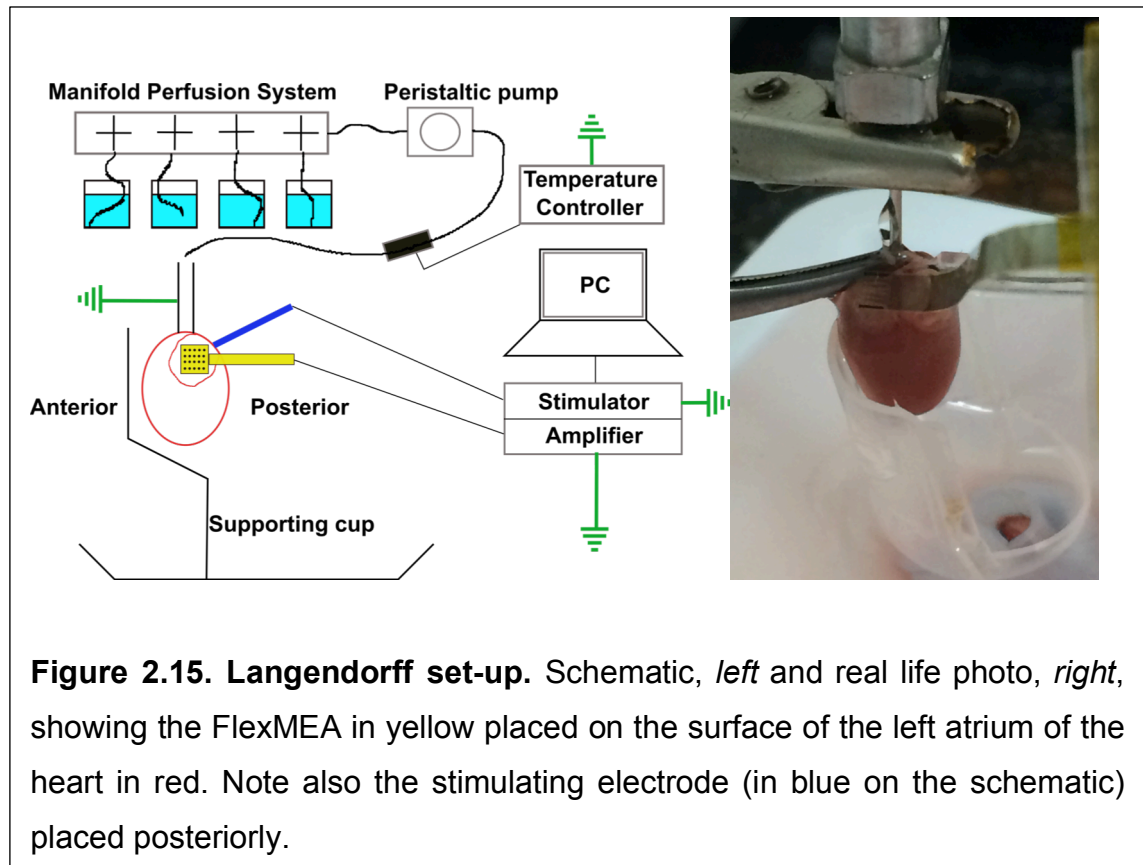
A commercially available flexible microelectrode array was used, known as FlexMEA for short (Multichannel systems, Germany). This is made of flexible polyimide 2611 foil with 32 circular titanium nitride electrodes of diameter 30 μ m and interelectrode distance of 300 μ m (see Figure 2.14). Two further electrodes act as reference electrodes and another 2 electrodes ground the array to help eliminate noise. The polyimide foil is perforated with holes of 30 μ m diameter to help ensure optimal tissue contact that make the FlexMEA ideal for recording from whole heart preparations. Each electrode records a local UEGM, or, extracellular field potential.



The FlexMEA is mounted on to a 32 channel miniature pre-amplifier (MPA32I, Multichannel Systems, Germany) using an adapter (ADPT-FM-32, Multichannel Systems, Germany), and then connected to a portable filter amplifier (USB-ME32-FAI-System, Multichannel Systems, Germany) for data acquisition via PC with accompanying software (MC Rack v4.6.2, Multichannel Systems, Germany).

The FlexMEA was held in place with a clamp stand on the surface of the right atrial appendage for experiments of spontaneous sinus rate, and that of the left atrial appendage for experiments with pacing protocols. The set-up for position

and orientation of the FlexMEA did not differ between preparations of the same experiments. Positioning the FlexMEA in this way could ensure large and sharp atrial electrograms for analysis and only small far-field ventricular electrograms (see Figure 2.16 bottom panel). Similarly, for protocols involving pacing of the heart, a custom-made unipolar platinum electrode was then always positioned on the posterior aspect of the heart in-between the two atria and directly adjacent to the left atrium. Figure 2.15 demonstrates a schematic of the set-up.



Pacing was performed via 1ms biphasic 2V stimuli using a stimulus generator (STG4002, Multichannel Systems) as programmed using its dedicated software interface (MC_Stimulus II, Multichannel Systems, Germany). Such stimuli were adopted as standard for all preparations through experience of having produced consistent and reliable tissue capture whilst also not saturating the electrogram signal. The programmed electrical stimulation (PES) protocol consisted of a drive train of eight paced beats (S1) at cycle length (CL) 120ms each followed by an extra stimulus (S2) every ninth beat. After the first drive train the S1-S2 interval was set at 120ms and after each subsequent drive train the S1-S2 interval reduced by 2ms until refractoriness was reached.

2.8.3 FlexMEA Signal Analysis

Signals recorded through the MC Rack software are stored as *.mcd* files and then were converted to *.h5* files before analysis using a modified Matlab script known as "*EcgSplitter*" (see Figure 2.16). Dr Malcolm Finlay, University College London and Queen Mary University of London, developed the *EcgSplitter* from a signal analysis graphical user interface (GUI, *wave_inspector.m*) created by David Western, University College London. *EcgSplitter* is a simple GUI allowing import, analysis and export of signals imported from a commercial electrophysiology system such as the FlexMEA system.

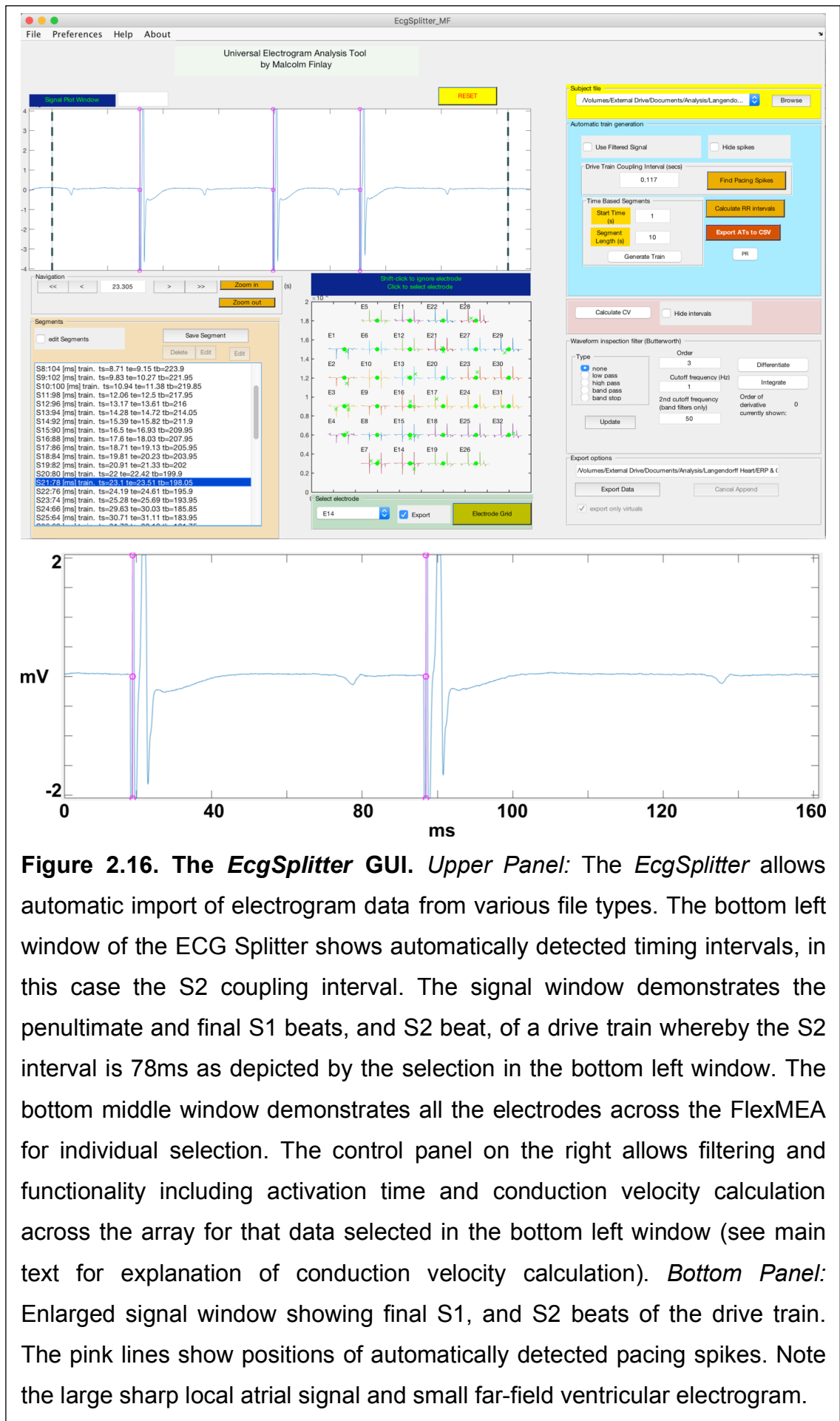


Figure 2.16. The *EcgSplitter* GUI. *Upper Panel:* The *EcgSplitter* allows automatic import of electrogram data from various file types. The bottom left window of the ECG Splitter shows automatically detected timing intervals, in this case the S2 coupling interval. The signal window demonstrates the penultimate and final S1 beats, and S2 beat, of a drive train whereby the S2 interval is 78ms as depicted by the selection in the bottom left window. The bottom middle window demonstrates all the electrodes across the FlexMEA for individual selection. The control panel on the right allows filtering and functionality including activation time and conduction velocity calculation across the array for that data selected in the bottom left window (see main text for explanation of conduction velocity calculation). *Bottom Panel:* Enlarged signal window showing final S1, and S2 beats of the drive train. The pink lines show positions of automatically detected pacing spikes. Note the large sharp local atrial signal and small far-field ventricular electrogram.

Dr Finlay's adaptations allow recognition of pacing spikes (by time differential of signal and signal magnitude), QRS complexes, as well as functionality involving selection of electrogram channels for analysis. A key adaptation was automatic recognition of the final 3 complexes in an S1-S2 pacing protocol drive train. After inputting the drive train constant, the script was able to recognise the final beats of a drive train, and select these for export. These "snippets" of the large electrogram data could then be checked for accuracy. Given the PES protocol brought the S2 down in 2ms intervals, ERP was taken as 1ms longer than the shortest coupled S2 that did not activate the tissue. 32 signals were obtained for each beat. In wild-type mice the atrial ERP can be of the order of 20ms (Kaese & Verheule, 2012). In the case of steady state conduction velocity measurement, the signals of the final two S1 activations (at CL 120ms) are taken to ensure an adequate number of beats of the drive train to overdrive the tissue. If, for example, the ERP is 20ms, this would constitute 11 time points and a total ~35,000 electrograms to assess over the course of a 20 minute experiment. In order to maintain fidelity via manual checking of every electrogram, for steady state conduction velocity, this was rationalised by including only the first 3 drive trains of the PES protocol for each time point of the experiment. Activation was defined as the point of most negative dV/dt of the electrogram. Having rationalised the number of electrograms to be included in the analysis, manual checking of every electrogram took place. Grossly fragmented electrograms, where no clear dominant negative intrinsicoid deflection of the field potential could be visualised and thus ambiguity existed as to the point of most negative dV/dt , were excluded from the analysis. *EcgSplitter* can present signal-averaged data from a manually selected drive train and manually selected electrodes. It presents the averaged data for that drive train across all the selected electrodes depicting the $\text{mean} \pm 2\text{SD}$ of the final two S1 beats in red, and that of the S2 beats in blue (see Figure 2.17). The data is presented with respect to time from the pacing spike such that S2 data is later than S1 data due to activation delay at shorter coupling intervals. The user then selects a window from this data to exclude, for example, any remnant artefact from the pacing spike, and *EcgSplitter* then measures the activation time for **all** manually included drive trains and electrode data as the time from the pacing spike detection to the point of the most negative dV/dt within the time window manually selected. If, in selecting the window, the drive train with the

shortest coupled S2 is used, and the window is placed at the end of the S2 triggered electrogram, the window should incorporate all electrogram data timed from a pacing spike for all the manually included drive trains.

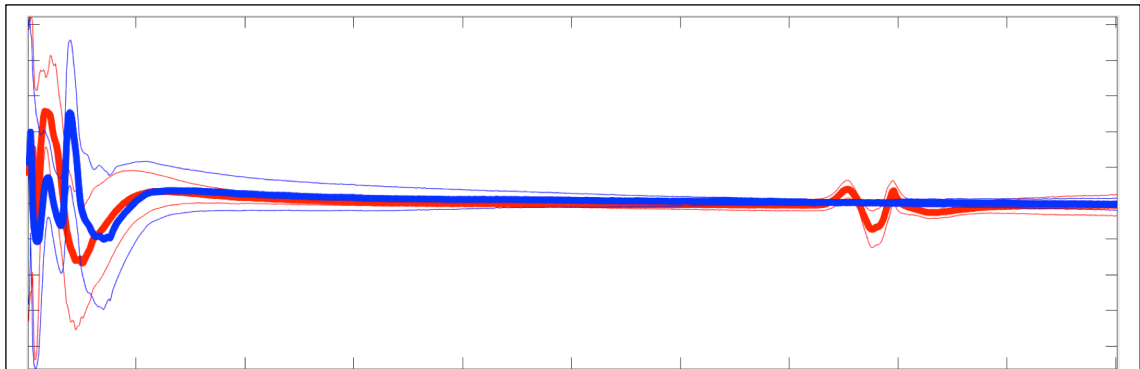


Figure 2.17. The *EcgSplitter* manual window selection tool. Mean (bold lines) and 2 standard deviations either side of the mean are presented for all manually selected electrodes for data pertaining to a particular drive train. Red represents the final 2 S1 beats of the drive train and blue the S2 beats. Note the small far field ventricular data to the right of the window in red corresponding to that from the S1 beats. That from the S2 beats is not shown as it falls too late due to activation delay. See also main text for details.

Classical measurement of conduction velocity via measurement of the time for impulse propagation between two points relies on knowledge of the path of activation and in a 2D planar surface this can be complex to determine. For example, the path may not be linear which would confound the final measurement. Alternatively, the overall activation gradient as measured across the entire tissue can be calculated. For each manually included beat, and also as per the windowing function, the activation time for each included electrode is plotted to its corresponding point on the array. A topographical function fits a 2D least-squares regression surface to activation time data across the entire electrode array grid. The distance between each electrode is known (300 μ m) and given the "grid" nature of the FlexMEA, is equal in both the x and y planes. Activation gradients (time/distance) can be measured at each point of the fitted surface corresponding to each included electrode data point. The gradient (G) has vector directionality and at each point is calculated in a Cartesian fashion whereby $G = \sqrt{G_x^2 + G_y^2}$ (see figure 2.18). This circumvents the potential confounding of non-linear activation. The inverse of the activation gradient $1/G$

is the conduction velocity at that point. The mean of these was then taken as the overall conduction velocity across the FlexMEA. The mean is then taken of data from all beats pertaining to a particular coupling interval. Hence, in the case of steady state conduction velocity at CL 120ms, seeing as the final 2 S1 beats of the drive train were used and the first 3 drive trains of the PES protocol, the final CV measurement will be the average from 6 beats. In the case of CV restitution, in order to take a mean of a number of beats, data was averaged from 5 beats, that of the S2 interval in question, and the 2 intervals either side of that S2 interval. A potential limitation of this method using the present materials in the whole heart, is that the FlexMEA rests solely on the epicardial surface of the heart and conduction could also proceed perpendicular to the FlexMEA or, at least, not truly parallel to it. Care was taken to ensure activation maps supported propagation parallel to the FlexMEA and where this was not the case data were excluded from analysis. Figure 2.18 demonstrates a typical activation map from the experiments where propagation appeared parallel to the FlexMEA. It is colour coded for activation time where like colours are isochrones (red = early, blue = late). The method for CV calculation has been validated previously (Finlay *et al.*, 2014).

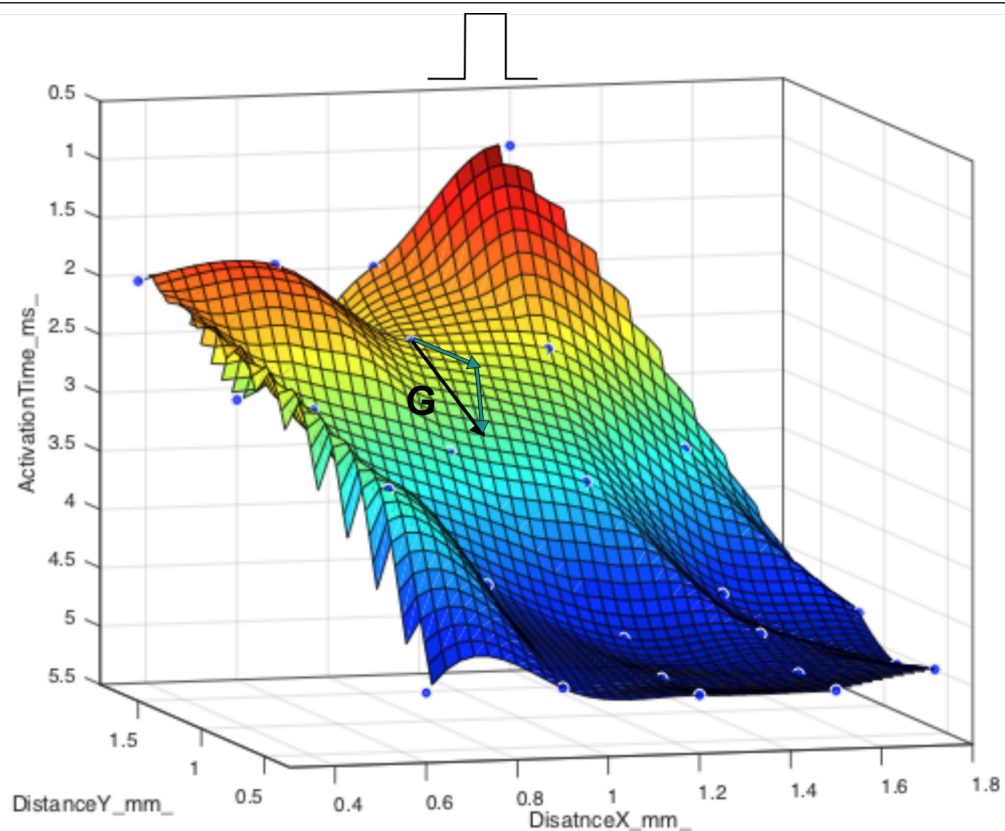


Figure 2.18. Calculation of conduction velocity from a regression surface. A typical regression surface for calculation of conduction velocity is shown. The x and y axes represent 2D positions. The height of the blue dots gives the activation time measured at that location. This z axis is inverted (early activation = high, late activation = low). A regression surface is fitted to these co-ordinates, which here is colour-scaled to represent activation time (red = early, blue = late, note also the square pulse indicating point of stimulus). At any point on this surface, the slope (G) can be calculated in a Cartesian fashion $G = \sqrt{(G_x^2 + G_y^2)}$, where G_x is the gradient in the x plane and G_y that in the y plane. The inverse $1/G$ is the conduction velocity at that point. The mean is then taken of all conduction velocity points across the array to give the overall conduction velocity for that beat.

In the absence of pacing spikes *EcgSplitter* recognises the QRS complex and also has the functionality to set a manual threshold level for detection. This is useful since when the FlexMEA is placed on the surface of the atrial appendage, atrial electrograms are sharper and have greater amplitude (see Figure 2.16). Thus, for measurement of spontaneous sinus rate, the mean of the last 10 R-R intervals (for atrial electrograms) for a particular time point was taken.

2.9 Calcium Transient Measurement from HL-1 Syncytia

Given the tendency of HL-1 cells to beat spontaneously in clusters, I utilised this property to investigate the effects of K_{ATP} activation or inhibition on this spontaneous beating.

Referring to section 2.1.2, HL-1 cells were seeded such that they would be confluent as syncytia in a 5.5cm² MEA perfusion chamber on the day of experiments. 10µL of DMSO was added to 50µg of fluo-4 acetoxymethyl ester (Fluo-4,AM) (Thermofisher Scientific) making a 5mM stock. Fluo-4 is a labelled calcium indicator molecule that exhibits an increase in fluorescence upon binding Ca^{2+} . It has high fluorescence excitation at 488nm. Cells may be loaded with the AM ester form of Fluo-4 that allows cell permeation, by adding dissolved indicator directly to dishes containing cultured cells.

5µL of the Fluo-4,AM/DMSO 5mM stock was added to HL-1 syncytia in 1ml of Claycomb medium such that the concentration of Fluo-4,AM was ~20µM. Syncytia were allowed to incubate with the Fluo-4-AM for 20 minutes before the medium was changed to 1ml of oxygenated Krebs with the same contents as described in section 2.8.2. The temperature of the Krebs solution was maintained at 37°C by use of a temperature controller (TC02, Multichannel Systems, Germany). The syncytia were imaged with a Nikon Eclipse TE200 inverted microscope with an integrated digital CMOS camera (ORCA Flash4.0 V2 C11440-22CU; Hamamatsu Photonics UK Limited, Hertfordshire, UK). A light emitting diode illumination system was synchronised with the camera for epifluorescence. Recordings were taken at 100fps.

Syncytia would tend to display spontaneous calcium transients in the form of organised wavefronts across the MEA and in a rotational fashion. After a 5 minute period of stabilisation, recordings (1min) of spontaneous calcium transients were made under baseline conditions, after 3 minutes incubation with diazoxide 100µM, after 3 minutes incubation with diazoxide 200µM and finally after 3 minutes incubation with diazoxide 200µM / tolbutamide 100µM. Drugs were added sequentially directly to the bath.

Recordings were processed as stacks using the public domain software Image J (<http://imagej.nih.gov/ij>) to measure the frequency of activating wavefronts by selecting a small area of the array encroached by the wavefront. The absolute size of this area was kept uniform between arrays. Where representation of calcium transients is depicted, the median fluorescence over the whole recording has been subtracted in an attempt to reduce the confounding of the background signal likely to be due largely to non-esterified Fluo-4 bound to extracellular calcium.

Various limitations apply to the use of the calcium transient solely as an indicator of wave front propagation. Firstly, activation time is not accurately delineated by any parameter of the calcium transient given changes in membrane potential defining the action potential do not coincide directly or ubiquitously with changes in cytosolic calcium. Isolated calcium sparks or release events from the SR may not trigger activation or be related to a propagating wave front. Voltage sensitive dyes demonstrate changes in membrane potential and action potential morphology and a measurement of the maximum rate of change of the upstroke of the action potential can be defined as the true activation time (duBell *et al.*, 1991; Herron *et al.*, 2012; Jaimes *et al.*, 2016). Similarly calcium transient duration does not mirror action potential duration and the calcium transient usually outlasts the action potential, partly due to a calcium-buffering effect of many calcium sensitive dyes, though there tends to be correlation between the two (Jaimes *et al.*, 2016). Thus, it is not reliable to use calcium transients to measure conduction velocity or activation-recovery intervals and propagation maps have to be interpreted with an element of caution. That said, macroscopic wave front propagation can be clearly visualised through the above calcium imaging in HL-1 syncytia, and demonstration of this propagation with time through peak measurement of the transient is possible, recognising it as a surrogate of any true activation time.

2.10 Statistical Analyses

Statistical analyses were carried out using GraphPad Prism V6.0h (GraphPad Software, Inc., California) with, where appropriate: the independent samples Student's *t* test for comparison of two independent parametric means, the paired samples Student's *t* test for comparison of two paired parametric data sets, ordinary one-way ANOVA for comparison of 3 or more independent parametric means, or repeated measures one-way or two-way ANOVA for comparison of 3 or more dependent parametric means and the effects of more than one independent variable. Tukey's post-hoc test was utilised when comparing every mean with every other mean, Dunnett's post-hoc test in the instance of comparing means to the mean at baseline, and Bonferroni post-hoc test when comparing a specific selection of means. Fisher's exact test or Chi-square test were used to compare categorical data. Data are presented as mean±SEM. A *p* value of <0.05 was regarded as statistically significant. Where markers of statistical significance are shown, **p* < 0.05, ***p* < 0.01, ****p* < 0.001, *****p* < 0.0001.

Section 3: Results

3.1 Confirmation of Selective Pharmacology of K_{ATP} Openers and Inhibitors using HEK293 Stable Cell Lines

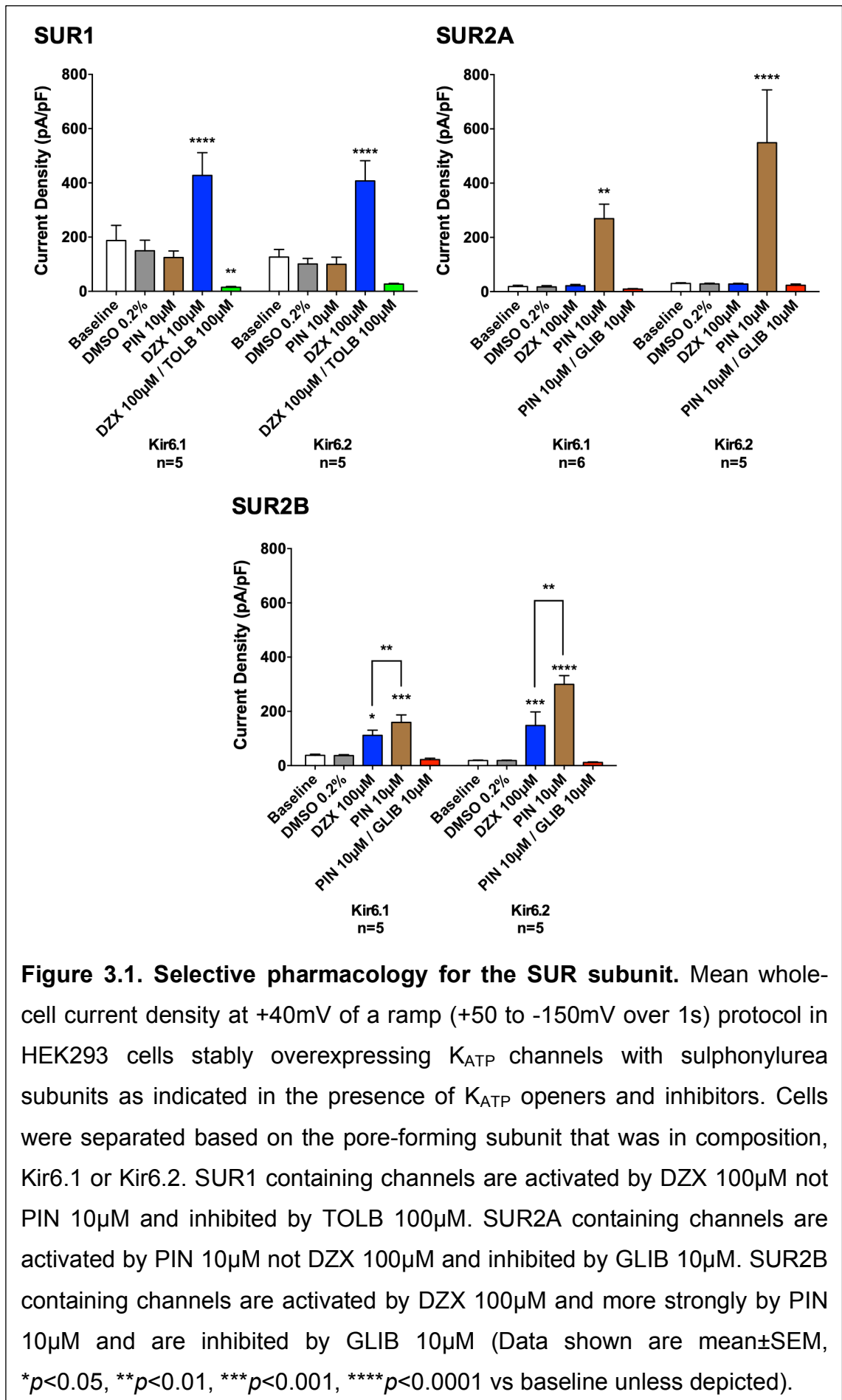
Further to the current knowledge and some of the contentions regarding K_{ATP} modulator specificity as delineated in section 1.3.2, the first task was to demonstrate in my own hands the ability of various openers and inhibitors to be selective with regards particular K_{ATP} subunit composition. I therefore set about performing a comprehensive and systematic approach utilising HEK293 cell lines stably overexpressing K_{ATP} channels of every homomultimeric Kir6x/SURx composition. I subjected isolated cells to whole-cell patch clamp and chose drug concentrations empirically guided by previous literature. The aim was to develop a repertoire of drugs at specific concentrations that, in my hands and under the intracellular/extracellular conditions set by the experimental solutions, would be able to delineate the underlying subunits contributing to a K_{ATP} current.

3.1.1 SURx subunit pharmacology

Openers

SUR1-containing channels were strongly activated by diazoxide 100 μ M (DZX) but in the same cells pinacidil 10 μ M (PIN) failed to activate current (Kir6.1/SUR1: baseline, 187 \pm 56; PIN, 125 \pm 24; DZX, 427 \pm 84 pA/pF; n=5; PIN vs baseline, $p > 0.05$; DZX vs baseline, $p < 0.0001$; Kir6.2/SUR1: baseline, 127 \pm 28; PIN, 100 \pm 27; DZX, 407 \pm 75 pA/pF; n=5; PIN vs baseline, $p > 0.05$; DZX vs baseline, $p < 0.0001$). (See Figure 3.1).

The opposite was true for channels containing SUR2A subunits in that pinacidil 10 μ M strongly activated current but in the same cells diazoxide 100 μ M failed to activate current (Kir6.1/SUR2A: baseline, 19 \pm 5; DZX, 22 \pm 5; PIN, 269 \pm 53 pA/pF; n=6; DZX vs baseline, $p > 0.05$; PIN vs baseline, $p < 0.01$; Kir6.2/SUR2A: baseline, 30 \pm 3; DZX, 28 \pm 3; PIN, 549 \pm 195 pA/pF; n=5; DZX vs baseline, $p > 0.05$; PIN vs baseline, $p < 0.0001$). (See Figure 3.1).



In the case of K_{ATP} channels with SUR2B subunits, both diazoxide 100 μ M and pinacidil 10 μ M activated current, though pinacidil more so (Kir6.1/SUR2B: baseline, 38 ± 4 ; DZX, 111 ± 19 ; PIN, 160 ± 28 pA/pF; n=5; DZX vs baseline, $p < 0.05$; PIN vs baseline, $p < 0.001$; PIN vs DZX, $p < 0.01$; Kir6.2/SUR2B: baseline, 19 ± 2 ; DZX, 148 ± 50 ; PIN, 300 ± 32 pA/pF; n=5; DZX vs baseline, $p < 0.001$; PIN vs baseline, $p < 0.0001$; PIN vs DZX, $p < 0.01$). (See Figure 3.1).

Inhibitors

For SUR1-containing channels, and in repeated measures from the experiments with openers, tolbutamide 100 μ M abolished the diazoxide 100 μ M activated current and inhibited a basally active current when added sequentially to the bath solution (Kir6.1/SUR1: baseline, 187 ± 56 ; DZX/TOLB, 15 ± 3 pA/pF; n=5; $p < 0.01$; Kir6.2/SUR1: baseline, 127 ± 28 ; DZX/TOLB, 27 ± 3 pA/pF; n=5; $p > 0.05$). (See Figure 3.1).

In the case of SUR2A and SUR2B containing channels, and in repeated measures from the experiments with openers, glibenclamide 10 μ M completely inhibited the pinacidil 10 μ M activated current when added sequentially to the bath solution (Kir6.1/SUR2A: baseline, 19 ± 5 ; PIN/GLIB, 10 ± 1 pA/pF; n=6; $p > 0.05$; Kir6.2/SUR2A: baseline, 30 ± 3 ; PIN/GLIB, 24 ± 5 pA/pF; n=5; $p > 0.05$; Kir6.1/SUR2B: baseline, 38 ± 4 ; PIN/GLIB, 22 ± 5 pA/pF; n=5; $p > 0.05$; Kir6.2/SUR2B: baseline, 19 ± 2 ; PIN/GLIB, 12 ± 2 pA/pF; n=5; $p > 0.05$). (See Figure 3.1).

To investigate the effects of HMR1098, I inferred from the results encountered above. As such I investigated the fractional inhibition of inhibitor-sensitive peak-activated current (using diazoxide 100 μ M/tolbutamide 100 μ M in the case of SUR1 containing channels, and pinacidil 10 μ M/glibenclamide 10 μ M in the case of SUR2A containing channels) for HMR1098. No difference was found between the inhibitory effects of HMR1098 10 μ M after peak activation for Kir6.2/SUR1 or Kir6.2/SUR2A channels. (Kir6.2/SUR1: 0.99 ± 0.03 , n=5; Kir6.2/SUR2A: 0.95 ± 0.01 , n=6; $p > 0.05$). (See Figure 3.2).

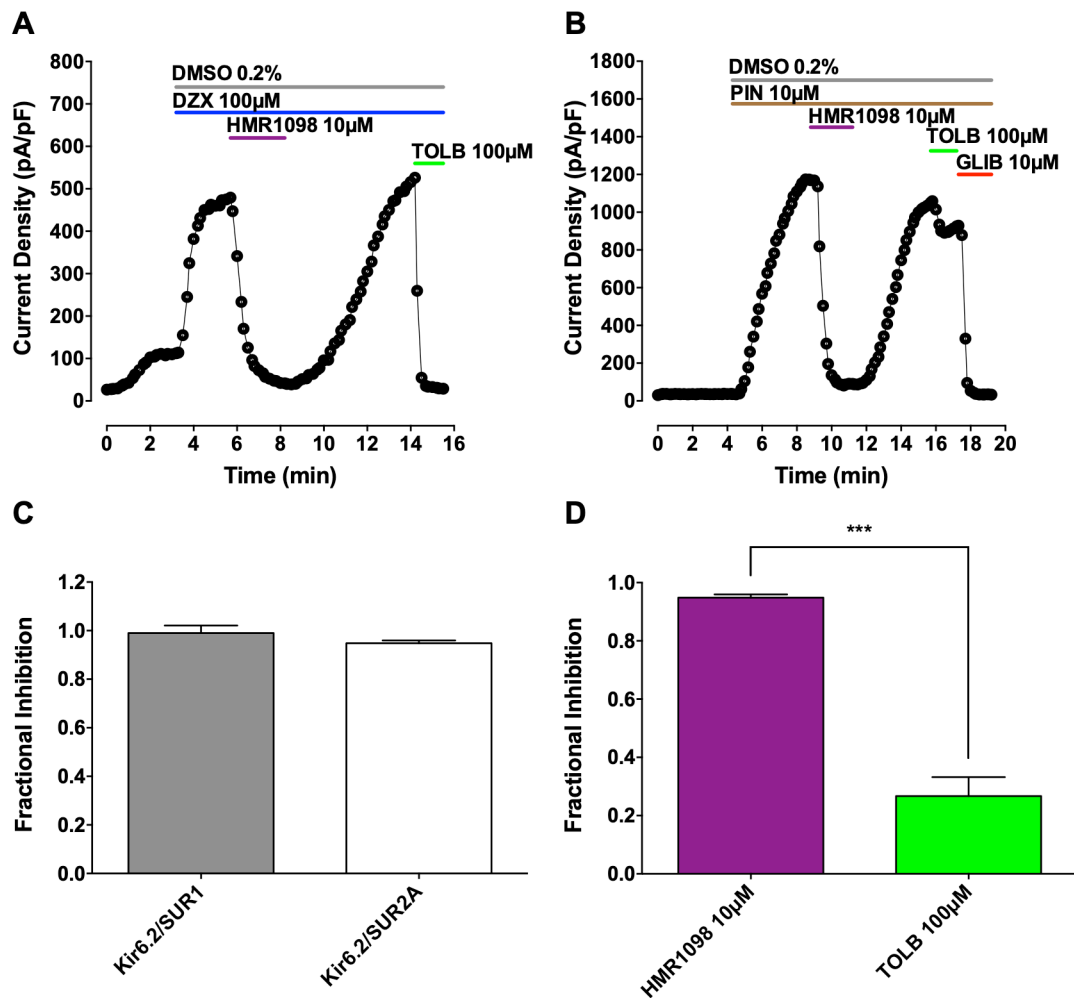


Figure 3.2. Effects of HMR1098 and Tolbutamide. HMR1098 10µM inhibits both SUR1 and SUR2A containing channels whilst TOLB 100µM only inhibits those containing SUR1. Representative whole-cell current density trace for HEK293 cells overexpressing Kir6.2/SUR1 (**A**) and Kir6.2/SUR2A (**B**) channels in the presence of K_{ATP} activators and inhibitors. (**C**) Mean fractional inhibition by HMR1098 10µM of the inhibitor-sensitive peak-activated K_{ATP} current in HEK293 cells overexpressing K_{ATP} channels (DZX 100µM activation / TOLB 100µM inhibition for Kir6.2/SUR1 channels, $n=5$; PIN 10µM activation / GLIB 10µM inhibition for Kir6.2/SUR2A channels, $n=6$). (**D**) Mean fractional inhibition by HMR1098 10µM and TOLB 100µM of the inhibitor-sensitive peak-activated K_{ATP} current (PIN 10µM activation / GLIB 10µM inhibition) in HEK293 cells overexpressing Kir6.2/SUR2A channels, $n=6$ (Data shown are mean±SEM; *** $p<0.001$).

Fractional inhibition of the inhibitor-sensitive peak-activated current (pinacidil 10 μ M / glibenclamide 10 μ M) was then compared between HMR1098 10 μ M and tolbutamide 100 μ M in repeated measures for cells overexpressing Kir6.2/SUR2A channels. Tolbutamide was found to be a weak inhibitor of these channels indicative of its more SUR1-specific effects. (HMR: 0.95 ± 0.01 ; TOLB: 0.27 ± 0.06 ; $n=6$; $p < 0.001$). (See Figure 3.2).

3.1.2 Kir6x subunit pharmacology

Fractional inhibition of the inhibitor-sensitive peak-activated current (diazoxide 100 μ M/tolbutamide 100 μ M in the case of SUR1 containing channels and pinacidil 10 μ M/glibenclamide 10 μ M in the case of SUR2A containing channels) was then investigated for the suggested pore blocker PNU37883A at 50 μ M. This concentration was chosen based on its representation in existing literature depicting ~70% inhibition of Kir6.1-containing channels and ~10% inhibition of Kir6.2-containing channels (Surah-Narwal *et al.*, 1999; Kovalev *et al.*, 2004). I sought to reproduce similar results under the given experimental conditions as this would serve as a pharmacological tool to distinguish between the two pore-forming subunits. A stark and reproducible difference was found between channels containing the two different pore types with a selectivity of inhibition for channels containing Kir6.1 pore-forming subunits as shown in figure 3.3. (SUR1-containing channels: Kir6.1, 0.93 ± 0.004 , $n=5$; Kir6.2, 0.19 ± 0.02 , $n=5$; $p < 0.0001$; SUR2A-containing channels: Kir6.1, 0.94 ± 0.02 , $n=5$; Kir6.2, -0.06 ± 0.06 , $n=5$; $p < 0.0001$; SUR2B-containing channels: Kir6.1, 0.95 ± 0.01 , $n=5$; Kir6.2, 0.13 ± 0.05 , $n=5$; $p < 0.0001$). Given the reproducibility of this pore selective inhibition regardless of the SUR subunit, summative data are also presented combining recordings from all channels with the same pore-forming subunit as shown in figure 3.3. (Kir6.1, 0.94 ± 0.01 , $n=15$; Kir 6.2, 0.09 ± 0.04 , $n=15$; $p < 0.0001$).

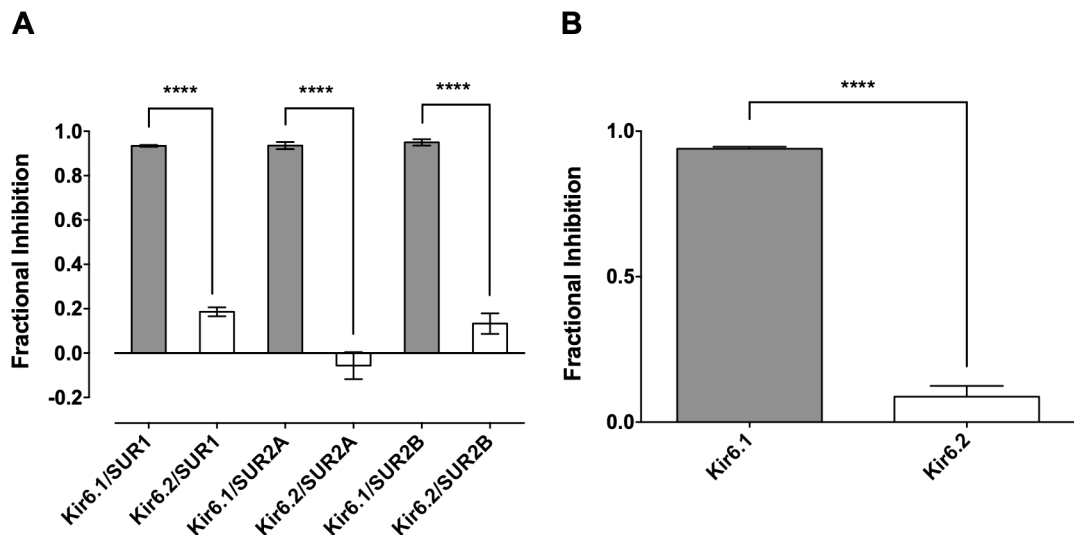
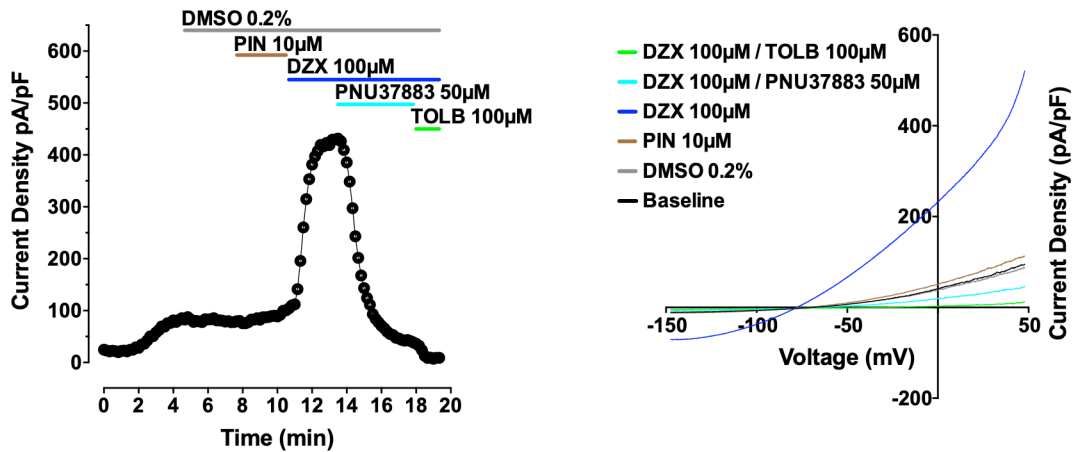


Figure 3.3. PNU37883A K_{ATP} pore selectivity. PNU 50 μ M selectively inhibits Kir6.1 containing channels not Kir6.2. **(A)** Mean fractional inhibition by PNU37883A 50 μ M of the inhibitor-sensitive peak-activated K_{ATP} current in HEK293 cells overexpressing K_{ATP} channels (DZX 100 μ M activation / TOLB 100 μ M inhibition for SUR1 containing channels; PIN 10 μ M activation / GLIB 10 μ M inhibition for SUR2A and SUR2B containing channels; n=5 for all channel compositions). **(B)** Mean summative data of that in (A) combining that from all channels with the same pore-forming subunit, n=15 for each pore type. (Data shown are mean \pm SEM; **** p <0.0001).

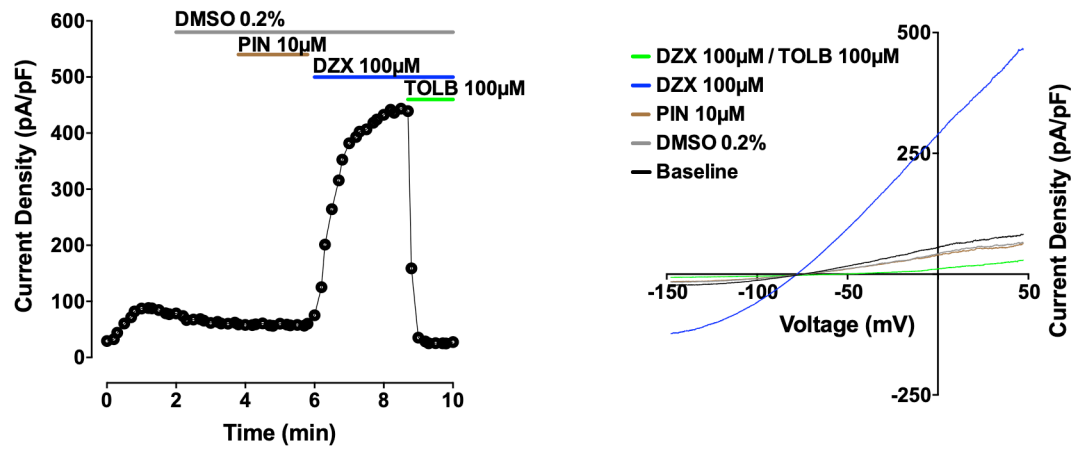
3.1.3 Representative recordings

Figures 3.4, 3.5 and 3.6 demonstrate representative traces of whole-cell current density with time, and corresponding I-V plots, for HEK293 cells stably overexpressing K_{ATP} channels as indicated and in the presence of the K_{ATP} openers and inhibitors. In the case of cells with Kir6.2/SUR1 and Kir6.2/SUR2A channels, PNU37883A was investigated on a separate cell set, hence, the traces are presented on separate graphs.

Kir6.1/SUR1



Kir6.2/SUR1



Kir6.2/SUR1 with PNU37883 50 μ M

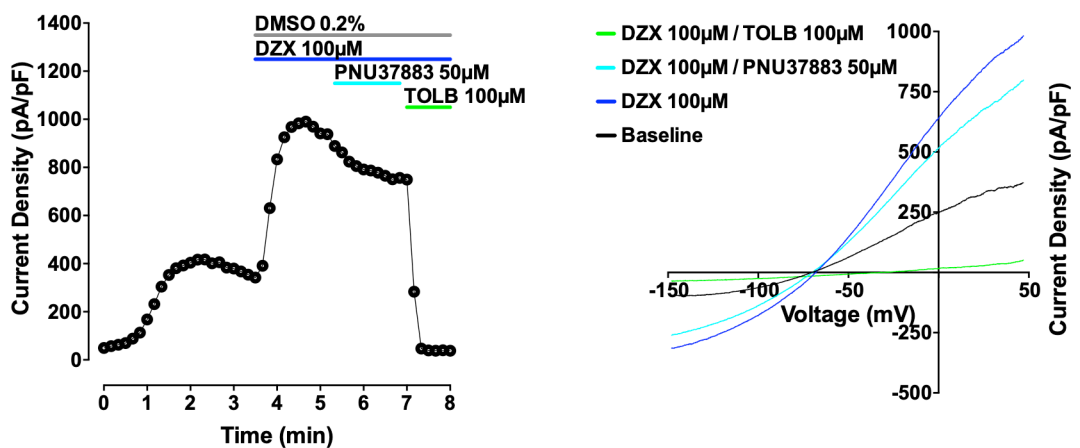
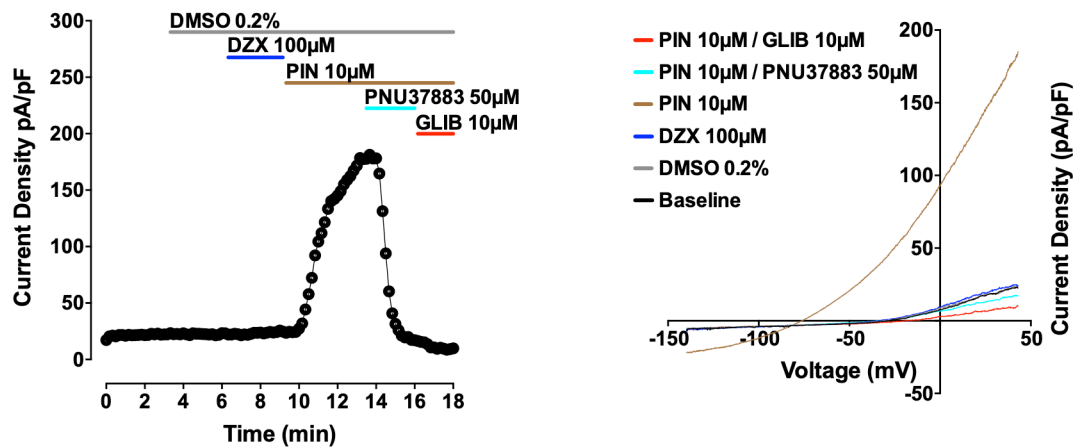
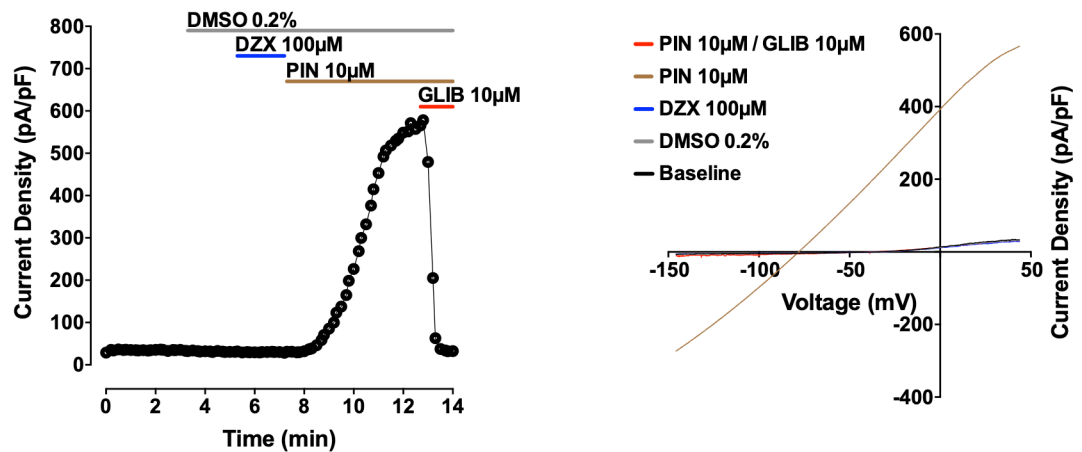


Figure 3.4. Representative recordings for SUR1 containing channels. Whole-cell current density (left panels) and corresponding I-V plots at plateau of activation / inhibition (right panels) of HEK293 cells stably overexpressing SUR1 containing K_{ATP} channels (pore as indicated) in the presence of K_{ATP} openers and inhibitors.

Kir6.1/SUR2A



Kir6.2/SUR2A



Kir6.2/SUR2A with PNU37883 50μM

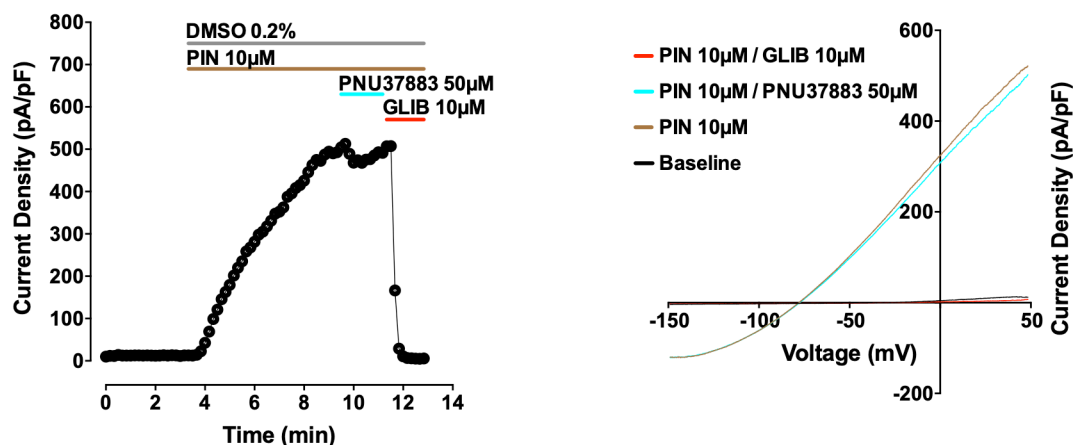
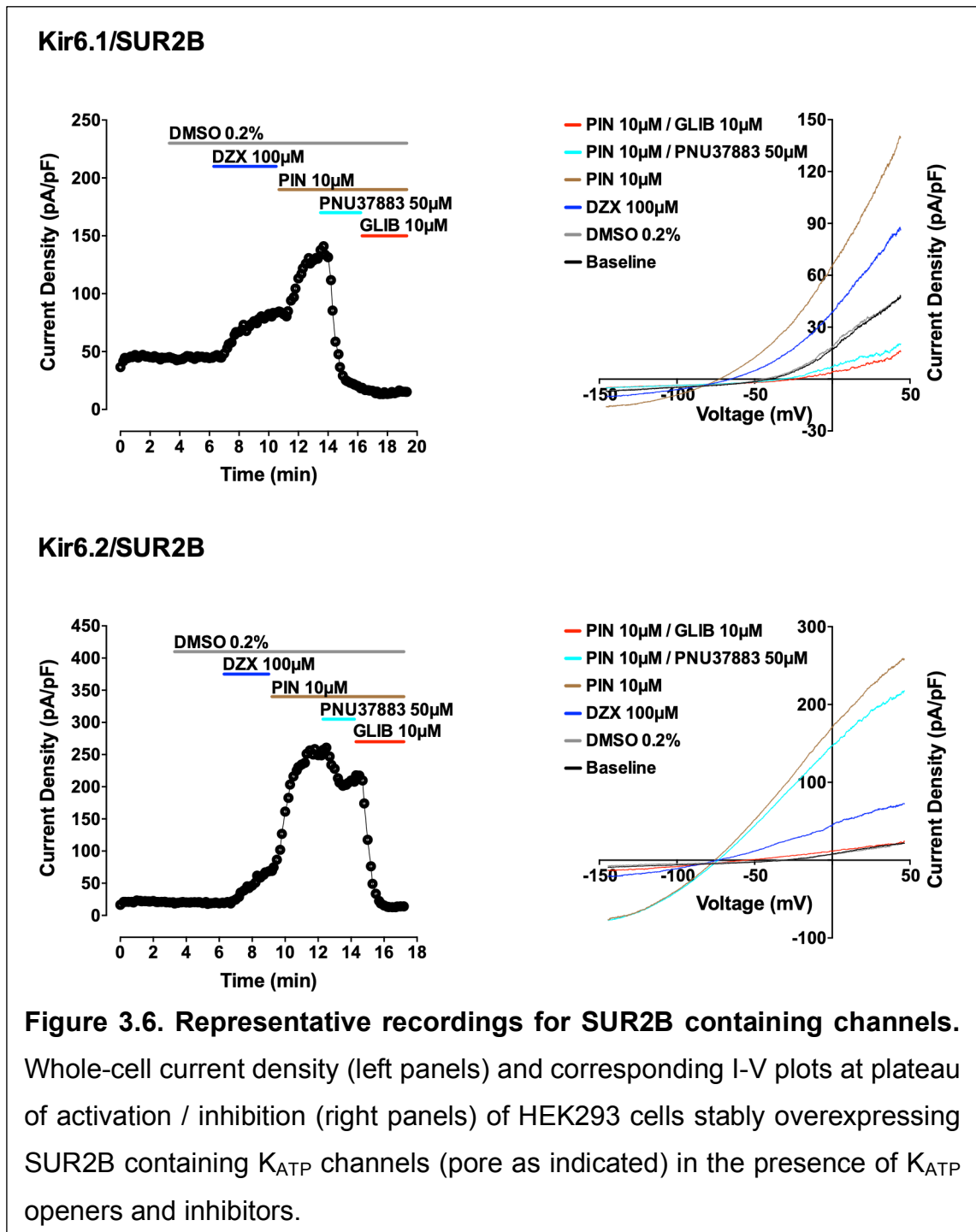


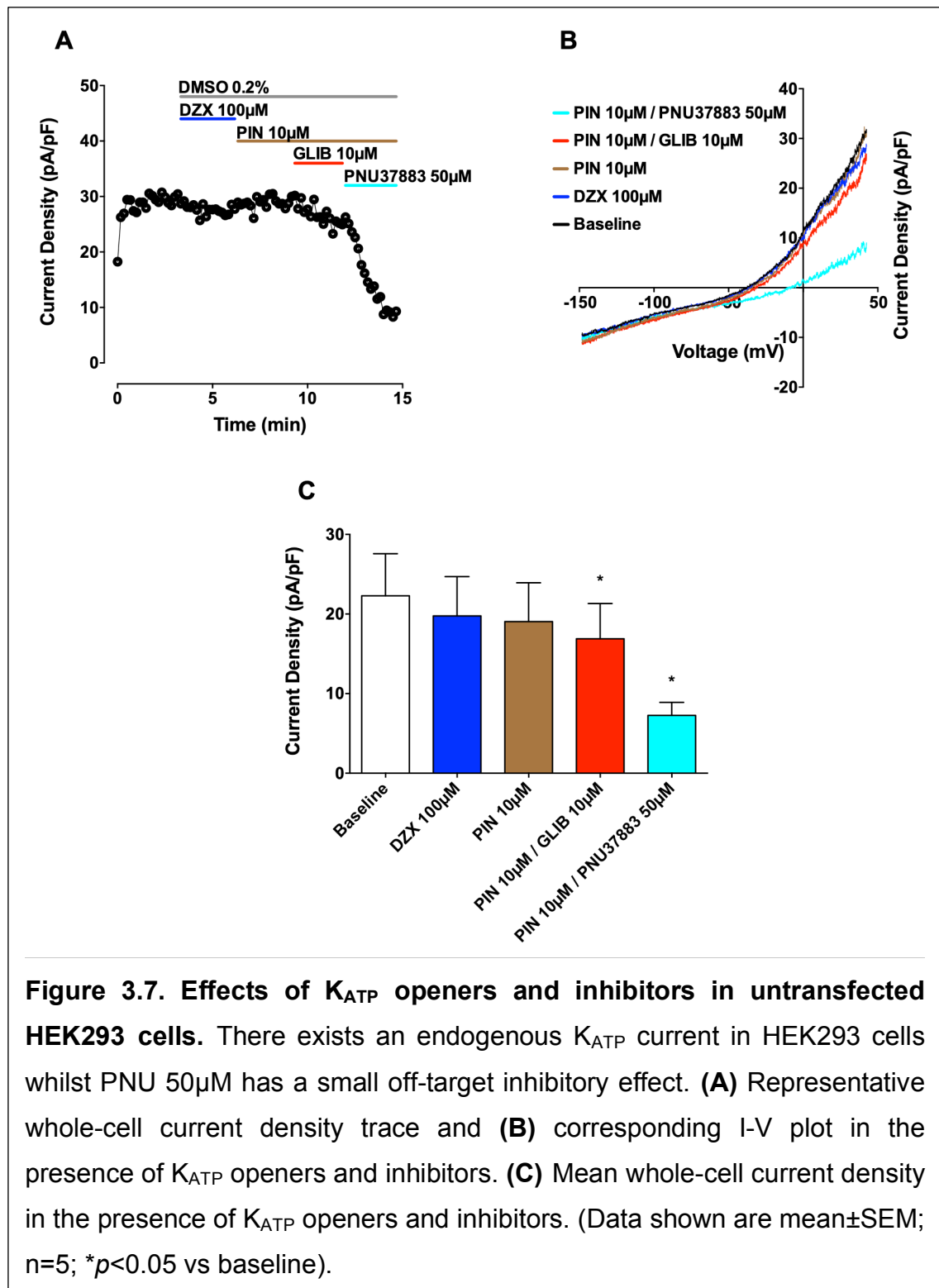
Figure 3.5. Representative recordings for SUR2A containing channels. Whole-cell current density (left panels) and corresponding I-V plots at plateau of activation / inhibition (right panels) of HEK293 cells stably overexpressing SUR2A containing K_{ATP} channels (pore as indicated) in the presence of K_{ATP} openers and inhibitors.



3.1.4 Untransfected HEK293 cells

To demonstrate the above effects were not due to other endogenous currents, the same experiments were repeated on HEK293 cells not transfected with K_{ATP} subunits. The openers diazoxide 100µM and pinacidil 10µM had no effect on the baseline current. Glibenclamide 10µM inhibited a basal current and PNU37883A 50µM provided further inhibition of this basal current. (Baseline, 22

± 5 ; DZX, 20 ± 5 ; PIN, 19 ± 5 ; PIN/GLIB, 17 ± 4 ; PIN/PNU, 7 ± 2 pA/pF; $n=5$; GLIB vs baseline, $p < 0.05$; PNU vs baseline, $p < 0.05$). (See Figure 3.7).



3.1.5 Summary

The above provides a very useful pharmacological tool to distinguish the subunits present of any K_{ATP} channel population as a whole expressed at the cell membrane. This may well contain a mixture of channels of varying subunit composition, and indeed some channels may even be heteromultimers. Nevertheless the pharmacological tools can confirm or refute the presence of a particular K_{ATP} subunit. There appears to be a small endogenous basally active K_{ATP} current in HEK293 cells. The results suggest PNU37883A weakly inhibits currents other than K_{ATP} , but this only strengthens the data showing its specificity for blocking Kir6.1, as compared to Kir6.2 where it produced ~90% inhibition. Even off-target effects are not likely to cloud its inhibitory effects on Kir6.1-containing channels. The weak inhibition (~10%) seen in HEK293 cells overexpressing K_{ATP} channels with Kir6.2 pore forming subunits, however, could be explained in part, by its action on a non- K_{ATP} current, and not much inhibition of Kir6.2 at all. Table 2 summarises the findings.

SUBUNIT	OPENERS	INHIBITORS
Kir6.1		PNU37883A 50 μ M - strong
Kir6.2		PNU37883A 50 μ M - weak/nil
SUR1	diazoxide 100 μ M - strong pinacidil 10 μ M - nil	tolbutamide 100 μ M - strong HMR1098 10 μ M - strong
SUR2A	pinacidil 10 μ M - strong diazoxide 100 μ M - nil	glibenclamide 10 μ M - strong HMR1098 10 μ M - strong tolbutamide 100 μ M - weak
SUR2B	pinacidil 10 μ M - strong diazoxide 100 μ M - moderate	glibenclamide 10 μ M - strong

Table 2. Summary of the investigated effects of K_{ATP} openers and inhibitors.

3.2 Generation of knockout mice

3.2.1 Attempt to generate a cardiomyocyte conditional *Kcnj8* knockout mouse

The initial aim was to produce a mouse with cardiomyocyte conditional knockout of Kir6.1 (Kir6.1-cKO) to investigate the importance of this pore-forming subunit with particular respect to heart muscle electrophysiology and arrhythmia. A conditional knockout would potentially circumvent concerns that the hypertensive phenotype of a global knockout (see section 1.3.1) might lead to electrophysiological changes indirectly, through an increased afterload-induced tissue substrate of both fibrosis, and stretch-induced K_{ATP} opening, or from ischaemia (Miki *et al.*, 2002; Chutkow *et al.*, 2002; Lader *et al.*, 2011).

Figure 3.8 demonstrates the PCR products from genomic DNA in the Kir6.1-cKO knockout line. The "floxed" allele gives rise to a 600bp product that is larger than the wild-type 474bp product due to additional FRT and loxP elements. The presence of Cre recombinase (under control of the alphaMHC promoter) is detected by a 650bp product.

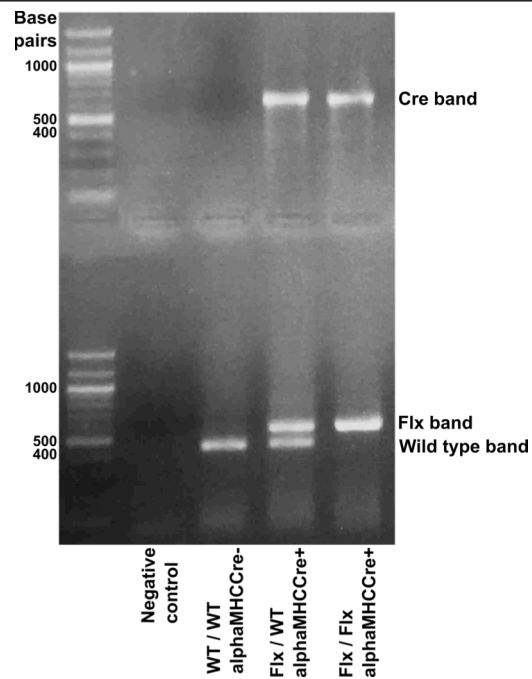
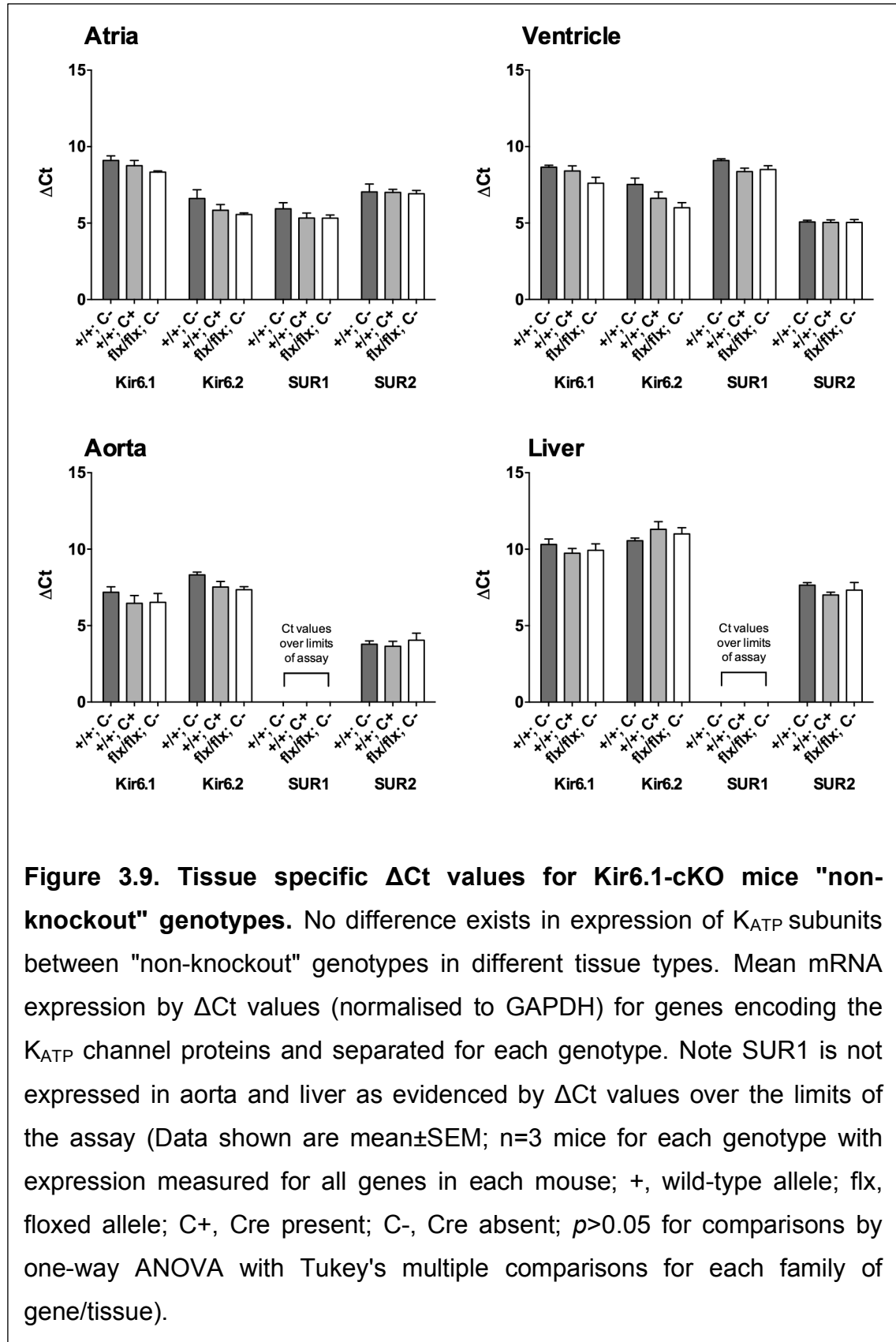


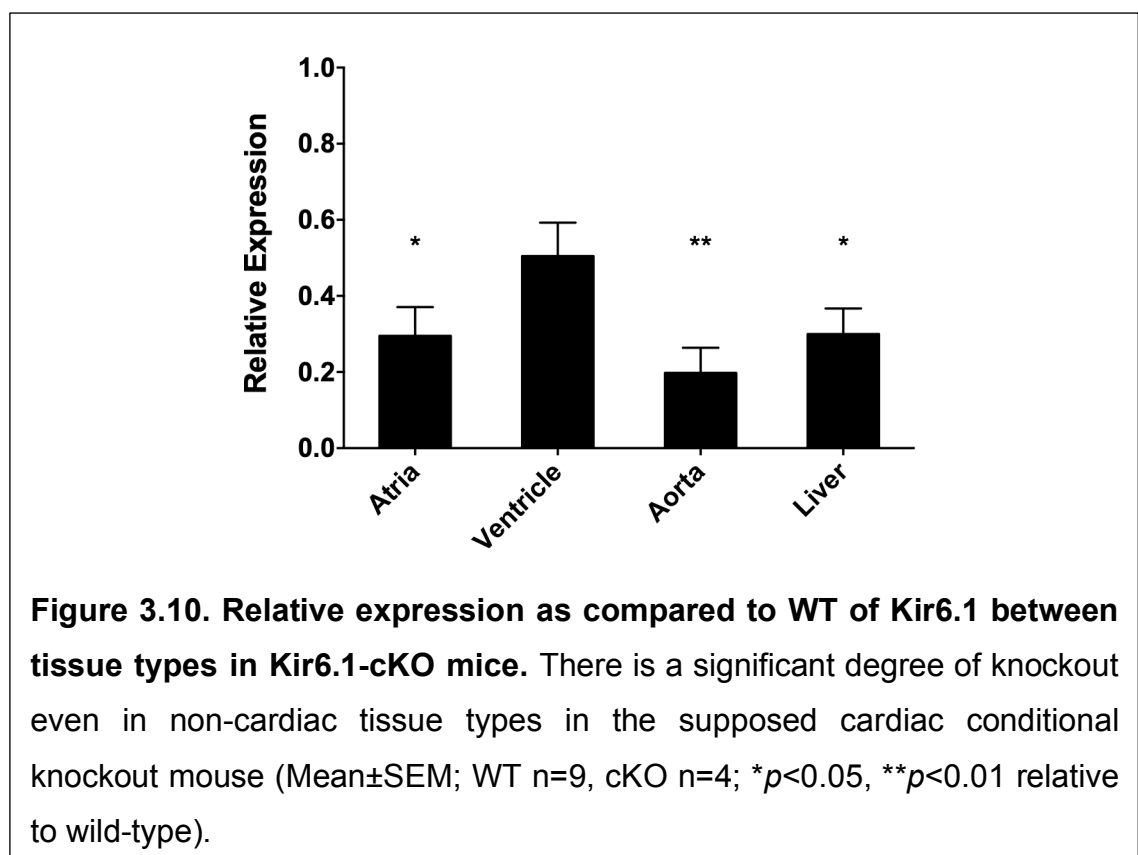
Figure 3.8. Genomic DNA PCR for the cardiomyocyte conditional Kir6.1 knockout mice. Top half shows the Cre band and bottom half the "floxed" and wild-type bands. The alphaMHCCre gives rise to a 650bp product, "floxed" allele a 600bp product and WT band a 474bp product. The "floxed" allele is longer given it contains FRT and loxP elements.

Using qRT-PCR, I demonstrated that there was no difference between the Δ Ct values for all K_{ATP} subunits, and with respect to tissue type, when comparing the "non-knockout" genotypes (wt/wt alphaMHCCre-; wt/wt alphaMHCCre+, flx/flx alphaMHCCre-). This is presented in figure 3.9.



Based on these findings "non-knockout" genotypes were pooled as wild-type (WT) mice going forward. Of note, indications were SUR1 was not expressed at all in wild-type aorta and liver.

Figure 3.10 shows the results of qRT-PCR relative quantification using the $2^{-\Delta\Delta Ct}$ method for Kir6.1-cKO mice as compared to littermate WT animals between tissue types. There was a high degree of knockout in all tissue types not just the heart (relative expression in cKO compared to WT: atria 0.29 ± 0.08 , $p < 0.05$; ventricle 0.51 ± 0.09 , $p = 0.12$; aorta 0.20 ± 0.07 , $p < 0.01$; liver 0.30 ± 0.07 , $p < 0.05$; WT n=9, KO n=4).



Given the heterogeneous mix of cell type in whole heart tissue, cardiomyocyte conditional knockout would be expected to produce a relative knockdown of ~50% (Pinto *et al.*, 2016). However, this degree of knockdown was also seen in the aorta and liver suggesting that the alphaMHCcre could have been "leaky" so as not to be cardiomyocyte conditional.

3.2.2 *Kcnj8* global knockout

With the uncertainty of cardiomyocyte conditional knockout of Kir6.1 in the cKO mouse line, I decided to focus my attention on a global knockout where I could be sure of genetic deletion. Whilst the concerns about indirect afterload effects on electrophysiological substrate could be argued, the degree of knockdown in the aorta in the cKO mouse line was also significant. In terms of a model for the effects of Kir6.1 modulation on single cell and tissue electrophysiology, a global knockout has its advantages given naturally occurring germ line loss of function mutations, or indeed pharmacological manipulation, are not likely to be cardiomyocyte specific.

Figure 3.11 demonstrates the PCR products from genomic DNA in the Kir6.1 global knockout mouse (Kir6.1-gKO). The wild-type allele PCR gives rise to a 474bp product, just as it did in the cKO mouse given the same primers were used and the wild-type allele contains no loxP or FRT site (see also Figure 2.3). The knockout allele PCR gives rise to a 724bp product only if the critical region has been removed. If this does not take place, then the product would be too large to amplify with the given PCR conditions, and no band would be seen on gel electrophoresis.

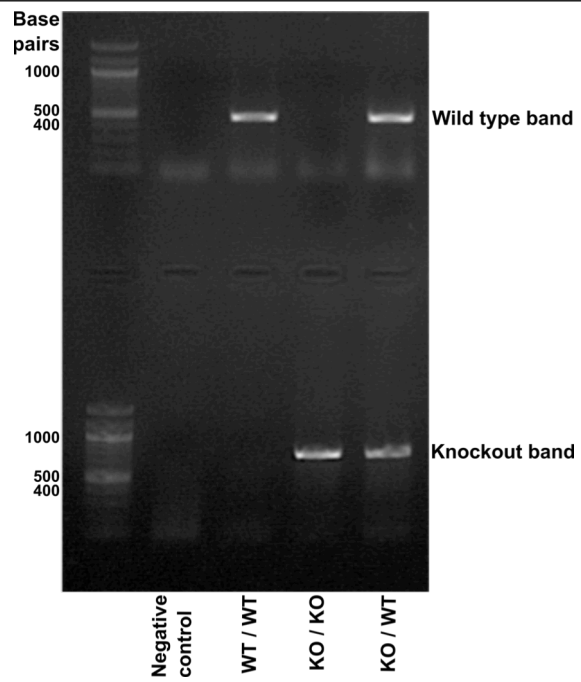
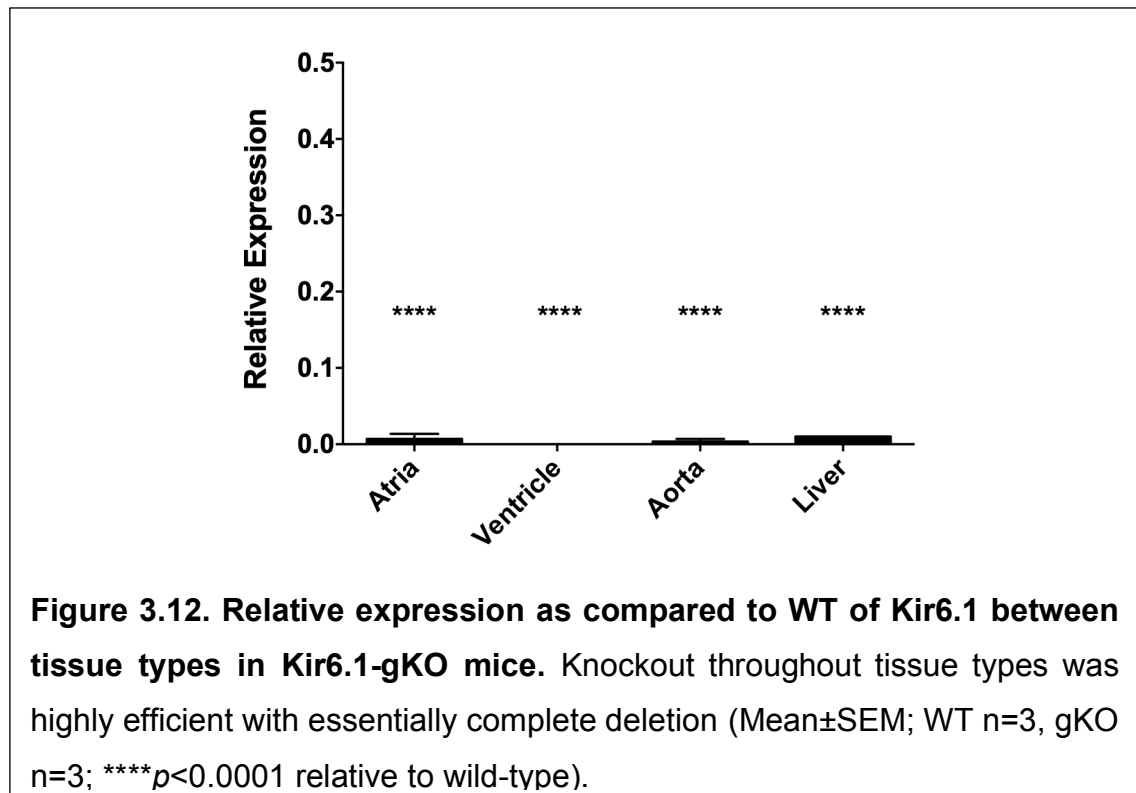


Figure 3.11. Genomic DNA PCR for the Kir6.1 global knockout mouse. Top half shows WT band (474bp product) and bottom half KO band (724bp) product, which is only amplified under the given conditions if the critical region of the gene is knocked out allowing for a shorter product.

Figure 3.12 shows the results of qRT-PCR relative quantification of the Kir6.1-gKO mice when compared to littermate WT animals between tissue types. There was essentially complete knockout in all tissue types (relative expression in gKO compared to WT: atria 0.01 ± 0.01 , $p < 0.0001$; ventricle 0.00 ± 0.00 , $p < 0.0001$; aorta 0.00 ± 0.00 , $p < 0.0001$; liver 0.01 ± 0.00 , $p < 0.0001$; WT n=3, KO n=3).



I then compared the relative expression of the different K_{ATP} subunits in the Kir6.1-gKO heart. This is presented in figure 3.13. Statistical significance was found for a down-regulation of *Abcc8* (coding for SUR1) in the atria. The functional significance of what this finding might mean was not completely clear. Whilst this was whole heart RNA the finding could be examined further when measuring the K_{ATP} current density in atrial cardiomyocytes by patch clamp (expression relative to WT: Kir6.2, atria 1.1 ± 0.2 , ventricle 0.5 ± 0.2 ; SUR1, atria 0.3 ± 0.1 $p < 0.05$, ventricle 0.5 ± 0.2 ; SUR2, atria 0.8 ± 0.2 , ventricle 0.7 ± 0.2 ; WT n=3, KO n=3).

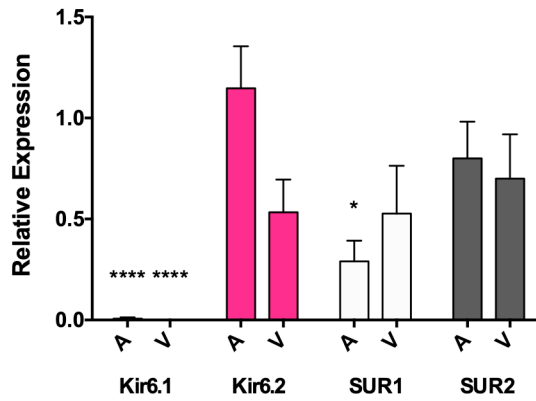


Figure 3.13. Relative expression compared to WT of K_{ATP} subunits in the Kir6.1-gKO heart. There appeared to be a down-regulation of SUR1 in the atria of knockout mice but no change in the other subunits (Mean±SEM; A - atria, V - ventricles; WT n=3, KO n=3; **p*<0.05, *****p*<0.0001 relative to wild-type).

3.2.3 *Kcnj11* global knockout

As discussed in section 2.2 the Kir6.2 global knockout mouse (Kir6.2-gKO) was engineered at The Medical Research Council Centre for Mouse Genetics, Harwell Campus, Oxfordshire, UK (MRC Harwell) in collaboration with the International Mouse Phenotyping Consortium. Mice were genotyped and delivered to order. Further characterisation by qRT-PCR was then carried out.

Figure 3.14 shows the results of qRT-PCR relative quantification of the Kir6.2-gKO mice when compared to littermate WT animals between tissue types. There was essentially complete knockout in all tissue types (expression in gKO relative to WT: atria 0.00 ± 0.00, *p* < 0.001; ventricle 0.00 ± 0.00, *p* < 0.001; aorta 0.03 ± 0.01, *p* < 0.01; liver 0.03 ± 0.01, *p* < 0.0001; WT n=4, KO n=4).

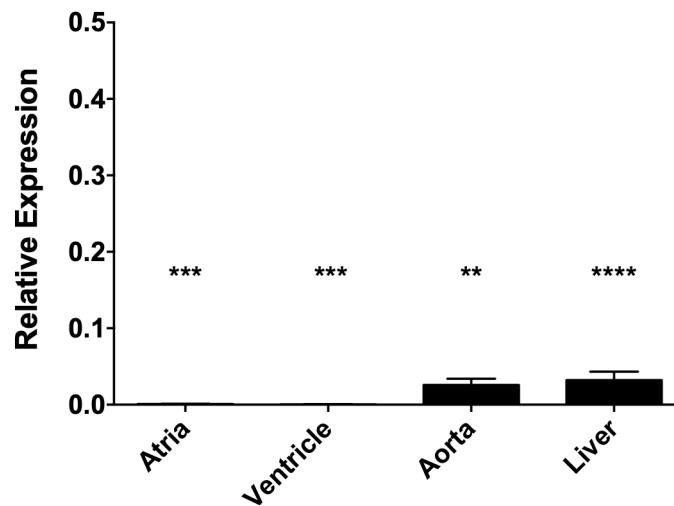


Figure 3.14. Relative expression compared to WT of Kir6.2 between tissue types in Kir6.2-gKO mice. Knockout throughout tissue types was highly efficient with essentially complete deletion (Mean±SEM; WT n=4, gKO n=4; ** $p < 0.01$, *** $p < 0.001$, **** $p < 0.0001$ relative to wild-type).

I then compared the relative expression of the different K_{ATP} subunits in the Kir6.2-gKO heart. This is presented in figure 3.15. Statistical significance was found for an up-regulation of *Kcnj8* in the ventricle. The functional significance of this was not clear. I did not plan to perform patch clamp on ventricular myocytes and expanding on the meaning of this finding would fall out of the scope of the project (relative expression compared to WT: Kir6.1, atria 1.2 ± 0.1 , ventricle 1.4 ± 0.1 $p < 0.05$; SUR1, atria 1.5 ± 0.4 , ventricle 1.6 ± 0.1 ; SUR2, atria 1.3 ± 0.1 , ventricle 1.1 ± 0.04 ; WT n=4, KO n=4).

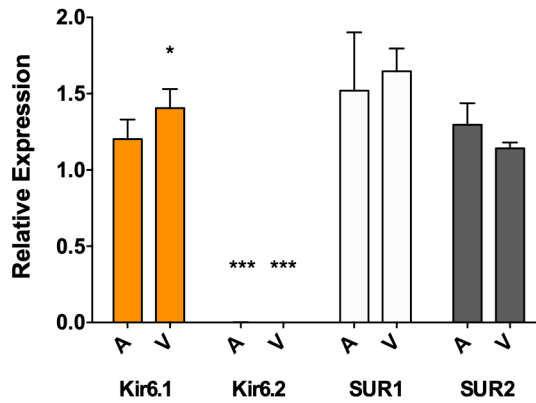


Figure 3.15. Relative expression compared to WT of K_{ATP} subunits in the Kir6.2-gKO heart. There appeared to be an up-regulation of Kir6.2 in the ventricles of knockout mice but no change in the other subunits (Mean±SEM; A - atria, V - ventricles; WT n=4, KO n=4; * p <0.05, *** p <0.001 relative to wild-type).

3.2.4 Summary

Whilst knockdown in off-target tissues in the Kir6.1-cKO mouse might be related to cardiomyocyte knockdown, I could not be sure that the alphaMHCCre was functioning as intended. The Kir6.1-gKO mouse appeared robust with essentially complete knockdown of Kir6.1 in all tissues as expected and so too was the case with Kir6.2 in the Kir6.2-gKO mouse. Together with being able to make comparisons between both global knockouts, potential advantages exist of a global knockout as a model for effects that might be produced by naturally occurring germ line loss of function mutations, and indeed pharmacological manipulation, which are not likely to be cardiomyocyte specific. Thus I used the global knockouts for further experiments.

3.3 Isolated murine atrial cardiomyocytes demonstrate a functional expression and predominance for sarcolemmal K_{ATP} channels comprising Kir6.2/SUR1 subunits

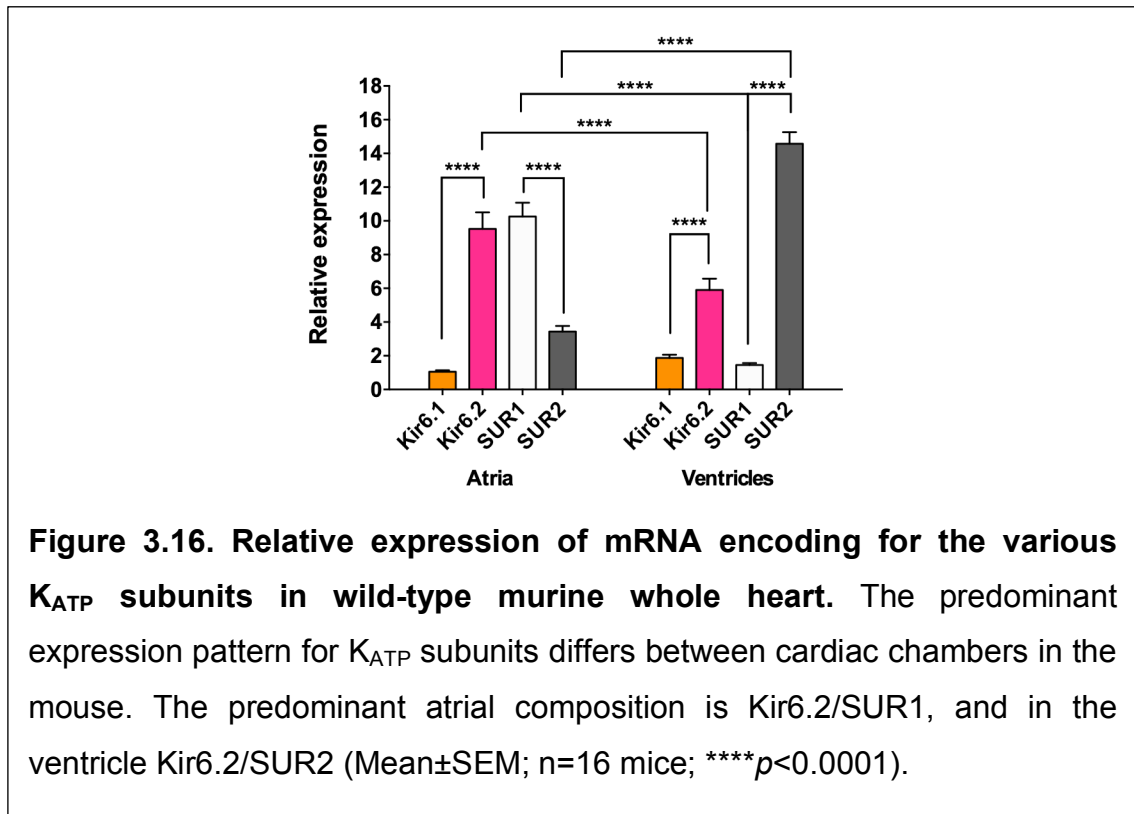
A body of evidence has already delineated that Kir6.2/SUR1 appears as the prominent K_{ATP} subunit composition at the sarcolemma of murine atrial cardiomyocytes (Saegusa *et al.*, 2005; Flagg *et al.*, 2008; Glukhov *et al.*, 2010). This drove initial excitement for a translatable therapeutic target for atrial arrhythmias as the classic ventricular K_{ATP} subunit composition was defined as Kir6.2/SUR2A (Inagaki *et al.*, 1996; Babenko *et al.*, 1998; Suzuki *et al.*, 2001; Chutkow *et al.*, 2001). Thus, SUR1 might be an atrial specific drug target that would not have any off-target detrimental effects in the ventricle. This excitement was blunted by further human studies suggesting that SUR1 was not an important K_{ATP} subunit in the human heart, at least not in non-failing heart (Zünkler *et al.*, 1997; Fedorov *et al.*, 2011).

Mouse models with knockout of either pore-forming subunit and sulphonylurea receptor subunits have been extensively investigated for the ventricle, and to some degree, the sulphonylurea receptor in the atria, but there has been a paucity of studies looking at the effects of knockout of the pore-forming subunits in murine atria. I therefore sought to directly compare, with identical experiments, the effects of global knockout of either pore-forming subunit on the atria of these mice. I wanted to further delineate any contribution of Kir6.1 to the sarcolemmal current in murine atrial cardiomyocytes as has been previously suggested in other rodent models (Baron *et al.*, 1999; Poitry *et al.*, 2003; van Bever *et al.*, 2004).

3.3.1 Differential cardiac K_{ATP} subunit mRNA expression

I first investigated the relative expression of mRNA encoding for the various K_{ATP} subunits in wild-type whole heart mRNA. The results are displayed in figure 3.16. Kir6.2 and SUR1 were more abundantly expressed than their alternative subunits in the atria, and Kir6.2 and SUR2 in the ventricles. There was still evidence for Kir6.1 expression in both chambers. There was

significantly more expression of SUR1 in the atria relative to the ventricles and for SUR2 in the ventricles relative to the atria. (Expression normalised to GAPDH and relative to the mean of atrial Kir6.1: Atria - Kir6.1 1.1 ± 0.1 , Kir6.2 9.5 ± 1.0 , $p < 0.0001$; SUR1 10.3 ± 0.8 , SUR2 3.4 ± 0.3 , $p < 0.0001$. Ventricles - Kir6.1 1.8 ± 0.2 , Kir6.2 5.9 ± 0.7 , $p < 0.0001$; SUR1 1.5 ± 0.1 , SUR2 14.6 ± 0.7 , $p < 0.0001$; SUR1 atria vs ventricle, $p < 0.0001$; SUR2 atria vs ventricle, $p < 0.0001$. n=16 mice).



3.3.2 Kir6.2 deletion, but not Kir6.1 deletion, abolishes the K_{ATP} current in isolated murine atrial cardiomyocytes

To investigate the functional consequences of deletion of each pore-forming subunit on atrial cardiomyocytes, isolated cells from Kir6.1-gKO, Kir6.2-gKO and WT mice were subjected to whole-cell patch clamp. In both WT and Kir6.1-gKO, diazoxide 100 μ M but not pinacidil 10 μ M activated current, and addition of tolbutamide 100 μ M but not PNU37883A inhibited the current activated by diazoxide 100 μ M. No difference was seen in the peak activated current between right and left atria in these genotypes (WT n=8-15 cells from 13 mice

(see figure 3.17): RA; baseline 22 ± 6 , PIN 18 ± 3 , DZX 137 ± 29 , DZX/PNU 142 ± 30 , DZX/TOLB 19 ± 6 pA/pF; DZX and DZX/PNU vs baseline, $p < 0.0001$. LA; baseline 18 ± 2 , PIN 19 ± 3 , DZX 141 ± 28 , DZX/PNU 137 ± 34 , DZX/TOLB 11 ± 2 pA/pF; DZX and DZX/PNU vs baseline, $p < 0.0001$. Kir6.1-gKO n=4-8 cells from 4 mice (see figure 3.18): RA; baseline 46 ± 14 , PIN 48 ± 14 , DZX 244 ± 58 , DZX/PNU 301 ± 46 , DZX/TOLB 22 ± 4 pA/pF; DZX and DZX/PNU vs baseline, $p < 0.0001$. LA; baseline 22 ± 5 , PIN 25 ± 6 , DZX 185 ± 39 , DZX/PNU 163 ± 39 , DZX/TOLB 13 ± 4 pA/pF; DZX vs baseline, $p < 0.001$; DZX/PNU vs baseline, $p < 0.01$).

In the case of Kir6.2-gKO atrial cardiomyocytes, neither diazoxide $100\mu\text{M}$ or pinacidil $10\mu\text{M}$ activated current. Both tolbutamide $100\mu\text{M}$ and glibenclamide $10\mu\text{M}$ failed to significantly inhibit any baseline endogenous current. However, PNU37883A $50\mu\text{M}$ did inhibit a baseline endogenous current (Kir6.2-gKO n=4-8 cells from 5 mice (see figure 3.19): RA; baseline 17 ± 3 , PIN 16 ± 4 , DZX 15 ± 2 , DZX/TOLB 14 ± 2 , DZX/GLIB 13 ± 2 , DZX/PNU 5 ± 1 pA/pF; DZX/PNU vs baseline, $p < 0.01$. LA; baseline 20 ± 3 , PIN 18 ± 2 , DZX 16 ± 2 , DZX/TOLB 16 ± 2 , DZX/GLIB 12 ± 2 , DZX/PNU 5 ± 1 pA/pF; DZX/PNU vs baseline, $p < 0.001$).

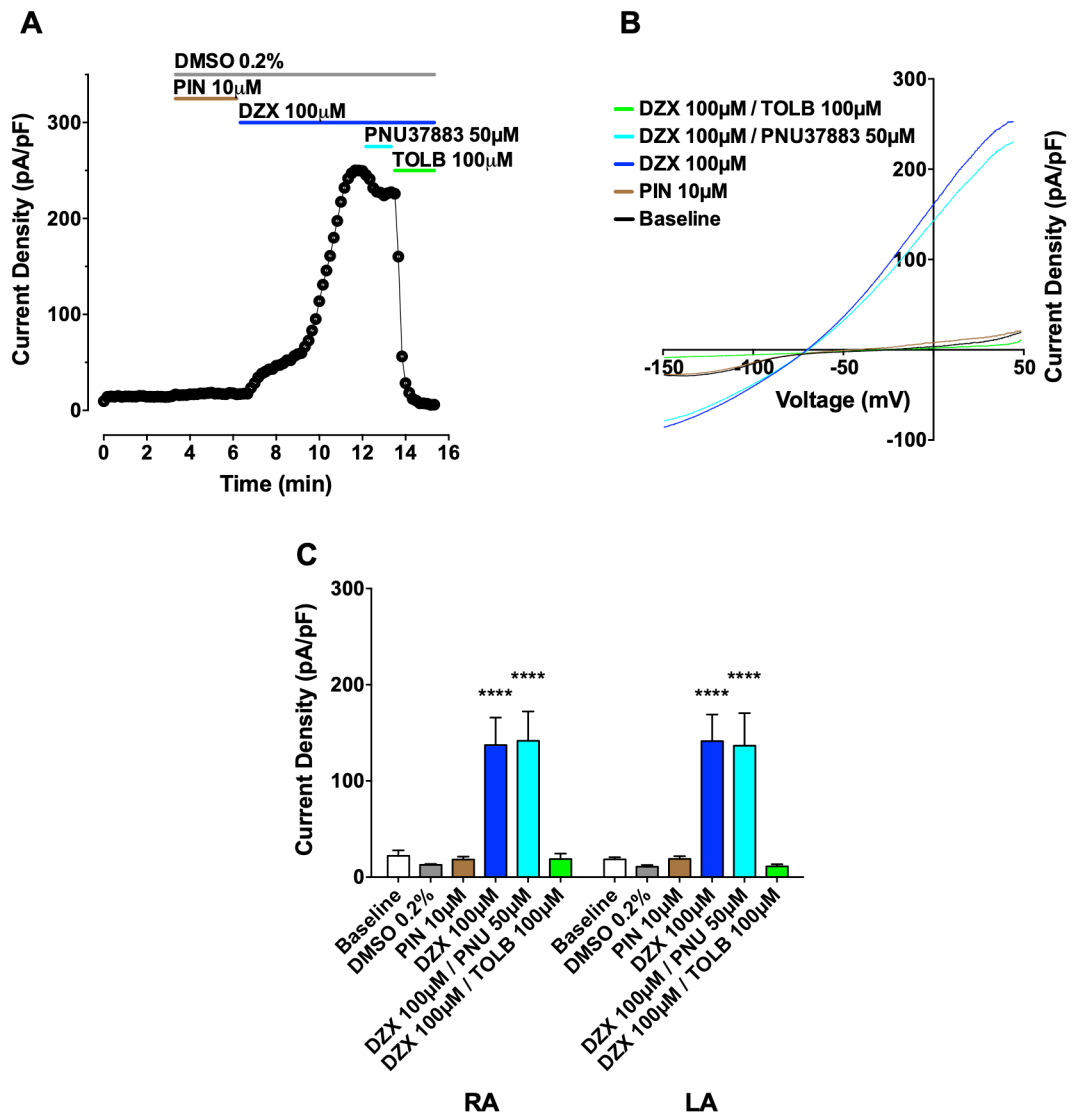
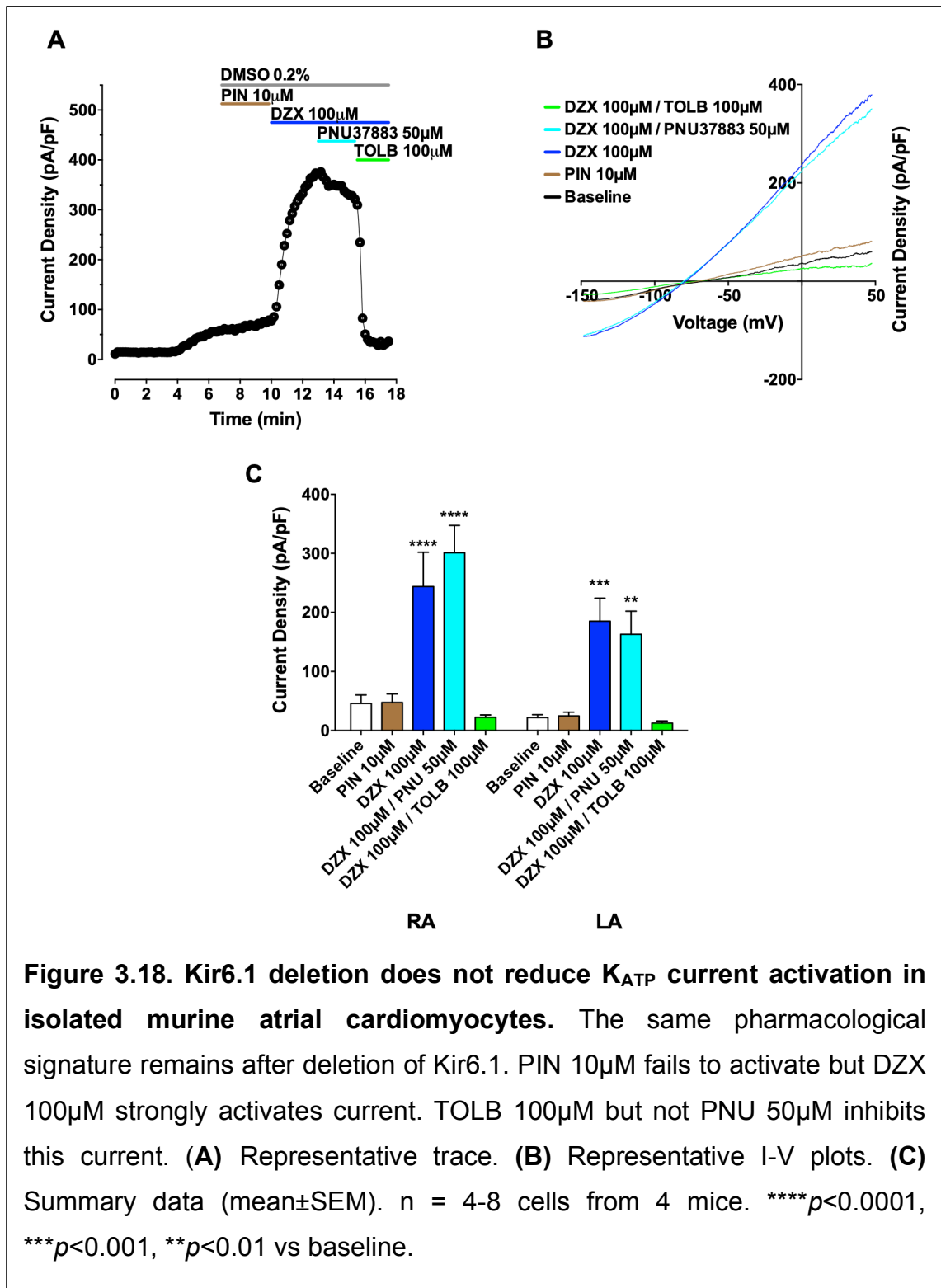
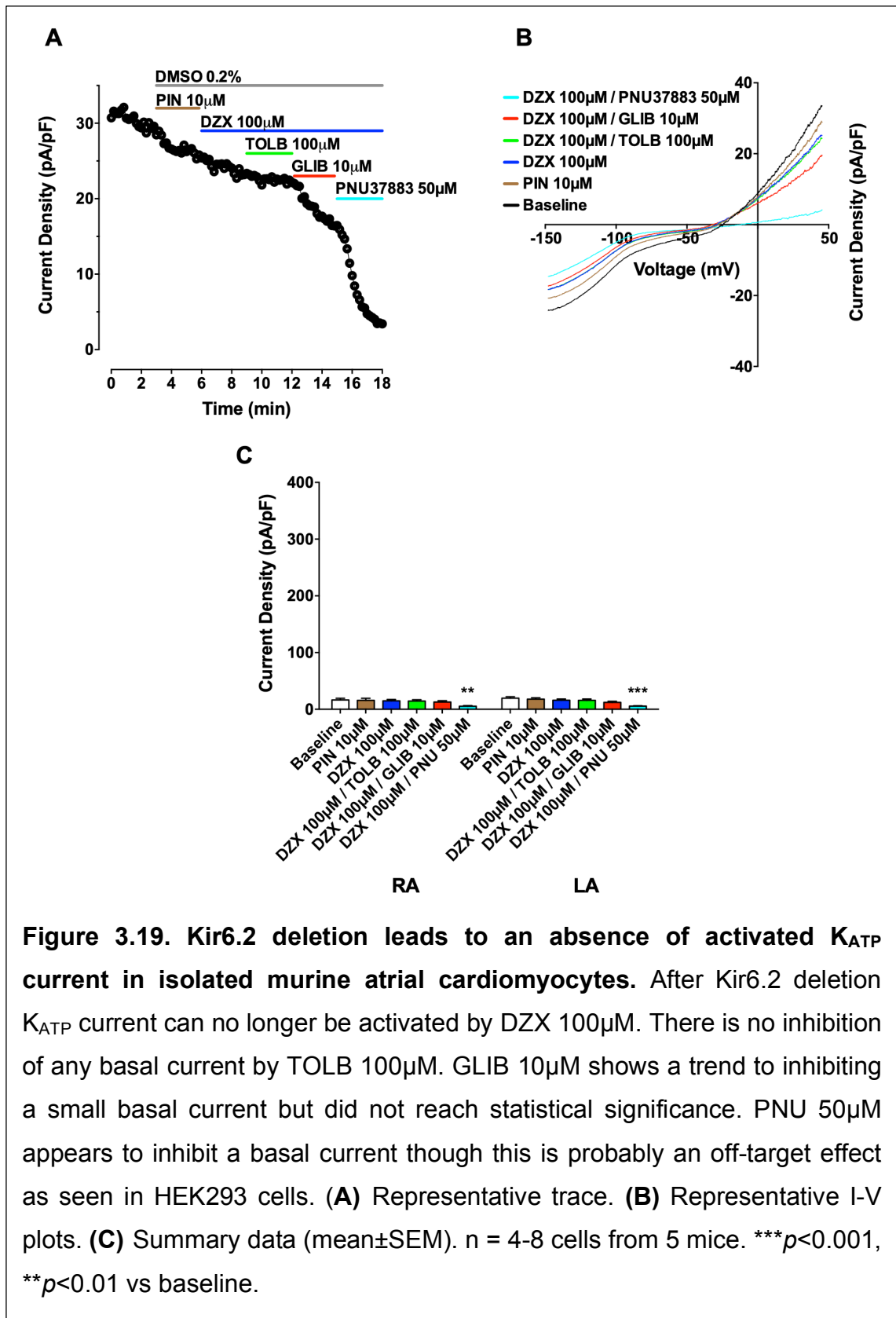
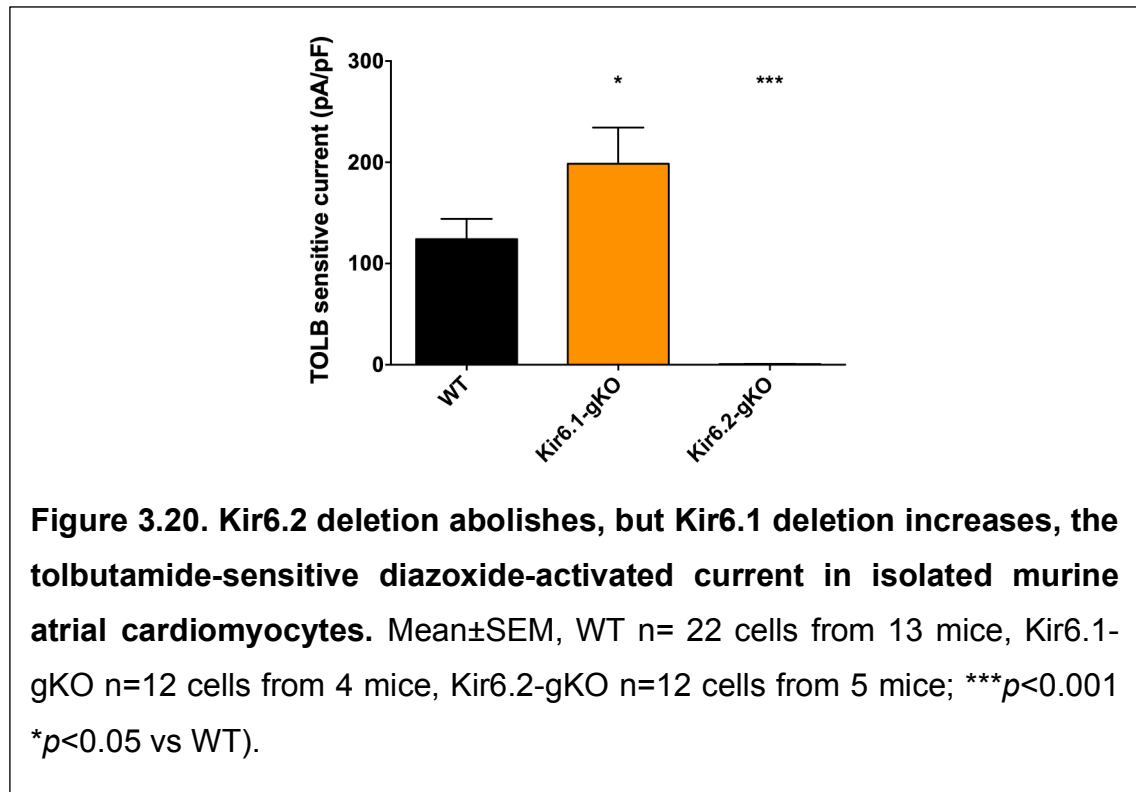


Figure 3.17. Demonstration of a K_{ATP} current in wild-type murine atrial cardiomyocytes with the pharmacological signature of Kir6.2/SUR1 subunits. In wild-type murine atrial cardiomyocytes PIN 10 μ M fails to activate but DZX 100 μ M strongly activates current. TOLB 100 μ M but not PNU 50 μ M inhibits this current which is indicative of Kir6.2/SUR1 K_{ATP} channels. **(A)** Representative trace. **(B)** Representative I-V plots. **(C)** Summary data (mean \pm SEM). n = 8-15 cells from 13 mice. **** p <0.0001 vs baseline.





Further, the tolbutamide-sensitive diazoxide-activated current was abolished in the Kir6.2-gKO murine atrial cardiomyocytes but it was increased in the Kir6.1-gKO mouse (WT n=22 cells from 13 mice: 120 ± 20 pA/pF; Kir6.1-gKO n=12 cells from 4 mice: 199 ± 36 pA/pF, $p < 0.05$ vs WT; Kir6.2-gKO n=12 cells from 5 mice: 0.7 ± 0.3 pA/pF, $p < 0.001$ vs WT see figure 3.20).



3.3.3 Kir6.2 but not Kir6.1 contributes to the resting membrane potential in isolated murine atrial cardiomyocytes

The equilibrium potential, taken as the clamped voltage on the ramp protocol where no current flowed, was taken as the resting membrane potential (RMP). Resting membrane potential did not differ between WT and Kir6.1g-KO atrial cardiomyocytes but those in the Kir6.2-gKO were more depolarised (WT n=28 cells from 13 mice: -41 ± 3 mV; Kir6.1-gKO n=14 cells from 4 mice: -49 ± 5 mV; Kir6.2-gKO n=14 cells from 5 mice: -27 ± 2 mV, $p < 0.01$ vs WT) see figure 3.21).

Further, on activation of K_{ATP} current by diazoxide, resting membrane potential was hyperpolarised in WT and Kir6.1-gKO atrial cardiomyocytes, an effect that was reversed by addition of tolbutamide. No such effect was seen in atrial cardiomyocytes from Kir6.2-gKO mice. (WT n=21 cells from 13 mice: baseline -42 ± 3 , DZX -73 ± 2 , DZX/TOLB -28 ± 5 mV; DZX vs baseline, $p < 0.0001$; DZX/TOLB vs baseline, $p < 0.01$; Kir6.1-gKO n=10 cells from 4 mice: baseline -53 ± 6 mV, DZX -75 ± 2 , DZX/TOLB -38 ± 7 mV; DZX vs baseline, $p < 0.01$; DZX/TOLB vs baseline $p < 0.05$; Kir6.2-gKO n=11 cells from 5 mice: baseline -26 ± 2 , DZX -25 ± 2 , DZX/TOLB -26 ± 2 mV, see figure 3.21).

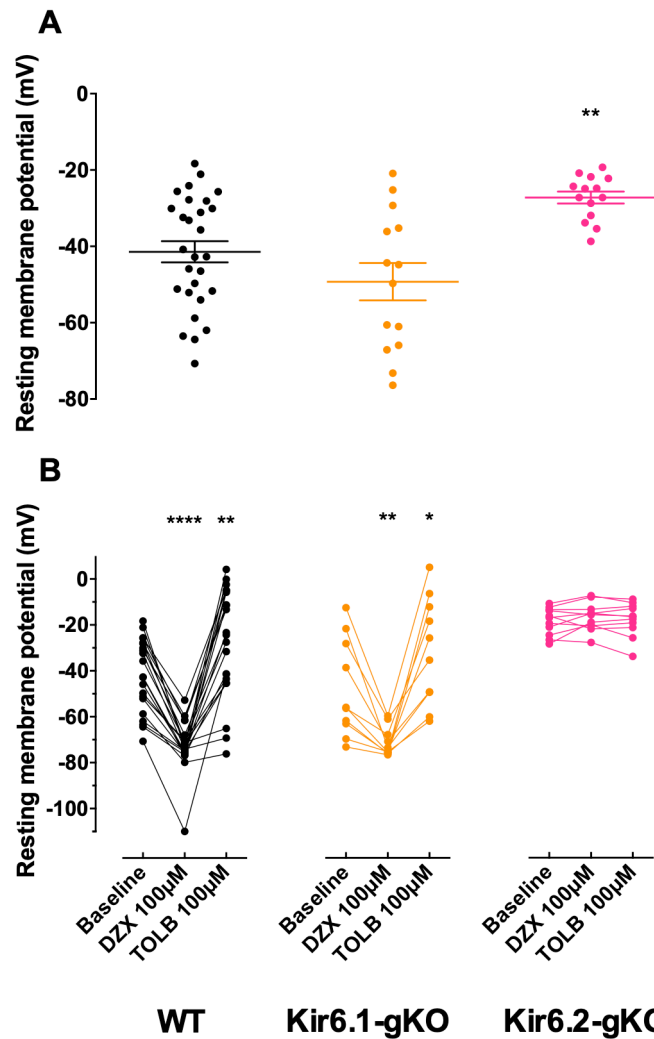
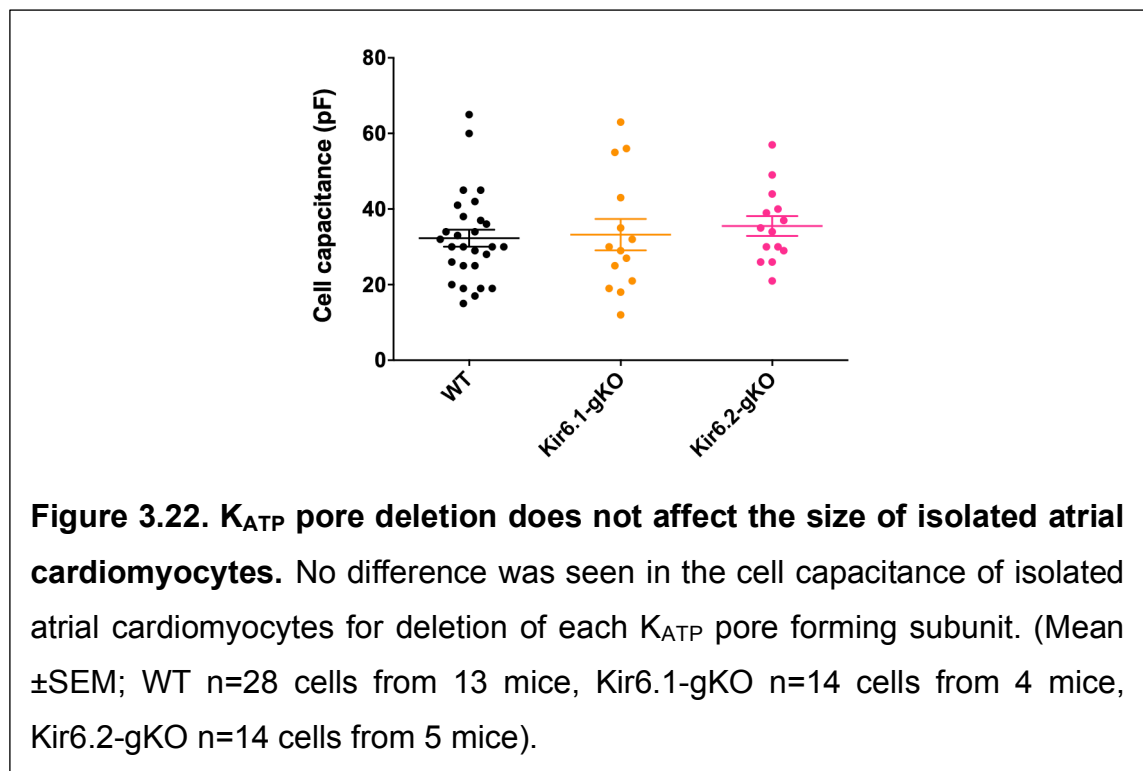


Figure 3.21. Kir6.2 deletion but not Kir6.1 deletion leads to a more depolarised resting membrane potential in isolated murine atrial cardiomyocytes. (A) Mean resting membrane potential at baseline. Kir6.1 deletion does not affect the RMP but Kir6.2 deletion leads to more depolarised cells (Data shown are mean±SEM; WT n=28 cells from 13 mice; Kir6.1g-KO n=14 cells from 4 mice; Kir6.2-gKO n=14 cells from 5 mice; ** p <0.01 vs WT). (B) Like WT atrial cardiomyocytes, Kir6.1-gKO cells also hyperpolarise on application of diazoxide, an effect reversed with tolbutamide, but none of these effects are seen after Kir6.2 deletion (repeated measures WT n=21 cells from 13 mice; Kir6.1g-KO n=10 cells from 4 mice; Kir6.2-gKO n=11 cells from 5 mice; * p <0.001, ** p <0.01, * p <0.05 vs baseline).**

3.3.4 Knockout of either K_{ATP} pore-forming subunit does not lead to hypertrophy in isolated atrial cardiomyocytes

Cell capacitance can be measured via capacitance transient cancellation after going into the whole-cell configuration during patch clamp. The capacitance of the cell is a surrogate for cell size as it is proportional to the membrane surface area, which, assuming the cell as a sphere, is itself proportional to the volume of the cell. No difference was seen in the capacitance of isolated atrial cardiomyocytes from WT, Kir6.1-gKO or Kir6.2-gKO mice (WT n=28 cells from 13 mice, 32 ± 2 ; Kir6.1-gKO n= 14 cells from 4 mice; 33 ± 4 , Kir6.2-gKO n=14 cells from 5 mice; 36 ± 3 pF see figure 3.22).

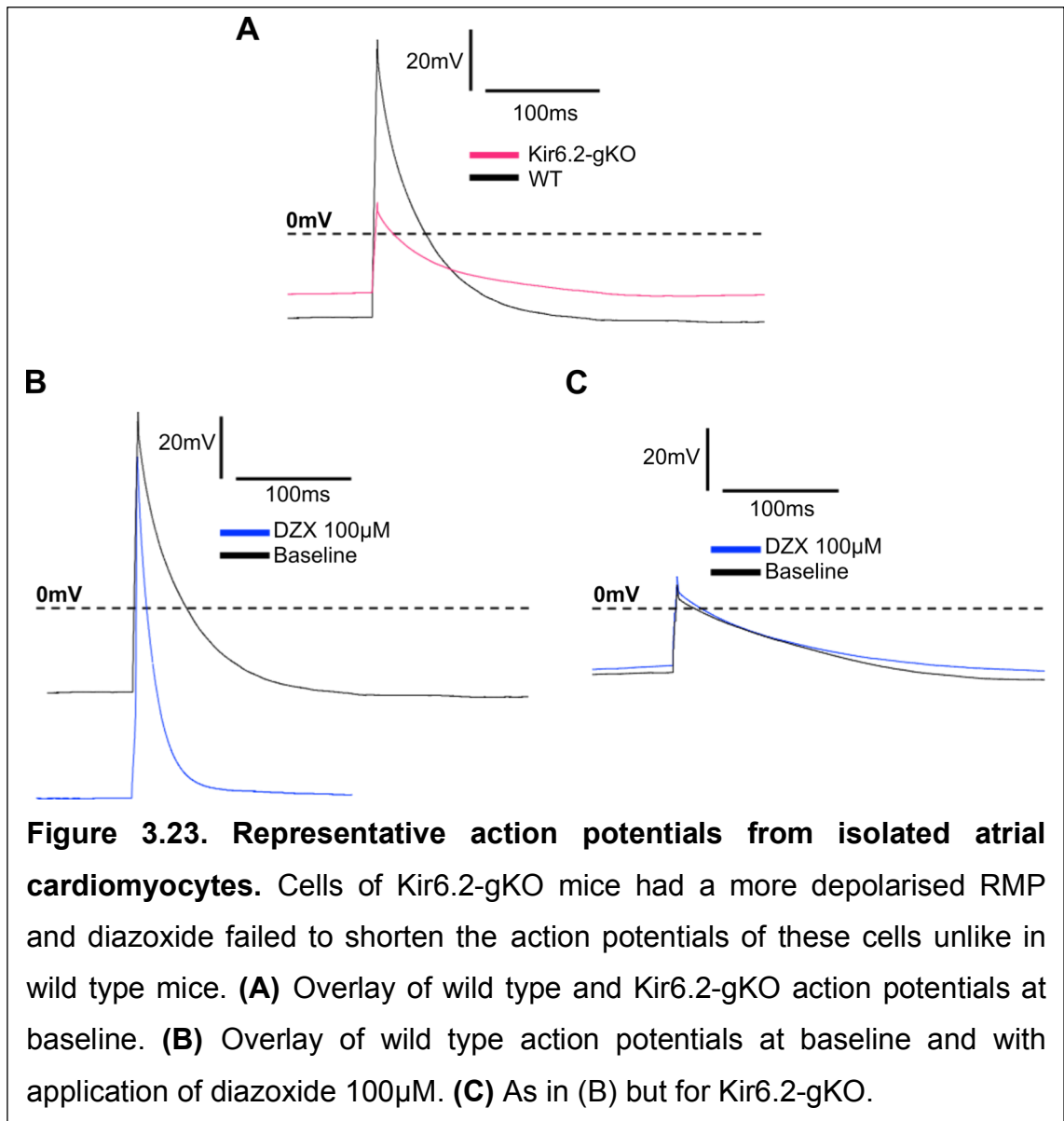


3.3.5 Kir6.2 contributes to the resting membrane potential in isolated atrial cardiomyocytes - reproducible with whole-cell action potential analysis

To confirm the effects of Kir6.2 deletion seen on the resting membrane potential of isolated atrial cardiomyocytes, my colleague Dr Aziz measured whole-cell action potentials triggered at 1Hz by 600pA/5ms square pulses in wild type and Kir6.2-gKO mice. Again, we found that the resting membrane potential, but also

the maximum diastolic potential (MDP), were both more depolarised in the Kir6.2-gKO mouse. Trends were also seen for a reduction in V_{\max} and a lesser degree of change of membrane potential during the action potential (delta, Δ) (RMP: WT -30 ± 3 , Kir6.2-gKO, -21 ± 1 mV, $p < 0.05$; MDP: WT -34 ± 4 , Kir6.2-gKO -24 ± 2 mV, $p < 0.05$; V_{\max} : WT 17 ± 2 , Kir6.2-gKO 11 ± 2 mV/ms, $p = 0.06$; Delta: WT 78 ± 10 , Kir6.2-gKO 51 ± 10 mV, $p = 0.06$; WT $n=10$ cells from 6 mice, Kir6.2-gKO $n=11$ cells from 5 mice; see figures 3.23 and 3.24).

Furthermore, in the absence of Kir6.2, again we found that the application of diazoxide was unable to hyperpolarise the RMP like it did in wild type isolated atrial cardiomyocytes (Paired data for RMP: WT $n=5$ cells from 3 mice, baseline -37 ± 4 , DZX -57 ± 7 mV, $p < 0.05$; Kir6.2-gKO $n=10$ cells from 5 mice, baseline -22 ± 1 , DZX -20 ± 2 mV; see figures 3.23 and 3.24).



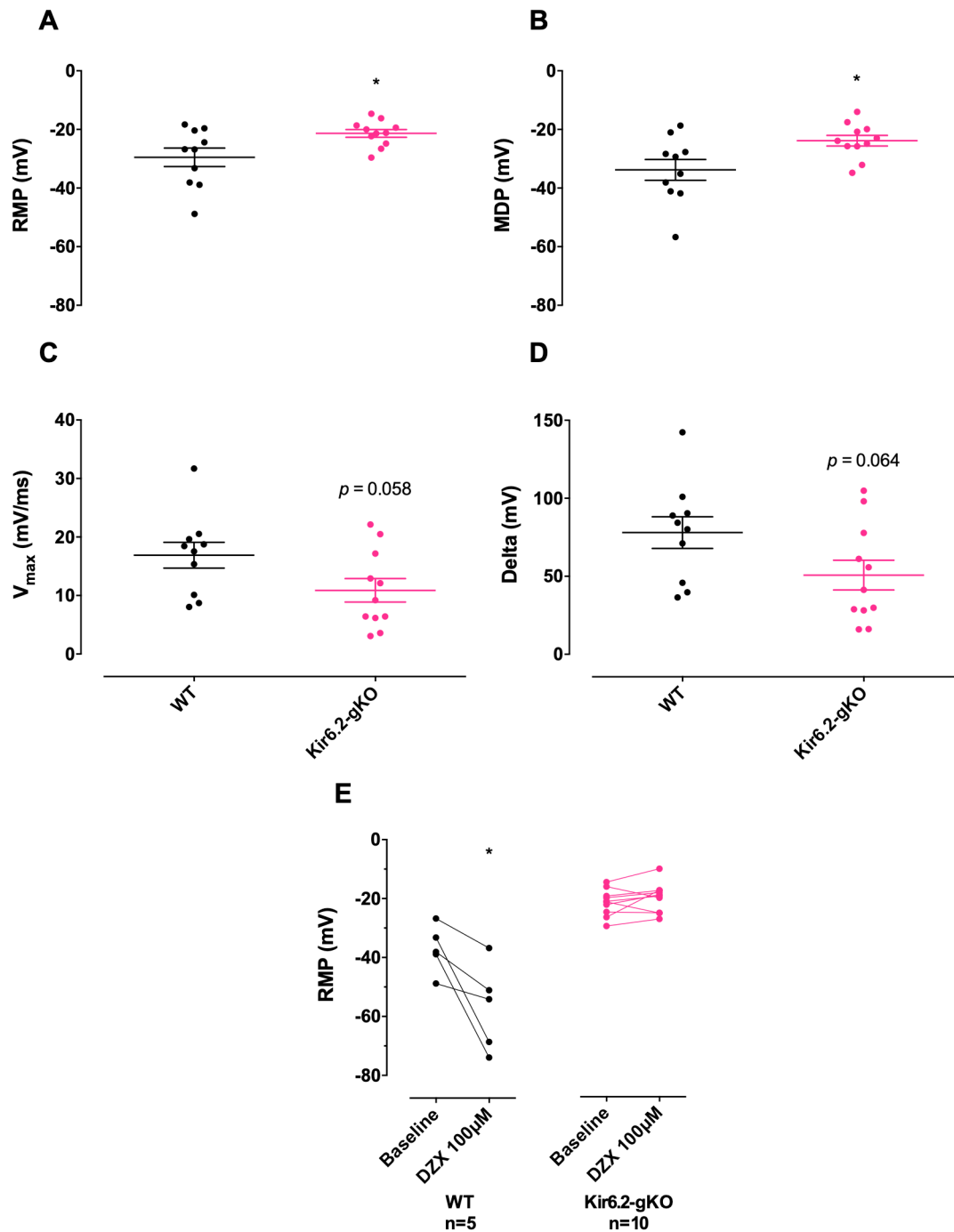


Figure 3.24. Kir6.2 deletion leads to changes in the parameters of the action potential in isolated atrial cardiomyocytes. Both RMP (A) and MDP (B) are more depolarised, and a trend is also seen for a reduction in V_{max} (C) and a lesser degree of change of membrane potential during the action potential (D), in isolated atrial cardiomyocytes of the Kir6.2-gKO mouse. (WT n=10 cells from 6 mice, Kir6.2-gKO n=11 cells from 5 mice, * $p < 0.05$). (E) Diazoxide fails to hyperpolarise the RMP of isolated atrial cardiomyocytes of the Kir6.2-gKO mouse like it does in the wild type (* $p < 0.05$).

3.3.6 Kir6.2 deletion leads to a failure of action potential shortening on K_{ATP} activation

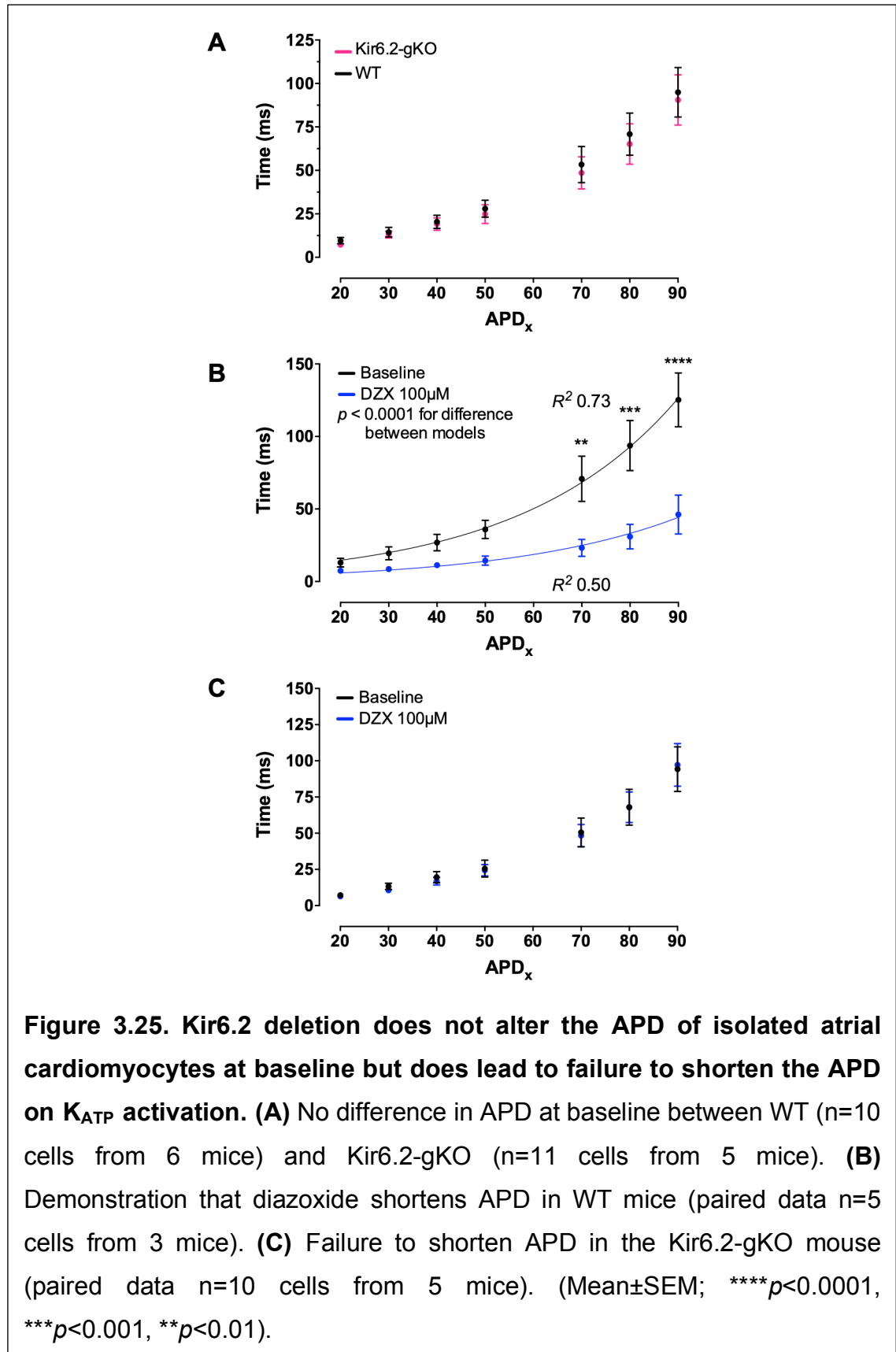
Whilst cells were more depolarised at rest, action potentials of Kir6.2-gKO atrial cardiomyocytes did not differ in duration at any point of repolarisation compared to wild type as can be seen by figure 3.25. Models of best fit were applied to the data. This was performed for two reasons. Firstly, to aid in comprehensive statistical comparisons, and secondly, to later extrapolate data on ERP from a whole heart tissue model back into the single cell model (see section 4.3). Data were best represented by an exponential growth model given by

$$Y = Y_0 \cdot e^{kx}$$

where Y is the action potential duration at the percentage repolarisation of interest and x is that percentage repolarisation. This was also visible by morphology of the action potentials such as in figure 3.23. Best fits were applied using the least squares method and the preferred model was a unifying fit for both wild type and Kir6.2-gKO (WT: $n=10$ cells from 6 mice, Y_0 6.0 ± 2.1 , k 0.031 ± 0.004 , R^2 0.58; Kir6.2-gKO: $n=11$ cells from 5 mice, Y_0 5.0 ± 1.9 , k 0.032 ± 0.005 , R^2 0.55; $p = 0.7115$ for a difference between models; unifying model Y_0 5.5 ± 1.4 , k 0.032 ± 0.003 , R^2 0.56).

Paired data were then analysed before and after application of diazoxide demonstrating shortening of action potentials in wild type mice but not in the Kir6.2-gKO. Again an exponential growth model could be best fitted to the data whereby separate fits were the preferred models for baseline and after diazoxide for wild type ($n=5$ cells from 3 mice; baseline Y_0 7.9 ± 2.8 , k 0.031 ± 0.004 , R^2 0.73; DZX Y_0 3.3 ± 1.7 , k 0.029 ± 0.006 , R^2 0.50; $p < 0.0001$) but a unifying model for Kir6.2-gKO ($n=10$ cells from 5 mice; baseline Y_0 5.1 ± 2.0 , k 0.033 ± 0.005 , R^2 0.56; DZX Y_0 4.0 ± 1.5 , k 0.036 ± 0.005 , R^2 0.65; $p = 0.9$, unifying model Y_0 4.5 ± 1.2 , k 0.034 ± 0.003 , R^2 0.60). When wild type data were subjected to repeated measures two-way ANOVA with Tukey's correction for multiple comparisons, an overall effect was seen for diazoxide in line with the difference between models with non-linear regression (repeated measures two-way ANOVA $p < 0.01$ by interaction) and significance specifically also for APD_{90} (baseline 125 ± 19 , DZX 46 ± 13 ms, $p < 0.0001$), APD_{80} (baseline $94 \pm$

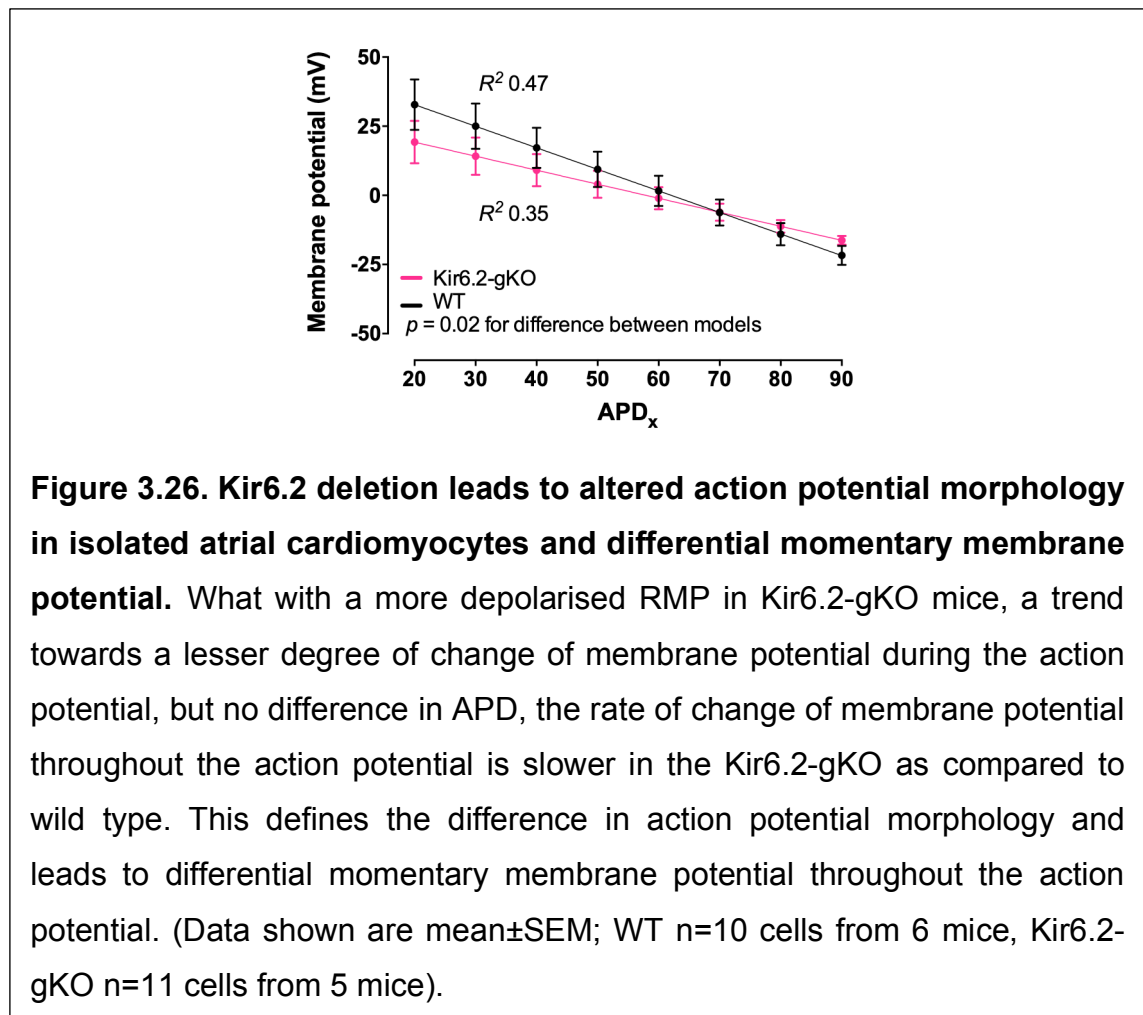
17, DZX 31 ± 8 ms, $p < 0.001$) and APD_{70} (baseline 71 ± 16 , DZX 23 ± 6 ms, $p < 0.01$).



Given the APD did not differ between WT and Kir6.2-gKO at baseline but RMP and MDP both did, an expected difference was found for the membrane potential at each time point of repolarisation, a factor defining the difference in AP morphology between the genotypes. Data were best represented by a linear function

$$Y = mx + c$$

where Y is the membrane potential at the percentage repolarisation of interest and x is that percentage repolarisation. Best fits were applied using the least squares method and the preferred model was one of two separate fits for WT and Kir6.2-gKO (WT $n=10$ cells from 6 mice, $m -0.78 \pm 0.09$, $c 48 \pm 6$, $R^2 0.47$; KO $n=11$ cells from 5 mice, $m -0.51 \pm 0.07$, $c 29 \pm 4$, $R^2 0.35$; $p < 0.05$; see figure 3.26).



3.3.7 Summary

The message from these data are that Kir6.2 and SUR1 are, in line with previous literature, the predominant subunits that make up the sarcolemmal K_{ATP} current in isolated murine atrial cardiomyocytes. The relative expression of mRNA and pharmacological signature through whole-cell patch clamp both support this. A current was present that was activated by diazoxide and not pinacidil, and was inhibited by tolbutamide but not PNU37883A. However, Kir6.1 may make up a small contributing proportion to the K_{ATP} current. Whilst there was no reduction in current with Kir6.1 deletion, there was an increase in current, and this could be manifested by a compensatory increase in Kir6.2 expression at the sarcolemma in place of deleted Kir6.1. Kir6.2 pore-forming subunits have an approximately double unitary conductance compared to Kir6.1 and, thus, if Kir6.2 compensates for loss of Kir6.1, one could expect the whole-cell current to be larger. With these data the apparent down-regulation of SUR1 in the Kir6.1-gKO did not appear to manifest any functional significance given the K_{ATP} current was increased in the Kir6.1-gKO.

A deletion of either pore, but particularly Kir6.2, might be expected to lead to cell hypertrophy if action potential duration is prolonged and there are greater influxes of calcium leading to secondary messenger switch on of hypertrophy genes by the calcineurin/NFAT pathway. Cell capacitance was not different between the genotypes suggesting this was not the case. The mice were, however, not stressed in the lead up to experiments. Data exist that deletion of Kir6.2 leads to a maladaptive response to stress and ischaemia in the murine heart, particularly with respect to the ventricle. This compromises contractile function and increases the incidence of arrhythmias, and that this is in large part due to an inability to shorten the action potential and leads to calcium handling abnormalities (Suzuki *et al.*, 2001; 2002; Zingman *et al.*, 2002; Suzuki *et al.*, 2003). I did not see a difference in action potential duration at baseline but deletion of Kir6.2 did lead to a failure of action potential shortening on application of the K_{ATP} opener diazoxide, a finding not reported in isolated atrial cardiomyocytes before. Another finding not previously reported in the literature is that Kir6.2 appears to contribute to the resting membrane potential given by the more depolarised state in the Kir6.2-gKO. The action potential morphology

in this knockout is also different with a shallower change of membrane potential through repolarisation back to the more depolarised resting state. This might well contribute to differences in refractoriness of cells and tissue, and the more depolarised resting state could induce periods of post-repolarisation refractoriness due to failure of recovery from inactivation of a significant population of sodium channels.

3.4 K_{ATP} activation slows automaticity in a murine atrial tissue model utilising HL-1 cells

HL-1 cells are immortalised cells derived from murine atrial cardiomyocytes that retain their differentiated adult phenotype and continue to beat spontaneously despite repeated culture. When cultured as syncytia they set up cell-to-cell communication via gap junctions and are a useful model of a 2D tissue sheet. They share electrophysiological properties of both murine atrial and SAN cardiomyocytes which also lends them as a good model for an ectopic atrial automatic focus (White *et al.*, 2004; Yang & Murray, 2011). A proposed mechanism for the drivers of atrial fibrillation are automatic or triggered activity emanating from the inter-digitating cardiomyocyte sleeves of the pulmonary veins (Haïssaguerre *et al.*, 1998; Chen *et al.*, 1999; 2001). HL-1 cells are a reasonable model for such cells.

3.4.1 HL-1 cells exhibit a K_{ATP} current and the functional expression is one of Kir6.2/SUR1 subunit composition

I first sought to look for a K_{ATP} current in HL-1 cells and characterise it using whole-cell patch clamp. Isolated HL-1 cells were kindly cultured by Dr Muriel Nobles.

In isolated HL-1 cells pinacidil 10 μ M failed to activate current but diazoxide 100 μ M strongly activated current. This current was completely inhibited by the subsequent application of tolbutamide 100 μ M. (Baseline 6.7 ± 0.6 , PIN 7.2 ± 1.0 , DZX 13 ± 2 , DZX/TOLB 5.5 ± 0.6 pA/pF; n=18 cells; DZX vs baseline $p < 0.01$; see figure 3.27).

In a separate set of cells the effect of PNU37883A was investigated. After activation with diazoxide, PNU37883A did not significantly inhibit the current. (Baseline 10.8 ± 3.5 , DZX 27.2 ± 7.5 , DZX/PNU 22.2 ± 6.3 , DZX/TOLB 3.8 ± 2.7 pA/pF; n=6 cells; DZX and DZX/PNU vs baseline $p < 0.05$; see figure 3.28).

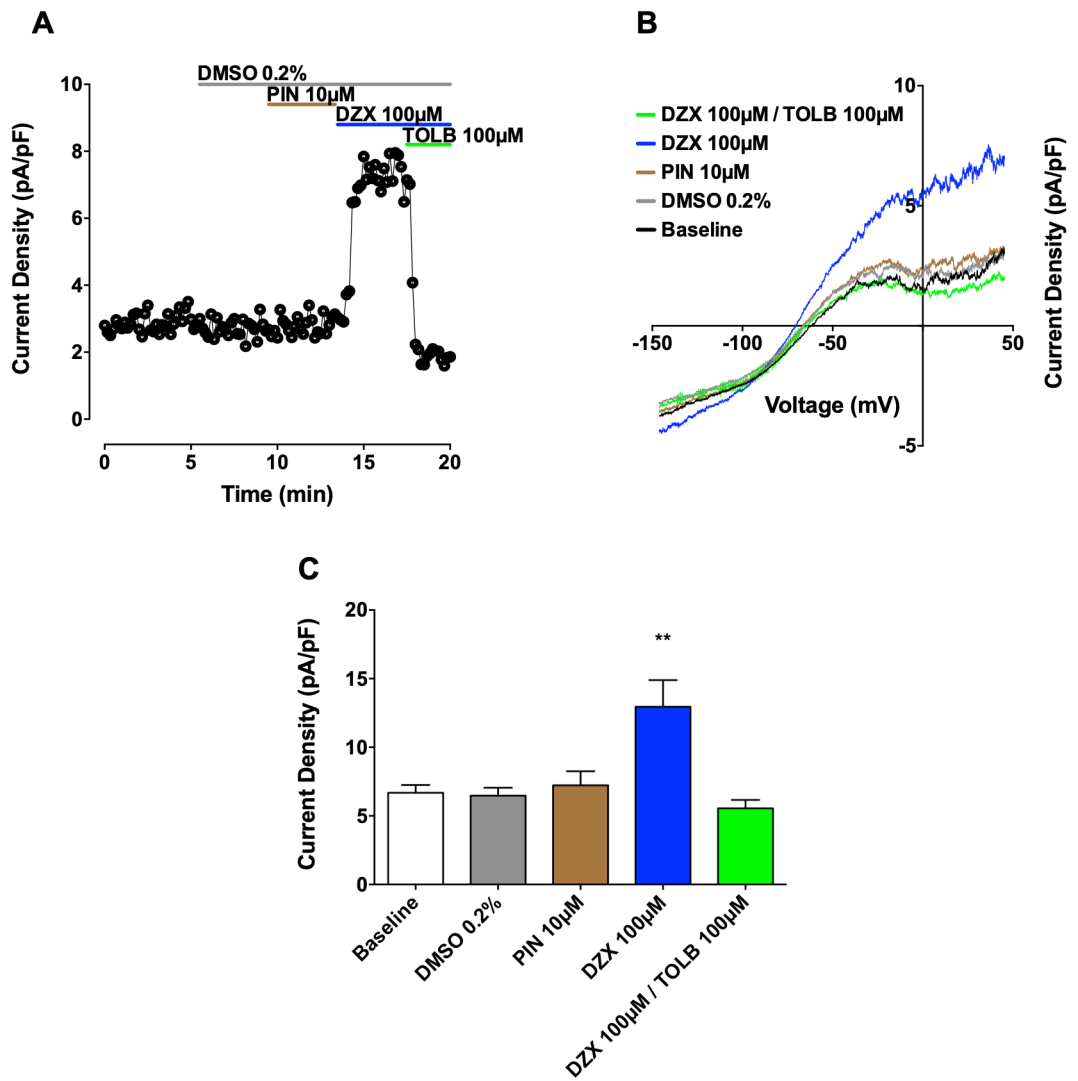


Figure 3.27. HL-1 cells exhibit a K_{ATP} current activated by diazoxide but not pinacidil. (A) Representative trace. (B) Representative I-V plot. (C) Summary data. (Mean \pm SEM; n=18 cells, ** p <0.01 vs baseline).

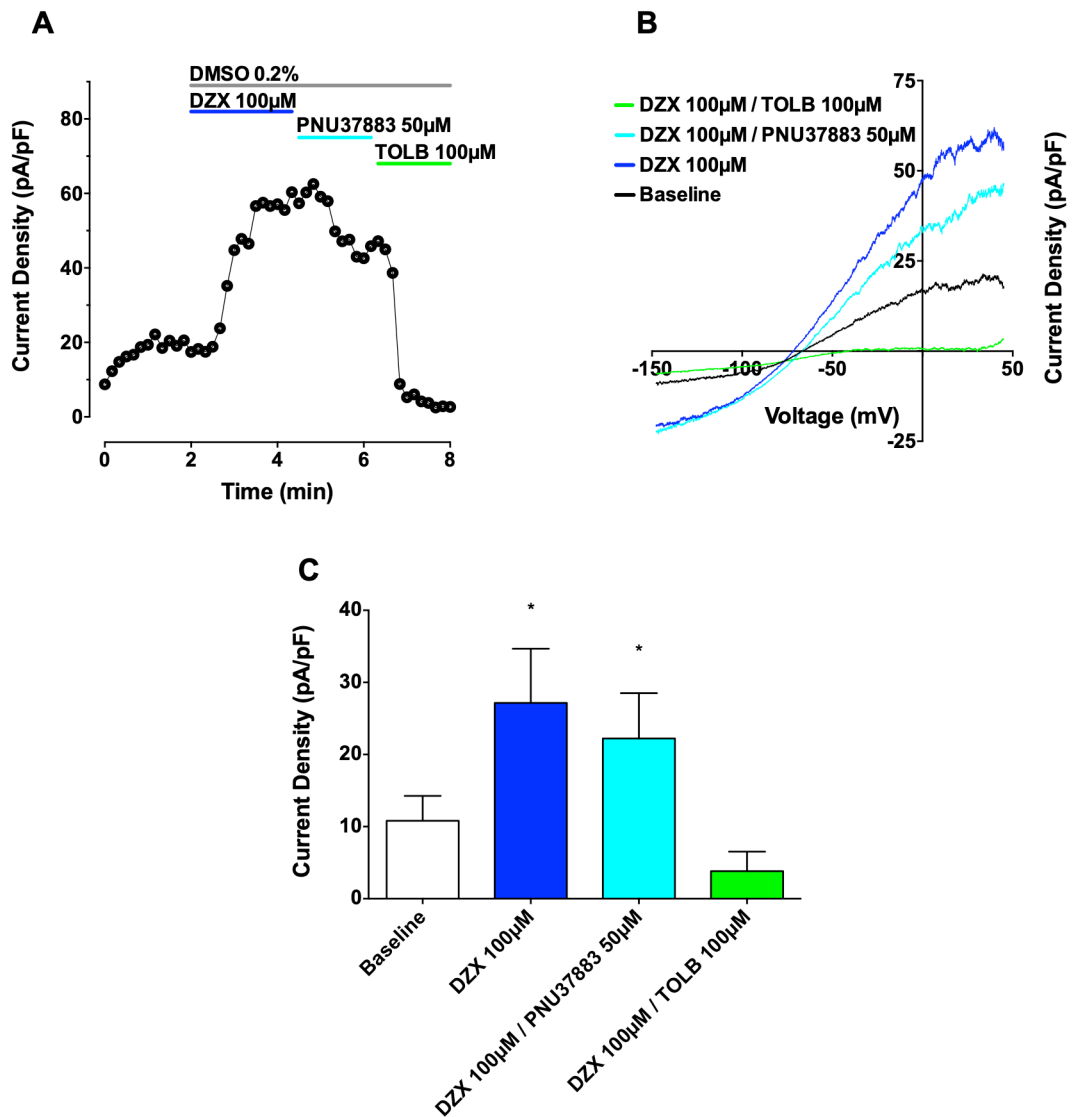
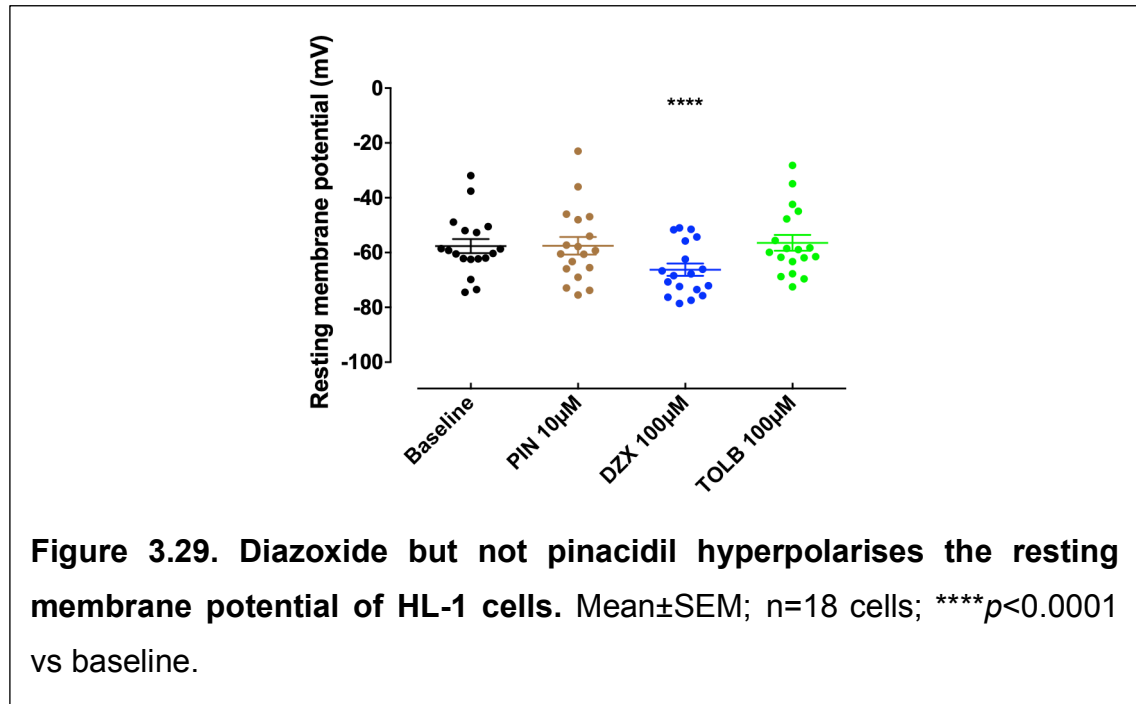


Figure 3.28. The K_{ATP} current in HL-1 cells is inhibited by tolbutamide but not PNU37883A. **(A)** Representative trace. **(B)** Representative I-V plot. **(C)** Summary data. (Mean \pm SEM; n=6 cells, * p <0.05 vs baseline).

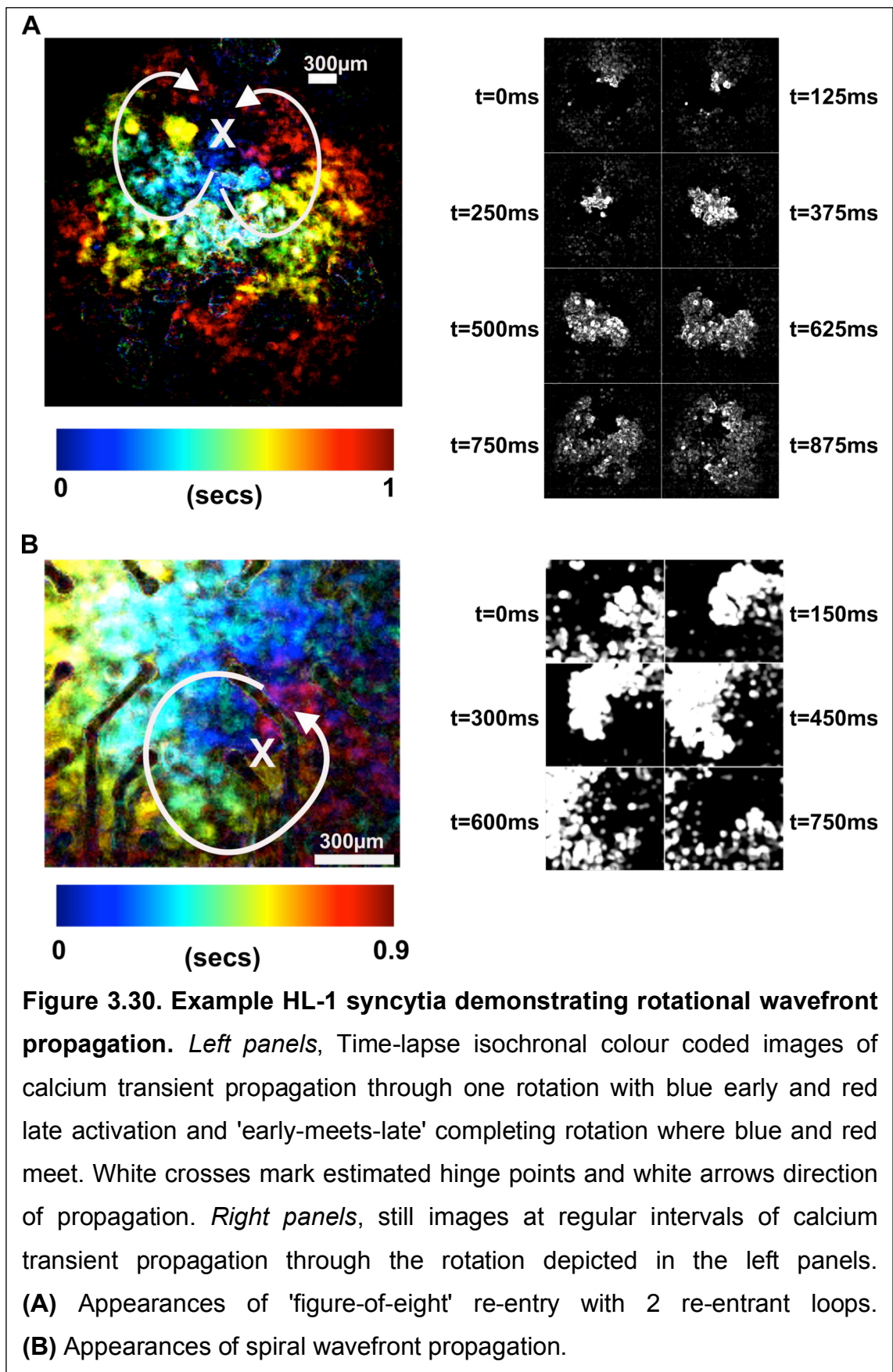
Furthermore, the resting membrane potential, taken as the clamped voltage on the ramp protocol where no current flowed, was hyperpolarised by the application of diazoxide but not pinacidil, an effect reversed by the subsequent application of tolbutamide. (RMP: baseline -58 ± 3 , PIN -58 ± 3 , DZX -66 ± 2 , DZX/TOLB -56 ± 3 mV; $n=18$ cells; DZX vs baseline $p < 0.0001$; see figure 3.29).



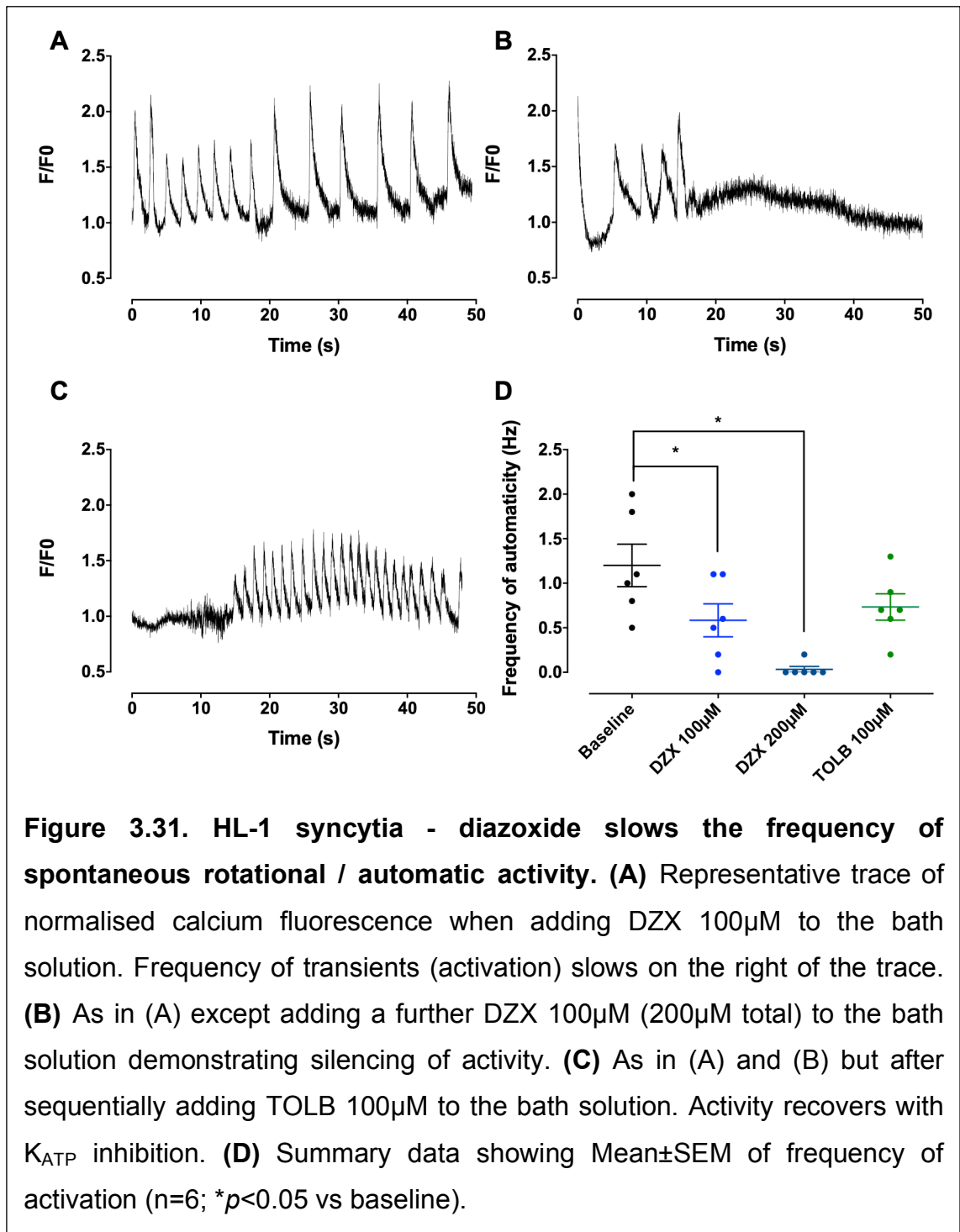
3.4.2 HL-1 cell syncytia exhibit spontaneous rotational activity that can be abolished by application of the K_{ATP} opener diazoxide

Syncytia of HL-1 cells were cultured in an MEA (Multichannel Systems, Germany). They have a circular dish 1600 μ m in diameter with 60 flat electrodes 30 μ m in diameter spaced 200 μ m apart in an 8x8 grid fashion for measuring field potentials as necessary. I did not utilise the function to measure field potentials and focussed on recording calcium transients as described in section 2.9. The MEA was used as it provided a convenient vessel for culture that could also be temperature-controlled at 37 $^{\circ}$ C for experiments, as it was compatible with the TC02 temperature controller (Multichannel Systems, Germany).

Syncytia would typically set up spontaneous rotational wavefronts of activation. Examples are shown in figure 3.30.



The frequency of spontaneous wavefront activation was recorded after application of diazoxide and tolbutamide as described in section 2.9. Diazoxide 100 μ M slowed the frequency of activation in all syncytia, and re-organised the activation wavefront from that of rotational activity to a straight and flat wave front spreading uniformly across the array in 5 out of 6 syncytia ($p < 0.05$ by Fisher's exact test). Adding a further diazoxide 100 μ M (200 μ M total) would abolish activation and silence the syncytia in all but 1 out of the 6. In the syncytium where diazoxide 200 μ M did not abolish activation, the frequency of activation was still slowed considerably further to that in the presence of diazoxide 100 μ M. Adding tolbutamide 100 μ M would recover activity in the 5 syncytia that were silenced by diazoxide 200 μ M, and increased the frequency of activation in the syncytium that was not silenced. (Frequency of activation $n=6$: Baseline 1.2 ± 0.24 , DZX 100 μ M 0.58 ± 0.19 , DZX 200 μ M 0.03 ± 0.03 , DZX 200 μ M/TOLB 100 μ M 0.73 ± 0.15 Hz; DZX 100 μ M vs baseline $p < 0.05$, DZX 200 μ M vs baseline $p < 0.05$; see figure 3.31).



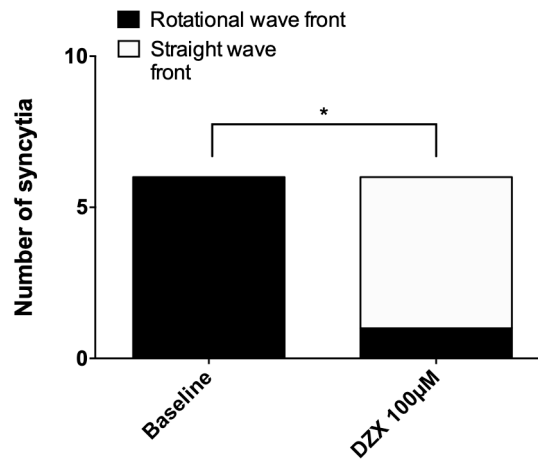


Figure 3.32. HL-1 syncytia - diazoxide can re-organise activation wavefronts from rotational to straight and uniform. * $p < 0.05$ by Fisher's exact test.

3.4.3 Summary

HL-1 cells exhibit a K_{ATP} current that has the pharmacological signature of a subunit composition given by Kir6.2/SUR1, the same predominant composition as that in murine atrial cardiomyocytes. This finding is somewhat unsurprising, but nonetheless reassuring, given HL-1 cells are derived from murine atrial cardiomyocytes. K_{ATP} activation hyperpolarises HL-1 cells in isolation.

HL-1 cells have been shown to express gap junction proteins and evidence on the arrays through calcium fluorescence shows they exhibit cell-to-cell conduction and set up spontaneous activation wavefronts in a rotational fashion. K_{ATP} activation slows the frequency of this activation in a dose dependent manner. At a high dose K_{ATP} activation can silence activation completely. K_{ATP} activation also re-organises rotational activation wavefronts to straight and uniform wavefronts. Such findings are interesting from a translational perspective in terms of arrhythmia mechanisms and potential therapies. If automatic or micro-re-entrant circuits in, for example, the extending myocardial sleeves of left atrium into pulmonary vein are at play in driving atrial arrhythmias, then K_{ATP} channel activation might be a pharmacological therapeutic target.

3.5 K_{ATP} activation during hypoxia contributes to sinus node depression, but pharmacological activation alone does not

Further to the findings from the experiments with the HL-1 syncytia where spontaneous activation was slowed by K_{ATP} activation, I sought to investigate whether K_{ATP} activation could slow spontaneous sinus node activation. Evidence from our lab has uncovered that Kir6.1 contributes to a K_{ATP} current in the murine sinus node. Whilst a proportion of isolated cells displayed current activation with pinacidil 10 μ M, the vast majority of cells displayed a current with the pharmacological signature of the SUR1 sulphonylurea receptor subunit and activation by diazoxide 100 μ M (Aziz *et al.*, 2018). The K_{ATP} openers pinacidil and cromakalim have been shown to hyperpolarise and slow spontaneous activation in isolated rabbit SAN cells and another group has demonstrated that Kir6.2 deletion reverses hypoxia driven slowing of sinus node spontaneous activation in a whole heart Langendorff model (Han *et al.*, 1996; Fukuzaki *et al.*, 2008).

3.5.1 Pharmacological K_{ATP} activation does not slow sinus node rate in a whole heart model

I first tested whether K_{ATP} activation in a whole heart Langendorff model would slow spontaneous sinus node activation. The Langendorff set up and signal recording via the FlexMEA (Multichannel Systems, Germany) has been described in sections 2.8.2 and 2.8.3. After a period of stabilisation the spontaneous cycle length of Langendorff beating wild type hearts was recorded at baseline, after 3 minutes perfusion of diazoxide 100 μ M, and then followed by 3 minutes perfusion with diazoxide 200 μ M. No change in spontaneous cycle length was seen. (Cycle length: baseline 145 \pm 11, DZX 100 μ M 143 \pm 8, DZX 200 μ M 142 \pm 6 ms; n=8 hearts; see figure 3.33).

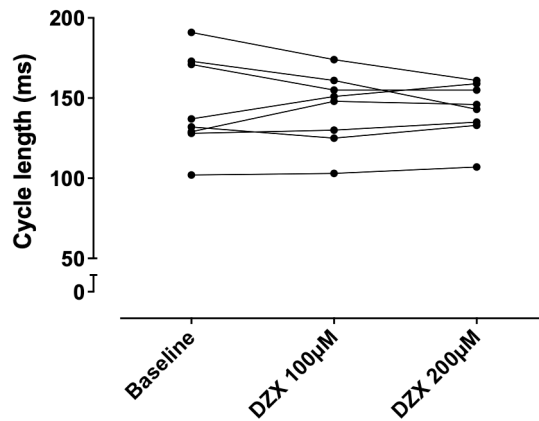


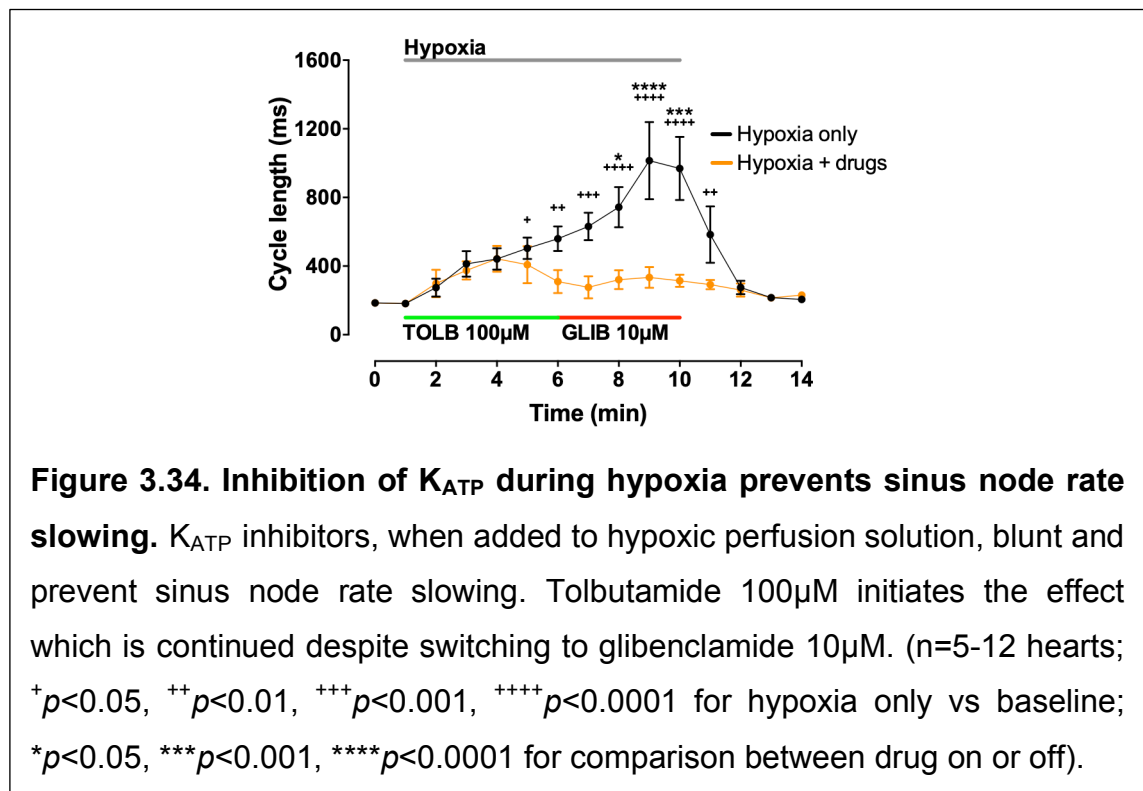
Figure 3.33. Pharmacological K_{ATP} activation does not slow spontaneous sinus node rate in the whole heart. Perfusate containing up to diazoxide 200µM did not slow sinus node rate in the Langendorff mouse heart (n=8).

3.5.2 Inhibition of K_{ATP} during hypoxia prevents sinus node rate slowing

Langendorff wild type mouse hearts were then subjected to hypoxic conditions. As described in section 2.8.2 this was achieved by pre-bubbling Krebs solution with 95% N_2 / 5% CO_2 . After a period of stabilisation hearts were perfused with the hypoxic solution continuously for 9 minutes followed by 4 minutes washout with oxygenated Krebs solution. A separate set of hearts were perfused with hypoxic solution containing tolbutamide 100µM for 5 minutes, and then switched to hypoxic solution containing glibenclamide 10µM for 4 minutes, before washout with oxygenated Krebs for 4 minutes.

Hypoxia caused marked sinus node rate slowing, see figure 3.34 (selected time points, cycle length: baseline, 182 ± 16 ms; 5mins hypoxia, 560 ± 72 ms, $p < 0.01$ vs baseline; 9mins hypoxia, 969 ± 184 ms, $p < 0.0001$ vs baseline; 4mins washout, 206 ± 12 ms; n=5-12 hearts). With the addition of K_{ATP} inhibitors there was no significant difference to baseline of sinus node rate (selected time points, cycle length: baseline, 182 ± 16 ms; 5mins hypoxia with TOLB 100µM, 309 ± 67 ms; 9mins hypoxia with 4mins GLIB 10µM, 315 ± 36 ms; 4mins washout, 231 ± 20 ms; n=5-12 hearts).

On comparisons between the condition of having K_{ATP} inhibitors added to the perfusate and hypoxia alone at each time point, the blunting effect of K_{ATP} inhibitors on sinus node slowing during hypoxia was seen further (cycle length: 7 minutes of hypoxia alone, 744 ± 117 ms, $n=7$ hearts vs 7 minutes hypoxia with K_{ATP} inhibitors (5 minutes tolbutamide $100\mu\text{M}$ / 2 minutes glibenclamide $10\mu\text{M}$), 321 ± 55 ms, $n=5$ hearts; $p < 0.05$ for comparison; 8 minutes of hypoxia alone, 1015 ± 225 ms, $n=7$ hearts vs 8 minutes hypoxia with K_{ATP} inhibitors (5 minutes tolbutamide $100\mu\text{M}$ / 3 minutes glibenclamide $10\mu\text{M}$), 334 ± 60 ms, $n=5$ hearts; $p < 0.0001$ for comparison; 9 minutes of hypoxia alone, 969 ± 184 ms, $n=7$ hearts vs 9 minutes hypoxia with K_{ATP} inhibitors (5 minutes tolbutamide $100\mu\text{M}$ / 4 minutes glibenclamide $10\mu\text{M}$), 315 ± 36 ms, $n=5$ hearts; $p < 0.001$ for comparison, see figure 3.34.



3.5.3 Summary

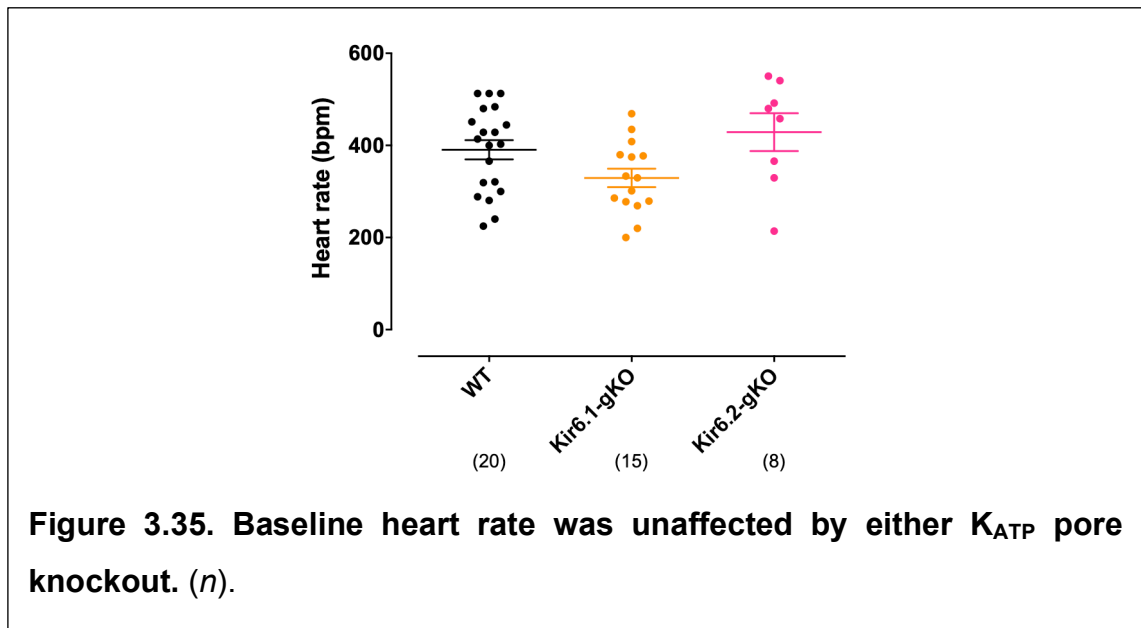
Pharmacological activation alone is unable to slow the spontaneous sinus node rate in wild type Langendorff mouse hearts. Hypoxia appears to produce a much more profound effect on sinus node rate causing considerable depression. This is, in at least part, due to K_{ATP} activation during hypoxia as other investigators have shown that Kir6.2 deletion causes an absence of this effect (Fukuzaki *et al.*, 2008), and I have shown that pharmacological K_{ATP} inhibition produces the same effect. In line with our lab's previous work suggesting that the pharmacological signature of the sinus node K_{ATP} current is one of SUR1 as the sulphonylurea subunit, tolbutamide 100 μ M is able to reverse sinus node rate slowing during hypoxia.

3.6 Both K_{ATP} pore-forming subunits contribute to tissue-level electrophysiology of the atria in murine whole heart

Given that the HL-1 syncytia atrial model demonstrated that K_{ATP} activation had an important impact on cardiac myocyte activity and arrhythmia generation, I wanted to next investigate the effects of K_{ATP} inhibition on parameters thought widely to affect arrhythmogenicity, ERP and conduction velocity. The data had suggested there was an, albeit small, Kir6.1 contribution to the sarcolemmal K_{ATP} current in isolated atrial cardiomyocytes, delineated by an increase in current in the Kir6.1-gKO atrial cells which may well be due to compensation by Kir6.2 with its larger unitary conductance. I was keen to investigate any differences in electrophysiology of tissue in the Kir6.1-gKO that would support this. On top of this, a complete dissection of these electrophysiological parameters directly comparing both pore-forming knockout mice had not been reported in the literature. As such, hearts from both pore-forming knockout mice were subjected to programmed electrical stimulation in a Langendorff set-up, and ERP and CV measured using the FlexMEA (Multichannel Systems, Germany) as described in sections 2.8.2 and 2.8.3. Experiments were repeated at various time points during perfusion of hypoxic solution to activate a K_{ATP} current. After a period of stabilisation and baseline recordings, hypoxia was induced by switching to a Krebs solution pre-bubbled with 95% N_2 / 5% CO_2 . Hypoxia was maintained for 12 minutes. For a cohort of wild type and Kir6.1-gKO hearts, between minutes 8 to 12 the perfusing solution was changed to a hypoxic one also containing tolbutamide 100 μ M. The final 6 minutes of the protocol were washout back to an oxygenated perfusing solution with no drugs. Programmed electrical stimulation was performed every 2 minutes.

3.6.1 Both K_{ATP} pore-forming subunits affect the atrial effective refractory period, and Kir6.2 is crucial to preventing its prolongation during hypoxia

Baseline heart rate was recorded. No significant difference was seen between the genotypes (WT, 391 \pm 21 bpm, n=20; Kir6.1-gKO, 329 \pm 20 bpm, n=15; Kir6.2-gKO, 429 \pm 41 bpm, n=8; see figure 3.35).



Baseline ERP was prolonged in both Kir6.1-gKO and Kir6.2-gKO atria (WT, 26 ± 2 ms, $n=20$; Kir6.1-gKO, 47 ± 5 ms, $n=15$, $p < 0.0001$ vs WT; Kir6.2-gKO, 42 ± 4 ms, $n=8$, $p < 0.05$ vs WT). ERP after 8 minutes of hypoxia was also prolonged in both knockout mice, and Kir6.2-gKO more prolonged than Kir6.1-gKO (WT, 21 ± 2 ms, $n=16$; Kir6.1-gKO, 46 ± 9 ms, $n=12$, $p < 0.05$ vs WT; Kir6.2-gKO, 74 ± 11 ms, $n=8$, $p < 0.0001$ vs WT, $p < 0.05$ vs Kir6.1-gKO). In the cohort of wild type hearts that were also given tolbutamide $100\mu\text{M}$ in the hypoxic perfusate, after hypoxia for 12 minutes, ERP was prolonged in the tolbutamide group (No TOLB, 22 ± 3 ms, $n=11$; +TOLB, 44 ± 10 ms, $n=6$; $p < 0.05$; see figure 3.36).

Whilst atrial ERP was prolonged compared to wild type in terms of absolute values for both knockouts, when normalised to baseline, like the WT, Kir6.1-gKO atria maintained their ERP through hypoxia. In the Kir6.2-gKO mouse, however, ERP prolonged out even further (selected time points % change in ERP compared to baseline: 6 minutes hypoxia - WT, $-7 \pm 8\%$, $n=17$; Kir6.1-gKO, $-17 \pm 11\%$, $n=11$; Kir6.2-gKO, $+60 \pm 17\%$, $n=8$, $p < 0.001$ vs WT; 12 minutes hypoxia - WT, $-9 \pm 9\%$, $n=11$; Kir6.1-gKO, $-41 \pm 11\%$, $n=4$; Kir6.2-gKO, $+114 \pm 47\%$, $n=7$, $p < 0.0001$ vs WT; after 8 minutes washout - WT, $+17 \pm 9\%$, $n=12$; Kir6.1-gKO, $+13 \pm 20\%$, $n=5$; Kir6.2-gKO, $+66 \pm 22\%$, $n=7$, $p < 0.05$ vs WT). In the cohort of WT and Kir6.1-gKO hearts that were also given tolbutamide in the hypoxic perfusate, ERP prolonged out in a similar fashion to

Kir6.2-gKO hearts in the absence of tolbutamide (ERP % change compared to baseline at 12 minutes hypoxia: WT no TOLB, $-9 \pm 9\%$, $n=11$; WT+TOLB, $+74 \pm 33\%$, $n=6$, $p < 0.0001$; Kir6.1-gKO no TOLB, $-41 \pm 11\%$, $n=4$ Kir6.1-gKO+TOLB, $+56 \pm 20\%$, $n=7$, $p < 0.01$; see figure 3.36).

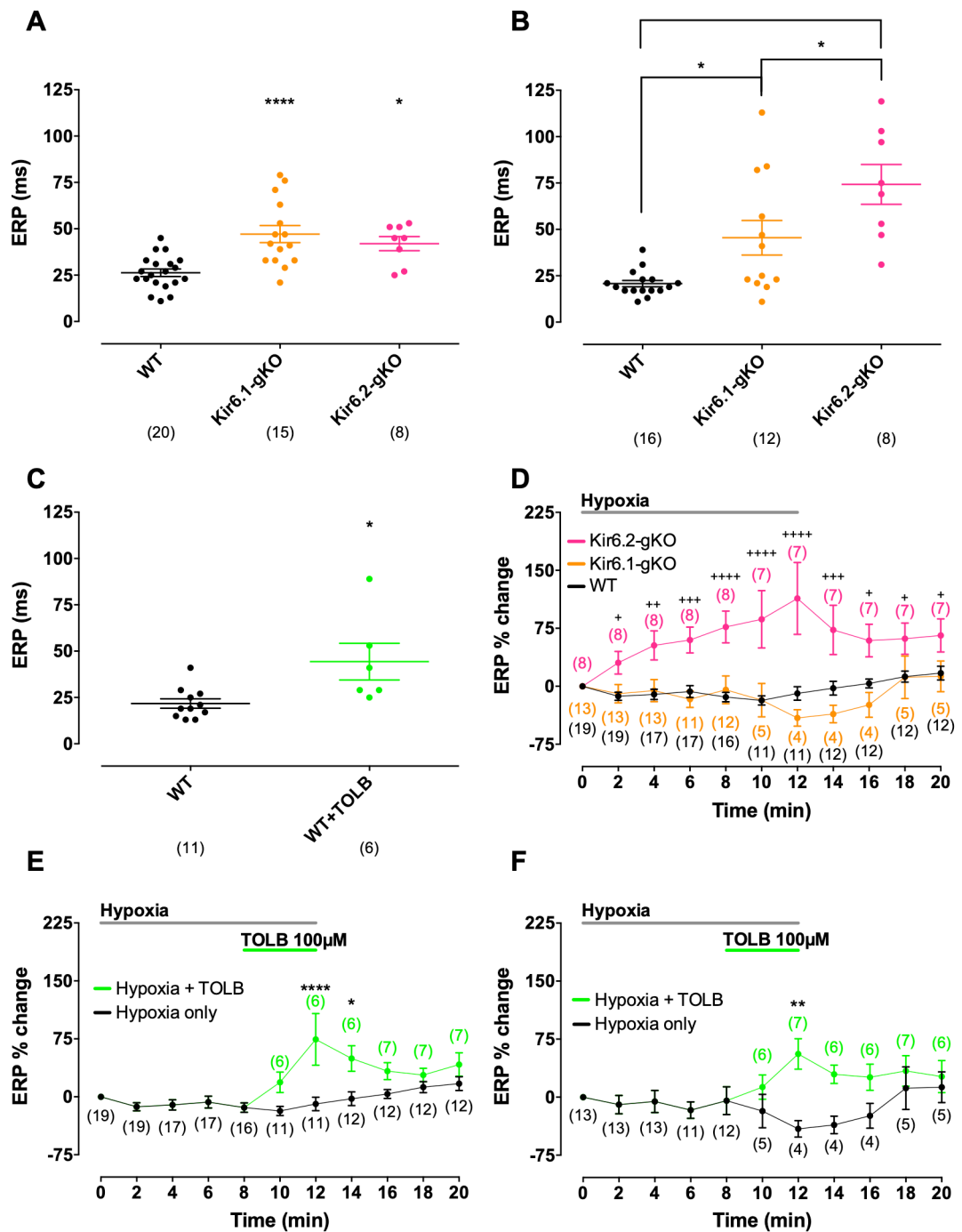


Figure 3.36. Atrial ERP is prolonged in both K_{ATP} pore knockout mice and Kir6.2 is crucial to maintain it during hypoxia. (A) Baseline ERP (significance shown vs WT) **(B)** ERP after 8 mins hypoxia **(C)** WT ERP after 12 mins hypoxia with/without TOLB **(D)** ERP % change compared to baseline in all genotypes (significance shown vs WT) **(E)** as for (D) but WT with and without TOLB (significance shown vs no TOLB) **(F)** as for (E) but Kir6.1-gKO (significance shown vs no TOLB). (n); * $p < 0.05$, **/ $+++p < 0.01$, $+++p < 0.001$, ****/ $++++p < 0.0001$.

3.6.2 Both K_{ATP} pore-forming subunits affect the atrial conduction velocity

A trend was observed in a lower baseline steady state CV in both knockout mice (WT, 0.66 ± 0.04 m/s, $n=19$; Kir6.1-gKO, 0.52 ± 0.06 m/s, $n=13$, $p = 0.05$ vs WT; Kir6.2-gKO, 0.55 ± 0.03 m/s, $n=8$, $p = 0.26$ vs WT). This finding was reinforced when examining CV restitution at progressively shorter coupling intervals down to ERP, whereby the knockout atria developed consistently lower CV compared to WT (CV at selected coupling intervals: S2-100ms - WT, 0.63 ± 0.04 m/s, $n=19$; Kir6.1-gKO, 0.44 ± 0.06 m/s, $n=13$, $p < 0.01$ vs WT; Kir6.2-gKO, 0.44 ± 0.07 m/s, $n=8$, $p < 0.05$ vs WT; S2-60ms - WT, 0.52 ± 0.04 m/s, $n=19$; Kir6.1-gKO, 0.32 ± 0.06 , $n=8$, $p < 0.05$ vs WT; Kir6.2-gKO, 0.31 ± 0.06 m/s, $n=7$, $p < 0.05$ vs WT). Steady state CV after 8 minutes of hypoxia was also lower in both knockout mice (WT, 0.46 ± 0.04 m/s, $n=15$; Kir6.1-gKO, 0.32 ± 0.05 m/s, $n=10$, $p < 0.05$ vs WT; Kir6.2-gKO, 0.30 ± 0.04 m/s, $n=8$, $p < 0.05$ vs WT). This finding was reinforced when examining CV restitution after 8 minutes hypoxia. At progressively shorter coupling intervals down to ERP, the knockout atria had consistently lower CV compared to WT (CV at 8 minutes hypoxia, selected coupling intervals: S2-100ms - WT, 0.47 ± 0.05 m/s, $n=15$; Kir6.1-gKO, 0.31 ± 0.05 m/s, $n=9$, $p < 0.05$ vs WT; Kir6.2-gKO, 0.25 ± 0.03 , $n=6$, $p < 0.01$ vs WT; S2-60ms - WT, 0.41 ± 0.04 m/s, $n=15$; Kir6.1-gKO, 0.19 ± 0.03 , $n=7$, $p < 0.01$ vs WT; Kir6.2-gKO, 0.17 ± 0.06 m/s, $n=3$, $p < 0.05$ vs WT). In the cohort of wild type hearts that were also given tolbutamide $100\mu\text{M}$ in the hypoxic perfusate, after hypoxia for 12 minutes steady state CV was no different in the tolbutamide group (No TOLB, 0.37 ± 0.04 m/s, $n=10$; +TOLB, 0.39 ± 0.04 m/s, $n=6$). No difference was seen either in CV restitution between the hypoxia only group and that with tolbutamide (see figure 3.37). Example isochronal activation maps are presented in figure 3.38.

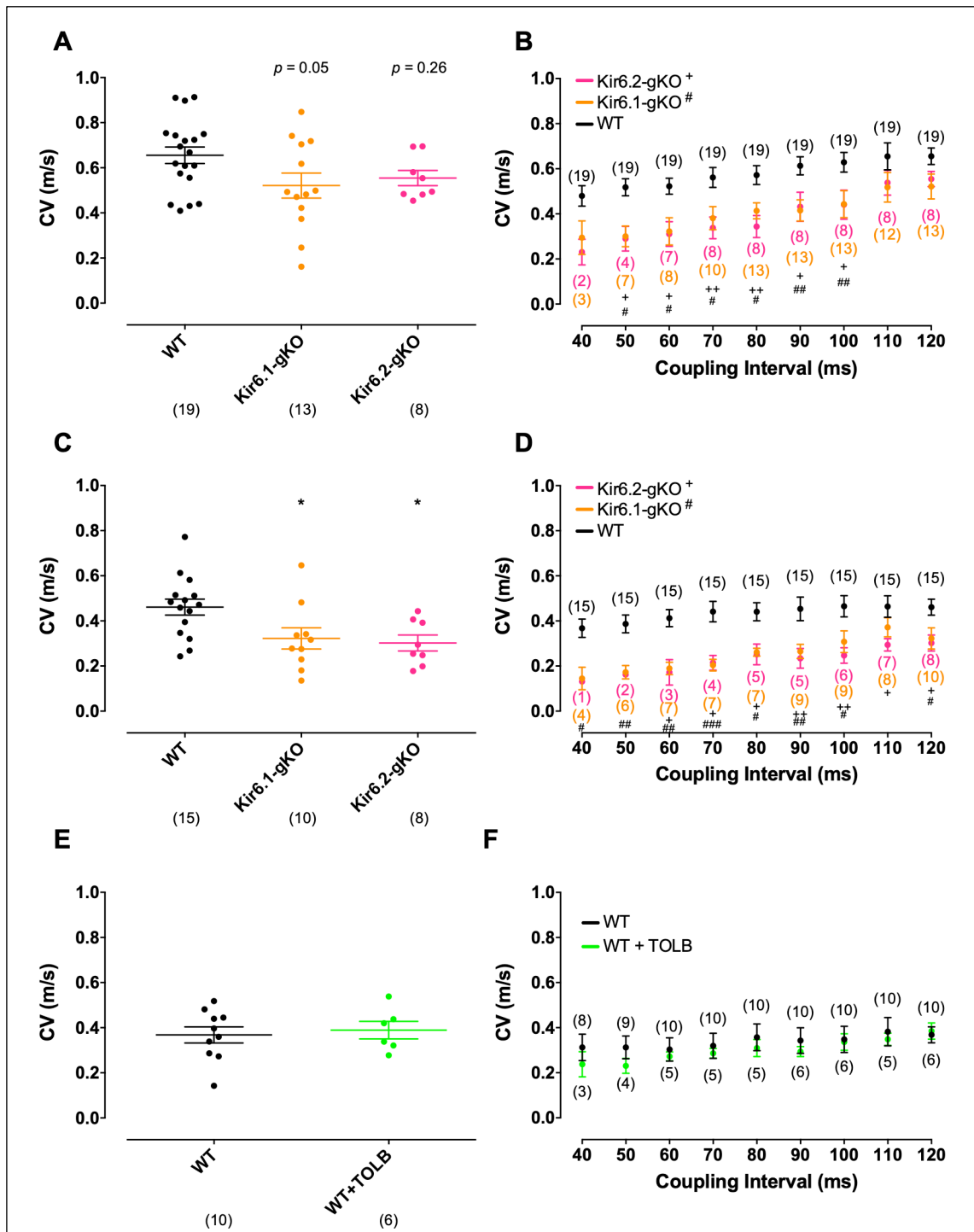
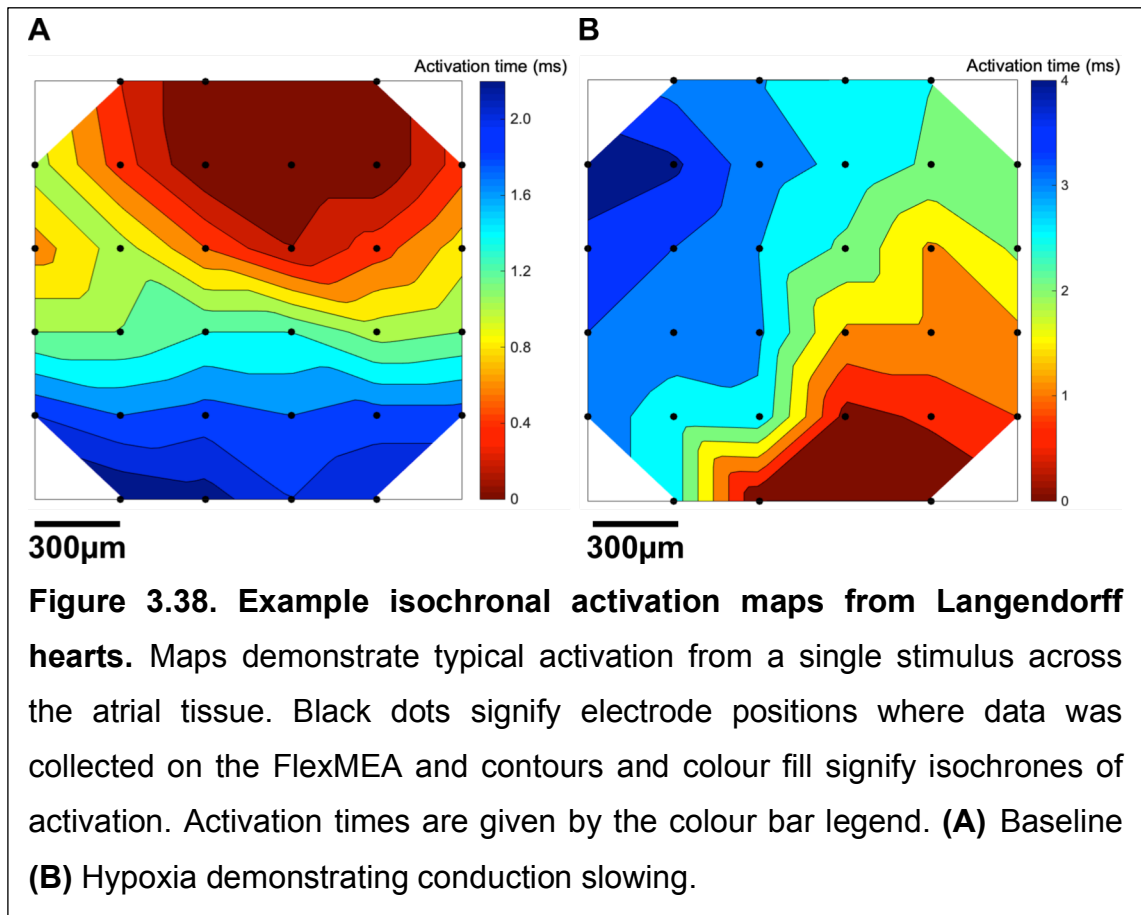
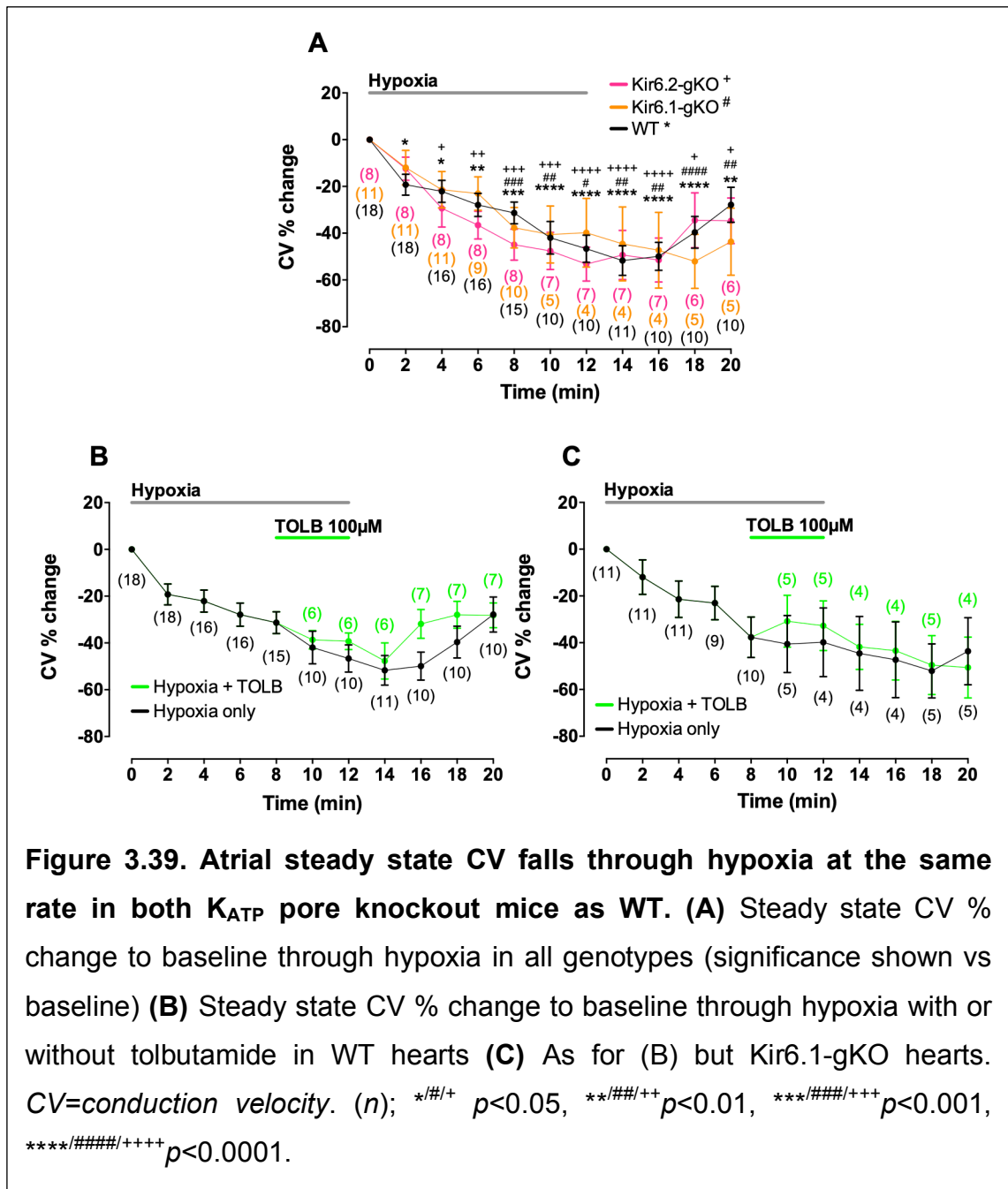


Figure 3.37. Atrial CV is lower in both K_{ATP} pore knockout mice. (A) Baseline steady state CV (B) Baseline CV restitution (significance shown vs WT) (C) Steady state CV at 8mins hypoxia (D) CV restitution at 8mins hypoxia (significance shown vs WT) (E) Steady state CV at 12mins hypoxia with or without tolbutamide in the WT (F) CV restitution at 12mins hypoxia with or without tolbutamide in the WT. CV=conduction velocity. (n); */#/+ $p < 0.05$, ##/++ $p < 0.01$, ### $p < 0.001$.



When normalised to baseline, like the WT, both K_{ATP} pore knockout atria had further reductions in CV through hypoxia (selected time points % change in CV compared to baseline: 12 minutes hypoxia - WT, $-47 \pm 6\%$, $n=10$, $p < 0.0001$ vs baseline; Kir6.1-gKO, $-40 \pm 15\%$, $n=4$, $p < 0.05$ vs baseline; Kir6.2-gKO, $-53 \pm 7\%$, $n=7$, $p < 0.0001$ vs baseline; after 8 minutes washout - WT, $-28 \pm 7\%$, $n=10$, $p < 0.01$ vs baseline; Kir6.1-gKO, $-44 \pm 14\%$ $n=5$ $p < 0.01$ vs baseline; Kir6.2-gKO, $-35 \pm 10\%$, $n=6$, $p < 0.05$ vs baseline). In the cohort of WT and Kir6.1-gKO hearts that were also given tolbutamide in the hypoxic perfusate, there was no difference in the percentage change in steady state CV in the tolbutamide groups, as compared to no tolbutamide, through hypoxia (CV % change compared to baseline at 12 minutes hypoxia: WT no TOLB, $-47 \pm 6\%$, $n=10$; WT+TOLB, $-39 \pm 4\%$, $n=6$; Kir6.1-gKO no TOLB, $-40 \pm 15\%$, $n=4$; Kir6.1-gKO+TOLB, $-33 \pm 11\%$, $n=5$; see figure 3.39).



3.6.3 Kir6.2 deletion, and pharmacological K_{ATP} inhibition, cause prolongation of atrial minimum wavefront path length during hypoxia

Measurements of ERP and steady state CV were then used to calculate the minimum wavefront path length (WFPL) of the tissue through hypoxia given by their product. Despite a prolonged ERP in both K_{ATP} pore knockouts at baseline, a reduction in CV compensated in that there was no difference in WFPL (WT, 1.7 ± 0.2 cm, $n=19$; Kir6.1-gKO, 2.5 ± 0.4 cm, $n=13$; Kir6.2-gKO, 2.3 ± 0.3 cm, $n=8$). At 8 minutes of hypoxia, due to the prolongation in ERP with fall in CV, the WFPL was maintained in the Kir6.2-gKO and, as such, became longer than

the WT. This was not the case in the Kir6.1-gKO where the ERP was maintained during hypoxia with a fall in CV leading to a shorter WFPL, akin to the WT (WFPL at 8mins hypoxia: WT, 0.9 ± 0.1 cm, $n=15$; Kir6.1-gKO, 1.6 ± 0.5 cm, $n=10$; Kir6.2-gKO, 2.3 ± 0.5 cm, $n=8$, $p < 0.05$ vs WT). At 12 minutes hypoxia, K_{ATP} inhibition with tolbutamide produced a prolongation in ERP that was not accompanied by a fall in CV, leading to a longer WFPL (WT no TOLB, 0.7 ± 0.1 cm, $n=10$; WT+TOLB, 1.7 ± 0.3 cm, $n=6$, $p < 0.01$ for comparison, see figure 3.40).

The change in absolute values of WFPL is well summarised by the percentage change compared to baseline through hypoxia. In both WT and Kir6.1-gKO atria, the maintenance of ERP together with a fall of CV led to a fall in WFPL, whereas in the Kir6.2-gKO, the prolongation of ERP compensated the fall in CV and WFPL was maintained through hypoxia. (Selected time points % change in WFPL compared to baseline: 6 minutes hypoxia - WT, $-32 \pm 7\%$, $n=16$, $p < 0.05$ vs baseline; Kir6.1-gKO, $-30 \pm 15\%$, $n=9$; Kir6.2-gKO, $-3 \pm 9\%$, $n=8$; 12 minutes hypoxia - WT, $-49 \pm 8\%$, $n=10$, $p < 0.001$ vs baseline; Kir6.1-gKO, $-66 \pm 11\%$, $n=4$, $p < 0.01$ vs baseline; Kir6.2-gKO, $-4 \pm 27\%$, $n=7$, $p < 0.01$ vs WT; after 8 minutes washout - WT, $-16 \pm 10\%$, $n=10$; Kir6.1-gKO, $-43 \pm 11\%$ $n=5$; Kir6.2-gKO, $+2 \pm 14\%$, $n=6$). Similarly, K_{ATP} inhibition with tolbutamide led to a prolongation in ERP which compensated the fall in CV, and the ensuing fall in WFPL was reversed (WFPL % change compared to baseline at 12 minutes hypoxia: WT no TOLB, $-49 \pm 8\%$, $n=10$; WT+TOLB, $+1 \pm 13\%$, $n=6$, $p < 0.05$; Kir6.1-gKO no TOLB, $-66 \pm 11\%$, $n=4$; Kir6.1-gKO+TOLB, $+8 \pm 22\%$, $n=5$, $p < 0.05$, see figure 3.40).

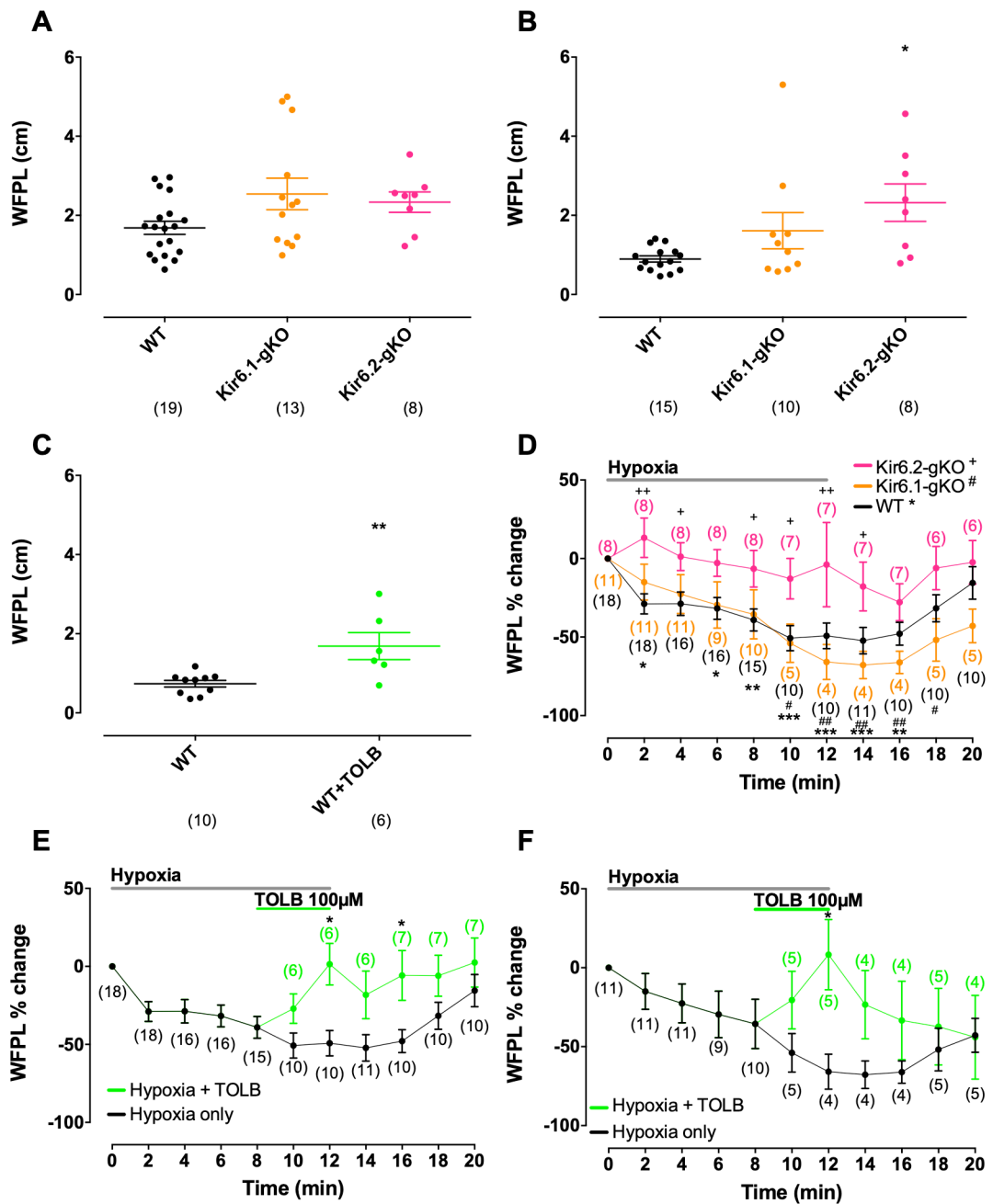


Figure 3.40. Kir6.2 deletion, and pharmacological K_{ATP} inhibition, cause prolongation of atrial minimum wavefront path length during hypoxia. (A) Baseline WFPL (B) WFPL after 8 mins hypoxia (C) WT WFPL after 12 mins hypoxia with/without TOLB (D) WFPL % change compared to baseline in all genotypes ($^+p<0.05$, $^{++}p<0.01$ vs WT; $^{*/#}p<0.05$, $^{/###}p<0.01$, $^{***}p<0.001$ vs baseline) (E) as for (D) but WT with and without TOLB ($^*p<0.05$ vs no TOLB) (F) as for (E) but Kir6.1-gKO ($^*p<0.05$ vs no TOLB). (n).**

3.6.4 Kir6.2 deleted mice display reduced arrhythmia inducibility to programmed electrical stimulation during hypoxia / reperfusion

Arrhythmias induced by programmed electrical stimulation (PES) were observed. A run of 500ms or longer was considered a sustained atrial arrhythmia. At baseline sustained atrial arrhythmia was observed in WT 1/20 hearts, Kir6.1-gKO 1/15 hearts, Kir6.2-gKO 0/8 hearts. Where hearts with data existed for the duration of the hypoxia/washout 20-minute protocol, sustained atrial arrhythmia was observed in WT 6/11 hearts, Kir6.1-gKO 5/7 hearts, Kir6.2-gKO 0/7 hearts ($p < 0.05$ Kir6.2-gKO vs WT by Fisher's exact test). It can be noticed, and it is important to point out, that in only one heart in the Kir6.2-gKO group could data not be extracted for the duration of the protocol and as such this heart was omitted from this part of the analysis. However, even up to 8 minutes of the protocol where data could be extracted in this heart, still no sustained atrial arrhythmia was observed. During the period of 4 minutes hypoxia with or without tolbutamide (8-12min of protocol), sustained atrial arrhythmia was observed in WT with no tolbutamide 3/11 hearts and WT with tolbutamide 0/6 hearts. Sustained atrial arrhythmia was observed similarly in Kir6.1-gKO with no tolbutamide 1/4 hearts and Kir6.1-gKO with tolbutamide 0/6 hearts. See figures 3.41 and 3.42.

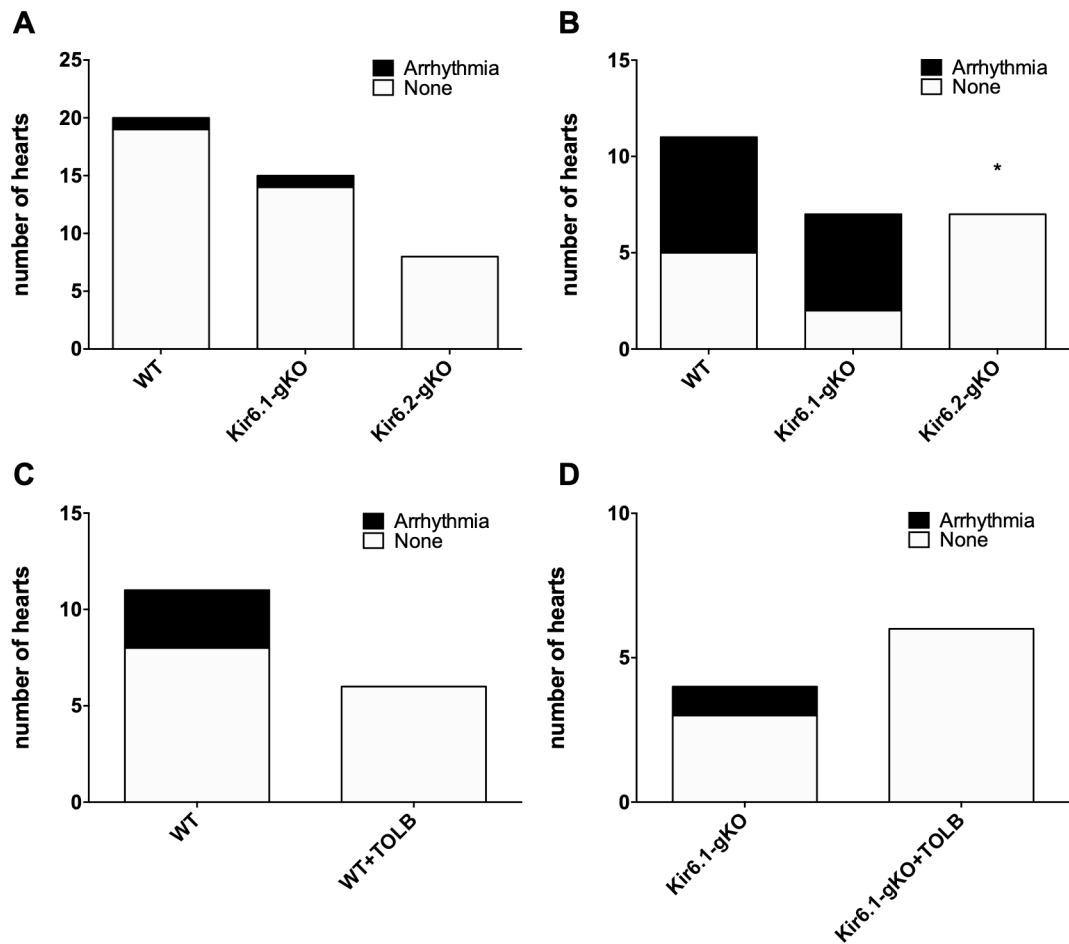


Figure 3.41. Kir6.2 deleted mice display reduced arrhythmia inducibility to programmed electrical stimulation (PES) during hypoxia/reperfusion. Proportions of hearts with PES-induced sustained atrial arrhythmia (500ms or longer): **(A)** At baseline **(B)** during the hypoxia/washout 20-minute protocol **(C)** 8-12mins of hypoxia with and without tolbutamide in the WT **(D)** as (C) but for Kir6.1-gKO. (Significance shown vs WT, * $p < 0.05$ by Fisher's exact test).

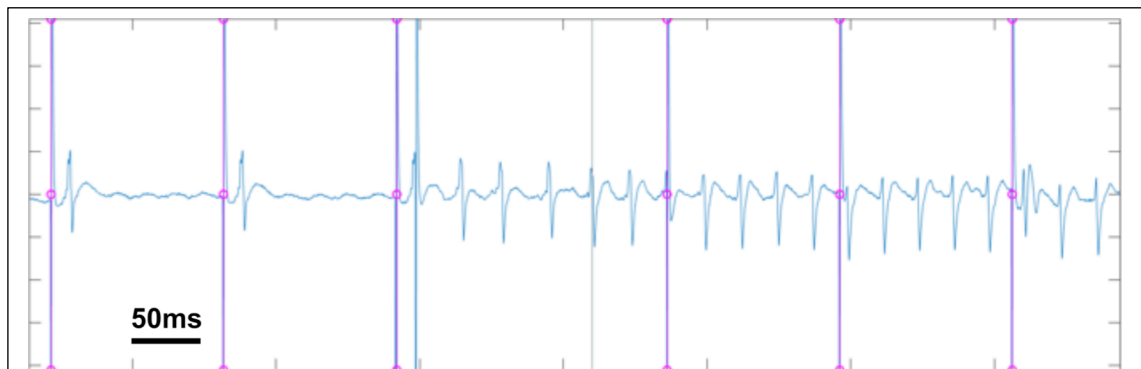


Figure 3.42. Example trace of arrhythmia induced by programmed electrical stimulation. Trace showing the final 3 beats of a drive train with preceding pacing artefact (purple), followed by the S2 with shorter coupling interval with preceding pacing artefact (blue), followed by what appears to be atrial fibrillation (further pacing artefact is also present from the next drive train in the automated sequence), which on this occasion went on to last for 25 beats and ~700ms.

3.6.5 Summary

I have shown in section 3.3 that in line with previous literature, Kir6.2 is a crucial subunit of a sarcolemmal K_{ATP} current in murine atria and this further work demonstrating its contribution to atrial tissue electrophysiology supports this. In section 3.3 I also demonstrated that Kir6.1 deletion leads to an increase in K_{ATP} current in isolated atrial cardiomyocytes. I postulated that this might be due to a small population of Kir6.1-containing K_{ATP} channels whereby Kir6.1 deletion could lead to substitution by Kir6.2, which has a larger unitary conductance. This would be expected to enhance effects of hypoxia on K_{ATP} activation and the prolongation of ERP and reduction in CV seen in the Kir6.1 deleted mouse is counter-intuitive to this argument. It may be, however, that Kir6.1 deletion has different effects in tissue to that of isolated cells and it could be, for example, a factor of its subcellular localisation that is more important in tissue than in the isolated cell. This or there is an indirect effect of Kir6.1 deletion, either via the vascular smooth muscle or endothelium, that leads to the changes seen on atrial tissue electrophysiology. Whether or not Kir6.1 is present in an atrial sarcolemmal K_{ATP} current, the data demonstrate that global modulation of the

current will have effects on parameters known to affect arrhythmia inducibility, just as with Kir6.2 modulation. The presence of Kir6.2 in the Kir6.1 knockout continues to compensate for the electrophysiological changes seen during hypoxia and maintains the ERP just as in the wild type. Pharmacological blockade of K_{ATP} , via inhibition at the SUR1 subunit using tolbutamide, recapitulates the effects of Kir6.2 deletion in wild type and Kir6.1 knockout mice.

Kir6.2-deleted mice display reduced arrhythmia inducibility to programmed electrical stimulation during hypoxia. This is likely to reflect the absence of wavefront path length shortening displayed by the Kir6.2-gKO that was observed in WT and Kir6.1-gKO mice.

3.7 Whole heart RNA quantification suggests the presence of all K_{ATP} subunits except SUR1 in the human heart

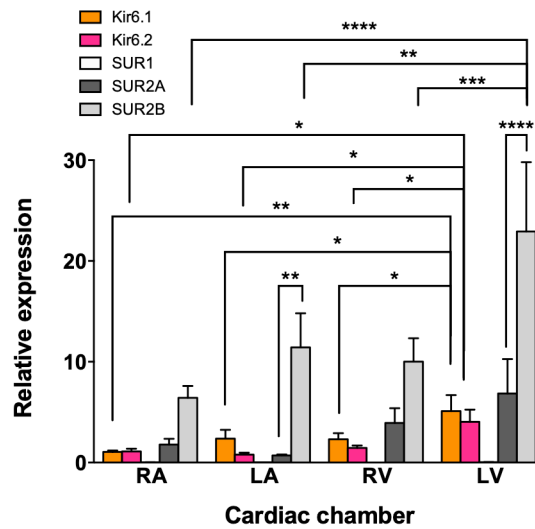
I began to examine the contribution of the various K_{ATP} subunits to a sarcolemmal K_{ATP} current in the human heart by performing relative quantification of mRNA transcripts encoding the subunits.

3.7.1 Commercially available human whole heart RNA

Isolated human total RNA from all four heart chambers (right atrium, left atrium, right ventricle and left ventricle) from three separate donors said to be "normal" with regards to no past medical history and normal cardiac structure and function, was purchased from AMS Biotechnology (Europe) Limited. Donors consisted of a 49 year old male, 69 year old male and 65 year old male.

Two runs of qRT-PCR were performed for all samples. Samples were analysed in triplicate and the mean Ct values were taken. Quantification was normalised to GAPDH. Data were grouped from all 3 donors in terms of subunit and chamber, and after normalising to GAPDH, quantification was made relative to the mean of the right atrial GAPDH normalised Kir6.1 value.

There was no significant difference in relative quantity of Kir6.1 and Kir6.2 transcripts within each cardiac chamber, but the left ventricle had consistently greater relative quantity of both pore-forming transcripts than all the other chambers. This was also the case for SUR2B transcripts, which were significantly more abundant in the left ventricle than all the other chambers. SUR2B transcripts were also significantly more abundant than SUR2A within the left ventricle and left atrium. There was a consistent signal suggesting that no SUR1 transcripts were present in human whole, "normal heart", RNA. See figure 3.43.



CHAMBER	SUBUNIT	RELATIVE QUANTIFICATION
RA	Kir6.1	1.06 ± 0.14
	Kir6.2	1.10 ± 0.27
	SUR1	0.03 ± 0.01
	SUR2A	1.78 ± 0.57
	SUR2B	6.42 ± 1.19
LA	Kir6.1	2.38 ± 0.87
	Kir6.2	0.78 ± 0.20
	SUR1	0.02 ± 0.01
	SUR2A	0.71 ± 0.10
	SUR2B	11.43 ± 3.38
RV	Kir6.1	2.31 ± 0.60
	Kir6.2	1.45 ± 0.25
	SUR1	0.01 ± 0.01
	SUR2A	3.93 ± 1.47
	SUR2B	10.02 ± 2.32
LV	Kir6.1	5.11 ± 1.59
	Kir6.2	4.04 ± 1.20
	SUR1	0.04 ± 0.02
	SUR2A	6.85 ± 3.42
	SUR2B	22.92 ± 6.88

Figure 3.43. Relative quantification of K_{ATP} subunit transcripts in human whole "normal heart" RNA. Data from 2 runs of triplicates, 3 donors.. * p <0.05, ** p <0.01, *** p <0.001, **** p <0.0001.

3.7.2 Human whole heart RNA from The Barts Cardiovascular Registry

To confirm the findings from the commercially available human whole heart RNA, I performed identical experiments on the RNA extracted from the samples of atria I collected from 5 patients in the cardiothoracic theatre. Patients were all male, ages 56, 62, 59, 74, 61, non-diabetic with normal valvular and preserved LV systolic function undergoing coronary artery bypass grafting. Samples were obtained from right and left atrium from all 5 patients. The data from these samples complemented the atrial data from the commercially available samples in an almost identical pattern. See figure 3.44.

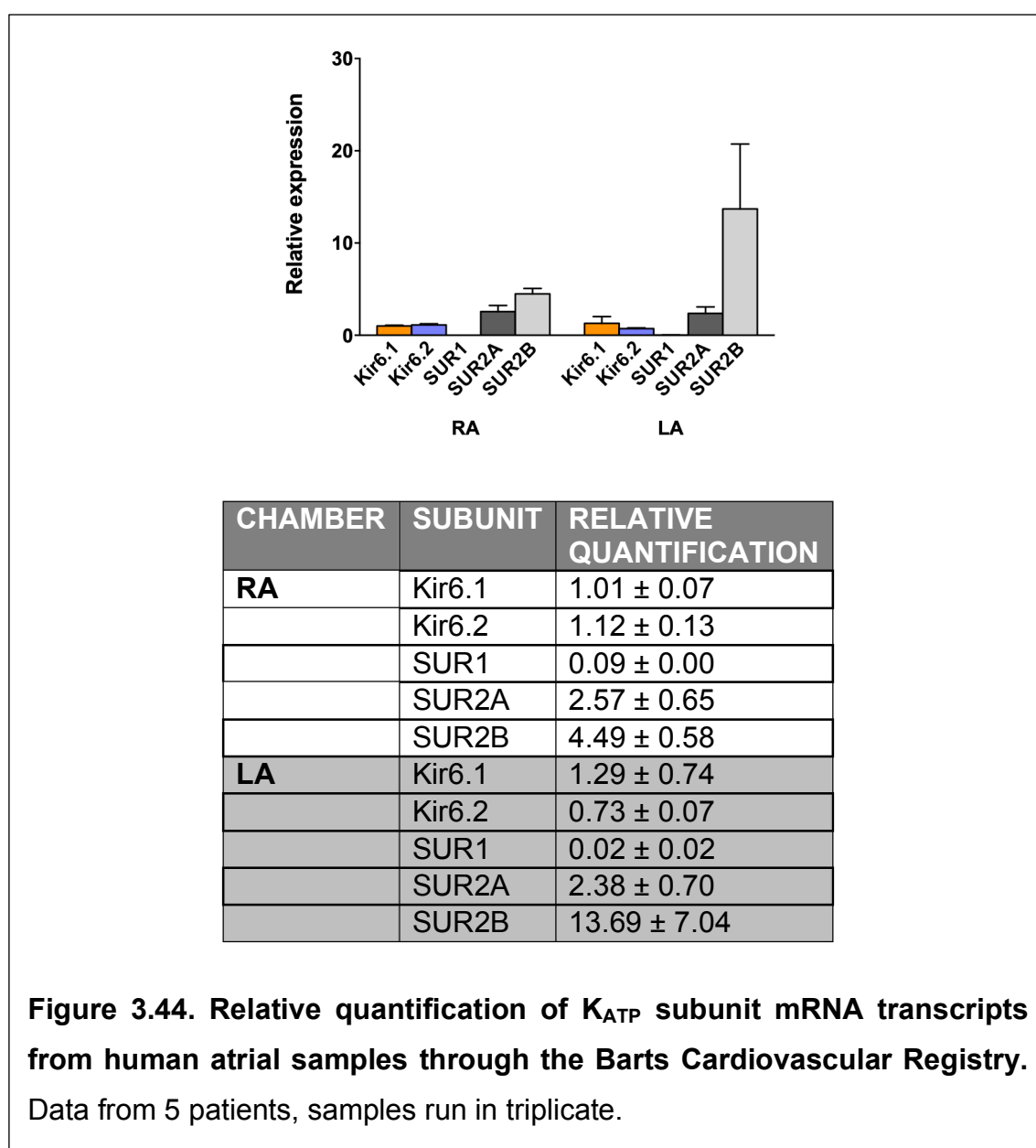


Figure 3.44. Relative quantification of K_{ATP} subunit mRNA transcripts from human atrial samples through the Barts Cardiovascular Registry. Data from 5 patients, samples run in triplicate.

3.7.3 Summary

These data are in keeping with reports in the literature that SUR1 is not an important subunit in the composition of K_{ATP} in the normal human heart (Fedorov *et al.*, 2011). It does, however, suggest that there may be an equal contribution of both pore-forming subunits throughout the heart. SUR2B is expressed in abundance throughout the heart. With the data being from whole heart RNA, it is impossible to make inferences about what cellular populations the transcripts are emanating from, and it may be the large proportion of SUR2B is in large part provided by vascular smooth muscle or endothelium. Similarly, the equal proportions of the pore-forming subunit transcripts might look very different if RNA could be isolated solely from cardiomyocytes. Nonetheless, the findings make pursuing further investigations in this vein worthwhile, and the stark difference to the proportionality found in mouse whole heart RNA is clear.

Section 4: Discussion

4.1 Unique findings and addressment of the hypotheses and aims

Aims of this project were to further define the K_{ATP} subunit expression and current characteristics in murine atria with a view to comparing with human atria, and to explore any effect on cardiac rhythm generation of K_{ATP} modulation.

These were based on hypotheses that, in addition to literature demonstrating an importance for Kir6.2 as the major atrial sarcolemmal pore-forming K_{ATP} subunit in the mouse, Kir6.1 is also present, and that both pore-forming subunits contribute to murine atrial electrophysiology. Further, a differential subunit expression existed between the atria and ventricles that could be exploited pharmacologically in the event of anti-arrhythmic mechanisms of K_{ATP} modulation. With this in mind I postulated that K_{ATP} activation would be anti-arrhythmic in the case of reducing automaticity through membrane hyperpolarisation, whilst K_{ATP} inhibition would also be anti-arrhythmic by increasing minimum wavefront path length and reducing the chances of perseveration of re-entry.

Mice with global deletion of Kir6.1 and Kir6.2 were bred. Whole cell patch clamp of isolated wild-type murine atrial cardiomyocytes demonstrated an activation of current with diazoxide 100 μ M that was strongly inhibited by tolbutamide 100 μ M but not PNU37883A 50 μ M. Pinacidil 10 μ M failed to activate current in these cells. This was in keeping with a pharmacological signature of Kir6.2/SUR1 as that making up the predominant sarcolemmal K_{ATP} current in these cells. In keeping with this, genetic deletion of Kir6.2 abolished a K_{ATP} current in these cells. However, Kir6.1 deletion caused an increase in K_{ATP} current and K_{ATP} inhibitors still produced an effect, albeit subtle, after Kir6.2 deletion. When atrial tissue electrophysiology was investigated in a whole heart model, both pore-forming knockout mice showed pronounced changes with ERP prolongation and CV reduction as compared to wild-type littermate control mice. Kir6.2 appeared more important, particularly with regards to adaptation to hypoxic conditions. Thus, both pore-forming subunits contribute to atrial electrophysiology in the mouse. In keeping with this whole heart mRNA

quantification demonstrated greater expression of Kir6.2 and SUR1 subunits compared to Kir6.1 and SUR2 in the atria, though the latter were still present. The data pertaining to the direct comparison of the K_{ATP} pore-forming knockouts in isolated murine atrial myocytes is novel, and the suggestion that Kir6.1 contributes to a murine sarcolemmal atrial K_{ATP} current has not been reported before. A direct assessment and comparison of atrial tissue electrophysiology between K_{ATP} pore-forming knockouts has also not been performed before and these findings are also novel.

Kir6.2 deletion, or K_{ATP} pharmacological inhibition, led to increases in minimum wavefront path length and this was accompanied by trends towards reduced arrhythmia inducibility to programmed electrical stimulation, suggesting a reduction in re-entrant activity. Conversely, K_{ATP} activation first organised rotational wavefronts to straight and uniform wavefronts in spontaneously beating syncytia of HL-1 cells, and then silenced these syncytia completely in a dose-dependent fashion. Both the characterisation of the K_{ATP} current in HL-1 cells, and the effects on rotational wavefronts of K_{ATP} activation are novel findings. Both K_{ATP} activation and inhibition appear to have anti-arrhythmic effects by different means.

In the mouse heart, mRNA quantification supported existing literature that the ventricles have a different K_{ATP} subunit expression profile to the atria whereby Kir6.2/SUR2A predominates in the ventricle (Suzuki *et al.*, 2001; Chutkow *et al.*, 2001; Flagg *et al.*, 2008). Human whole heart mRNA quantification did not show the same results. The pore-forming subunits were equally expressed throughout the four heart chambers, SUR1 appeared to not be expressed, and SUR2B was consistently expressed more than SUR2A. Whilst this was whole heart RNA and does not explore expression in different cellular populations, it infers that human cardiac K_{ATP} expression is different to the mouse as suggested by existing literature (Fedorov *et al.*, 2011). Thus, it may well be possible to create an atrial specific anti-arrhythmic therapy using K_{ATP} modulation in the mouse, but whether this can be translated to humans requires further dissection.

4.2 K_{ATP} subunit pharmacology

I utilised HEK293 cells overexpressing K_{ATP} channels of varying subunit composition. With 3mM ATP and 1mM ADP in the intracellular solution I was able to delineate through whole cell patch clamp of these cells, that diazoxide 100µM is a relatively specific activator of SUR1-containing channels though also activates weakly SUR2B-containing channels. Pinacidil 10µM is an activator of SUR2A- and SUR2B-containing channels. Tolbutamide 100µM is a relatively specific inhibitor for SUR1-containing channels. This is all in keeping with current literature (Ashfield *et al.*, 1999; Uhde *et al.*, 1999; Babenko *et al.*, 2000; Moreau *et al.*, 2000; Dabrowski *et al.*, 2002; Moreau *et al.*, 2005a; 2005b).

Of perhaps more interest, is that I found PNU37883A 50µM to be a relatively specific inhibitor for all Kir6.1-containing channels relative to those containing Kir6.2. Some groups have demonstrated a specificity for Kir6.1- over Kir6.2-containing K_{ATP} channels when expressed with SUR1 or SUR2B in *Xenopus laevis* oocytes, and activated pharmacologically by diazoxide (Surah-Narwal *et al.*, 1999; Kovalev *et al.*, 2004). The IC₅₀ for Kir6.1/SUR1 was ~30µM and for Kir6.1/SUR2B ~5µM. This is in contrast to the results seen by another group, whereby SUR2B-containing channels in general were inhibited selectively regardless of the pore-forming subunit, with an IC₅₀ of 15.2µM for Kir6.2-containing channels, and 6µM for Kir6.1-containing channels (Cui *et al.*, 2003). In the same series of experiments 100µM of PNU37883A was required to inhibit to only less than 40% of the BaCl₂ sensitive current in Kir6.2/SUR1 and Kir6.2/SUR2A channels, thus demonstrating a SUR2B-containing channel selectivity of the drug. The results of Cui and colleagues do not dispute the pore as the site of block. The current from a truncated form of Kir6.2 (Kir6.2Δ26), which can be expressed at the cell surface in the absence of SUR, was also inhibited by PNU37883A (Cui *et al.*, 2003). Kovalev and colleagues also demonstrated that the C-terminus of the pore was important for drug effect (Kovalev *et al.*, 2004). However, the experiments of Cui and colleagues delineated an interaction of the SUR subtype in composition with the pore, which then conferred selective inhibition to the drug. There were differences in the experimental conditions between the studies. Cui and colleagues, for

example, expressed channels in HEK293 cells and used metabolic inhibition to activate current. The authors stipulate that differences in nucleotide concentrations can affect the action of both KCOs and inhibitors as evidenced by various studies (Jahangir *et al.*, 1994; Gribble *et al.*, 1997b; D'hahan *et al.*, 1999; Reimann *et al.*, 2003). In my experiments HEK293 cells were used ruling out this as the cause for the differences, and activating pharmacologically with 3mM ATP/ 1mM ADP in the pipette solution, PNU37883A 50µM appears to selectively inhibit Kir6.1-containing channels over those containing Kir6.2.

PNU37883A 50µM also had off-target effects as indicated by its inhibition of basal current beyond that induced with the non-specific K_{ATP} inhibitor glibenclamide. A caveat to this is that the inhibitory effects of both PNU37883A and glibenclamide are potentiated in each others' presence (Ohrnberger *et al.*, 1993). Though in my experiments the drugs were applied separately and PNU37883A has been seen to have effects on other non- K_{ATP} targets in other studies (Teramoto, 2006a). Despite this, given the clarity of PNU37883A inhibition for Kir6.1-containing channels after pharmacological K_{ATP} activation in my experiments, under certain experimental conditions the drug appears to be a reasonable tool to distinguish between each pore-forming subunit.

Also of note, discrepancies exist between the results of selective inhibition by HMR1098 (Gögelein *et al.*, 1998; Russ *et al.*, 2001; Manning Fox *et al.*, 2002; Zhang *et al.*, 2011). Under the experimental conditions in this study, no apparent selectivity was seen, and HMR1098 10µM inhibited both SUR1- and SUR2A-containing channels equally, thus limiting its utility at distinguishing between them.

4.3 Kir6.2 is the predominant pore-forming subunit, but is there a role for Kir6.1 in murine atrial cardiomyocytes?

An overwhelming message from these experiments is that Kir6.2 is the predominant sarcolemmal K_{ATP} pore-forming subunit in murine atrial cardiomyocytes. Whilst not thought to be active under baseline physiological conditions due to inhibiting concentrations of ATP, the data from this study suggest that Kir6.2 does contribute to the resting membrane potential in isolated cells. Kir6.2 deletion produced more depolarised cells at baseline. Kir6.1-containing channels have an inherent greater open probability at rest due to differing sensitivity to the co-expressed SUR in combination, and differing sensitivity to ADP (Satoh *et al.*, 1998; Babenko & Bryan, 2001). Vascular smooth muscle cells contain Kir6.1-containing K_{ATP} channels (Cui *et al.*, 2002) and in vascular smooth muscle, K_{ATP} channels have been shown to contribute to the resting membrane potential even under resting conditions (Teramoto, 2006b). Whilst Kir6.2 is strongly inhibited by Mg^{2+} -independent ATP, co-expression with SUR sensitises the K_{ATP} pore to release from ATP inhibition by Mg^{2+} -dependent ATP hydrolysis to MgADP, with ensuing conformational change of the channel and pore opening. SUR1 in particular is more sensitising than, for example, SUR2A (Babenko & Bryan, 2001). Whilst I did not see a significant inhibition beyond baseline on application of tolbutamide in wild-type atrial cardiomyocytes, this was administered alongside diazoxide and not in isolation, and in HEK293 cells overexpressing Kir6.2/SUR1 K_{ATP} channels there was always a degree of run-up of current at baseline during dialysis of pipette solution (see representative trace in figure 3.4). This run-up was seen to a lesser degree in murine atrial cardiomyocytes (see figure 3.17). The data suggest there is at least a small population of K_{ATP} channels open under basal conditions in these atrial cardiomyocytes, contributing to setting of the resting membrane potential, and Kir6.2 deletion removes this. An alternative explanation is that there is an indirect effect through other ion channel remodelling but this was not investigated. There were other consistencies, not least that the tolbutamide-sensitive current was abolished with Kir6.2 deletion. Kir6.2-deleted atrial cardiomyocytes were not hyperpolarised on application of diazoxide in comparison to wild type and Kir6.1-gKO cells. Similarly, unlike control cells, diazoxide failed to shorten the APD in Kir6.2-gKO atrial

cardiomyocytes. Kir6.2 is crucial to the sarcolemmal K_{ATP} current in murine atrial cardiomyocytes and this is consistent with the existing literature.

What is interesting is the increase in tolbutamide-sensitive current in the Kir6.1-gKO. This might be due to a replacement of Kir6.1 by Kir6.2 with its greater unitary conductance. The relative expression of Kir6.2 mRNA was not increased in the Kir6.1-gKO, but this does not alone rule out a greater expression of surface protein. One group has demonstrated the presence of a K_{ATP} current in neonatal rat atrial appendage cardiomyocytes with a single channel conductance of 58pS (Baron *et al.*, 1999). This is intermediate between that of Kir6.1 and Kir6.2 and suggests the possibility of a heteromultimeric pore. This was re-enforced when the group also demonstrated a significant band for Kir6.1 on RT-PCR of RNA extracted from these cultured cells. Another group recognised a differential basal activity of wild-type atrial and ventricular rat cardiomyocytes in the presence of 84 μ M intracellular ADP suggesting that there might be a presence of Kir6.1 (Poitry *et al.*, 2003), and others demonstrated reductions in K_{ATP} current after separately electroporating pore-loop-mutated Kir6.1 and Kir6.2 constructs into both rat atrial and ventricular cardiomyocytes (van Bever *et al.*, 2004). This all suggests there is the presence of at least some sarcolemmal Kir6.1 in rodent atrial cardiomyocytes and would support my findings. Any contribution of Kir6.1 is small, and not able to compensate for complete deletion of Kir6.2 as demonstrated by a failure to see a pharmacologically activated K_{ATP} current in these cells. Any pharmacologically activated current might also be very subtle if the Kir6.1 population is already open at baseline. Whilst it did not reach statistical significance, there was always a very small inhibition compared to baseline with glibenclamide in these cells.

The tissue electrophysiology of whole heart atria is, therefore, even more intriguing. The ERP at baseline was prolonged in both the Kir6.1-gKO and the Kir6.2-gKO when compared to WT. In the latter this can be explained by the data pertaining to the more depolarised resting membrane potential in the Kir6.2-gKO, and the difference in slopes and crossover of the models for momentary membrane potential during the action potential between the knockout and wild type. Whilst the APDs were not different, ERP prolongation

here is almost certainly as a factor of a mechanism akin to post-repolarisation refractoriness (Cranefield *et al.*, 1971; Lazzara *et al.*, 1975; Davidenko & Antzelevitch, 1986). It is likely in the Kir6.2-gKO that there is a reduced proportion of the sodium channel population that has recovered from inactivation at any moment during repolarisation, particularly towards the end of repolarisation where the models cross at APD₇₀. Beyond this point in the models, the Kir6.2-gKO has a more positive membrane potential than the WT. Markov models predict that the availability of sodium channels, and calcium channels with a longer period of recovery from inactivation, will be reduced for any shorter coupled extra-stimulus arriving in this critical period (O'Hara *et al.*, 2011). Activation of the tissue is less likely as the peak amplitude of the source current will be reduced, and the sink too is likely to have a higher resistance due to the more depolarised state of the tissue as a whole, with a reduced probability of activating surrounding cells whose inactivation-recovered sodium channel population is also depleted (Davidenko & Antzelevitch, 1986).

If the unifying model for APD at any particular percentage repolarisation in the isolated cells (see section 3.3.6) is extrapolated using the mean measured values for ERP of the tissue, the ERP of the WT corresponds to ~APD₅₀ and the ERP of the Kir6.2-gKO corresponds to ~APD₆₀. Isolated myocytes were stimulated at 1Hz and the S1 drive train interval for programmed electrical stimulation of tissue was 120ms and this will incur differences in APD, but bearing this in mind estimates using the models can be made. For example, using the separate models for membrane potential at any particular percentage repolarisation (see section 3.3.6), at ERP in the WT the membrane potential approximates ~9mV and in the Kir6.2-gKO ~-3mV. There are a number of ways to interpret this. These of course are only approximate values from a model, and isolated cells are not tissue. Had monophasic action potentials or transmembrane action potentials been recorded from the tissue then different models may have been produced, and the ERPs might have fallen longer than a crossover point in models for membrane potential at any percentage of repolarisation. This would have set up a simpler explanation that the WT exhibited less post-repolarisation refractoriness secondary to more hyperpolarised membrane potentials in the critical late repolarisation zone. Alternatively, the values are taken on face value, and it is not inconceivable that

the Kir6.2-gKO tissue would need a more negative membrane potential at moment of stimulus to propagate activation through the tissue as a whole based on the concepts as previously described with regards effects of the sink (Cranefield *et al.*, 1971; Lazzara *et al.*, 1975; Davidenko & Antzelevitch, 1986).

It follows that steady state conduction velocity and that at shorter coupling intervals, should be reduced in the Kir6.2-gKO on similar grounds to that of ERP prolongation. There was a trend to a reduction in V_{\max} of the upstroke of the action potential in isolated atrial cardiomyocytes of the Kir6.2-gKO mouse.

It is perhaps unsurprising then that Kir6.2 deletion should lead to profound effects on ERP during hypoxia. Hypoxia reduces activity of all membrane currents in cardiomyocytes, barring the late persistent sodium current, reverse mode of the $I_{Na/Ca}$ current, and of course K_{ATP} (Saint *et al.*, 1992; Ju *et al.*, 1996; Hammarström & Gage, 2002; Wang *et al.*, 2007; Shimoda & Polak, 2011; Tang *et al.*, 2012). As a result the action potential amplitude is reduced, action potential duration is shortened, and the resting membrane potential becomes more depolarised. I have shown how deletion of Kir6.2 causes a more depolarised resting membrane potential even under baseline conditions. Further compromise to this during hypoxia without compensation by deleted Kir6.2-containing K_{ATP} channels, would almost certainly lead to ERP prolongation through further post-repolarisation refractoriness. APD is also likely to be longer in hypoxic Kir6.2-deleted atrial cardiomyocytes, as suggested by a lack of APD shortening with diazoxide in this study, and demonstration of this previously with metabolic inhibition in cardiomyocytes (Nichols *et al.*, 1991). These mechanisms are presumably at play for tolbutamide's effects in the WT and Kir6.1-gKO, owing to a block of the active Kir6.2-containing population. Ultimately, it is a purpose of K_{ATP} , to prevent complete hypoxic contractile failure due to failure of other membrane currents and cellular depolarisation. Action potential shortening also leads to reduced toxic calcium loading on the cell, both through reduced L-type calcium current entry, and given a localisation of K_{ATP} channels in the Z-groove, most probably reduced calcium-induced calcium release at the sarcoplasmic reticulum (Korchev *et al.*, 2000). Kir6.2 is crucial to this in murine atria and the murine heart as a whole.

If the tolbutamide-sensitive current in isolated Kir6.1-gKO atrial myocytes is increased, it is paradoxical that ERP should be prolonged and the CV reduced in atrial tissue of these mice. Possibilities include an up-regulation of Kir6.2 only in isolated cells, or that there might be a subcellular localisation of Kir6.1-containing channels that is important only in tissue. For example, K_{ATP} channels are known to localise to the Z-groove, and also associate with junctional proteins at the intercalated disk in cardiac myocytes (Korchev *et al.*, 2000; Hong *et al.*, 2012). K_{ATP} , like other potassium channels, are likely to be very important in modulating and improving saltatory conduction between cardiac myocytes through this junctional protein interaction (Vermij *et al.*, 2017). If Kir6.1 were to preferentially localise to channels at the intercalated disk, deletion would be expected to have a significant effect on tissue conduction properties as we have seen in this study, and have a similar effect on tissue refractoriness to that of Kir6.2 deletion. An up-regulation of compensatory Kir6.2 may only be detectable in membranes of enzymatically-dissociated cells where the intercalated disk has been disrupted. An alternative explanation is that the electrophysiological effects of Kir6.1 deletion are indirect and occur through its deletion in other cellular populations. Kir6.1 is a prominent vascular smooth muscle cell K_{ATP} subunit and mice with global deletion of Kir6.1 exhibit coronary ischaemia and hypertension (Miki *et al.*, 2002; Aziz *et al.*, 2014). Kir6.1 has also been shown to be the pore-forming subunit making up the endothelial K_{ATP} channel and endothelial conditional knockout leads to a failure to vasodilate the coronary bed during hypoxia leading to larger infarct size (Aziz *et al.*, 2017). The effects of increased afterload and ischaemia in a Kir6.1 global knockout might lead to widespread cardiac fibrosis. Absence of a cardioprotective effect of Kir6.2 deletion might also lead to the same. I have as yet not looked for histological changes in the atria of either pore-forming knockout mice but one might expect to see such changes. With cellular injury fibroblasts differentiate into myofibroblasts, which cause a degree of cellular uncoupling and conduction slowing due to differences in ion channel expression and inefficiencies in saltatory cardiac conduction (Rohr, 2012). Where they do form gap junctions, they exert a depolarising effect on adjacent cardiomyocytes as they themselves sit at a more depolarised resting membrane potential (Nguyen *et al.*, 2014). This effect would tend to produce a similar functional consequence as seen in the action potentials of the Kir6.2-gKO isolated atrial cardiomyocytes and may

well offer another reasonable explanation behind the changes in tissue electrophysiology seen in the Kir6.1-gKO.

In keeping with the critical mass hypothesis, in that a threshold size of tissue would be required to sustain a re-entrant arrhythmia, early thoughts were the mouse heart, and in particular murine atria, would be too small to fibrillate (Garrey, 1914; 1924). This has been subsequently challenged by various models of AF in the mouse (Riley *et al.*, 2012). The ratio of murine atrial circumference to atrial wavefront path length is also not dissimilar to that of larger mammals (Kaese & Verheule, 2012).

However, whilst the consensus for the duration of a sustained arrhythmia in the human is defined as 30 seconds, there is no such consensus for the mouse. The multitude of published models of murine AF display a variety of cut-offs for duration of sustained arrhythmia, and they also demonstrate a variety of methods to induce arrhythmia including both programmed electrical stimulation and burst pacing (Riley *et al.*, 2012). Arguments could be made then that the exact arrhythmogenic mechanism being explored actually differs between these studies, re-entrant vs triggered. In general, certainly clinically in humans, arrhythmias induced to programmed electrical stimulation are thought to represent re-entrant activity. In attempting, then, to explore the effects of wavefront path length on re-entrant arrhythmia inducibility, I used programmed electrical stimulation to induce arrhythmia. Utilising the existing literature, I used a conservative cut-off of 500ms or longer for an arrhythmia to be considered sustained.

Kir6.2-gKO atria displayed an absence of arrhythmia inducibility to programmed electrical stimulation through the hypoxia/washout 20-minute protocol. This was not observed in the Kir6.1-gKO. A natural explanation for this is the absence of minimum wavefront path length shortening in the Kir6.2-gKO compared to the WT and Kir6.1-gKO mice, such that re-entrant activity is favoured in the WT and Kir6.1-gKO. The effects of tolbutamide administration on PES-induced arrhythmia inducibility in hypoxic WT and Kir6.1-gKO murine atria was also compared. Whilst sustained arrhythmias were seen in the atria of untreated hearts, none were seen in tolbutamide-treated hearts though this did not reach

statistical significance. Small numbers, though, might have led to an inappropriately powered study in this aspect.

4.4 K_{ATP} channel activation organises rotational wavefronts to straight uniform wavefronts, and slows automaticity

The finding of this project that potassium channel activation can lead to organisation of rotational wavefronts is very intriguing. The classic theories behind re-entry, either functional or around an anatomical obstacle, revolve around the notion of a critical mass of tissue required to set up the wavefronts (Garrey, 1914; Rensma *et al.*, 1988; Kim *et al.*, 1997). This critical mass is in part dependent on the minimum wavefront path length required to set up a re-entrant wave, and this is defined by the product of conduction velocity and effective refractory period of the tissue (Allessie *et al.*, 1977). Any intervention that leads to prolongation of ERP, would lead to WFPL prolongation and a reduced likelihood of re-entrant waves sustaining themselves. On this basis the mode of action of anti-arrhythmic drugs is thought mainly to be driven by ERP prolongation, though more recently, reduction of tissue excitability by sodium channel blockade has been apportioned to the anti-arrhythmic effects of flecainide on spiral waves, through reducing the angle of curvature at the centre of the rotor and increasing the excitable gap (Coronel *et al.*, 2012; Pandit & Jalife, 2013; Osadchii, 2017). This too can be expected to increase the WFPL and for a given tissue mass reduce the likelihood of multiple re-entrant waves. However, pharmacological intervention, or invasive catheter ablation of AF are not always met with success. The basic premise of catheter ablation is isolation of the pulmonary veins from the body of the left atrium to eliminate drivers from the pulmonary veins (Haïssaguerre *et al.*, 1998). Techniques evolved to demonstrate that wide antral circumferential ablation was superior to ostial pulmonary vein isolation (Proietti *et al.*, 2014). This was deemed due to not only eliminating exit of drivers from the pulmonary veins, but also debulking the left atrium in general and reducing the volume of tissue that could sustain re-entry.

The opening of K_{ATP} channels leads to faster repolarisation and a shorter QT interval on the surface ECG, a marker of the activation-recovery interval (Kubota *et al.*, 1993; Lu *et al.*, 2008). In turn this gives a reduced effective refractory period, which in principle can predispose to re-entrant circuits and a pro-fibrillatory state. Pro-fibrillatory effects of K_{ATP} openers have been shown in the ventricle in numerous animal models and a major factor in this is likely to

involve heterogeneous dispersion of APD effects both in an interventricular, and intraventricular manner between layers of the myocardium (Wolleben *et al.*, 1989; Chi *et al.*, 1990; Furukawa *et al.*, 1991; Di Diego & Antzelevitch, 1993; Wolk *et al.*, 1999; Uchida *et al.*, 1999; Quintanilla *et al.*, 2013).

The corollary is that blocking K_{ATP} would be anti-arrhythmic. Studies in rat and canine models have looked at ventricular fibrillatory potential in the context of ischaemia and shown that this is reduced in the presence of K_{ATP} blocking drugs (Wolleben *et al.*, 1989; Kantor *et al.*, 1990; Billman *et al.*, 1998). This has been replicated in a Langendorff-perfused explanted cardiomyopathic human heart model (Farid *et al.*, 2011).

Studies have also investigated arrhythmia inducibility in atrial preparations. In a rat model isoproterenol-induced metabolic stress led to a reduced intracellular ATP concentration and an increased atrial tachyarrhythmia inducible state that was reversed with the K_{ATP} inhibitor glibenclamide (Kim *et al.*, 2012). In a murine model with salt-induced hypertension, atrial K_{ATP} upregulation was seen coinciding with shortened APD and ERP and increased atrial arrhythmia inducibility (Lader *et al.*, 2011). In human hearts obtained at transplantation, KCOs were seen to increase atrial arrhythmia inducibility that was then terminated with a K_{ATP} inhibitor (Fedorov *et al.*, 2011).

It has also been demonstrated, however, that AF initiation is dependent on other factors such as APD and CV restitution at shorter coupling intervals, where steeper restitution slopes (>1) are associated with enhanced wavebreak and fibrillatory conduction (Qu *et al.*, 1999; Weiss *et al.*, 1999). The spatiotemporal heterogeneity of restitution is also important in causing wavebreak (Cao *et al.*, 1999; Banville & Gray, 2002). More recently, it has also been shown that conduction slowing is important at the moment of AF initiation, as is a heterogeneity of conduction slowing across the atria for perseveration of AF (Narayan *et al.*, 2008; Lalani *et al.*, 2012; Krummen *et al.*, 2012; Lim *et al.*, 2017; Honarbakhsh *et al.*, 2018). Potassium channel blocking drugs such as sotalol demonstrate reverse use dependence with greater block at longer diastolic intervals and steepen the APD restitution slope (Lathrop *et al.*, 1989; 1990). I saw a hyperpolarisation of the resting membrane potential with K_{ATP}

activation in HL-1 cells. Potassium channel activation, by hyperpolarising the membrane potential, could actually serve to increase conduction velocity by increasing sodium channel availability. Atria are less thick than the ventricles and the degree of transmural and spatial heterogeneity of K_{ATP} expression across the atria has not been described like it has in the ventricle. The effects of K_{ATP} opening in the HL-1 syncytia might be a uniform phenomenon and serve to homogenise conduction velocity across the tissue sheet. Increasing conduction velocity should serve to increase the minimum wavefront path length and reduce the likelihood of re-entrant activation. K_{ATP} opening may also reduce APD and CV restitution slopes, or at least shift them leftwards to shorter coupling intervals, and in a uniform manner if there is no significant gradient of ion channel expression, like what might be expected in the HL-1 syncytia. This would need to be explored further to prove but might explain the organisation of rotational activity seen.

Whilst channel opening might open up tissue to the increased likelihood of re-entry, in the case of abnormal automaticity or triggered activity, it is also possible that hyperpolarisation of the membrane will lead to the arrhythmia being extinguished. Effects of K_{ATP} modulation on automaticity have largely been investigated in isolated nodal cell or Purkinje fibre preparations and confirm that an increased outward potassium flux and membrane hyperpolarisation on channel opening slows spontaneous firing rate and suppresses automaticity (Yanagisawa & Taira, 1981; Satoh & Hashimoto, 1984; Imanishi *et al.*, 1984; Lathrop *et al.*, 1990). In my series of experiments, further to organising rotational wavefronts, K_{ATP} activation then silenced HL-1 syncytia in a dose-dependent fashion. This could be explained by further hyperpolarisation leading to reduced automaticity. Similarly, it may merely be an effect of reduced excitability of the HL-1 syncytia, that prevented curvature of rotational wavefronts, and organisation to a straight wavefronts.

4.5 Pharmacological K_{ATP} activation does not impact on sinus node automaticity

Further to the finding that increased doses of diazoxide could silence HL-1 syncytia, and work from our lab that a large proportion of murine SAN cells were diazoxide-sensitive (Aziz *et al.*, 2018), I sought to establish whether pharmacological K_{ATP} activation could have an SAN slowing effect. This was not the case but K_{ATP} inhibition was able to blunt the SAN slowing effects of hypoxia. Similar effects have been shown in a Kir6.2 $-/-$ mouse (Fukuzaki *et al.*, 2008). Hypoxia and metabolic inhibition are inherently potent activators of K_{ATP} and perhaps more so than pharmacological activation alone, especially if the current density for K_{ATP} is small in the sinus node compared to atria as our lab has demonstrated through this and a previous study ($\sim 20\text{pA/pF}$ vs $\sim 130\text{pA/pF}$ in atrial cardiomyocytes) (Aziz *et al.*, 2018). During hypoxia, the activity of the inward calcium currents and calcium release from the sarcoplasmic reticulum are reduced (Shimoda & Polak, 2011), and a reduction in circulating cAMP from reduced availability of ATP is likely to contribute to reduced I_f current. Taken together hyperpolarisation from hypoxia induced K_{ATP} activation is likely to slow diastolic depolarisation and pacemaker activity further.

4.6 Human cardiac K_{ATP}

The data from this project suggests one major difference in the subunit composition of the K_{ATP} current in the human heart as compared to that of the mouse. SUR1 expression appeared very low in the "normal" human heart. One group have demonstrated a failure to shorten action potential duration on administration of diazoxide in non-failing human heart atria, but the opposite in the failing heart (Fedorov *et al.*, 2011). Pinacidil was able to shorten action potentials in both scenarios. A high dose of diazoxide was used, 300 μ M, and thus this could represent SUR2B activation, or even SUR2A activation in the presence of a high concentration of MgADP. Another group have shown a lack of inhibition by tolbutamide in human right atrial cardiac myocytes (Zünkler *et al.*, 1997). SUR2-specific K_{ATP} openers have also been shown to activate current in human atrial cardiomyocytes (Pelzmann *et al.*, 2001; Balana *et al.*, 2003). Inferences on the differential cardiomyocyte composition of subunits other than SUR1 is difficult when utilising whole heart RNA. SUR2B is likely to be expressed in the endothelium and smooth muscle cell populations that make up the total RNA, and this probably explains a large relative expression of this subunit in my results given that non-myocytes in the heart constitute ~70% of cells, and endothelial cells alone are said to constitute >60% of this non-myocyte population (Pinto *et al.*, 2016). Single cell RNA quantification from isolated cardiomyocytes is likely to yield more meaningful information, and single cell electrophysiology using the pharmacological tools established in this project could further delineate the subunit composition of human cardiomyocytes.

4.7 Clinical implications and translational aspects

In a murine model, this study has demonstrated K_{ATP} inhibition to have anti-arrhythmic effects on the atria in the context of ischaemia. Conduction velocity is slowed during hypoxia, and thus inhibition of a potassium channel that is strongly activated by hypoxia, and shortens APD during hypoxia, will counter these WFPL shortening effects by prolonging the ERP. This paradigm might be useful in the context of ischaemia driven atrial arrhythmias during, for example, the peri-procedural period of cardiac surgery where there is a high burden of post-operative AF and potassium channel blocking drugs such as amiodarone already provide a benefit (Budeus *et al.*, 2006). If an atrial selective K_{ATP} blocker can be developed then this might also have benefit during the peri-myocardial-infarct period where AF burden is also high. Amiodarone is the most effective drug in this context but carries with it the risk of many side effects. There are various series commenting on the pro- and anti-arrhythmic effects of sulphonylureas used in diabetic patients. These were usually in the context of ischaemia, specifically with respect to ventricular fibrillation, and the findings are equivocal (Leonard *et al.*, 2017). These series are also observational and naturally, therefore, heterogeneous. There are no such data pertaining to the prevalence of atrial arrhythmias or its burden amongst this patient cohort.

The alternative paradigm raised by this study is that potassium channel activation can be anti-arrhythmic. Myocardial sleeves and strands extend from the left atrium into the pulmonary veins producing a distinct architecture including areas of fibrosis and conduction slowing (Saito *et al.*, 2000; Ho *et al.*, 2001; Mueller-Hoecker *et al.*, 2008). Fibroblast differentiation to myfibroblasts is a precursor step to the development of fibrosis and the latter are more depolarised at rest lacking the ionic currents required of specialised cardiomyocytes (Camelliti *et al.*, 2005; Nguyen *et al.*, 2014). This contributes to conduction slowing and, through electrotonic interaction, is likely to have a depolarising effect on adjacent pulmonary vein (PV) myocytes, and those in the atrial body, where a fibrotic histopathological substrate is also stipulated in the mechanism of chronic AF (Schotten *et al.*, 2011; Rohr, 2012; Nguyen *et al.*, 2014). PV myocytes have been shown to have a more depolarised resting membrane potential, lower peak amplitude and shorter action potential duration

(Ehrlich *et al.*, 2003). They also display automaticity with expression of pacemaker-like currents including I_{CaT} and a hyperpolarisation-activated cation current akin to the "funny" current (Cheung, 1981a; Chen *et al.*, 2004; Ehrlich *et al.*, 2004). Enrichment of transcription factors, PITX2 and SHOX2, known to control the development of nodal and pacemaking regions of the heart, has been shown at the LA-PV junction (Yeh *et al.*, 2013). PV myocytes have also displayed calcium-handling abnormalities and develop EADs and DADs that can give rise to triggered activity, and atrial cardiomyocytes from patients with chronic AF demonstrate abnormal calcium handling with enhanced SR calcium leak and $I_{Na/Ca}$ function (Cheung, 1981b; Chen *et al.*, 1999; Wit & Boyden, 2007; Schotten *et al.*, 2011; Voigt *et al.*, 2012). Whilst cholinergic activity would be expected to shorten APD and increase the likelihood of re-entry, M3 muscarinic receptors also lead to increased calcium release from SR stores via the G_q receptor pathway and it may be that calcium handling is an all-important factor here in the generation of cholinergic AF. It is conceivable, therefore, that potassium channel activation alone, in reducing calcium loading on the cell and providing an opposing current to depolarisation, reduce the likelihood of triggered or automatic activity that might drive AF. It might also have a homogenising effect on conduction velocity and APD restitution that serves to reduce the likelihood of wavebreak and acts to organise rotational wavefronts as has been seen in this study.

K_{ATP} opening has cardioprotective effects not least owing to reducing the calcium load on the myocyte. There may be other, indirect, positive cardiac effects of K_{ATP} activation. Diazoxide was first explored clinically for its anti-hypertensive effect through vascular smooth muscle relaxation (McNair *et al.*, 1983). In the more modern era it is used to suppress insulin secretion in hyperinsulinaemic hypoglycaemic patients (Nessa *et al.*, 2016). It is a drug with fully established pharmacokinetics and safety characteristics with no associated increased risk of arrhythmias (Welters *et al.*, 2015).

It has also been shown through its pancreatic and central effects, to improve glycaemic control in type 1 diabetics, ameliorate beta-cell function in type 2 diabetics, and lead to weight loss in obese patients (Qvigstad *et al.*, 2004; Schreuder *et al.*, 2005; van Boekel *et al.*, 2008; Radtke *et al.*, 2010). Recent

good evidence shows that obesity and epicardial fat have a clear association with promoting an AF substrate. Diazoxide could have a multi-dimensional action in reducing the burden of AF not only via a direct electrophysiological effect of K_{ATP} opening, but also by favourable metabolic effects.

4.8 Limitations

Further to limitations previously mentioned through the discussion, attention must be drawn to others.

The mouse model brings with it limitations with regards differences in action potential characteristics compared to human, owing to differences in calcium handling and repolarising currents. The K_{ATP} subunit composition in the murine heart is likely to be different from that of the human as has been alluded to.

In the quantitative mRNA analysis, GAPDH was used as a sole reference gene. An ideal reference gene is one that has completely stable expression across developmental stages, disease states, different tissue/cell types and different tissue preparations. No commonly used reference gene can be said to truly exhibit this though some show more stability than others and GAPDH tends to be one of the more stable (Vandesompele *et al.*, 2002; Brattelid *et al.*, 2010). Knockout of the pore-forming subunits in itself may have affected GAPDH expression stability, though demonstration of the absence of expression of the pore-forming subunit in question in each of the global knockout mice is not in doubt given the clear and profound evidence for deletion in the quantification analysis. Caution must, however, be exercised when analysing expression differences between the other subunits. Equally we do not know the exact contribution of different cell types in each of the tissue samples used, though the mean of various preparations was taken, and the variation is accounted for in the statistical testing. Whilst making inferences into absolute expression differences and proportions would be unwise, it is reasonable to observe and accept the trends in differences in subunit expression, and much of the data pertaining to quantitative mRNA analysis in the mouse is supported by the electrophysiology and pharmacology also presented. The same qualms described above would apply to the human quantitative mRNA analysis. Undoubtedly the purest and most ideal approach, is to use the geometric mean of a number, usually a minimum of three, different reference genes deemed most stable amongst the different cell types in the tissue preparation of interest (Vandesompele *et al.*, 2002).

HL-1 syncytia are representative of 2D sheets of tissue and not likely to be more than 2 to 3 cells thick. Whole heart tissue is not a 2D sheet and cardiac conduction is a 3D phenomenon. A corollary to this is the measurement of conduction velocity in the Langendorff preparation was performed solely on the epicardial surface in a 2D format and does not account for wavefront paths passing transmurally. Whilst also there was a large drive to manually check the quality of electrograms, and the method used to measure conduction velocity has been validated previously (Finlay *et al.*, 2014), there is always the possibility of error with regards electrogram quality.

Arrhythmia induction protocols have already been mentioned in that they could be more aggressive. The definition of arrhythmia including a single ectopic could be seen as too sensitive, though this was a standardised approach and ectopy was only taken in response to programmed electrical stimulation.

4.9 Future directions

A thorough assessment of the K_{ATP} current in isolated human cardiomyocytes is needed. The pharmacological tools with patch clamp demonstrated in this project could be used. It is my plan to perform this on isolated cardiomyocytes from tissue obtained from patients undergoing cardiothoracic surgery under the auspices of The Barts Cardiovascular Registry. I would also include an assessment of nicorandil in these experiments. Isolated cardiomyocyte single cell RNA quantification could also be compared. Atrial tissue is easier to obtain from a risk balance perspective, though it may also be possible to obtain ventricular myocardial samples from, for example, septal myectomy patients with hypertrophic cardiomyopathy, and also make a direct comparison of atrial and ventricular K_{ATP} pharmacology through patch clamp of these cells.

Further assessments of the conduction velocity across the HL-1 syncytia would be possible through utilisation of the electrograms obtained through the MEA. An assessment of calcium transient characteristics under control circumstances, and in response to diazoxide, including peak amplitude, duration at half-maximum amplitude, time to peak and tau could all be assessed under uniform frequency by pacing through the MEA. After-depolarisations could also be assessed both through stimulation at high frequencies to induce calcium loading, or even in the presence of caffeine, and any suppression of diazoxide examined. This could also be performed in Langendorff preparations looking at ectopic and arrhythmia burden in control and knockout mouse hearts in response to diazoxide +/- caffeine.

Given diazoxide is a fully established drug with known safety profile and pharmacokinetics, it is conceivable that a clinical trial be performed looking at its effects in patients with AF. Similarly, given nicorandil is a widely used drug in patients with cardiac ischaemia for improved symptoms of angina, and that it does not appear to have pro-arrhythmic effects in the ventricle, it too could be assessed for an atrial anti-arrhythmic effect.

Section 5: References

- Abed HS, Wittert GA, Leong DP, Shirazi MG, Bahrami B, Middeldorp ME, Lorimer MF, Lau DH, Antic NA, Brooks AG, Abhayaratna WP, Kalman JM & Sanders P (2013). Effect of weight reduction and cardiometabolic risk factor management on symptom burden and severity in patients with atrial fibrillation: a randomized clinical trial. *JAMA* **310**, 2050–2060.
- Abriel H (2007). Roles and regulation of the cardiac sodium channel Na^v 1.5: recent insights from experimental studies. *Cardiovasc Res* **76**, 381–389.
- Aguilar-Bryan L, Nichols CG, Wechsler SW, Clement JP, Boyd AE, Gonzalez G, Herrera-Sosa H, Nguy K, Bryan J & Nelson DA (1995). Cloning of the beta cell high-affinity sulfonylurea receptor: a regulator of insulin secretion. *Science* **268**, 423–426.
- Ahir BK & Pratten MK (2014). Structure and function of gap junction proteins: role of gap junction proteins in embryonic heart development. *Int J Dev Biol* **58**, 649–662.
- Allessie MA, Bonke FIM & Schopman FJ (1977). Circus movement in rabbit atrial muscle as a mechanism of tachycardia. III. The “leading circle” concept: a new model of circus movement in cardiac tissue without the involvement of an anatomical obstacle. *Circ Res* **41**, 9–18.
- Allessie MA, Lammers WJEP, Bonke FIM & Hollen SJ (1985). Experimental evaluation of Moe’s multiple wavelet hypothesis of atrial fibrillation. In *Cardiac Electrophysiology and Arrhythmias*, ed. Zipes DP & Jalife J, pp. 265–275. NY: Grune & Stratton.
- Alves-Cabrato L, García-Gil M, Comas-Cufí M, Ponjoan A, Martí-Lluch R, Parramon D, Blanch J, Elosua-Bayes M & Ramos R (2017). Statins and new-onset atrial fibrillation in a cohort of patients with hypertension. Analysis of electronic health records, 2006-2015. ed. Wright JM. *PLoS ONE* **12**, e0186972.
- Antcliff JF, Haider S, Proks P, Sansom MSP & Ashcroft FM (2005). Functional analysis of a structural model of the ATP-binding site of the KATP channel Kir6.2 subunit. *EMBO J* **24**, 229–239.
- Antzelevitch C (2012). Genetic, molecular and cellular mechanisms underlying the J wave syndromes. *Circ J* **76**, 1054–1065.
- Antzelevitch C & Burashnikov A (2011). Overview of Basic Mechanisms of Cardiac Arrhythmia. *Card Electrophysiol Clin* **3**, 23–45.
- Antzelevitch C, Sicouri S, Litovsky SH, Lukas A, Krishnan SC, Di Diego JM, Gintant GA & Liu DW (1991). Heterogeneity within the ventricular wall. Electrophysiology and pharmacology of epicardial, endocardial, and M cells. *Circ Res* **69**, 1427–1449.

- Arbelo E, Brugada J, Hindricks G, Maggioni A, Tavazzi L, Vardas P, Anselme F, Inama G, Jaïs P, Kalarus Z, Kautzner J, Lewalter T, Mairesse G, Perez-Villacastin J, Riahi S, Taborsky M, Theodorakis G, Trines Son behalf of the Atrial Fibrillation Ablation Pilot Study Investigators (2012). ESC-EURObservational Research Programme: the Atrial Fibrillation Ablation Pilot Study, conducted by the European Heart Rhythm Association. *Europace* **14**, 1094–1103.
- Ariyaratnam V & Spodick DH (2006). The Bachmann Bundle and interatrial conduction. *Cardiol Rev* **14**, 194–199.
- Armstrong CM (2006). Na channel inactivation from open and closed states. *Proc Natl Acad Sci USA* **103**, 17991–17996.
- Ashcroft FM (1988). Adenosine 5'-triphosphate-sensitive potassium channels. *Annu Rev Neurosci* **11**, 97–118.
- Ashfield R, Gribble FM, Ashcroft SJ & Ashcroft FM (1999). Identification of the high-affinity tolbutamide site on the SUR1 subunit of the K(ATP) channel. *Diabetes* **48**, 1341–1347.
- Axon Instruments Inc (1993). *The Axon guide for electrophysiology & biophysics laboratory techniques*. Axon Instruments Inc.
- Aziz Q, Finlay M, Montaigne D, Ojake L, Li Y, Anderson N, Ludwig A & Tinker A (2018). ATP-sensitive potassium channels in the sinoatrial node contribute to heart rate control and adaptation to hypoxia. *J Biol Chem* **293**, 8912–8921.
- Aziz Q, Li Y, Anderson N, Ojake L, Tsisanova E & Tinker A (2017). Molecular and functional characterization of the endothelial ATP-sensitive potassium channel. *J Biol Chem* **292**, 17587–17597.
- Aziz Q, Thomas AM, Gomes J, Ang R, Sones WR, Li Y, Ng K-E, Gee L & Tinker A (2014). The ATP-sensitive potassium channel subunit, Kir6.1, in vascular smooth muscle plays a major role in blood pressure control. *Hypertension* **64**, 523–529.
- Babenko AP & Bryan J (2001). A conserved inhibitory and differential stimulatory action of nucleotides on K(IR)6.0/SUR complexes is essential for excitation-metabolism coupling by K(ATP) channels. *J Biol Chem* **276**, 49083–49092.
- Babenko AP & Bryan J (2003). Sur domains that associate with and gate KATP pores define a novel gatekeeper. *J Biol Chem* **278**, 41577–41580.
- Babenko AP, Gonzalez G & Bryan J (1999). The tolbutamide site of SUR1 and a mechanism for its functional coupling to K(ATP) channel closure. *FEBS Lett* **459**, 367–376.
- Babenko AP, Gonzalez G & Bryan J (2000). Pharmacology-topology of sulfonylurea receptors. Separate domains of the regulatory subunits of K(ATP) channel isoforms are required for selective interaction with K(+) channel openers. *J Biol Chem* **275**, 717–720.

- Babenko AP, Gonzalez G, Aguilar-Bryan L & Bryan J (1998). Reconstituted human cardiac KATP channels: functional identity with the native channels from the sarcolemma of human ventricular cells. *Circ Res* **83**, 1132–1143.
- Babenko AP, Polak M, Cavé H, Busiah K, Czernichow P, Scharfmann R, Bryan J, Aguilar-Bryan L, Vaxillaire M & Froguel P (2006). Activating mutations in the ABCC8 gene in neonatal diabetes mellitus. *N Engl J Med* **355**, 456–466.
- Balana B, Dobrev D, Wettwer E, Christ T, Knaut M & Ravens U (2003). Decreased ATP-sensitive K(+) current density during chronic human atrial fibrillation. *J Mol Cell Cardiol* **35**, 1399–1405.
- Banville I & Gray RA (2002). Effect of action potential duration and conduction velocity restitution and their spatial dispersion on alternans and the stability of arrhythmias. *J Cardiovasc Electrophysiol* **13**, 1141–1149.
- Bao L, Kefaloyianni E, Lader J, Hong M, Morley G, Fishman GI, Sobie EA & Coetzee WA (2011). Unique properties of the ATP-sensitive K⁺ channel in the mouse ventricular cardiac conduction system. *Circ Arrhythm Electrophysiol* **4**, 926–935.
- Barajas-Martínez H, Hu D, Ferrer T, Onetti CG, Wu Y, Burashnikov E, Boyle M, Surman T, Urrutia J, Veltmann C, Schimpf R, Borggreffe M, Wolpert C, Ibrahim BB, Sánchez-Chapula JA, Winters S, Haïssaguerre M & Antzelevitch C (2012). Molecular genetic and functional association of Brugada and early repolarization syndromes with S422L missense mutation in KCNJ8. *Heart Rhythm* **9**, 548–555.
- Barajas-Martínez H, Hu D, Goodrow RJ, Joyce F & Antzelevitch C (2013). Electrophysiologic characteristics and pharmacologic response of human cardiomyocytes isolated from a patient with hypertrophic cardiomyopathy. *Pacing Clin Electrophysiol* **36**, 1512–1515.
- Baron A, van Bever L, Monnier D, Roatti A & Baertschi AJ (1999). A novel K(ATP) current in cultured neonatal rat atrial appendage cardiomyocytes. *Circ Res* **85**, 707–715.
- Baumann P, Poitry S, Roatti A & Baertschi AJ (2002). Plasmalemmal KATP channels shape triggered calcium transients in metabolically impaired rat atrial myocytes. *Am J Physiol Heart Circ Physiol* **283**, H2296–H2305.
- Bean BP (1985). Two kinds of calcium channels in canine atrial cells. Differences in kinetics, selectivity, and pharmacology. *J Gen Physiol* **86**, 1–30.
- Beaumont J, Davidenko N, Davidenko JM & Jalife J (1998). Spiral waves in two-dimensional models of ventricular muscle: formation of a stationary core. *Biophys J* **75**, 1–14.
- Beech DJ, Zhang H, Nakao K & Bolton TB (1993). K channel activation by nucleotide diphosphates and its inhibition by glibenclamide in vascular smooth muscle cells. *Br J Pharmacol* **110**, 573–582.
- Bers DM (2002). Cardiac excitation-contraction coupling. *Nature* **415**, 198–205.

- Bers DM (2008). Calcium cycling and signaling in cardiac myocytes. *Annu Rev Physiol* **70**, 23–49.
- Bienengraeber M, Alekseev AE, Abraham MR, Carrasco AJ, Moreau C, Vivaudou M, Dzeja PP & Terzic A (2000). ATPase activity of the sulfonylurea receptor: a catalytic function for the KATP channel complex. *FASEB J* **14**, 1943–1952.
- Bienengraeber M, Olson TM, Selivanov VA, Kathmann EC, O'Coilain F, Gao F, Karger AB, Ballew JD, Hodgson DM, Zingman LV, Pang Y-P, Alekseev AE & Terzic A (2004). ABCC9 mutations identified in human dilated cardiomyopathy disrupt catalytic KATP channel gating. *Nat Genet* **36**, 382–387.
- Billman GE, Englert HC & Schölkens BA (1998). HMR 1883, a novel cardioselective inhibitor of the ATP-sensitive potassium channel. Part II: effects on susceptibility to ventricular fibrillation induced by myocardial ischemia in conscious dogs. *J Pharmacol Exp Ther* **286**, 1465–1473.
- Blaustein MP & Lederer WJ (1999). Sodium/calcium exchange: its physiological implications. *Physiol Rev* **79**, 763–854.
- Bogdanov KY, Vinogradova TM & Lakatta EG (2001). Sinoatrial nodal cell ryanodine receptor and Na(+)-Ca(2+) exchanger: molecular partners in pacemaker regulation. *Circ Res* **88**, 1254–1258.
- Borisov AB & Claycomb WC (1995). Proliferative potential and differentiated characteristics of cultured cardiac muscle cells expressing the SV40 T oncogene. *Ann N Y Acad Sci* **752**, 80–91.
- Bouabe H & Okkenhaug K (2013). Gene targeting in mice: a review. *Methods Mol Biol* **1064**, 315–336.
- Boukens BJ, Rivaud MR, Rentschler S & Coronel R (2014). Misinterpretation of the mouse ECG: 'musing the waves of *Mus musculus*'. *J Physiol (Lond)* **592**, 4613–4626.
- Boyett MR, Honjo H & Kodama I (2000). The sinoatrial node, a heterogeneous pacemaker structure. *Cardiovasc Res* **47**, 658–687.
- Brattelid T, Winer LH, Levy FO, Liestøl K, Sejersted OM & Andersson KB (2010). Reference gene alternatives to Gapdh in rodent and human heart failure gene expression studies. *BMC Mol Biol* **11**, 22.
- Braz JC et al. (2004). PKC-alpha regulates cardiac contractility and propensity toward heart failure. *Nat Med* **10**, 248–254.
- Brodde OE & Michel MC (1999). Adrenergic and muscarinic receptors in the human heart. *Pharmacol Rev* **51**, 651–690.
- Brown SDM & Moore MW (2012). The International Mouse Phenotyping Consortium: past and future perspectives on mouse phenotyping. *Mamm Genome* **23**, 632–640.

- Brownstein CA, Towne MC, Luquette LJ, Harris DJ, Marinakis NS, Meinecke P, Kutsche K, Campeau PM, Yu TW, Margulies DM, Agrawal PB & Beggs AH (2013). Mutation of KCNJ8 in a patient with Cantú syndrome with unique vascular abnormalities - support for the role of K(ATP) channels in this condition. *Eur J Med Genet* **56**, 678–682.
- Brundel BJ, Van Gelder IC, Henning RH, Tuinenburg AE, Wietses M, Grandjean JG, Wilde AA, Van Gilst WH & Crijns HJ (2001). Alterations in potassium channel gene expression in atria of patients with persistent and paroxysmal atrial fibrillation: differential regulation of protein and mRNA levels for K⁺ channels. *J Am Coll Cardiol* **37**, 926–932.
- Buch E, Share M, Tung R, Benharash P, Sharma P, Koneru J, Mandapati R, Ellenbogen KA & Shivkumar K (2016). Long-term clinical outcomes of focal impulse and rotor modulation for treatment of atrial fibrillation: A multicenter experience. *Heart Rhythm* **13**, 636–641.
- Budeus M, Hennersdorf M, Perings S, Röhlen S, Schnitzler S, Felix O, Reimert K, Feindt P, Gams E, Lehmann N, Wieneke H, Sack S, Erbel R & Perings C (2006). Amiodarone prophylaxis for atrial fibrillation of high-risk patients after coronary bypass grafting: a prospective, double-blinded, placebo-controlled, randomized study. *Eur Heart J* **27**, 1584–1591.
- Burashnikov A & Antzelevitch C (2003). Reinduction of atrial fibrillation immediately after termination of the arrhythmia is mediated by late phase 3 early afterdepolarization-induced triggered activity. *Circulation* **107**, 2355–2360.
- Burashnikov A & Antzelevitch C (2006). Late-phase 3 EAD. A unique mechanism contributing to initiation of atrial fibrillation. *Pacing Clin Electrophysiol* **29**, 290–295.
- Camelliti P, Borg TK & Kohl P (2005). Structural and functional characterisation of cardiac fibroblasts. *Cardiovasc Res* **65**, 40–51.
- Camm AJ et al. (2010). Guidelines for the management of atrial fibrillation: the Task Force for the Management of Atrial Fibrillation of the European Society of Cardiology (ESC). *Eur Heart J* **31**, 2369–2429.
- Camm AJ, Lip GYH, De Caterina R, Savelieva I, Atar D, Hohnloser SH, Hindricks G, Kirchhof PESC Committee for Practice Guidelines (CPG) (2012). 2012 focused update of the ESC Guidelines for the management of atrial fibrillation: an update of the 2010 ESC Guidelines for the management of atrial fibrillation. Developed with the special contribution of the European Heart Rhythm Association. *Eur Heart J* **33**, 2719–2747.
- Cantwell CD, Roney CH, Ng FS, Siggers JH, Sherwin SJ & Peters NS (2015). Techniques for automated local activation time annotation and conduction velocity estimation in cardiac mapping. *Comput Biol Med* **65**, 229–242.
- Cao JM, Qu Z, Kim YH, Wu TJ, Garfinkel A, Weiss JN, Karagueuzian HS & Chen PS (1999). Spatiotemporal heterogeneity in the induction of ventricular fibrillation by rapid pacing: importance of cardiac restitution properties. *Circ Res* **84**, 1318–1331.

- Carmeliet E (1987). Slow inactivation of the sodium current in rabbit cardiac Purkinje fibres. *Pflugers Arch* **408**, 18–26.
- Carrasco AJ, Dzeja PP, Alekseev AE, Pucar D, Zingman LV, Abraham MR, Hodgson D, Bienengraeber M, Puceat M, Janssen E, Wieringa B & Terzic A (2001). Adenylate kinase phosphotransfer communicates cellular energetic signals to ATP-sensitive potassium channels. *Proc Natl Acad Sci USA* **98**, 7623–7628.
- Cartier EA, Conti LR, Vandenberg CA & Shyng SL (2001). Defective trafficking and function of KATP channels caused by a sulfonylurea receptor 1 mutation associated with persistent hyperinsulinemic hypoglycemia of infancy. *PNAS* **98**, 2882–2887.
- Catterall WA (2011). Voltage-gated calcium channels. *Cold Spring Harb Perspect Biol* **3**, a003947.
- Chard M & Tabrizchi R (2009). The role of pulmonary veins in atrial fibrillation: a complex yet simple story. *Pharmacol Ther* **124**, 207–218.
- Chen SA, Hsieh MH, Tai CT, Tsai CF, Prakash VS, Yu WC, Hsu TL, Ding YA & Chang MS (1999). Initiation of atrial fibrillation by ectopic beats originating from the pulmonary veins: electrophysiological characteristics, pharmacological responses, and effects of radiofrequency ablation. *Circulation* **100**, 1879–1886.
- Chen Y-C, Chen S-A, Chen Y-J, Tai C-T, Chan P & Lin C-I (2004). T-type calcium current in electrical activity of cardiomyocytes isolated from rabbit pulmonary vein. *J Cardiovasc Electrophysiol* **15**, 567–571.
- Chen YJ, Chen SA, Chen YC, Yeh HI, Chan P, Chang MS & Lin CI (2001). Effects of rapid atrial pacing on the arrhythmogenic activity of single cardiomyocytes from pulmonary veins: implication in initiation of atrial fibrillation. *Circulation* **104**, 2849–2854.
- Cheng WWL, Tong A, Flagg TP & Nichols CG (2008). Random assembly of SUR subunits in K(ATP) channel complexes. *Channels (Austin)* **2**, 34–38.
- Cheung DW (1981a). Electrical activity of the pulmonary vein and its interaction with the right atrium in the guinea-pig. *J Physiol (Lond)* **314**, 445–456.
- Cheung DW (1981b). Pulmonary vein as an ectopic focus in digitalis-induced arrhythmia. *Nature* **294**, 582–584.
- Chi L, Uprichard AC & Lucchesi BR (1990). Profibrillatory actions of pinacidil in a conscious canine model of sudden coronary death. *J Cardiovasc Pharmacol* **15**, 452–464.
- Chinushi M, Kasai H, Tagawa M, Washizuka T, Hosaka Y, Chinushi Y & Aizawa Y (2002). Triggers of ventricular tachyarrhythmias and therapeutic effects of nicorandil in canine models of LQT2 and LQT3 syndromes. *J Am Coll Cardiol* **40**, 555–562.

- Choi E-K, Chang P-C, Lee Y-S, Lin S-F, Zhu W, Maruyama M, Fishbein MC, Chen Z, Rubart-von der Lohe M, Field LJ & Chen P-S (2012). Triggered firing and atrial fibrillation in transgenic mice with selective atrial fibrosis induced by overexpression of TGF- β 1. *Circ J* **76**, 1354–1362.
- Christel CJ, Cardona N, Mesirca P, Herrmann S, Hofmann F, Striessnig J, Ludwig A, Mangoni ME & Lee A (2012). Distinct localization and modulation of Cav1.2 and Cav1.3 L-type Ca²⁺ channels in mouse sinoatrial node. *J Physiol (Lond)* **590**, 6327–6342.
- Chutkow WA, Pu J, Wheeler MT, Wada T, Makielski JC, Burant CF & McNally EM (2002). Episodic coronary artery vasospasm and hypertension develop in the absence of Sur2 K(ATP) channels. *J Clin Invest* **110**, 203–208.
- Chutkow WA, Samuel V, Hansen PA, Pu J, Valdivia CR, Makielski JC & Burant CF (2001). Disruption of Sur2-containing K(ATP) channels enhances insulin-stimulated glucose uptake in skeletal muscle. *Proc Natl Acad Sci USA* **98**, 11760–11764.
- Chutkow WA, Simon MC, Le Beau MM & Burant CF (1996). Cloning, tissue expression, and chromosomal localization of SUR2, the putative drug-binding subunit of cardiac, skeletal muscle, and vascular KATP channels. *Diabetes* **45**, 1439–1445.
- Claycomb WC, Lanson NA, Stallworth BS, Egeland DB, Delcarpio JB, Bahinski A & Izzo NJ (1998). HL-1 cells: a cardiac muscle cell line that contracts and retains phenotypic characteristics of the adult cardiomyocyte. *Proc Natl Acad Sci USA* **95**, 2979–2984.
- Clement JP, Kunjilwar K, Gonzalez G, Schwanstecher M, Panten U, Aguilar-Bryan L & Bryan J (1997). Association and stoichiometry of K(ATP) channel subunits. *Neuron* **18**, 827–838.
- Comtois P, Kneller J & Nattel S (2005). Of circles and spirals: bridging the gap between the leading circle and spiral wave concepts of cardiac reentry. *Europace* **7 Suppl 2**, 10–20.
- Cooper PE, Sala-Rabanal M, Lee SJ & Nichols CG (2015). Differential mechanisms of Cantú syndrome-associated gain of function mutations in the ABCC9 (SUR2) subunit of the KATP channel. *J Gen Physiol* **146**, 527–540.
- Coppen SR, Kodama I, Boyett MR, Dobrzynski H, Takagishi Y, Honjo H, Yeh HI & Severs NJ (1999). Connexin45, a major connexin of the rabbit sinoatrial node, is co-expressed with connexin43 in a restricted zone at the nodal-crista terminalis border. *J Histochem Cytochem* **47**, 907–918.
- Coronel R, de Bakker JMT, Wilms-Schopman FJG, Opthof T, Linnenbank AC, Belterman CN & Janse MJ (2006). Monophasic action potentials and activation recovery intervals as measures of ventricular action potential duration: experimental evidence to resolve some controversies. *Heart Rhythm* **3**, 1043–1050.

- Coronel R, Janse MJ, Opthof T, Wilde AA & Taggart P (2012). Postrepolarization refractoriness in acute ischemia and after antiarrhythmic drug administration: action potential duration is not always an index of the refractory period. *Heart Rhythm* **9**, 977–982.
- Cosío FG & Delpón E (2002). New antiarrhythmic drugs for atrial flutter and atrial fibrillation: a conceptual breakthrough at last? *Circulation* **105**, 276–278.
- Craig TJ, Shimomura K, Holl RW, Flanagan SE, Ellard S & Ashcroft FM (2009). An in-frame deletion in Kir6.2 (KCNJ11) causing neonatal diabetes reveals a site of interaction between Kir6.2 and SUR1. *J Clin Endocrinol Metab* **94**, 2551–2557.
- Cranefield PF, Klein HO & Hoffman BF (1971). Conduction of the cardiac impulse. 1. Delay, block, and one-way block in depressed Purkinje fibers. *Circ Res* **28**, 199–219.
- Crawford RM, Jovanović S, Budas GR, Davies AM, Lad H, Wenger RH, Robertson KA, Roy DJ, Ranki HJ & Jovanović A (2003). Chronic mild hypoxia protects heart-derived H9c2 cells against acute hypoxia/reoxygenation by regulating expression of the SUR2A subunit of the ATP-sensitive K⁺ channel. *J Biol Chem* **278**, 31444–31455.
- Crawford RM, Ranki HJ, Botting CH, Budas GR & Jovanović A (2002). Creatine kinase is physically associated with the cardiac ATP-sensitive K⁺ channel in vivo. *FASEB J* **16**, 102–104.
- Cui Y, Gibling JP, Clapp LH & Tinker A (2001). A mechanism for ATP-sensitive potassium channel diversity: Functional coassembly of two pore-forming subunits. *Proc Natl Acad Sci USA* **98**, 729–734.
- Cui Y, Tinker A & Clapp LH (2003). Different molecular sites of action for the KATP channel inhibitors, PNU-99963 and PNU-37883A. *Br J Pharmacol* **139**, 122–128.
- Cui Y, Tran S, Tinker A & Clapp LH (2002). The molecular composition of K(ATP) channels in human pulmonary artery smooth muscle cells and their modulation by growth. *Am J Respir Cell Mol Biol* **26**, 135–143.
- D'hahan N, Moreau C, Prost AL, Jacquet H, Alekseev AE, Terzic A & Vivaudou M (1999). Pharmacological plasticity of cardiac ATP-sensitive potassium channels toward diazoxide revealed by ADP. *Proc Natl Acad Sci USA* **96**, 12162–12167.
- Dabrowski M, Ashcroft FM, Ashfield R, Lebrun P, Pirotte B, Egebjerg J, Bondo Hansen J & Wahl P (2002). The novel diazoxide analog 3-isopropylamino-7-methoxy-4H-1,2,4-benzothiadiazine 1,1-dioxide is a selective Kir6.2/SUR1 channel opener. *Diabetes* **51**, 1896–1906.
- Davidenko JM & Antzelevitch C (1986). Electrophysiological mechanisms underlying rate-dependent changes of refractoriness in normal and segmentally depressed canine Purkinje fibers. The characteristics of post-repolarization refractoriness. *Circ Res* **58**, 257–268.

- Davis LD & Temte JV (1969). Electrophysiological actions of lidocaine on canine ventricular muscle and Purkinje fibers. *Circ Res* **24**, 639–655.
- Davis LM, Rodefeld ME, Green K, Beyer EC & Saffitz JE (1995). Gap junction protein phenotypes of the human heart and conduction system. *J Cardiovasc Electrophysiol* **6**, 813–822.
- de Tombe PP (2003). Cardiac myofilaments: mechanics and regulation. *J Biomech* **36**, 721–730.
- DeFelice LJ (1997). *Electrical Properties of Cells*. Springer US.
- Delaney JT, Muhammad R, Blair MA, Kor K, Fish FA, Roden DM & Darbar D (2012). A KCNJ8 mutation associated with early repolarization and atrial fibrillation. *Europace* **14**, 1428–1432.
- Di Diego JM & Antzelevitch C (1993). Pinacidil-induced electrical heterogeneity and extrasystolic activity in canine ventricular tissues. Does activation of ATP-regulated potassium current promote phase 2 reentry? *Circulation* **88**, 1177–1189.
- Dias P, Desplantez T, El-Harasis MA, Chowdhury RA, Ullrich ND, Cabestrero de Diego A, Peters NS, Severs NJ, MacLeod KT & Dupont E (2014). Characterisation of connexin expression and electrophysiological properties in stable clones of the HL-1 myocyte cell line. ed. Barnes S. *PLoS ONE* **9**, e90266.
- DiFrancesco D (2010). The role of the funny current in pacemaker activity. *Circ Res* **106**, 434–446.
- DiFrancesco D & Tortora P (1991). Direct activation of cardiac pacemaker channels by intracellular cyclic AMP. *Nature* **351**, 145–147.
- Dobrev D, Friedrich A, Voigt N, Jost N, Wettwer E, Christ T, Knaut M & Ravens U (2005). The G protein-gated potassium current I(K,ACh) is constitutively active in patients with chronic atrial fibrillation. *Circulation* **112**, 3697–3706.
- Doshi RN, Wu TJ, Yashima M, Kim YH, Ong JJ, Cao JM, Hwang C, Yashar P, Fishbein MC, Karagueuzian HS & Chen PS (1999). Relation between ligament of Marshall and adrenergic atrial tachyarrhythmia. *Circulation* **100**, 876–883.
- Drain P, Li L & Wang J (1998). KATP channel inhibition by ATP requires distinct functional domains of the cytoplasmic C terminus of the pore-forming subunit. *Proc Natl Acad Sci USA* **95**, 13953–13958.
- duBell WH, Boyett MR, Spurgeon HA, Talo A, Stern MD & Lakatta EG (1991). The cytosolic calcium transient modulates the action potential of rat ventricular myocytes. *J Physiol (Lond)* **436**, 347–369.
- Durrer D, van Dam RT, Freud GE, Janse MJ, Meijler FL & Arzbaecher RC (1970). Total excitation of the isolated human heart. *Circulation* **41**, 899–912.

- Echt DS, Liebson PR, Mitchell LB, Peters RW, Obias-Manno D, Barker AH, Arensberg D, Baker A, Friedman L & Greene HL (1991). Mortality and morbidity in patients receiving encainide, flecainide, or placebo. The Cardiac Arrhythmia Suppression Trial. *N Engl J Med* **324**, 781–788.
- Ehrlich JR, Cha T-J, Zhang L, Chartier D, Melnyk P, Hohnloser SH & Nattel S (2003). Cellular electrophysiology of canine pulmonary vein cardiomyocytes: action potential and ionic current properties. *J Physiol (Lond)* **551**, 801–813.
- Ehrlich JR, Cha T-J, Zhang L, Chartier D, Villeneuve L, Hébert TE & Nattel S (2004). Characterization of a hyperpolarization-activated time-dependent potassium current in canine cardiomyocytes from pulmonary vein myocardial sleeves and left atrium. *J Physiol (Lond)* **557**, 583–597.
- Eisner DA & Sipido KR (2004). Sodium calcium exchange in the heart: necessity or luxury? *Circ Res* **95**, 549–551.
- Elrod JW, Harrell M, Flagg TP, Gundewar S, Magnuson MA, Nichols CG, Coetzee WA & Lefer DJ (2008). Role of sulfonylurea receptor type 1 subunits of ATP-sensitive potassium channels in myocardial ischemia/reperfusion injury. *Circulation* **117**, 1405–1413.
- Enkvetchakul D, Jeliaskova I, Bhattacharyya J & Nichols CG (2007). Control of inward rectifier K channel activity by lipid tethering of cytoplasmic domains. *J Gen Physiol* **130**, 329–334.
- Erginel-Unaltuna N, Yang WP & Blannar MA (1998). Genomic organization and expression of KCNJ8/Kir6.1, a gene encoding a subunit of an ATP-sensitive potassium channel. *Gene* **211**, 71–78.
- Fang W-T, Li H-J, Zhang H & Jiang S (2012). The role of statin therapy in the prevention of atrial fibrillation: a meta-analysis of randomized controlled trials. *Br J Clin Pharmacol* **74**, 744–756.
- Farid TA, Nair K, Massé S, Azam MA, Maguy A, Lai PFH, Umapathy K, Dorian P, Chauhan V, Varró A, Al-Hesayen A, Waxman M, Nattel S & Nanthakumar K (2011). Role of KATP channels in the maintenance of ventricular fibrillation in cardiomyopathic human hearts. *Circ Res* **109**, 1309–1318.
- Farzaneh T & Tinker A (2008). Differences in the mechanism of metabolic regulation of ATP-sensitive K⁺ channels containing Kir6.1 and Kir6.2 subunits. *Cardiovasc Res* **79**, 621–631.
- Fedorov VV, Glukhov AV, Ambrosi CM, Kosteki G, Chang R, Janks D, Schuessler RB, Moazami N, Nichols CG & Efimov IR (2011). Effects of KATP channel openers diazoxide and pinacidil in coronary-perfused atria and ventricles from failing and non-failing human hearts. *J Mol Cell Cardiol* **51**, 215–225.
- Field LJ (1988). Atrial natriuretic factor-SV40 T antigen transgenes produce tumors and cardiac arrhythmias in mice. *Science* **239**, 1029–1033.

- Finlay MC, Ahmed AK, Sugrue A, Bhar-Amato J, Quarta G, Pantazis A, Ciaccio EJ, Syrris P, Sen-Chowdhry S, Ben-Simon R, Chow AW, Lowe MD, Segal OR, McKenna WJ & Lambiase PD (2014). Dynamic conduction and repolarisation changes in early arrhythmogenic right ventricular cardiomyopathy versus benign outflow tract ectopy demonstrated by high density mapping & paced surface ECG analysis. *PLoS ONE* **9**, e99125.
- Flagg TP, Enkvetchakul D, Koster JC & Nichols CG (2010). Muscle KATP channels: recent insights to energy sensing and myoprotection. *Physiol Rev* **90**, 799–829.
- Flagg TP, Kurata HT, Masia R, Caputa G, Magnuson MA, Lefer DJ, Coetzee WA & Nichols CG (2008). Differential structure of atrial and ventricular KATP: atrial KATP channels require SUR1. *Circ Res* **103**, 1458–1465.
- Fox JEM, Jones L & Light PE (2005). Identification and pharmacological characterization of sarcolemmal ATP-sensitive potassium channels in the murine atrial HL-1 cell line. *J Cardiovasc Pharmacol* **45**, 30–35.
- Fozzard HA (2002). Cardiac sodium and calcium channels: a history of excitatory currents. *Cardiovasc Res* **55**, 1–8.
- Fukuzaki K, Sato T, Miki T, Seino S & Nakaya H (2008). Role of sarcolemmal ATP-sensitive K⁺ channels in the regulation of sinoatrial node automaticity: an evaluation using Kir6.2-deficient mice. *J Physiol (Lond)* **586**, 2767–2778.
- Furukawa T, Kimura S, Furukawa N, Bassett AL & Myerburg RJ (1991). Role of cardiac ATP-regulated potassium channels in differential responses of endocardial and epicardial cells to ischemia. *Circ Res* **68**, 1693–1702.
- Gaborit N, Le Bouter S, Szuts V, Varró A, Escande D, Nattel S & Demolombe S (2007). Regional and tissue specific transcript signatures of ion channel genes in the non-diseased human heart. *J Physiol (Lond)* **582**, 675–693.
- Gaeta M, Bandera F, Tassinari F, Lorenzo C, Cargnelutti M, Pelissero G, Malavazos AE & Ricci C (2017). Is epicardial fat depot associated with atrial fibrillation? A systematic review and meta-analysis. *Europace* **19**, 747–752.
- Garrey WE (1914). The nature of fibrillary contraction of the heart.- its relation to tissue mass and form. *Am J Physiol* **33**, 397–414.
- Garrey WE (1924). Auricular fibrillation. *Physiol Rev* **4**, 215–250.
- Giblin JP, Cui Y, Clapp LH & Tinker A (2002). Assembly limits the pharmacological complexity of ATP-sensitive potassium channels. *J Biol Chem* **277**, 13717–13723.
- Gintant GA (1995). Regional differences in IK density in canine left ventricle: role of IK_s in electrical heterogeneity. *Am J Physiol* **268**, H604–H613.
- Girard CAJ, Shimomura K, Proks P, Absalom N, Castano L, Perez de Nanclares G & Ashcroft FM (2006). Functional analysis of six Kir6.2 (KCNJ11) mutations causing neonatal diabetes. *Pflugers Arch* **453**, 323–332.

- Glitsch HG (2001). Electrophysiology of the sodium-potassium-ATPase in cardiac cells. *Physiol Rev* **81**, 1791–1826.
- Gloyn AL et al. (2004). Activating mutations in the gene encoding the ATP-sensitive potassium-channel subunit Kir6.2 and permanent neonatal diabetes. *N Engl J Med* **350**, 1838–1849.
- Gloyn AL, Weedon MN, Owen KR, Turner MJ, Knight BA, Hitman G, Walker M, Levy JC, Sampson M, Halford S, McCarthy MI, Hattersley AT & Frayling TM (2003). Large-scale association studies of variants in genes encoding the pancreatic beta-cell KATP channel subunits Kir6.2 (KCNJ11) and SUR1 (ABCC8) confirm that the KCNJ11 E23K variant is associated with type 2 diabetes. *Diabetes* **52**, 568–572.
- Glukhov AV, Flagg TP, Fedorov VV, Efimov IR & Nichols CG (2010). Differential K(ATP) channel pharmacology in intact mouse heart. *J Mol Cell Cardiol* **48**, 152–160.
- Goette A, Schön N, Kirchhof P, Breithardt G, Fetsch T, Häusler KG, Klein HU, Steinbeck G, Wegscheider K & Meinertz T (2012). Angiotensin II-antagonist in paroxysmal atrial fibrillation (ANTIPAF) trial. *Circ Arrhythm Electrophysiol* **5**, 43–51.
- Gordan R, Gwathmey JK & Xie L-H (2015). Autonomic and endocrine control of cardiovascular function. *World J Cardiol* **7**, 204–214.
- Gögelein H, Hartung J, Englert HC & Schölkens BA (1998). HMR 1883, a novel cardioselective inhibitor of the ATP-sensitive potassium channel. Part I: effects on cardiomyocytes, coronary flow and pancreatic beta-cells. *J Pharmacol Exp Ther* **286**, 1453–1464.
- Grant AO (2009). Cardiac ion channels. *Circ Arrhythm Electrophysiol* **2**, 185–194.
- Gribble FM, Tucker SJ & Ashcroft FM (1997a). The essential role of the Walker A motifs of SUR1 in K-ATP channel activation by Mg-ADP and diazoxide. *EMBO J* **16**, 1145–1152.
- Gribble FM, Tucker SJ & Ashcroft FM (1997b). The interaction of nucleotides with the tolbutamide block of cloned ATP-sensitive K⁺ channel currents expressed in *Xenopus* oocytes: a reinterpretation. *J Physiol (Lond)* **504** (Pt 1), 35–45.
- Gribble FM, Tucker SJ, Seino S & Ashcroft FM (1998). Tissue specificity of sulfonylureas: studies on cloned cardiac and beta-cell K(ATP) channels. *Diabetes* **47**, 1412–1418.
- Gross GJ & Auchampach JA (1992). Blockade of ATP-sensitive potassium channels prevents myocardial preconditioning in dogs. *Circ Res* **70**, 223–233.

- Haïssaguerre M, Chatel S, Sacher F, Weerasooriya R, Probst V, Lousouarn G, Horlitz M, Liersch R, Schulze-Bahr E, Wilde A, Kääb S, Koster J, Rudy Y, Le Marec H & Schott J (2009). Ventricular fibrillation with prominent early repolarization associated with a rare variant of KCNJ8/KATP channel. *J Cardiovasc Electrophysiol* **20**, 93–98.
- Haïssaguerre M, Jaïs P, Shah DC, Takahashi A, Hocini M, Quiniou G, Garrigue S, Le Mouroux A, Le Métayer P & Clémenty J (1998). Spontaneous initiation of atrial fibrillation by ectopic beats originating in the pulmonary veins. *N Engl J Med* **339**, 659–666.
- Hambrock A, Kayar T, Stumpp D & Osswald H (2004). Effect of two amino acids in TM17 of Sulfonylurea receptor SUR1 on the binding of ATP-sensitive K⁺ channel modulators. *Diabetes* **53 Suppl 3**, S128–S134.
- Hambrock A, Löffler-Walz C, Kloor D, Delabar U, Horio Y, Kurachi Y & Quast U (1999). ATP-Sensitive K⁺ channel modulator binding to sulfonylurea receptors SUR2A and SUR2B: opposite effects of MgADP. *Mol Pharmacol* **55**, 832–840.
- Hamill OP, Marty A, Neher E, Sakmann B & Sigworth FJ (1981). Improved patch-clamp techniques for high-resolution current recording from cells and cell-free membrane patches. *Pflugers Arch* **391**, 85–100.
- Hammarström AKM & Gage PW (2002). Hypoxia and persistent sodium current. *Eur Biophys J* **31**, 323–330.
- Hamming KSC, Soliman D, Matemisz LC, Niazi O, Lang Y, Gloyn AL & Light PE (2009). Coexpression of the type 2 diabetes susceptibility gene variants KCNJ11 E23K and ABCC8 S1369A alter the ATP and sulfonylurea sensitivities of the ATP-sensitive K(+) channel. *Diabetes* **58**, 2419–2424.
- Han X, Light PE, Giles WR & French RJ (1996). Identification and properties of an ATP-sensitive K⁺ current in rabbit sino-atrial node pacemaker cells. *J Physiol (Lond)* **490 (Pt 2)**, 337–350.
- Hancox JC & Mitcheson JS (1997). Ion channel and exchange currents in single myocytes isolated from the rabbit atrioventricular node. *Can J Cardiol* **13**, 1175–1182.
- Harakalova M et al. (2012). Dominant missense mutations in ABCC9 cause Cantú syndrome. *Nat Genet* **44**, 793–796.
- Harvey RD & Belevych AE (2003). Muscarinic regulation of cardiac ion channels. *Br J Pharmacol* **139**, 1074–1084.
- Heijman J, Voigt N, Nattel S & Dobrev D (2014). Cellular and molecular electrophysiology of atrial fibrillation initiation, maintenance, and progression. *Circ Res* **114**, 1483–1499.
- Herron TJ, Lee P & Jalife J (2012). Optical imaging of voltage and calcium in cardiac cells & tissues. *Circ Res* **110**, 609–623.

- Hibino H, Inanobe A, Furutani K, Murakami S, Findlay I & Kurachi Y (2010). Inwardly rectifying potassium channels: their structure, function, and physiological roles. *Physiol Rev* **90**, 291–366.
- Hirano Y, Fozzard HA & January CT (1989). Characteristics of L- and T-type Ca²⁺ currents in canine cardiac Purkinje cells. *Am J Physiol* **256**, H1478–H1492.
- Ho SY, Cabrera JA, Tran VH, Farré J, Anderson RH & Sánchez-Quintana D (2001). Architecture of the pulmonary veins: relevance to radiofrequency ablation. *Heart* **86**, 265–270.
- Hobbs WJ, Van Gelder IC, Fitzpatrick AP, Crijns HJ & Garratt CJ (1999). The role of atrial electrical remodeling in the progression of focal atrial ectopy to persistent atrial fibrillation. *J Cardiovasc Electrophysiol* **10**, 866–870.
- Hodgkin AL & Huxley AF (1952). A quantitative description of membrane current and its application to conduction and excitation in nerve. *J Physiol (Lond)* **117**, 500–544.
- Honarbaksh S, Schilling RJ, Orini M, Providencia R, Keating E, Finlay M, Sporton S, Chow A, Earley MJ, Lambiase PD & Hunter RJ (2018). Structural remodeling and conduction velocity dynamics in the human left atrium: Relationship with reentrant mechanisms sustaining atrial fibrillation. *Heart Rhythm*; DOI: 10.1016/j.hrthm.2018.07.019.
- Hong M, Bao L, Kefaloyianni E, Agullo-Pascual E, Chkourko H, Foster M, Taskin E, Zhandre M, Reid DA, Rothenberg E, Delmar M & Coetzee WA (2012). Heterogeneity of ATP-sensitive K⁺ channels in cardiac myocytes: enrichment at the intercalated disk. *J Biol Chem* **287**, 41258–41267.
- Hopkins WF, Fatherazi S, Peter-Riesch B, Corkey BE & Cook DL (1992). Two sites for adenine-nucleotide regulation of ATP-sensitive potassium channels in mouse pancreatic beta-cells and HIT cells. *J Membrane Biol* **129**, 287–295.
- Hoppe UC, Jansen E, Südkamp M & Beuckelmann DJ (1998). Hyperpolarization-activated inward current in ventricular myocytes from normal and failing human hearts. *Circulation* **97**, 55–65.
- Hu D et al. (2014). ABCC9 is a novel Brugada and early repolarization syndrome susceptibility gene. *Int J Cardiol* **171**, 431–442.
- Hu X, Xu X, Huang Y, Fassett J, Flagg TP, Zhang Y, Nichols CG, Bache RJ & Chen Y (2008). Disruption of sarcolemmal ATP-sensitive potassium channel activity impairs the cardiac response to systolic overload. *Circ Res* **103**, 1009–1017.
- Huopio H, Reimann F, Ashfield R, Komulainen J, Lenko HL, Rahier J, Vauhkonen I, Kere J, Laakso M, Ashcroft F & Otonkoski T (2000). Dominantly inherited hyperinsulinism caused by a mutation in the sulfonylurea receptor type 1. *J Clin Invest* **106**, 897–906.

- Imanishi S, Arita M, Aomine M & Kiyosue T (1984). Antiarrhythmic effects of nicorandil on canine cardiac Purkinje fibers. *J Cardiovasc Pharmacol* **6**, 772–779.
- Inagaki N, Gono T & Seino S (1997). Subunit stoichiometry of the pancreatic beta-cell ATP-sensitive K⁺ channel. *FEBS Lett* **409**, 232–236.
- Inagaki N, Gono T, Clement JP, Namba N, Inazawa J, Gonzalez G, Aguilar-Bryan L, Seino S & Bryan J (1995a). Reconstitution of IKATP: an inward rectifier subunit plus the sulfonylurea receptor. *Science* **270**, 1166–1170.
- Inagaki N, Gono T, Clement JP, Wang CZ, Aguilar-Bryan L, Bryan J & Seino S (1996). A family of sulfonylurea receptors determines the pharmacological properties of ATP-sensitive K⁺ channels. *Neuron* **16**, 1011–1017.
- Inagaki N, Inazawa J & Seino S (1995b). cDNA sequence, gene structure, and chromosomal localization of the human ATP-sensitive potassium channel, uKATP-1, gene (KCNJ8). *Genomics* **30**, 102–104.
- IONA Study Group (2002). Effect of nicorandil on coronary events in patients with stable angina: the Impact Of Nicorandil in Angina (IONA) randomised trial. *Lancet* **359**, 1269–1275.
- Isidoro Tavares N, Philip-Couderc P, Papageorgiou I, Baertschi AJ, Lerch R & Montessuit C (2007). Expression and function of ATP-dependent potassium channels in late post-infarction remodeling. *J Mol Cell Cardiol* **42**, 1016–1025.
- Isomoto S, Kondo C, Yamada M, Matsumoto S, Higashiguchi O, Horio Y, Matsuzawa Y & Kurachi Y (1996). A novel sulfonylurea receptor forms with BIR (Kir6.2) a smooth muscle type ATP-sensitive K⁺ channel. *J Biol Chem* **271**, 24321–24324.
- Jackman CP, Shadrin IY, Carlson AL & Bursac N (2015). Human Cardiac Tissue Engineering: From Pluripotent Stem Cells to Heart Repair. *Curr Opin Chem Eng* **7**, 57–64.
- Jahangir A, Terzic A & Kurachi Y (1994). Intracellular acidification and ADP enhance nicorandil induction of ATP sensitive potassium channel current in cardiomyocytes. *Cardiovasc Res* **28**, 831–835.
- Jaimes R, Walton RD, Pasdois P, Bernus O, Efimov IR & Kay MW (2016). A technical review of optical mapping of intracellular calcium within myocardial tissue. *Am J Physiol Heart Circ Physiol* **310**, H1388–H1401.
- Jaïs P, Cauchemez B, Macle L, Daoud E, Khairy P, Subbiah R, Hocini M, Extramiana F, Sacher F, Bordachar P, Klein G, Weerasooriya R, Clémenty J & Haïssaguerre M (2008). Catheter ablation versus antiarrhythmic drugs for atrial fibrillation: the A4 study. *Circulation* **118**, 2498–2505.
- Janse MJ, Coronel R, Opthof T, Sosunov EA, Anyukhovskiy EP & Rosen MR (2012). Repolarization gradients in the intact heart: transmural or apico-basal? *Prog Biophys Mol Biol* **109**, 6–15.

- John SA, Weiss JN, Xie L-H & Ribalet B (2003). Molecular mechanism for ATP-dependent closure of the K⁺ channel Kir6.2. *J Physiol (Lond)* **552**, 23–34.
- Jovanović A, Jovanović S, Lorenz E & Terzic A (1998). Recombinant cardiac ATP-sensitive K⁺ channel subunits confer resistance to chemical hypoxia-reoxygenation injury. *Circulation* **98**, 1548–1555.
- Jovanović N, Jovanović S, Jovanović A & Terzic A (1999). Gene delivery of Kir6.2/SUR2A in conjunction with pinacidil handles intracellular Ca²⁺ homeostasis under metabolic stress. *FASEB J* **13**, 923–929.
- Joyner RW & van Capelle FJ (1986). Propagation through electrically coupled cells. How a small SA node drives a large atrium. *Biophys J* **50**, 1157–1164.
- Ju YK, Saint DA & Gage PW (1996). Hypoxia increases persistent sodium current in rat ventricular myocytes. *J Physiol (Lond)* **497 (Pt 2)**, 337–347.
- Kaese S & Verheule S (2012). Cardiac electrophysiology in mice: a matter of size. *Front Physiol* **3**, 345.
- Takei M & Noma A (1984). Adenosine-5'-triphosphate-sensitive single potassium channel in the atrioventricular node cell of the rabbit heart. *J Physiol (Lond)* **352**, 265–284.
- Kane GC, Behfar A, Dyer RB, O'Coilain DF, Liu X-K, Hodgson DM, Reyes S, Miki T, Seino S & Terzic A (2006). KCNJ11 gene knockout of the Kir6.2 KATP channel causes maladaptive remodeling and heart failure in hypertension. *Hum Mol Genet* **15**, 2285–2297.
- Kanno S & Saffitz JE (2001). The role of myocardial gap junctions in electrical conduction and arrhythmogenesis. *Cardiovasc Pathol* **10**, 169–177.
- Kantor PF, Coetzee WA, Carmeliet EE, Dennis SC & Opie LH (1990). Reduction of ischemic K⁺ loss and arrhythmias in rat hearts. Effect of glibenclamide, a sulfonylurea. *Circ Res* **66**, 478–485.
- Kapoor RR, Flanagan SE, James CT, McKiernan J, Thomas AM, Harmer SC, Shield JP, Tinker A, Ellard S & Hussain K (2011). Hyperinsulinaemic hypoglycaemia and diabetes mellitus due to dominant ABCC8/KCNJ11 mutations. *Diabetologia* **54**, 2575–2583.
- Kawase A, Ikeda T, Nakazawa K, Ashihara T, Namba T, Kubota T, Sugi K & Hirai H (2003). Widening of the excitable gap and enlargement of the core of reentry during atrial fibrillation with a pure sodium channel blocker in canine atria. *Circulation* **107**, 905–910.
- Kim S-J, Zhang H, Khaliulin I, Choisy SCM, Bond R, Lin H, Haou El S, Milnes JT, Hancox JC, Suleiman MS & James AF (2012). Activation of glibenclamide-sensitive ATP-sensitive K⁺ channels during β -adrenergically induced metabolic stress produces a substrate for atrial tachyarrhythmia. *Circ Arrhythm Electrophysiol* **5**, 1184–1192.

- Kim YH, Garfinkel A, Ikeda T, Wu TJ, Athill CA, Weiss JN, Karagueuzian HS & Chen PS (1997). Spatiotemporal complexity of ventricular fibrillation revealed by tissue mass reduction in isolated swine right ventricle. Further evidence for the quasiperiodic route to chaos hypothesis. *J Clin Invest* **100**, 2486–2500.
- Kirchhof P et al. (2016). 2016 ESC Guidelines for the management of atrial fibrillation developed in collaboration with EACTS. *Eur Heart J* **37**, 2893–2962.
- Kleppisch T & Nelson MT (1995). Adenosine activates ATP-sensitive potassium channels in arterial myocytes via A2 receptors and cAMP-dependent protein kinase. *PNAS* **92**, 12441–12445.
- Kneller J, Zou R, Vigmond EJ, Wang Z, Leon LJ & Nattel S (2002). Cholinergic atrial fibrillation in a computer model of a two-dimensional sheet of canine atrial cells with realistic ionic properties. *Circ Res* **90**, E73–E87.
- Knollmann BC, Katchman AN & Franz MR (2001). Monophasic action potential recordings from intact mouse heart: validation, regional heterogeneity, and relation to refractoriness. *J Cardiovasc Electrophysiol* **12**, 1286–1294.
- Konarzewska H, Peeters GA & Sanguinetti MC (1995). Repolarizing K⁺ currents in nonfailing human hearts. Similarities between right septal subendocardial and left subepicardial ventricular myocytes. *Circulation* **92**, 1179–1187.
- Kondo C, Repunte VP, Satoh E, Yamada M, Horio Y, Matsuzawa Y, Pott L & Kurachi Y (1998). Chimeras of Kir6.1 and Kir6.2 reveal structural elements involved in spontaneous opening and unitary conductance of the ATP-sensitive K⁺ channels. *Recept Channels* **6**, 129–140.
- Kondo T, Kubota I, Tachibana H, Yamaki M & Tomoike H (1996). Glibenclamide attenuates peaked T wave in early phase of myocardial ischemia. *Cardiovasc Res* **31**, 683–687.
- Korchev YE, Negulyaev YA, Edwards CR, Vodyanoy I & Lab MJ (2000). Functional localization of single active ion channels on the surface of a living cell. *Nat Cell Biol* **2**, 616–619.
- Koschak A, Reimer D, Huber I, Grabner M, Glossmann H, Engel J & Striessnig J (2001). alpha 1D (Cav1.3) subunits can form I-type Ca²⁺ channels activating at negative voltages. *J Biol Chem* **276**, 22100–22106.
- Kovalev H, Quayle JM, Kamishima T & Lodwick D (2004). Molecular analysis of the subtype-selective inhibition of cloned KATP channels by PNU-37883A. *Br J Pharmacol* **141**, 867–873.
- Krummen DE, Bayer JD, Ho J, Ho G, Smetak MR, Clopton P, Trayanova NA & Narayan SM (2012). Mechanisms of human atrial fibrillation initiation: clinical and computational studies of repolarization restitution and activation latency. *Circ Arrhythm Electrophysiol* **5**, 1149–1159.

- Kubota I, Yamaki M, Shibata T, Ikeno E, Hosoya Y & Tomoike H (1993). Role of ATP-sensitive K⁺ channel on ECG ST segment elevation during a bout of myocardial ischemia. A study on epicardial mapping in dogs. *Circulation* **88**, 1845–1851.
- Kus T & Sasyniuk BI (1975). Electrophysiological actions of disopyramide phosphate on canine ventricular muscle and Purkinje fibers. *Circ Res* **37**, 844–854.
- Kusano KF (2013). Brugada syndrome: Recent understanding of pathophysiological mechanism and treatment. *Journal of Arrhythmia* **29**, 77–82.
- Kühlkamp V, Schirdewan A, Stangl K, Homberg M, Ploch M & Beck OA (2000). Use of metoprolol CR/XL to maintain sinus rhythm after conversion from persistent atrial fibrillation: a randomized, double-blind, placebo-controlled study. *J Am Coll Cardiol* **36**, 139–146.
- Lader JM, Vasquez C, Bao L, Maass K, Qu J, Kefalogianni E, Fishman GI, Coetzee WA & Morley GE (2011). Remodeling of atrial ATP-sensitive K⁺ channels in a model of salt-induced elevated blood pressure. *Am J Physiol Heart Circ Physiol* **301**, H964–H974.
- Lafuente-Lafuente C, Valembois L, Bergmann J-F & Belmin J (2015). Antiarrhythmics for maintaining sinus rhythm after cardioversion of atrial fibrillation. ed. Lafuente-Lafuente C. *Cochrane Database Syst Rev* **3**, CD005049.
- Lakatta EG & DiFrancesco D (2009). What keeps us ticking: a funny current, a calcium clock, or both? *J Mol Cell Cardiol* **47**, 157–170.
- Lalani GG, Schricker A, Gibson M, Rostamian A, Krummen DE & Narayan SM (2012). Atrial conduction slows immediately before the onset of human atrial fibrillation: a bi-atrial contact mapping study of transitions to atrial fibrillation. *J Am Coll Cardiol* **59**, 595–606.
- Lanson NA, Glembotski CC, Steinhilber ME, Field LJ & Claycomb WC (1992). Gene expression and atrial natriuretic factor processing and secretion in cultured AT-1 cardiac myocytes. *Circulation* **85**, 1835–1841.
- Lathrop DA, Nánási PP & Varro A (1990). In vitro cardiac models of dog Purkinje fibre triggered and spontaneous electrical activity: effects of nicorandil. *Br J Pharmacol* **99**, 119–123.
- Lathrop DA, Varro A & Schwartz A (1989). Rate-dependent electrophysiological effects of OPC-8212: comparison to sotalol. *Eur J Pharmacol* **164**, 487–496.
- Lavie CJ, Pandey A, Lau DH, Alpert MA & Sanders P (2017). Obesity and Atrial Fibrillation Prevalence, Pathogenesis, and Prognosis: Effects of Weight Loss and Exercise. *J Am Coll Cardiol* **70**, 2022–2035.
- Lazzara R, El-Sherif N & Scherlag BJ (1975). Disorders of cellular electrophysiology produced by ischemia of the canine His bundle. *Circ Res* **36**, 444–454.

- Lederer WJ & Nichols CG (1989). Nucleotide modulation of the activity of rat heart ATP-sensitive K⁺ channels in isolated membrane patches. *J Physiol (Lond)* **419**, 193–211.
- Lederer WJ, Nichols CG & Smith GL (1989). The mechanism of early contractile failure of isolated rat ventricular myocytes subjected to complete metabolic inhibition. *J Physiol (Lond)* **413**, 329–349.
- Lee KPK, Chen J & MacKinnon R (2017). Molecular structure of human KATP in complex with ATP and ADP. *Elife*; DOI: 10.7554/eLife.32481.
- Lemoine MD, Krause T, Koivumäki JT, Prondzynski M, Schulze ML, Girdauskas E, Willems S, Hansen A, Eschenhagen T & Christ T (2018). Human Induced Pluripotent Stem Cell-Derived Engineered Heart Tissue as a Sensitive Test System for QT Prolongation and Arrhythmic Triggers. *Circ Arrhythm Electrophysiol* **11**, e006035.
- Leonard CE, Hennessy S, Han X, Siscovick DS, Flory JH & Deo R (2017). Pro- and Antiarrhythmic Actions of Sulfonylureas: Mechanistic and Clinical Evidence. *Trends Endocrinol Metab* **28**, 561–586.
- Lerman BB & Belardinelli L (1991). Cardiac electrophysiology of adenosine. Basic and clinical concepts. *Circulation* **83**, 1499–1509.
- Li D, Zhang L, Kneller J & Nattel S (2001). Potential ionic mechanism for repolarization differences between canine right and left atrium. *Circ Res* **88**, 1168–1175.
- Li L, Wang J & Drain P (2000a). The I182 region of k(ir)6.2 is closely associated with ligand binding in K(ATP) channel inhibition by ATP. *Biophys J* **79**, 841–852.
- Li N, Wu J-X, Ding D, Cheng J, Gao N & Chen L (2017). Structure of a Pancreatic ATP-Sensitive Potassium Channel. *Cell* **168**, 101–110.e110.
- Li RA, Leppo M, Miki T, Seino S & Marban E (2000b). Molecular basis of electrocardiographic ST-segment elevation. *Circ Res* **87**, 837–839.
- Light PE, Cordeiro JM & French RJ (1999). Identification and properties of ATP-sensitive potassium channels in myocytes from rabbit Purkinje fibres. *Cardiovasc Res* **44**, 356–369.
- Lim B, Hwang M, Song J-S, Ryu A-J, Joung B, Shim EB, Ryu H & Pak H-N (2017). Effectiveness of atrial fibrillation rotor ablation is dependent on conduction velocity: An in-silico 3-dimensional modeling study. *PLoS ONE* **12**, e0190398.
- Lip GYH & Tse H-F (2007). Management of atrial fibrillation. *Lancet* **370**, 604–618.
- Liu DW, Gintant GA & Antzelevitch C (1993). Ionic bases for electrophysiological distinctions among epicardial, midmyocardial, and endocardial myocytes from the free wall of the canine left ventricle. *Circ Res* **72**, 671–687.

- Liu X-K, Yamada S, Kane GC, Alekseev AE, Hodgson DM, O'Coilain F, Jahangir A, Miki T, Seino S & Terzic A (2004). Genetic disruption of Kir6.2, the pore-forming subunit of ATP-sensitive K⁺ channel, predisposes to catecholamine-induced ventricular dysrhythmia. *Diabetes* **53 Suppl 3**, S165–S168.
- Livak KJ & Schmittgen TD (2001). Analysis of relative gene expression data using real-time quantitative PCR and the 2(-Delta Delta C(T)) Method. *Methods* **25**, 402–408.
- Lu HR, Vlamincx E, Hermans AN, Rohrbacher J, Van Ammel K, Towart R, Pugsley M & Gallacher DJ (2008). Predicting drug-induced changes in QT interval and arrhythmias: QT-shortening drugs point to gaps in the ICHS7B Guidelines. *Br J Pharmacol* **154**, 1427–1438.
- Lympelopoulou A, Rengo G & Koch WJ (2013). Adrenergic nervous system in heart failure: pathophysiology and therapy. *Circ Res* **113**, 739–753.
- Maier LS & Sossalla S (2013). The late Na current as a therapeutic target: where are we? *J Mol Cell Cardiol* **61**, 44–50.
- Mangold KE, Brumback BD, Angsutararux P, Voelker TL, Zhu W, Kang PW, Moreno JD & Silva JR (2017). Mechanisms and models of cardiac sodium channel inactivation. *Channels (Austin)* **11**, 517–533.
- Mangoni ME, Couette B, Bourinet E, Platzer J, Reimer D, Striessnig J & Nargeot J (2003). Functional role of L-type Cav1.3 Ca²⁺ channels in cardiac pacemaker activity. *PNAS* **100**, 5543–5548.
- Manning Fox JE, Kanji HD, French RJ & Light PE (2002). Cardioselectivity of the sulphonylurea HMR 1098: studies on native and recombinant cardiac and pancreatic K(ATP) channels. *Br J Pharmacol* **135**, 480–488.
- Marott SCW, Nielsen SF, Benn M & Nordestgaard BG (2014). Antihypertensive treatment and risk of atrial fibrillation: a nationwide study. *Eur Heart J* **35**, 1205–1214.
- Marrouche NF, Brachmann J, Andresen D, Siebels J, Boersma L, Jordaens L, Merkely B, Pokushalov E, Sanders P, Proff J, Schunkert H, Christ H, Vogt J, Bänsch DCastle-AF Investigators (2018). Catheter Ablation for Atrial Fibrillation with Heart Failure. *N Engl J Med* **378**, 417–427.
- Marthinet E, Bloc A, Oka Y, Tanizawa Y, Wehrle-Haller B, Bancila V, Dubuis J-M, Philippe J & Schwitzgebel VM (2005). Severe congenital hyperinsulinism caused by a mutation in the Kir6.2 subunit of the adenosine triphosphate-sensitive potassium channel impairing trafficking and function. *J Clin Endocrinol Metab* **90**, 5401–5406.
- Martin GM, Yoshioka C, Rex EA, Fay JF, Xie Q, Whorton MR, Chen JZ & Shyng S-L (2017). Cryo-EM structure of the ATP-sensitive potassium channel illuminates mechanisms of assembly and gating. *Elife*; DOI: 10.7554/eLife.24149.

- Matsuo M, Tanabe K, Kioka N, Amachi T & Ueda K (2000). Different binding properties and affinities for ATP and ADP among sulfonylurea receptor subtypes, SUR1, SUR2A, and SUR2B. *J Biol Chem* **275**, 28757–28763.
- Matsuoka T, Matsushita K, Katayama Y, Fujita A, Inageda K, Tanemoto M, Inanobe A, Yamashita S, Matsuzawa Y & Kurachi Y (2000). C-terminal tails of sulfonylurea receptors control ADP-induced activation and diazoxide modulation of ATP-sensitive K(+) channels. *Circ Res* **87**, 873–880.
- McNair A, Andreasen F & Nielsen PE (1983). Antihypertensive effect of diazoxide given intravenously in small repeated doses. *Eur J Clin Pharmacol* **24**, 151–156.
- McPherson CD, Pierce GN & Cole WC (1993). Ischemic cardioprotection by ATP-sensitive K⁺ channels involves high-energy phosphate preservation. *Am J Physiol* **265**, H1809–H1818.
- Medeiros-Domingo A, Tan B-H, Crotti L, Tester DJ, Eckhardt L, Cuoretti A, Kroboth SL, Song C, Zhou Q, Kopp D, Schwartz PJ, Makielski JC & Ackerman MJ (2010). Gain-of-function mutation S422L in the KCNJ8-encoded cardiac K(ATP) channel Kir6.1 as a pathogenic substrate for J-wave syndromes. *Heart Rhythm* **7**, 1466–1471.
- Melamed-Frank M, Terzic A, Carrasco AJ, Nevo E, Avivi A & Levy AP (2001). Reciprocal regulation of expression of pore-forming KATP channel genes by hypoxia. *Mol Cell Biochem* **225**, 145–150.
- Melgari D, Zhang Y, Harchi El A, Dempsey CE & Hancox JC (2015). Molecular basis of hERG potassium channel blockade by the class Ic antiarrhythmic flecainide. *J Mol Cell Cardiol* **86**, 42–53.
- Mesirca P, Torrente AG & Mangoni ME (2015). Functional role of voltage gated Ca(2+) channels in heart automaticity. *Front Physiol* **6**, 19.
- Mikhailov MV, Mikhailova EA & Ashcroft SJ (2001). Molecular structure of the glibenclamide binding site of the beta-cell K(ATP) channel. *FEBS Lett* **499**, 154–160.
- Miki T, Suzuki M, Shibasaki T, Uemura H, Sato T, Yamaguchi K, Koseki H, Iwanaga T, Nakaya H & Seino S (2002). Mouse model of Prinzmetal angina by disruption of the inward rectifier Kir6.1. *Nat Med* **8**, 466–472.
- Millar CK, Kralios FA & Lux RL (1985). Correlation between refractory periods and activation-recovery intervals from electrograms: effects of rate and adrenergic interventions. *Circulation* **72**, 1372–1379.
- Moe GK, Rheinboldt WC & Abildskov JA (1964). A computer model of atrial fibrillation. *Am Heart J* **67**, 200–220.
- Molina CE, Heijman J & Dobrev D (2016). Differences in Left Versus Right Ventricular Electrophysiological Properties in Cardiac Dysfunction and Arrhythmogenesis. *Arrhythm Electrophysiol Rev* **5**, 14–19.

- Molleman A (2003). *Patch Clamping: An Introductory Guide to Patch Clamp Electrophysiology*. Wiley.
- Moreau C, Gally F, Jacquet-Bouix H & Vivaudou M (2005a). The size of a single residue of the sulfonyleurea receptor dictates the effectiveness of K ATP channel openers. *Mol Pharmacol* **67**, 1026–1033.
- Moreau C, Jacquet H, Prost AL, D'hahan N & Vivaudou M (2000). The molecular basis of the specificity of action of K(ATP) channel openers. *EMBO J* **19**, 6644–6651.
- Moreau C, Prost A-L, Dérand R & Vivaudou M (2005b). SUR, ABC proteins targeted by KATP channel openers. *J Mol Cell Cardiol* **38**, 951–963.
- Mueller-Hoecker J, Beitinger F, Fernandez B, Bahlmann O, Assmann G, Troidl C, Dimomeletis I, Käab S & Deindl E (2008). Of rodents and humans: a light microscopic and ultrastructural study on cardiomyocytes in pulmonary veins. *Int J Med Sci* **5**, 152–158.
- Munk AA, Adjemian RA, Zhao J, Ogbaghebriel A & Shrier A (1996). Electrophysiological properties of morphologically distinct cells isolated from the rabbit atrioventricular node. *J Physiol (Lond)* **493 (Pt 3)**, 801–818.
- Murry CE, Jennings RB & Reimer KA (1986). Preconditioning with ischemia: a delay of lethal cell injury in ischemic myocardium. *Circulation* **74**, 1124–1136.
- Nakayama H, Bodi I, Maillet M, DeSantiago J, Domeier TL, Mikoshiba K, Lorenz JN, Blatter LA, Bers DM & Molkentin JD (2010). The IP3 receptor regulates cardiac hypertrophy in response to select stimuli. *Circ Res* **107**, 659–666.
- Narayan SM, Baykaner T, Clopton P, Schricker A, Lalani GG, Krummen DE, Shivkumar K & Miller JM (2014). Ablation of rotor and focal sources reduces late recurrence of atrial fibrillation compared with trigger ablation alone: extended follow-up of the CONFIRM trial (Conventional Ablation for Atrial Fibrillation With or Without Focal Impulse and Rotor Modulation). *J Am Coll Cardiol* **63**, 1761–1768.
- Narayan SM, Kazi D, Krummen DE & Rappel W-J (2008). Repolarization and activation restitution near human pulmonary veins and atrial fibrillation initiation: a mechanism for the initiation of atrial fibrillation by premature beats. *J Am Coll Cardiol* **52**, 1222–1230.
- Narayan SM, Krummen DE, Shivkumar K, Clopton P, Rappel W-J & Miller JM (2012). Treatment of atrial fibrillation by the ablation of localized sources: CONFIRM (Conventional Ablation for Atrial Fibrillation With or Without Focal Impulse and Rotor Modulation) trial. *J Am Coll Cardiol* **60**, 628–636.
- Nattel S (2002). New ideas about atrial fibrillation 50 years on. *Nature* **415**, 219–226.
- Nattel S (2003). Basic electrophysiology of the pulmonary veins and their role in atrial fibrillation: precipitators, perpetuators, and perplexers. *J Cardiovasc Electrophysiol* **14**, 1372–1375.

- Neagoe I & Schwappach B (2005). Pas de deux in groups of four--the biogenesis of KATP channels. *J Mol Cell Cardiol* **38**, 887–894.
- Nerbonne JM (2004). Studying cardiac arrhythmias in the mouse--a reasonable model for probing mechanisms? *Trends Cardiovasc Med* **14**, 83–93.
- Nerbonne JM & Guo W (2002). Heterogeneous expression of voltage-gated potassium channels in the heart: roles in normal excitation and arrhythmias. *J Cardiovasc Electrophysiol* **13**, 406–409.
- Nerbonne JM & Kass RS (2005). Molecular physiology of cardiac repolarization. *Physiol Rev* **85**, 1205–1253.
- Nessa A, Rahman SA & Hussain K (2016). Hyperinsulinemic Hypoglycemia - The Molecular Mechanisms. *Front Endocrinol (Lausanne)* **7**, 29.
- Nestorowicz A, Inagaki N, Gono T, Schoor KP, Wilson BA, Glaser B, Landau H, Stanley CA, Thornton PS, Seino S & Permutt MA (1997). A nonsense mutation in the inward rectifier potassium channel gene, Kir6.2, is associated with familial hyperinsulinism. *Diabetes* **46**, 1743–1748.
- Nguyen TP, Qu Z & Weiss JN (2014). Cardiac fibrosis and arrhythmogenesis: the road to repair is paved with perils. *J Mol Cell Cardiol* **70**, 83–91.
- Nichols CG, Ripoll C & Lederer WJ (1991). ATP-sensitive potassium channel modulation of the guinea pig ventricular action potential and contraction. *Circ Res* **68**, 280–287.
- Niwa N & Nerbonne JM (2010). Molecular determinants of cardiac transient outward potassium current (I_{to}) expression and regulation. *J Mol Cell Cardiol* **48**, 12–25.
- Noma A (1983). ATP-regulated K⁺ channels in cardiac muscle. *Nature* **305**, 147–148.
- O'Hara T, Virág L, Varró A & Rudy Y (2011). Simulation of the undiseased human cardiac ventricular action potential: model formulation and experimental validation. *PLoS Comput Biol* **7**, e1002061.
- Ohrnberger CE, Khan SA & Meisheri KD (1993). Synergistic effects of glyburide and U-37883A, two structurally different vascular ATP-sensitive potassium channel antagonists. *J Pharmacol Exp Ther* **267**, 25–30.
- Olson TM, Alekseev AE, Moreau C, Liu XK, Zingman LV, Miki T, Seino S, Asirvatham SJ, Jahangir A & Terzic A (2007). KATP channel mutation confers risk for vein of Marshall adrenergic atrial fibrillation. *Nat Clin Pract Cardiovasc Med* **4**, 110–116.
- Opel A, Nobles M, Montaigne D, Finlay M, Anderson N, Breckenridge R & Tinker A (2015). Absence of the Regulator of G-protein Signaling, RGS4, Predisposes to Atrial Fibrillation and Is Associated with Abnormal Calcium Handling. *J Biol Chem* **290**, 19233–19244.

- Opthof T, Coronel R & Janse MJ (2009). Is there a significant transmural gradient in repolarization time in the intact heart?: Repolarization Gradients in the Intact Heart. *Circ Arrhythm Electrophysiol* **2**, 89–96.
- Osadchii OE (2017). Effects of Na⁺ channel blockers on the restitution of refractory period, conduction time, and excitation wavelength in perfused guinea-pig heart. *PLoS ONE* **12**, e0172683.
- Otonkoski T, Ammälä C, Huopio H, Cote GJ, Chapman J, Cosgrove K, Ashfield R, Huang E, Komulainen J, Ashcroft FM, Dunne MJ, Kere J & Thomas PM (1999). A point mutation inactivating the sulfonylurea receptor causes the severe form of persistent hyperinsulinemic hypoglycemia of infancy in Finland. *Diabetes* **48**, 408–415.
- Pandit SV & Jalife J (2013). Rotors and the dynamics of cardiac fibrillation. *Circ Res* **112**, 849–862.
- Park DS & Fishman GI (2011). The cardiac conduction system. *Circulation* **123**, 904–915.
- Pathak RK, Middeldorp ME, Lau DH, Mehta AB, Mahajan R, Twomey D, Alasady M, Hanley L, Antic NA, McEvoy RD, Kalman JM, Abhayaratna WP & Sanders P (2014). Aggressive risk factor reduction study for atrial fibrillation and implications for the outcome of ablation: the ARREST-AF cohort study. *J Am Coll Cardiol* **64**, 2222–2231.
- Pathak RK, Middeldorp ME, Meredith M, Mehta AB, Mahajan R, Wong CX, Twomey D, Elliott AD, Kalman JM, Abhayaratna WP, Lau DH & Sanders P (2015). Long-Term Effect of Goal-Directed Weight Management in an Atrial Fibrillation Cohort: A Long-Term Follow-Up Study (LEGACY). *J Am Coll Cardiol* **65**, 2159–2169.
- Pelzmann B, Schaffer P, Bernhart E, Lang P, Mächler H, Rigler B & Koidl B (2001). Effects of K⁺ channel openers on I_{K(ATP)} of human atrial myocytes at physiological temperatures. *Naunyn-Schmied Arch Pharmacol* **363**, 125–132.
- Perez-Reyes E (2003). Molecular physiology of low-voltage-activated t-type calcium channels. *Physiol Rev* **83**, 117–161.
- Philip-Couderc P, Tavares NI, Roatti A, Lerch R, Montessuit C & Baertschi AJ (2008). Forkhead transcription factors coordinate expression of myocardial KATP channel subunits and energy metabolism. *Circ Res* **102**, e20–e35.
- Pinto AR, Ilinykh A, Ivey MJ, Kuwabara JT, D'Antoni ML, Debuque R, Chandran A, Wang L, Arora K, Rosenthal NA & Tallquist MD (2016). Revisiting Cardiac Cellular Composition. *Circ Res* **118**, 400–409.
- Po SS, Li Y, Tang D, Liu H, Geng N, Jackman WM, Scherlag B, Lazzara R & Patterson E (2005). Rapid and stable re-entry within the pulmonary vein as a mechanism initiating paroxysmal atrial fibrillation. *J Am Coll Cardiol* **45**, 1871–1877.

- Podd SJ, Freemantle N, Furniss SS & Sulke N (2016). First clinical trial of specific IKACH blocker shows no reduction in atrial fibrillation burden in patients with paroxysmal atrial fibrillation: pacemaker assessment of BMS 914392 in patients with paroxysmal atrial fibrillation. *Europace* **18**, 340–346.
- Poitry S, van Bever L, Coppex F, Roatti A & Baertschi AJ (2003). Differential sensitivity of atrial and ventricular K(ATP) channels to metabolic inhibition. *Cardiovasc Res* **57**, 468–476.
- Polontchouk L, Haefliger JA, Ebelt B, Schaefer T, Stuhlmann D, Mehlhorn U, Kuhn-Regnier F, De Vivie ER & Dhein S (2001). Effects of chronic atrial fibrillation on gap junction distribution in human and rat atria. *J Am Coll Cardiol* **38**, 883–891.
- Porciatti F, Pelzmann B, Cerbai E, Schaffer P, Pino R, Bernhart E, Koidl B & Mugelli A (1997). The pacemaker current I(f) in single human atrial myocytes and the effect of beta-adrenoceptor and A1-adenosine receptor stimulation. *Br J Pharmacol* **122**, 963–969.
- Potse M, Coronel R, Opthof T & Vinet A (2007). The positive T wave. *Anadolu Kardiyol Derg* **7 Suppl 1**, 164–167.
- Potse M, Vinet A, Opthof T & Coronel R (2009). Validation of a simple model for the morphology of the T wave in unipolar electrograms. *Am J Physiol Heart Circ Physiol* **297**, H792–H801.
- Pountney DJ, Sun ZQ, Porter LM, Nitabach MN, Nakamura TY, Holmes D, Rosner E, Kaneko M, Manaris T, Holmes TC & Coetzee WA (2001). Is the molecular composition of K(ATP) channels more complex than originally thought? *J Mol Cell Cardiol* **33**, 1541–1546.
- Priori SG & Corr PB (1990). Mechanisms underlying early and delayed afterdepolarizations induced by catecholamines. *Am J Physiol* **258**, H1796–H1805.
- Proietti R, Santangeli P, Di Biase L, Jozá J, Bernier ML, Wang Y, Sagone A, Viecca M, Essebag V & Natale A (2014). Comparative effectiveness of wide antral versus ostial pulmonary vein isolation: a systematic review and meta-analysis. *Circ Arrhythm Electrophysiol* **7**, 39–45.
- Qiagen (2010). *RNeasy® Fibrous Tissue Handbook*. Qiagen.
- Qiagen (2012). *Plasmid Purification Handbook*. Qiagen.
- Qu Z, Weiss JN & Garfinkel A (1999). Cardiac electrical restitution properties and stability of reentrant spiral waves: a simulation study. *Am J Physiol* **276**, H269–H283.
- Quintanilla JG, Moreno J, Archondo T, Chin A, Pérez-Castellano N, Usandizaga E, García-Torrent MJ, Molina-Morúa R, González P, Rodríguez-Bobada C, Macaya C & Perez-Villacastin J (2013). KATP channel opening accelerates and stabilizes rotors in a swine heart model of ventricular fibrillation. *Cardiovasc Res* **99**, 576–585.

- Qvigstad E, Kollind M & Grill V (2004). Nine weeks of bedtime diazoxide is well tolerated and improves beta-cell function in subjects with Type 2 diabetes. *Diabet Med* **21**, 73–76.
- Radtke MA, Neramoen I, Kollind M, Skeie S, Sørheim JI, Svartberg J, Hals I, Moen T, Dørflinger GH & Grill V (2010). Six months of diazoxide treatment at bedtime in newly diagnosed subjects with type 1 diabetes does not influence parameters of {beta}-cell function and autoimmunity but improves glycemic control. *Diabetes Care* **33**, 589–594.
- Raeis V, Philip-Couderc P, Roatti A, Habre W, Sierra J, Kalangos A, Beghetti M & Baertschi AJ (2010). Central venous hypoxemia is a determinant of human atrial ATP-sensitive potassium channel expression: evidence for a novel hypoxia-inducible factor 1alpha-Forkhead box class O signaling pathway. *Hypertension* **55**, 1186–1192.
- Ramanathan C, Jia P, Ghanem R, Ryu K & Rudy Y (2006). Activation and repolarization of the normal human heart under complete physiological conditions. *PNAS* **103**, 6309–6314.
- Ravens U & Odening KE (2016). Atrial fibrillation: Therapeutic potential of atrial K(+) channel blockers. *Pharmacol Ther* **176**, 13–21.
- Ravens U & Wettwer E (2011). Ultra-rapid delayed rectifier channels: molecular basis and therapeutic implications. *Cardiovasc Res* **89**, 776–785.
- Reiffel JA, Camm AJ, Belardinelli L, Zeng D, Karwatowska-Prokopczuk E, Olmsted A, Zareba W, Rosero S, Kowey PHARMONY Investigators (2015). The HARMONY Trial: Combined Ranolazine and Dronedarone in the Management of Paroxysmal Atrial Fibrillation: Mechanistic and Therapeutic Synergism. *Circ Arrhythm Electrophysiol* **8**, 1048–1056.
- Reimann F, Ashcroft FM & Gribble FM (2001). Structural basis for the interference between nicorandil and sulfonylurea action. *Diabetes* **50**, 2253–2259.
- Reimann F, Dabrowski M, Jones P, Gribble FM & Ashcroft FM (2003). Analysis of the differential modulation of sulphonylurea block of beta-cell and cardiac ATP-sensitive K⁺ (K(ATP)) channels by Mg-nucleotides. *J Physiol (Lond)* **547**, 159–168.
- Reimann F, Tucker SJ, Proks P & Ashcroft FM (1999). Involvement of the n-terminus of Kir6.2 in coupling to the sulphonylurea receptor. *J Physiol (Lond)* **518 (Pt 2)**, 325–336.
- Rensma PL, Allessie MA, Lammers WJEP, Bonke FIM & Schalij MJ (1988). Length of excitation wave and susceptibility to reentrant atrial arrhythmias in normal conscious dogs. *Circ Res* **62**, 395–410.
- Reyes S, Park S, Johnson BD, Terzic A & Olson TM (2009). KATP channel Kir6.2 E23K variant overrepresented in human heart failure is associated with impaired exercise stress response. *Hum Genet* **126**, 779–789.

- Reyes S, Terzic A, Mahoney DW, Redfield MM, Rodeheffer RJ & Olson TM (2008). K(ATP) channel polymorphism is associated with left ventricular size in hypertensive individuals: a large-scale community-based study. *Hum Genet* **123**, 665–667.
- Ribalet B, John SA & Weiss JN (2003). Molecular basis for Kir6.2 channel inhibition by adenine nucleotides. *Biophys J* **84**, 266–276.
- Ribalet B, John SA, Xie L-H & Weiss JN (2006). ATP-sensitive K⁺ channels: regulation of bursting by the sulphonylurea receptor, PIP₂ and regions of Kir6.2. *J Physiol (Lond)* **571**, 303–317.
- Riley G, Syeda F, Kirchhof P & Fabritz L (2012). An introduction to murine models of atrial fibrillation. *Front Physiol* **3**, 296.
- Rohr S (2004). Role of gap junctions in the propagation of the cardiac action potential. *Cardiovasc Res* **62**, 309–322.
- Rohr S (2012). Arrhythmogenic implications of fibroblast-myocyte interactions. *Circ Arrhythm Electrophysiol* **5**, 442–452.
- Rook MB, Evers MM, Vos MA & Bierhuizen MFA (2012). Biology of cardiac sodium channel Nav1.5 expression. *Cardiovasc Res* **93**, 12–23.
- Russ U, Lange U, Löffler-Walz C, Hambrock A & Quast U (2001). Interaction of the sulfonylthiourea HMR 1833 with sulfonylurea receptors and recombinant ATP-sensitive K(+) channels: comparison with glibenclamide. *J Pharmacol Exp Ther* **299**, 1049–1055.
- Saegusa N, Sato T, Saito T, Tamagawa M, Komuro I & Nakaya H (2005). Kir6.2-deficient mice are susceptible to stimulated ANP secretion: K(ATP) channel acts as a negative feedback mechanism? *Cardiovasc Res* **67**, 60–68.
- Saint DA, Ju YK & Gage PW (1992). A persistent sodium current in rat ventricular myocytes. *J Physiol (Lond)* **453**, 219–231.
- Saito T, Waki K & Becker AE (2000). Left atrial myocardial extension onto pulmonary veins in humans: anatomic observations relevant for atrial arrhythmias. *J Cardiovasc Electrophysiol* **11**, 888–894.
- Sakakibara Y, Wasserstrom JA, Furukawa T, Jia H, Arentzen CE, Hartz RS & Singer DH (1992). Characterization of the sodium current in single human atrial myocytes. *Circ Res* **71**, 535–546.
- Sakmann BF, Spindler AJ, Bryant SM, Linz KW & Noble D (2000). Distribution of a persistent sodium current across the ventricular wall in guinea pigs. *Circ Res* **87**, 910–914.
- Salameh A & Dhein S (2011). Adrenergic control of cardiac gap junction function and expression. *Naunyn-Schmied Arch Pharmacol* **383**, 331–346.
- Salazar NC, Chen J & Rockman HA (2007). Cardiac GPCRs: GPCR signaling in healthy and failing hearts. *Biochim Biophys Acta* **1768**, 1006–1018.

- Sarmast F, Kolli A, Zaitsev A, Parisian K, Dhamoon AS, Guha PK, Warren M, Anumonwo JMB, Taffet SM, Berenfeld O & Jalife J (2003). Cholinergic atrial fibrillation: I(K,ACh) gradients determine unequal left/right atrial frequencies and rotor dynamics. *Cardiovasc Res* **59**, 863–873.
- Sato T, Hata Y, Yamamoto M, Morita H, Mizuo K, Yamanari H, Saito D & Ohe T (1995). Early afterdepolarization abolished by potassium channel opener in a patient with idiopathic long QT syndrome. *J Cardiovasc Electrophysiol* **6**, 279–282.
- Satoh E, Yamada M, Kondo C, Repunte VP, Horio Y, Iijima T & Kurachi Y (1998). Intracellular nucleotide-mediated gating of SUR/Kir6.0 complex potassium channels expressed in a mammalian cell line and its modification by pinacidil. *J Physiol (Lond)* **511 (Pt 3)**, 663–674.
- Satoh H & Hashimoto K (1984). Effects of nicorandil on the membrane currents of rabbit sino-atrial node cells. *Jpn J Pharmacol* **34**, 411–415.
- Schotten U, Verheule S, Kirchhof P & Goette A (2011). Pathophysiological mechanisms of atrial fibrillation: a translational appraisal. *Physiol Rev* **91**, 265–325.
- Schram G, Pourrier M, Melnyk P & Nattel S (2002). Differential distribution of cardiac ion channel expression as a basis for regional specialization in electrical function. *Circ Res* **90**, 939–950.
- Schreuder T, Karreman M, Rennings A, Ruinemans-Koerts J, Jansen M & de Boer H (2005). Diazoxide-mediated insulin suppression in obese men: a dose-response study. *Diabetes Obes Metab* **7**, 239–245.
- Schwanstecher M, Sieverding C, Dörschner H, Gross I, Aguilar-Bryan L, Schwanstecher C & Bryan J (1998). Potassium channel openers require ATP to bind to and act through sulfonylurea receptors. *EMBO J* **17**, 5529–5535.
- Schwartz PJ, Crotti L & Insolia R (2012). Long-QT syndrome: from genetics to management. *Circ Arrhythm Electrophysiol* **5**, 868–877.
- Scirica BM, Morrow DA, Hod H, Murphy SA, Belardinelli L, Hedgepeth CM, Molhoek P, Verheugt FWA, Gersh BJ, McCabe CH & Braunwald E (2007). Effect of ranolazine, an antianginal agent with novel electrophysiological properties, on the incidence of arrhythmias in patients with non ST-segment elevation acute coronary syndrome: results from the Metabolic Efficiency With Ranolazine for Less Ischemia in Non ST-Elevation Acute Coronary Syndrome Thrombolysis in Myocardial Infarction 36 (MERLIN-TIMI 36) randomized controlled trial. *Circulation* **116**, 1647–1652.
- Selivanov VA, Alekseev AE, Hodgson DM, Dzeja PP & Terzic A (2004). Nucleotide-gated KATP channels integrated with creatine and adenylate kinases: amplification, tuning and sensing of energetic signals in the compartmentalized cellular environment. *Mol Cell Biochem* **256-257**, 243–256.

- Sharma N, Crane A, Clement JP, Gonzalez G, Babenko AP, Bryan J & Aguilar-Bryan L (1999). The C terminus of SUR1 is required for trafficking of KATP channels. *J Biol Chem* **274**, 20628–20632.
- Shimizu W & Antzelevitch C (2000). Effects of a K(+) channel opener to reduce transmural dispersion of repolarization and prevent torsade de pointes in LQT1, LQT2, and LQT3 models of the long-QT syndrome. *Circulation* **102**, 706–712.
- Shimoda LA & Polak J (2011). Hypoxia. 4. Hypoxia and ion channel function. *Am J Physiol Cell Physiol* **300**, C951–C967.
- Shyng S & Nichols CG (1997). Octameric stoichiometry of the KATP channel complex. *J Gen Physiol* **110**, 655–664.
- Shyng S, Ferrigni T & Nichols CG (1997). Regulation of KATP channel activity by diazoxide and MgADP. Distinct functions of the two nucleotide binding folds of the sulfonylurea receptor. *J Gen Physiol* **110**, 643–654.
- Shyng SL, Ferrigni T, Shepard JB, Nestorowicz A, Glaser B, Permutt MA & Nichols CG (1998). Functional analyses of novel mutations in the sulfonylurea receptor 1 associated with persistent hyperinsulinemic hypoglycemia of infancy. *Diabetes* **47**, 1145–1151.
- Simpson D & Wellington K (2004). Nicorandil: a review of its use in the management of stable angina pectoris, including high-risk patients. *Drugs* **64**, 1941–1955.
- Smith KJ, Chadburn AJ, Adomaviciene A, Minoretta P, Vignali L, Emanuele E & Tammaro P (2013). Coronary spasm and acute myocardial infarction due to a mutation (V734I) in the nucleotide binding domain 1 of ABCC9. *Int J Cardiol* **168**, 3506–3513.
- Smith PC, Karpowich N, Millen L, Moody JE, Rosen J, Thomas PJ & Hunt JF (2002). ATP binding to the motor domain from an ABC transporter drives formation of a nucleotide sandwich dimer. *Mol Cell* **10**, 139–149.
- Sola D, Rossi L, Schianca GPC, Maffioli P, Bigliocca M, Mella R, Corliano F, Fra GP, Bartoli E & Derosa G (2015). Sulfonylureas and their use in clinical practice. *Arch Med Sci* **11**, 840–848.
- Spinelli W, Sorota S, Siegal M & Hoffman BF (1991). Antiarrhythmic actions of the ATP-regulated K⁺ current activated by pinacidil. *Circ Res* **68**, 1127–1137.
- Steinberg JS, Shah Y, Bhatt A, Sichrovsky T, Arshad A, Hansinger E & Musat D (2017). Focal impulse and rotor modulation: Acute procedural observations and extended clinical follow-up. *Heart Rhythm* **14**, 192–197.
- Steinhilber ME, Lanson NA, Dresdner KP, Delcarpio JB, Wit AL, Claycomb WC & Field LJ (1990). Proliferation in vivo and in culture of differentiated adult atrial cardiomyocytes from transgenic mice. *Am J Physiol* **259**, H1826–H1834.

- Stevenson WG & Soejima K (2005). Recording techniques for clinical electrophysiology. *J Cardiovasc Electrophysiol* **16**, 1017–1022.
- Surah-Narwal S, Xu SZ, McHugh D, McDonald RL, Hough E, Cheong A, Partridge C, Sivaprasadarao A & Beech DJ (1999). Block of human aorta Kir6.1 by the vascular KATP channel inhibitor U37883A. *Br J Pharmacol* **128**, 667–672.
- Suzuki M, Li RA, Miki T, Uemura H, Sakamoto N, Ohmoto-Sekine Y, Tamagawa M, Ogura T, Seino S, Marban E & Nakaya H (2001). Functional roles of cardiac and vascular ATP-sensitive potassium channels clarified by Kir6.2-knockout mice. *Circ Res* **88**, 570–577.
- Suzuki M, Saito T, Sato T, Tamagawa M, Miki T, Seino S & Nakaya H (2003). Cardioprotective effect of diazoxide is mediated by activation of sarcolemmal but not mitochondrial ATP-sensitive potassium channels in mice. *Circulation* **107**, 682–685.
- Suzuki M, Sasaki N, Miki T, Sakamoto N, Ohmoto-Sekine Y, Tamagawa M, Seino S, Marbán E & Nakaya H (2002). Role of sarcolemmal K(ATP) channels in cardioprotection against ischemia/reperfusion injury in mice. *J Clin Invest* **109**, 509–516.
- Szentadrassy N, Banyasz T, Biro T, Szabo G, Toth BI, Magyar J, Lazar J, Varró A, Kovacs L & Nanasi PP (2005). Apico-basal inhomogeneity in distribution of ion channels in canine and human ventricular myocardium. *Cardiovasc Res* **65**, 851–860.
- Tamarro P, Proks P & Ashcroft FM (2006). Functional effects of naturally occurring KCNJ11 mutations causing neonatal diabetes on cloned cardiac KATP channels. *J Physiol (Lond)* **571**, 3–14.
- Taneja TK, Mankouri J, Karnik R, Kannan S, Smith AJ, Munsey T, Christesen HBT, Beech DJ & Sivaprasadarao A (2009). Sar1-GTPase-dependent ER exit of KATP channels revealed by a mutation causing congenital hyperinsulinism. *Hum Mol Genet* **18**, 2400–2413.
- Tang Q, Ma J, Zhang P, Wan W, Kong L & Wu L (2012). Persistent sodium current and Na⁺/H⁺ exchange contributes to the augmentation of the reverse Na⁺/Ca²⁺ exchange during hypoxia or acute ischemia in ventricular myocytes. *Pflugers Arch* **463**, 513–522.
- Teramoto N (2006a). Pharmacological Profile of U-37883A, a Channel Blocker of Smooth Muscle-Type ATP-Sensitive K Channels. *Cardiovasc Drug Rev* **24**, 25–32.
- Teramoto N (2006b). Physiological roles of ATP-sensitive K⁺ channels in smooth muscle. *J Physiol (Lond)* **572**, 617–624.
- Tester DJ, Tan B-H, Medeiros-Domingo A, Song C, Makielski JC & Ackerman MJ (2011). Loss-of-function mutations in the KCNJ8-encoded Kir6.1 K(ATP) channel and sudden infant death syndrome. *Circ Cardiovasc Genet* **4**, 510–515.

- Thomas P, Ye Y & Lightner E (1996). Mutation of the pancreatic islet inward rectifier Kir6.2 also leads to familial persistent hyperinsulinemic hypoglycemia of infancy. *Hum Mol Genet* **5**, 1809–1812.
- Tinker A & Harmer SC (2010). K⁺ channels in the heart: new insights and therapeutic implications. *Expert Rev Clin Pharmacol* **3**, 305–319.
- Tinker A, Aziz Q & Thomas A (2014). The role of ATP-sensitive potassium channels in cellular function and protection in the cardiovascular system. *Br J Pharmacol* **171**, 12–23.
- Tinker A, Finlay M, Nobles M & Opel A (2016). The contribution of pathways initiated via the Gq\11 G-protein family to atrial fibrillation. *Pharmacol Res* **105**, 54–61.
- Tiscornia G, Vivas EL & Izpisúa Belmonte JC (2011). Diseases in a dish: modeling human genetic disorders using induced pluripotent cells. *Nat Med* **17**, 1570–1576.
- Torrente AG, Mesirca P, Neco P, Rizzetto R, Dubel S, Barrere C, Sinegger-Brauns M, Striessnig J, Richard S, Nargeot J, Gomez AM & Mangoni ME (2016). L-type Cav1.3 channels regulate ryanodine receptor-dependent Ca²⁺ release during sino-atrial node pacemaker activity. *Cardiovasc Res* **109**, 451–461.
- Tricarico D, Mele A, Lundquist AL, Desai RR, George AL & Conte Camerino D (2006). Hybrid assemblies of ATP-sensitive K⁺ channels determine their muscle-type-dependent biophysical and pharmacological properties. *Proc Natl Acad Sci USA* **103**, 1118–1123.
- Tsai CF, Tai CT, Hsieh MH, Lin WS, Yu WC, Ueng KC, Ding YA, Chang MS & Chen SA (2000). Initiation of atrial fibrillation by ectopic beats originating from the superior vena cava: electrophysiological characteristics and results of radiofrequency ablation. *Circulation* **102**, 67–74.
- Tse G (2016). Mechanisms of cardiac arrhythmias. *Journal of Arrhythmia* **32**, 75–81.
- Tseng GN & Boyden PA (1989). Multiple types of Ca²⁺ currents in single canine Purkinje cells. *Circ Res* **65**, 1735–1750.
- Tucker SJ, Gribble FM, Proks P, Trapp S, Ryder TJ, Haug T, Reimann F & Ashcroft FM (1998). Molecular determinants of KATP channel inhibition by ATP. *EMBO J* **17**, 3290–3296.
- Tucker SJ, Gribble FM, Zhao C, Trapp S & Ashcroft FM (1997). Truncation of Kir6.2 produces ATP-sensitive K⁺ channels in the absence of the sulphonylurea receptor. *Nature* **387**, 179–183.
- Tzatzalos E, Abilez OJ, Shukla P & Wu JC (2016). Engineered heart tissues and induced pluripotent stem cells: Macro- and microstructures for disease modeling, drug screening, and translational studies. *Adv Drug Deliv Rev* **96**, 234–244.

- Uchida T, Yashima M, Gotoh M, Qu Z, Garfinkel A, Weiss JN, Fishbein MC, Mandel WJ, Chen PS & Karagueuzian HS (1999). Mechanism of acceleration of functional reentry in the ventricle: effects of ATP-sensitive potassium channel opener. *Circulation* **99**, 704–712.
- Ueda H, Nakayama Y, Tsumura K, Yoshimaru K, Hayashi T & Yoshikawa J (2004). Intravenous nicorandil can reduce the occurrence of ventricular fibrillation and QT dispersion in patients with successful coronary angioplasty in acute myocardial infarction. *Can J Cardiol* **20**, 625–629.
- Ueda K, Komine J, Matsuo M, Seino S & Amachi T (1999). Cooperative binding of ATP and MgADP in the sulfonylurea receptor is modulated by glibenclamide. *Proc Natl Acad Sci USA* **96**, 1268–1272.
- Uhde I, Toman A, Gross I, Schwanstecher C & Schwanstecher M (1999). Identification of the potassium channel opener site on sulfonylurea receptors. *J Biol Chem* **274**, 28079–28082.
- Ulbricht W (2005). Sodium channel inactivation: molecular determinants and modulation. *Physiol Rev* **85**, 1271–1301.
- Unudurthi SD, Wolf RM & Hund TJ (2014). Role of sinoatrial node architecture in maintaining a balanced source-sink relationship and synchronous cardiac pacemaking. *Front Physiol* **5**, 446.
- Valiunas V, Weingart R & Brink PR (2000). Formation of heterotypic gap junction channels by connexins 40 and 43. *Circ Res* **86**, E42–E49.
- van Bever L, Poitry S, Faure C, Norman RI, Roatti A & Baertschi AJ (2004). Pore loop-mutated rat KIR6.1 and KIR6.2 suppress KATP current in rat cardiomyocytes. *Am J Physiol Heart Circ Physiol* **287**, H850–H859.
- van Boekel G, Loves S, van Sorge A, Ruinemans-Koerts J, Rijnders T & de Boer H (2008). Weight loss in obese men by caloric restriction and high-dose diazoxide-mediated insulin suppression. *Diabetes Obes Metab* **10**, 1195–1203.
- van Bon BWM et al. (2012). Cantú syndrome is caused by mutations in ABCC9. *Am J Hum Genet* **90**, 1094–1101.
- van Campenhout MJH, Yaksh A, Kik C, de Jaegere PP, Ho SY, Allessie MA & de Groot NMS (2013). Bachmann's bundle: a key player in the development of atrial fibrillation? *Circ Arrhythm Electrophysiol* **6**, 1041–1046.
- van Veen AA, van Rijen HV & Opthof T (2001). Cardiac gap junction channels: modulation of expression and channel properties. *Cardiovasc Res* **51**, 217–229.
- Van Wagoner DR, Pond AL, Lamorgese M, Rossie SS, McCarthy PM & Nerbonne JM (1999). Atrial L-type Ca²⁺ currents and human atrial fibrillation. *Circ Res* **85**, 428–436.

- Vandenberg JI, Perry MD, Perrin MJ, Mann SA, Ke Y & Hill AP (2012). hERG K(+) channels: structure, function, and clinical significance. *Physiol Rev* **92**, 1393–1478.
- Vandesompele J, De Preter K, Pattyn F, Poppe B, Van Roy N, De Paepe A & Speleman F (2002). Accurate normalization of real-time quantitative RT-PCR data by geometric averaging of multiple internal control genes. *Genome Biol* **3**, RESEARCH0034.
- Vedovato N, Cliff E, Proks P, Poovazhagi V, Flanagan SE, Ellard S, Hattersley AT & Ashcroft FM (2016). Neonatal diabetes caused by a homozygous KCNJ11 mutation demonstrates that tiny changes in ATP sensitivity markedly affect diabetes risk. *Diabetologia* **59**, 1430–1436.
- Venkatesh N, Lamp ST & Weiss JN (1991). Sulfonylureas, ATP-sensitive K⁺ channels, and cellular K⁺ loss during hypoxia, ischemia, and metabolic inhibition in mammalian ventricle. *Circ Res* **69**, 623–637.
- Verheijck EE, van Kempen MJ, Veereschild M, Lurvink J, Jongsma HJ & Bouman LN (2001). Electrophysiological features of the mouse sinoatrial node in relation to connexin distribution. *Cardiovasc Res* **52**, 40–50.
- Verkerk AO & Remme CA (2012). Zebrafish: a novel research tool for cardiac (patho)electrophysiology and ion channel disorders. *Front Physiol* **3**, 255.
- Verma A, Jiang C-Y, Betts TR, Chen J, Deisenhofer I, Mantovan R, Macle L, Morillo CA, Haverkamp W, Weerasooriya R, Albenque J-P, Nardi S, Menardi E, Novak P, Sanders PSTAR AF II Investigators (2015). Approaches to catheter ablation for persistent atrial fibrillation. *N Engl J Med* **372**, 1812–1822.
- Verma A, Mantovan R, Macle L, De Martino G, Chen J, Morillo CA, Novak P, Calzolari V, Guerra PG, Nair G, Torrecilla EG & Khaykin Y (2010). Substrate and Trigger Ablation for Reduction of Atrial Fibrillation (STAR AF): a randomized, multicentre, international trial. *Eur Heart J* **31**, 1344–1356.
- Vermij SH, Abriel H & van Veen TAB (2017). Refining the molecular organization of the cardiac intercalated disc. *Cardiovasc Res* **113**, 259–275.
- Vinogradova TM, Bogdanov KY & Lakatta EG (2002). beta-Adrenergic stimulation modulates ryanodine receptor Ca(2⁺) release during diastolic depolarization to accelerate pacemaker activity in rabbit sinoatrial nodal cells. *Circ Res* **90**, 73–79.
- Viswanathan PC, Shaw RM & Rudy Y (1999). Effects of IKr and IKs heterogeneity on action potential duration and its rate dependence: a simulation study. *Circulation* **99**, 2466–2474.
- Vizzardi E, D'Aloia A, Quinzani F, Bonadei I, Rovetta R, Bontempi L, Curnis A & Dei Cas L (2012). A focus on antiarrhythmic properties of ranolazine. *J Cardiovasc Pharmacol Ther* **17**, 353–356.

- Voigt N, Heijman J, Wang Q, Chiang DY, Li N, Karck M, Wehrens XHT, Nattel S & Dobrev D (2014). Cellular and molecular mechanisms of atrial arrhythmogenesis in patients with paroxysmal atrial fibrillation. *Circulation* **129**, 145–156.
- Voigt N, Li N, Wang Q, Wang W, Trafford AW, Abu-Taha I, Sun Q, Wieland T, Ravens U, Nattel S, Wehrens XHT & Dobrev D (2012). Enhanced sarcoplasmic reticulum Ca²⁺ leak and increased Na⁺-Ca²⁺ exchanger function underlie delayed afterdepolarizations in patients with chronic atrial fibrillation. *Circulation* **125**, 2059–2070.
- Volders PGA, Stengl M, van Opstal JM, Gerlach U, Spätjens RLHMG, Beekman JDM, Sipido KR & Vos MA (2003). Probing the contribution of IKs to canine ventricular repolarization: key role for beta-adrenergic receptor stimulation. *Circulation* **107**, 2753–2760.
- Vozzi C, Dupont E, Coppens SR, Yeh HI & Severs NJ (1999). Chamber-related differences in connexin expression in the human heart. *J Mol Cell Cardiol* **31**, 991–1003.
- Wakimoto H, Maguire CT, Kooroor P, Hammer PE, Gehrman J, Triedman JK & Berul CI (2001). Induction of atrial tachycardia and fibrillation in the mouse heart. *Cardiovasc Res* **50**, 463–473.
- Wang J, Feng J & Nattel S (1994). Class III antiarrhythmic drug action in experimental atrial fibrillation. Differences in reverse use dependence and effectiveness between d-sotalol and the new antiarrhythmic drug ambasilide. *Circulation* **90**, 2032–2040.
- Wang W, Ma J, Zhang P & Luo A (2007). Redox reaction modulates transient and persistent sodium current during hypoxia in guinea pig ventricular myocytes. *Pflügers Arch* **454**, 461–475.
- Wang Z, Feng J & Nattel S (1995). Idiopathic atrial fibrillation in dogs: electrophysiologic determinants and mechanisms of antiarrhythmic action of flecainide. *J Am Coll Cardiol* **26**, 277–286.
- Wang Z, Feng J, Shi H, Pond A, Nerbonne JM & Nattel S (1999). Potential molecular basis of different physiological properties of the transient outward K⁺ current in rabbit and human atrial myocytes. *Circ Res* **84**, 551–561.
- Wang Z, Fermini B & Nattel S (1993). Sustained depolarization-induced outward current in human atrial myocytes. Evidence for a novel delayed rectifier K⁺ current similar to Kv1.5 cloned channel currents. *Circ Res* **73**, 1061–1076.
- Wang ZG, Pelletier LC, Talajic M & Nattel S (1990). Effects of flecainide and quinidine on human atrial action potentials. Role of rate-dependence and comparison with guinea pig, rabbit, and dog tissues. *Circulation* **82**, 274–283.

- Watanabe O, Okumura T, Takeda H, Nakamura W, Segawa K, Ito H & Yoshimoto N (1999). Nicorandil, a potassium channel opener, abolished torsades de pointes in a patient with complete atrioventricular block. *Pacing Clin Electrophysiol* **22**, 686–688.
- Weiss JN, Garfinkel A, Karagueuzian HS, Qu Z & Chen PS (1999). Chaos and the transition to ventricular fibrillation: a new approach to antiarrhythmic drug evaluation. *Circulation* **99**, 2819–2826.
- Welters A, Lerch C, Kummer S, Marquard J, Salgin B, Mayatepek E & Meissner T (2015). Long-term medical treatment in congenital hyperinsulinism: a descriptive analysis in a large cohort of patients from different clinical centers. *Orphanet J Rare Dis* **10**, 150.
- Wettwer E, Amos GJ, Posival H & Ravens U (1994). Transient outward current in human ventricular myocytes of subepicardial and subendocardial origin. *Circ Res* **75**, 473–482.
- Wheeler A, Wang C, Yang K, Fang K, Davis K, Styer AM, Mirshahi U, Moreau C, Revilloud J, Vivaudou M, Liu S, Mirshahi T & Chan KW (2008). Coassembly of different sulfonylurea receptor subtypes extends the phenotypic diversity of ATP-sensitive potassium (KATP) channels. *Mol Pharmacol* **74**, 1333–1344.
- White SM, Constantin PE & Claycomb WC (2004). Cardiac physiology at the cellular level: use of cultured HL-1 cardiomyocytes for studies of cardiac muscle cell structure and function. *Am J Physiol Heart Circ Physiol* **286**, H823–H829.
- White TW, Bruzzone R, Goodenough DA & Paul DL (1994). Voltage gating of connexins. *Nature* **371**, 208–209.
- Wijffels MC, Dorland R, Mast F & Allessie MA (2000). Widening of the excitable gap during pharmacological cardioversion of atrial fibrillation in the goat: effects of cibenzoline, hydroquinidine, flecainide, and d-sotalol. *Circulation* **102**, 260–267.
- Wilde AAM, Postema PG, Di Diego JM, Viskin S, Morita H, Fish JM & Antzelevitch C (2010). The pathophysiological mechanism underlying Brugada syndrome: depolarization versus repolarization. *J Mol Cell Cardiol* **49**, 543–553.
- Wilkins BJ & Molkentin JD (2004). Calcium-calcineurin signaling in the regulation of cardiac hypertrophy. *Biochem Biophys Res Commun* **322**, 1178–1191.
- Wit AL & Boyden PA (2007). Triggered activity and atrial fibrillation. *Heart Rhythm* **4**, S17–S23.
- Wolk R, Cobbe SM, Kane KA & Hicks MN (1999). Relevance of inter- and intraventricular electrical dispersion to arrhythmogenesis in normal and ischaemic rabbit myocardium: a study with cromakalim, 5-hydroxydecanoate and glibenclamide. *J Cardiovasc Pharmacol* **33**, 323–334.

- Wolleben CD, Sanguinetti MC & Siegl PK (1989). Influence of ATP-sensitive potassium channel modulators on ischemia-induced fibrillation in isolated rat hearts. *J Mol Cell Cardiol* **21**, 783–788.
- Wong CX, Ganesan AN & Selvanayagam JB (2017). Epicardial fat and atrial fibrillation: current evidence, potential mechanisms, clinical implications, and future directions. *Eur Heart J* **38**, 1294–1302.
- Workman AJ, Kane KA & Rankin AC (2008). Cellular bases for human atrial fibrillation. *Heart Rhythm* **5**, S1–S6.
- Wu G, Huang C-X, Tang Y-H, Jiang H, Wan J, Chen H, Xie Q & Huang Z-R (2005). Changes of IK, ATP current density and allosteric modulation during chronic atrial fibrillation. *Chin Med J* **118**, 1161–1166.
- Wyatt RF, Burgess MJ, Evans AK, Lux RL, Abildskov JA & Tsutsumi T (1981). Estimation of ventricular transmembrane action potential durations and repolarization times from unipolar electrograms. *Am J Cardiol* **47**, 488.
- Yamada M, Isomoto S, Matsumoto S, Kondo C, Shindo T, Horio Y & Kurachi Y (1997). Sulphonylurea receptor 2B and Kir6.1 form a sulphonylurea-sensitive but ATP-insensitive K⁺ channel. *J Physiol (Lond)* **499 (Pt 3)**, 715–720.
- Yamada S, Kane GC, Behfar A, Liu X-K, Dyer RB, Faustino RS, Miki T, Seino S & Terzic A (2006). Protection conferred by myocardial ATP-sensitive K⁺ channels in pressure overload-induced congestive heart failure revealed in KCNJ11 Kir6.2-null mutant. *J Physiol (Lond)* **577**, 1053–1065.
- Yan F-F, Lin Y-W, MacMullen C, Ganguly A, Stanley CA & Shyng S-L (2007). Congenital hyperinsulinism associated ABCC8 mutations that cause defective trafficking of ATP-sensitive K⁺ channels: identification and rescue. *Diabetes* **56**, 2339–2348.
- Yanagisawa T & Taira N (1981). Effect of 2-nicotinamidethyl nitrate (SG-75) on membrane potentials of canine Purkinje fibers. *Jpn J Pharmacol* **31**, 409–417.
- Yang Z & Murray KT (2011). Ionic mechanisms of pacemaker activity in spontaneously contracting atrial HL-1 cells. *J Cardiovasc Pharmacol* **57**, 28–36.
- Yeh Y-H, Kuo C-T, Lee Y-S, Lin Y-M, Nattel S, Tsai F-C & Chen W-J (2013). Region-specific gene expression profiles in the left atria of patients with valvular atrial fibrillation. *Heart Rhythm* **10**, 383–391.
- Yellon DM & Downey JM (2003). Preconditioning the myocardium: from cellular physiology to clinical cardiology. *Physiol Rev* **83**, 1113–1151.
- Yokoshiki H, Sunagawa M, Seki T & Sperelakis N (1998). ATP-sensitive K⁺ channels in pancreatic, cardiac, and vascular smooth muscle cells. *Am J Physiol* **274**, C25–C37.

- Yue AM (2007). Significant correlation between monophasic action potential (MAP) durations and activation-recovery intervals (ARIs) determined at the maximum positive slope of the positive T wave (conventional method). *Heart Rhythm* **4**, 120–1–authorreply121.
- Yue AM, Paisey JR, Robinson S, Betts TR, Roberts PR & Morgan JM (2004). Determination of human ventricular repolarization by noncontact mapping: validation with monophasic action potential recordings. *Circulation* **110**, 1343–1350.
- Zhang HX, Akrouh A, Kurata HT, Remedi MS, Lawton JS & Nichols CG (2011). HMR 1098 is not an SUR isotype specific inhibitor of heterologous or sarcolemmal K ATP channels. *J Mol Cell Cardiol* **50**, 552–560.
- Zheng Y, Wei D, Zhu X, Chen W, Fukuda K & Shimokawa H (2016). Transmural, interventricular, apicobasal and anteroposterior action potential duration gradients are all essential to the genesis of the concordant and realistic T wave: A whole-heart model study. *J Electrocardiol* **49**, 569–578.
- Zingman LV, Hodgson DM, Bast PH, Kane GC, Perez-Terzic C, Gumina RJ, Pucar D, Bienengraeber M, Dzeja PP, Miki T, Seino S, Alekseev AE & Terzic A (2002). Kir6.2 is required for adaptation to stress. *Proc Natl Acad Sci USA* **99**, 13278–13283.
- Zlatkovic J, Arrell DK, Kane GC, Miki T, Seino S & Terzic A (2009). Proteomic profiling of KATP channel-deficient hypertensive heart maps risk for maladaptive cardiomyopathic outcome. *Proteomics* **9**, 1314–1325.
- Zünkler BJ, Henning B, Ott T, Hildebrandt AG & Fleck E (1997). Effects of tolbutamide on ATP-sensitive K⁺ channels from human right atrial cardiac myocytes. *Pharmacol Toxicol* **80**, 69–75.
- Zygmunt AC, Eddlestone GT, Thomas GP, Nesterenko VV & Antzelevitch C (2001). Larger late sodium conductance in M cells contributes to electrical heterogeneity in canine ventricle. *Am J Physiol Heart Circ Physiol* **281**, H689–H697.
- Zygmunt AC, Nesterenko VV, Rajamani S, Hu D, Barajas-Martínez H, Belardinelli L & Antzelevitch C (2011). Mechanisms of atrial-selective block of Na⁺ channels by ranolazine: I. Experimental analysis of the use-dependent block. *Am J Physiol Heart Circ Physiol* **301**, H1606–H1614.